

1-1-1984

## Synthesis and characterization of polymers which mimic the functions of hemoglobin/

Amy Lee Finkenaur  
*University of Massachusetts Amherst*

Follow this and additional works at: [https://scholarworks.umass.edu/dissertations\\_1](https://scholarworks.umass.edu/dissertations_1)

---

### Recommended Citation

Finkenaur, Amy Lee, "Synthesis and characterization of polymers which mimic the functions of hemoglobin/" (1984). *Doctoral Dissertations 1896 - February 2014*. 684.  
<https://doi.org/10.7275/q44a-kg89> [https://scholarworks.umass.edu/dissertations\\_1/684](https://scholarworks.umass.edu/dissertations_1/684)

This Open Access Dissertation is brought to you for free and open access by ScholarWorks@UMass Amherst. It has been accepted for inclusion in Doctoral Dissertations 1896 - February 2014 by an authorized administrator of ScholarWorks@UMass Amherst. For more information, please contact [scholarworks@library.umass.edu](mailto:scholarworks@library.umass.edu).

UMASS/AMHERST



312066 0024 2842 0

SYNTHESIS AND CHARACTERIZATION OF POLYMERS  
WHICH MIMIC THE FUNCTIONS OF HEMOGLOBIN

A Dissertation Presented

By

AMY LEE FINKENAUER

Submitted to the Graduate School of the  
University of Massachusetts in partial fulfillment  
of the requirements for the degree of

DOCTOR OF PHILOSOPHY

February

1984

Polymer Science and Engineering


SYNTHESIS AND CHARACTERIZATION OF POLYMERS  
WHICH MIMIC THE FUNCTIONS OF HEMOGLOBIN

A Dissertation Presented


By

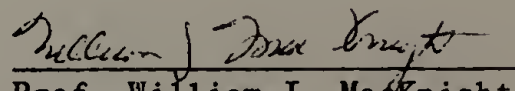
AMY LEE FINKENAUER

Approved as to style and content by:

  
Prof. James C.W. Chien, Chairperson of Committee

  
Prof. Frank E. Karasz, Member

  
Prof. Louis A. Carpino, Member

  
Prof. William J. MacKnight  
Department Head of Polymer  
Science and Engineering





Amy Lee Finkenaar

All Rights Reserved

For Paul, Nan and my parents, Allen and Virginia

### Acknowledgement

I wish to thank Professor James C.W. Chien for his support, invaluable discussions and for fostering my ability to think creatively and independently. I would also like to thank Professor Frank Karasz and Professor Louis Carpino for serving on my thesis committee and for providing helpful advice.

I would like to thank Dr. L. Charles Dickinson for daily encouragement and interaction which stimulated me intellectually and supported me emotionally.

Many of the faculty and students of the Department of Polymer Science and Engineering contributed intellectually to this dissertation. I would particularly like to thank Paul Russo for his advice on light scattering and polymer aggregation, Walt Bassett for his help with  $^{13}\text{C}$ -NMR studies, Brett Vanzo for helpful discussions concerning monomer synthesis and Yachin Cohen for electron microscopy of gel samples in aqueous systems. A special thanks is due Weishih Wu for providing invaluable assistance toward the completion of this dissertation and for teaching me more about myself than I could teach him about polymer science.

The friendships I have made in my research group enhanced my development as a scientist and made graduate school a fun and memorable experience. I would especially like to thank Jack Hirsch, Mike Schen and John Warakowski for their continuous support and companionship.

This dissertation would have never been accomplished without the steadfast love of my family. I can never repay my parents for giving me

curiosity, ambition, a good education, and their love. I am especially grateful to my twin sister Nan, who drew the figures in this dissertation, for understanding and loving me. Finally, I would like to thank my husband, Paul. He offered many helpful suggestions throughout the experimental work and writing process. Paul's love and encouragement have given sustenance to my work and have given me so much happiness.

## ABSTRACT

### SYNTHESIS AND CHARACTERIZATION OF POLYMERS WHICH MIMIC THE FUNCTIONS OF HEMOGLOBIN

(February 1984)

Amy Lee Finkenaur, B.S. University of Connecticut, 1979

M.S. University of Massachusetts, 1981

Ph.D. University of Massachusetts, 1984

Directed by: Professor James C.W. Chien

The objective of this dissertation was the synthesis of a water soluble vinyl polymer which could model some of the properties of hemoglobin such as oxygen and carbon dioxide carrying capacity, hydrophobic domains and rigidity.

The selection and synthesis of functional monomers was very important in the development of a model of hemoglobin. Derivatives of hemin, dimethylester (HDME), di-3-(1-imidazolyl)propylamide (HDA) and mono-3-(1-imidazolyl)-propylamide monomethylester (HMEMA), were synthesized to function as oxygen carriers. The bulk of the polymer was poly(styrene) whose function was to provide hydrophobic domains. Three monomers, methyl p-vinylbenzenesulfonate (MSS), 4-vinylpyridine (4VP) and p-vinylbenzylchloride (VBC), were incorporated in the polymer at 13 - 20 mol % and gave water solubility subsequent to hydrolysis of the ester, quaternization of the amine or substitution of the chlorine with a trialkylamine respectively. p-Azidophenyl methacrylate (APMA), a photoactive crosslinking agent, was polymerized to give structural rigidity. Amine moieties, 2-aminoethyl methacrylate (AEMA) and N-

methacrylylhexamethylenediamine (NAHD) were incorporated to carry carbon dioxide as a function of pH.

The reactivity of these monomers was characterized and the reactivity ratios were utilized to prepare ter- and tetrapolymers of known composition. Heme monomers behaved as chain terminators except in the presence of strong ligands for iron.

Polymeric subsets of the five different types of monomers were characterized as simple models of hemoglobin. The kinetics of the oxygenation of HMEMA showed that oxidation is due to dimerization. Polymer bound HMEMA was 1.5 times more stable to dimerization but also exhibited some autooxidation.

$^{13}\text{C}$ -NMR experiments, used to study the formation of carbamate as a function of pH in amine-containing polymers, proved that the  $\text{pK}_a$  of the amines was too high to bind  $^{13}\text{CO}_2$  at physiological pH.

Dye solubilization experiments demonstrated the presence of hydrophobic domains in the model polymers which were favored at high hydrophobe content and ionic strength and low solution concentration. These polymer molecules aggregated in solution at concentrations greater than 0.1 - 0.2 weight %. Preliminary evidence suggested that photolysis of APMA caused intramolecular crosslinking of the polymer. Novel hydrophobic polyampholyte gels were observed in polymers containing hydrophobic, anionic and cationic groups.

## Table of Contents

Dedication - - - - -	iv
Acknowledgement - - - - -	v
Abstract - - - - -	vii
List of Tables - - - - -	xiii
List of Figures - - - - -	xv
CHAPTER I. THE DESIGN OF A MODEL OF HEMOGLOBIN - - - - -	1
Introduction - - - - -	1
Fluorocarbon blood substitutes - - - - -	3
Hemoglobin structure and function - - - - -	5
Hemoglobin derivatives as oxygen carriers - - - - -	18
Heme derivatives as hemoglobin models - - - - -	19
Polymer based models of hemoglobin - - - - -	25
Research strategy - - - - -	30
References - - - - -	34
CHAPTER II. MONOMER SYNTHESIS - - - - -	42
Introduction - - - - -	42
Experimental procedure - - - - -	42
Purification - - - - -	44
Instrumentation - - - - -	44
Monomer synthesis - - - - -	44
p-(2-bromoethyl)benzenesulfonylchloride - - - - -	44
methyl p-(2-bromoethyl)benzenesulfonate - - - - -	45
methyl p-vinylbenzenesulfonate - - - - -	46
p-vinylbenzenesulfonylchloride - - - - -	46
N-ethyl-p-vinylpyridinium bromide - - - - -	47
ferric protoporphyrin IX dimethylester - - - - -	47
3-(1-imidazolyl)propylamine - - - - -	48
ferric protoporphyrin IX di-3-(1-imidazolyl)- propylamide - - - - -	49
ferric protoporphyrin IX mono-3-(1-imidazolyl)- propylamide monomethylester - - - - -	50
ferric protoporphyrin IX mono-3-(1-imidazolyl)- propylamide monodecylester - - - - -	51
ferric protoporphyrin IX mono-3-(1-imidazolyl)- propylamide monohexylester - - - - -	52
N- <u>tert</u> -butyloxycarbonyl-2-aminoethyl methacrylate - - -	53
N- <u>tert</u> -butyloxycarbonyl-1,6-diaminohexane·HCl - - - -	53
N- <u>tert</u> -butyloxycarbonyl-N'-(2-methacrylyl)- 1,6-diaminohexane - - - - -	54
p-azidostyrene - - - - -	55
p-azidoacetophenone - - - - -	56
1-(p-azidophenyl)ethanol - - - - -	56



p-azidostyrene - - - - -	57
2-azidoethyl methacrylate - - - - -	57
p-azidophenyl methacrylate - - - - -	58
Results and discussion - - - - -	59
Hydrophobic monomer - - - - -	59
Hydrophillic monomers - - - - -	59
Heme model compounds - - - - -	62
Amine monomers - - - - -	65
Photoactive crosslinking agents - - - - -	69
References - - - - -	77
 CHAPTER III. COPOLYMERIZATION - - - - -	79
Theory - - - - -	79
Experimental procedure - - - - -	82
Results and discussion - - - - -	84
Copolymerization of S/APMA - - - - -	84
Copolymerization of S/BAEMA - - - - -	96
Copolymerization of S/BNAHD - - - - -	100
Copolymerization of S/MSS - - - - -	106
Copolymerization of S/VBC - - - - -	112
Conclusions - - - - -	112
References - - - - -	121
 CHAPTER IV. COPOLYMERIZATION OF STYRENE WITH FERROUS AND FERRIC PROTOPORPHYRIN IX DERIVATIVES AND THE EFFECT OF LIGAND COMPLEXATION - - - - -	123
Introduction - - - - -	123
Experimental procedure - - - - -	124
Polymerizations - - - - -	124
S/Fe <sup>2+</sup> HDME - - - - -	125
S/Fe <sup>3+</sup> HDME·(CN) <sub>2</sub> <sup>-1</sup> - - - - -	125
S/Fe <sup>3+</sup> HDME·(IM) <sub>2</sub> - - - - -	130
S/Fe <sup>2+</sup> HDME·CO - - - - -	130
S/Fe <sup>3+</sup> HDA - - - - -	130
S/Fe <sup>3+</sup> HDA·CO - - - - -	130
S - - - - -	130
Results and discussion - - - - -	133
Polymerization and polymer composition - - - - -	133
Molecular weight studies - - - - -	144
Conclusions - - - - -	146
References - - - - -	150
 CHAPTER V. TAILORING THE COMPOSITION, PHYSICAL AND CHEMICAL PROPERTIES OF MODEL POLYMERS - - - - -	151
Introduction - - - - -	151
Composition - - - - -	151
Chemical and physical properties - - - - -	154
Molecular weight - - - - -	155
Experimental procedure - - - - -	158
Material - - - - -	158



Instrumentation - - - - -	158
Polymerization - - - - -	159
<sup>14</sup> C-AIBN labelled S/MSS/BNAHD - - - - -	159
S/MSS/APMA/HMEMA - - - - -	162
S/APMA - - - - -	162
Chemical modification of the polymer - - - - -	163
Hydrolysis of methylsulfonate - - - - -	163
Quaternization of polymerized 4VP - - - - -	164
Ammonium derivatives of polymerized VBC - - - - -	164
Removal of the <i>t</i> -butyloxycarbonyl protecting group - - - - -	165
Thermolysis of polymerized APMA - - - - -	166
Photolysis of S/APMA in organic solvents - - - - -	166
Photolysis of S/SS <sup>-</sup> /APMA in aqueous solution - - - - -	166
Results and discussion - - - - -	167
Composition - - - - -	167
Chemical modification of polymers - - - - -	173
Water solubility - - - - -	173
Removal of the <i>t</i> -BOC group - - - - -	179
Photolysis of the azide group - - - - -	182
Molecular weight studies - - - - -	185
Conclusions - - - - -	188
References - - - - -	191

## CHAPTER VI. THE OXIDATION KINETICS OF OXYGENATED

HEMOGLOBIN MODELS IN AN AQUEOUS ENVIRONMENT - - - - -	193
Introduction - - - - -	193
Experimental procedure - - - - -	194
Materials - - - - -	194
Sodium hydrosulfite (aprotic media) - - - - -	194
Sodium hydrosulfite (aqueous media) - - - - -	195
Ascorbate - - - - -	195
Aminoiminomethanesulfinic acid - - - - -	196
Solutions for oxygenation studies - - - - -	196
Heme monomers - - - - -	196
S/HDA; S/HDME - - - - -	196
S/SS <sup>-</sup> /HDA - - - - -	196
S/SS <sup>-</sup> /APMA/HMEMA - - - - -	197
Equipment - - - - -	197
Procedure - - - - -	200
Calculations - - - - -	203
Results and discussion - - - - -	203
Solution preparation - - - - -	203
Reducing agents - - - - -	206
Kinetic studies - - - - -	225
Conclusions - - - - -	241
References - - - - -	250

## CHAPTER VII. CHARACTERIZATION OF HYDROPHOBIC DOMAINS IN WATER SOLUBLE POLYMERS AND THE GELATION OF HYDROPHOBIC POLYAMPHOLYTES - - - - -

252

Introduction - - - - -	252
Experimental procedure - - - - -	256
Materials - - - - -	256
S/SS <sup>-</sup> /AEMA - - - - -	256
S/MSS/BNAHD - - - - -	257
Surfactant solutions - - - - -	257
Qualitative comparison of counterion effect - - - - -	258
Dye solubilization - - - - -	258
Composition effect - - - - -	258
Crosslinking effect - - - - -	259
Ionic strength effect - - - - -	259
pH effect - - - - -	260
Light scattering - - - - -	260
Electron microscopy - - - - -	261
Results and discussion - - - - -	262
Hydrophobic domains - - - - -	262
Hydrophobic polyampholyte complexes - - - - -	273
Conclusions - - - - -	285
References - - - - -	287

#### CHAPTER VIII. CARBAMATE FORMATION IN AMINE CONTAINING POLYMERS

TO MIMIC CO <sub>2</sub> TRANSPORT BY HEMOGLOBIN - - - - -	290
Introduction - - - - -	290
Experimental procedure - - - - -	295
Materials - - - - -	295
Standards - - - - -	295
Sample preparation - - - - -	296
<sup>13</sup> C Fourier transform NMR measurements - - - - -	297
Results and discussion - - - - -	297
Gated decoupling and the <sup>13</sup> C FT-NMR method - - - - -	297
HEPES as an internal pH standard - - - - -	301
<sup>13</sup> Carbamates in model systems - - - - -	301
Conclusions - - - - -	311
References - - - - -	313

#### CHAPTER IX. SUGGESTIONS FOR FUTURE WORK - - - - - 315

#### APPENDIX A. SPECTRA OF ORGANIC COMPOUNDS - - - - - 323

# List of Tables

## Table

1.1	Potential uses of artificial blood substitutes - - - - -	2
1.2	Identities of amino acids in hemoglobin and myoglobin - -	9
1.3	pK <sub>a</sub> values for valine - - - - -	16
3.1	Experimental parameters in the copolymerization of APMA (M <sub>1</sub> ) and styrene (M <sub>2</sub> ) - - - - -	85
3.2	Experimental parameters in the copolymerization of BAEMA (M <sub>1</sub> ) and styrene (M <sub>2</sub> ) - - - - -	86
3.3	Experimental parameters in the copolymerization of BNAHD (M <sub>1</sub> ) and styrene (M <sub>2</sub> ) - - - - -	87
3.4	Experimental parameters in the copolymerization of styrene (M <sub>1</sub> ) and MSS (M <sub>2</sub> ) - - - - -	88
3.5	Experimental parameters in the copolymerization of VBC (M <sub>1</sub> ) and styrene (M <sub>2</sub> ) - - - - -	89
3.6	Data for reactivity ratio analysis with M <sub>1</sub> = APMA and M <sub>2</sub> = styrene - - - - -	90
3.7	Data for reactivity ratio analysis with M <sub>1</sub> = BAEMA and M <sub>2</sub> = styrene - - - - -	97
3.8	Data for reactivity ratio analysis with M <sub>1</sub> = BNAHD and M <sub>2</sub> = styrene - - - - -	103
3.9	Data for reactivity ratio analysis with M <sub>1</sub> = styrene and M <sub>2</sub> = MSS - - - - -	107
3.10	Data for reactivity ratio analysis with M <sub>1</sub> = VBC and M <sub>2</sub> = styrene - - - - -	113
3.11	Summary of monomer reactivity - - - - -	116
4.1	Molecular weight data for styrene/iron porphyrin copolymers - - - - -	145
4.2	Molecular weight data for S/HDME·CO copolymers with varying heme concentrations - - - - -	147
5.1	Experimental parameters for terpolymerization - - - - -	160

5.2 Composition of terpolymers from Table 5.1 - - - - - 161

5.3 Theoretical values for elemental analysis - - - - - 170

5.4 A comparison of experimentally determined polymer  
compositions with those predicted from modification of the  
terpolymer equation - - - - - 172

5.5 The molecular weight of select ter- and tetrapolymers - - 186

6.1 Summary of the kinetics of the oxygenation/oxidation  
reactions of heme model systems - - - - - 249

7.1 Data for Oil Red EGN solubilization in terpolymers of  
S/4VPQ/NAHD - - - - - 264

## List of Figures

### Figure

1.1	The structure of a $\beta$ -subunit of human hemoglobin - - - -	7
1.2	The structure of ferrous protoporphyrin IX - - - - -	10
1.3	The heme group and its environment in the unliganded $\alpha$ -chain - - - - -	13
1.4	A schematic of the structure of novel heme derivatives -	21
1.5	Methods to attach heme groups to polymers - - - - -	27
1.6	A schematic of a heme-containing polymer which can mimic the functions of hemoglobin - - - - -	32
2.1	$^{13}\text{C}$ -NMR of 2-aminoethyl methacrylate and its tautomer N-(2-hydroxyethyl)methacrylamide - - - - -	67
2.2	The ultraviolet spectrum of APMA - - - - -	75
3.1	A Fineman-Ross plot for the copolymerization of APMA ( $M_1$ ) and styrene ( $M_2$ ) - - - - -	91
3.2	A Kelen-Tüdös plot for the copolymerization of APMA ( $M_1$ ) and styrene ( $M_2$ ) - - - - -	93
3.3	A Fineman-Ross plot for the copolymerization of BAEMA ( $M_1$ ) and styrene ( $M_2$ ) - - - - -	98
3.4	A Kelen-Tüdös plot for the copolymerization of BAEMA ( $M_1$ ) and styrene ( $M_2$ ) - - - - -	101
3.5	A Kelen-Tüdös plot for the copolymerization of BNAHD ( $M_1$ ) and styrene ( $M_2$ ) - - - - -	104
3.6	A Fineman-Ross plot for the copolymerization of styrene ( $M_1$ ) and MSS ( $M_2$ ) - - - - -	108
3.7	A Kelen-Tüdös plot for the copolymerization of styrene ( $M_1$ ) and MSS ( $M_2$ ) - - - - -	110
3.8	A Kelen-Tüdös plot for the copolymerization of VBC ( $M_1$ ) and styrene ( $M_2$ ) - - - - -	114
3.9	Dependence of the copolymer composition, $d[M_1]$ , on the mole percent styrene in the feed - - - - -	118



4.1	The visible spectra of ferric HDME - - - - -	126
4.2	The visible spectra of ferrous HDME - - - - -	128
4.3	The visible spectra of ferric HDA - - - - -	131
4.4	Polymer yield versus time for polystyrene, S/HDME (Fe II), S/HDME (Fe III) - - - - -	134
4.5	Polymer yield versus time for various ligated HDME monomers copolymerized with styrene under identical reaction conditions - - - - -	138
4.6	Polymer yield versus time for copolymers of styrene and iron protoporphyrin IX bis-3-(1-imidazolyl)propylamide -	141
5.1	Infrared spectra of S/4VP/BNAHD (60.9/23.5/15.5) before and after quaternization of the pyridine group - - - - -	175
5.2	The relative peak heights observed by infrared spectroscopy during quaternization of S/4VP/BNAHD as a function of time - - - - -	177
5.3	The infrared spectra of S/VBC before and after quaternization - - - - -	180
5.4	The infrared spectra of S/SS <sup>-</sup> /APMA before and after photolysis of the azide group - - - - -	183
6.1	A schematic of the low temperature dewar designed to regulate sample temperature for the Beckman Acta MVI spectrophotometer - - - - -	198
6.2	The visible sample cell used in kinetic studies of the oxidation of oxygenated heme models - - - - -	201
6.3	Representative visible spectra observed during kinetic studies - - - - -	204
6.4	The visible spectra of a S/HDME copolymer - - - - -	209
6.5	The visible spectra of HMEMA - - - - -	212
6.6	The decay in absorbance observed for the reaction of HMEMA from the oxygenated to the oxidized state using a dithionite reducing agent - - - - -	215
6.7	The decay in absorbance observed for the reaction of HMEMA from the oxygenated to the oxidized state using an ascorbate reducing agent - - - - -	219

6.8	A second-order plot of the kinetic data for the oxy/oxi equilibrium of HMEMA using an ascorbate reducing agent - - - - -	222
6.9	The visible spectra of S/HDA - - - - -	226
6.10	The effect of solvent on the visible spectra of S/SS <sup>-</sup> /HDA - - - - -	228
6.11	A second-order plot of the kinetic data for the oxy/oxi equilibrium of HMEMA using a dithionite reducing agent with hydroquinone as a free radical scavenger - - - - -	231
6.12	The visible spectra of S/SS <sup>-</sup> /APMA/HMEMA - - - - -	233
6.13	A second-order plot for the oxy/oxi equilibrium of S/SS <sup>-</sup> /APMA/HMEMA - - - - -	236
6.14	A first-order plot for the oxy/oxi equilibrium of S/SS <sup>-</sup> /APMA/HMEMA - - - - -	238
6.15	Visible spectra of S/SS <sup>-</sup> /APMA/HMEMA before and after irradiation with ultraviolet light - - - - -	242
7.1	The structure of polysoaps in solution - - - - -	253
7.2	Dye solubilization as a function of polymer composition and concentration for S/4VPQ/NAHD - - - - -	265
7.3	Solubilizing power versus sample concentration for two terpolymers of S/4VPQ/NAHD - - - - -	268
7.4	Dye solubilization as a function of ionic strength for S/4VPQ/NAHD - - - - -	271
7.5	Static light scattering as a function of angle for S/SS <sup>-</sup> /APMA - - - - -	275
7.6	The pH equilibration as a function of time for a solution of S/SS <sup>-</sup> /NAHD with the addition of NaOH - - - - -	277
7.7	A schematic of the structure proposed for a hydrophobic polyampholyte gel - - - - -	281
8.1	Titration curve of S/AEMA in water with NaOH and HCl - - - - -	293
8.2	The timing necessary to obtain gated decoupling - - - - -	299
8.3	The <sup>13</sup> C chemical shifts of HEPES as a function of pH - - - - -	302

8.4	Representative $^{13}\text{C}$ -NMR spectra of HEPES - - - - -	304
8.5	The chemical shift of the $^{13}\text{C}$ bicarbonate-carbonate resonance as a function of pH - - - - -	307
8.6	The $^{13}\text{C}$ -NMR of S/4VPQ/NAHD at pH = 7.3 - - - - -	309
9.1	Flow chart for the synthesis of a polymer which can mimic the functions of hemoglobin - - - - -	316
A.1	Proton NMR of methyl p-(2-bromoethyl)benzenesulfonate - -	324
A.2	Proton NMR of methyl p-vinylbenzenesulfonate - - - - -	326
A.3	Infrared spectrum of methyl p-vinylbenzenesulfonate - - -	328
A.4	Carbon-13 NMR of methyl p-vinylbenzenesulfonate - - - - -	330
A.5	Infrared spectrum of ferric protoporphyrin IX dimethylester - - - - -	332
A.6	Proton NMR of 3-(1-imidazolyl)propylamine - - - - -	334
A.7	Infrared spectrum of 3-(1-imidazolyl)propylamine - - - -	336
A.8	Infrared spectrum of ferric protoporphyrin IX di-3-(1-imidazolyl)propylamide - - - - -	338
A.9	Infrared spectrum of ferric protoporphyrin IX mono-3-(1-imidazolyl)propylamide monomethylester - - - - -	340
A.10	Infrared spectrum of N- <u>tert</u> -butyloxycarbonyl-2-aminoethyl methacrylate - - - - -	342
A.11	Proton NMR of N- <u>tert</u> -butyloxycarbonyl-2-aminoethyl methacrylate - - - - -	344
A.12	Carbon-13 NMR of N- <u>tert</u> -butyloxycarbonyl-2-aminoethyl methacrylate - - - - -	346
A.13	Infrared spectrum of N- <u>tert</u> -butyloxycarbonyl-N'-(2-methacrylyl)-1,6-diaminohexane - - - - -	348
A.14	Proton NMR of N- <u>tert</u> -butyloxycarbonyl-N'-(2-methacrylyl)-1,6-diaminohexane - - - - -	350
A.15	Carbon-13 NMR of N- <u>tert</u> -butyloxycarbonyl-N'-(2-methacrylyl)-1,6-diaminohexane - - - - -	352
A.16	Infrared spectrum of p-azidophenol - - - - -	354



A.17	Infrared spectrum of p-azidophenyl methacrylate	- - - -	356
A.18	Proton NMR of p-azidophenyl methacrylate	- - - - -	358
A.19	Carbon-13 NMR of p-azidophenyl methacrylate	- - - - -	360

## CHAPTER I

### THE DESIGN OF A MODEL OF HEMOGLOBIN

The synthesis of a molecule which can mimic the functions of hemoglobin is of great interest for application as an artificial blood and is a means of clarifying structure/function relationships in hemoglobin. In order for the molecule to be a good transport system for oxygen and carbon dioxide, it should have the following properties:<sup>1</sup>

- (1) The carrier should have a high affinity for oxygen at high partial pressures of oxygen such as are found in the lungs (100 mm Hg).
- (2) The carrier should have a lower oxygen affinity than the storage molecule, myoglobin, at lower partial pressures of oxygen.
- (3) The carrier must transport carbon dioxide from the tissue to the lungs.
- (4) The carrier should be chemically unchanged through the oxygenation/deoxygenation cycle (i.e. not oxidized) or by carbon dioxide transport.

The potential uses of an artificial blood are vast,<sup>2,3</sup> and a partial list of the applications are given in Table 1.1. Blood substitutes will complement the uses of natural blood. They have the advantage of being disease free and can be used without blood typing or other delays in emergency situations. They should be easy to store and sterilize with a good shelf life. Substitutes are particularly suited to organ perfusion

Table 1.1

## Potential Uses of Artificial Blood Substitutes

---

Anemias: aplastic, sickle cell and cancer associated anemias

Anaerobic infections

Blood loss: hemorrhage, emergencies, surgeries, shock

Vascular occlusions: thrombosis, atherosclerosis

Toxicity screening

Chemo-, immuno-therapy

Hormone transport and metabolism

Enzyme depletion and repletion

Studies on: hematoporesis, plasma protein metabolism, sleep, blood-

brain barrier, circulatory physiology and hemodynamics, rheology,

lymph and lymphatics

Animal surgery and medicine

Organ perfusion

Total body washout: remove toxins, viruses, etc.

---

and should allow the development of organ banks. Also, animal surgery would be greatly facilitated where no blood banks currently exist.

The total replacement of an animal's blood with a substitute would provide a powerful method to examine the action of plasma proteins, hormones, enzymes, chemicals etc. in the body. Artificial blood could also be used for total body washout to remove toxic chemicals, viruses, and other harmful substances.

Two approaches have been taken in the synthesis of an artificial blood. The first is the creation of a system which would mimic function without any effort to use hemoglobin as the structural template. The most successful work, using this idea, has been the development of fluorocarbon emulsions as blood substitutes. There is also significant effort in the synthesis of a cobalt containing system which can carry oxygen.<sup>4</sup>

#### Fluorocarbon Blood Substitutes

Fluorocarbon emulsions have received wide attention for use as artificial bloods since their unique properties were discovered by Dr. Leland Clark in 1966.<sup>5</sup> Hundreds of perfluorinated compounds have been evaluated as potential blood substitutes leading to the commercial preparation of Fluosol DA by the Green Cross Corporation of Japan.<sup>6</sup> Fluosol DA is a mixture of seven parts perfluorodecalin in three parts perfluorotripropylamine and utilizes the nonionic emulsifying agent Pluronic F-68 and yolk phospholipid to maintain a fine, stable emulsion in water.<sup>7</sup>

Fluorocarbons as blood substitutes have both significant advantages as well as disadvantages.<sup>8-11</sup> The utility of fluorocarbon emulsions is a result of their high capacity to dissolve gases of up to 27 volume %  $O_2$  and 57 volume %  $CO_2$  at  $37^\circ C$  with Henry's law behavior. These artificial bloods are free from disease, relatively inert and require no crosstyping. They are particularly advantageous in the treatment of tissues involved in trauma and shock because the fine particle size (less than  $0.2\ \mu m$ ) allows these oxygen carriers to penetrate tissues with the blood plasma while red blood cells are left behind. Brominated fluorocarbons are useful for tumor imaging as they are endocytosed by tumor cells and are radioopaque.<sup>12</sup>

Although fluorocarbon blood substitutes have been tested in several hundred humans, significant problems must be resolved to give safe and widespread application. Presently available emulsions must be stored in the frozen state and used immediately upon thawing. Emulsion stability, toxicity and body retention time are determined by the chemical composition. The vapor pressure of the perfluorinated substance must be less than 40 torr to prevent pulmonary embolism, which requires a chain length of at least eight carbons. Perfluorinated carbon-containing compounds have a short half-life in the body but form unstable emulsions. Incorporation of a hetero-atom, such as nitrogen, increases the stability of the emulsion while also increasing the uptake by the reticuloendothelial (RE) system and thus the half-life. Perfluorocarbons are removed from circulation by the RE system as well as excreted via exhalation and through the skin. Particle size must be

maintained at less than 0.2  $\mu\text{m}$  to avoid blockage of the RE system. Long term health effects due to retention of fluorocarbons in the liver and spleen are not well known.

Under atmospheric conditions perfluorocarbons don't have the same capacity to carry oxygen as whole blood. A 10 - 50 vol. % fluorocarbon emulsion in an atmosphere of 100% oxygen holds the same amount of oxygen as an equal volume of blood in air. For this reason blood substitution experiments must use an oxygen-rich atmosphere.

These fluorocarbon substitutes have been shown to be effective and will be of great value in medicine, however there is still room for improvement.

The second approach in the development of an artificial blood is the use of a heme-containing unit, either naturally occurring or totally synthetic to transport oxygen. The objective of this dissertation is the synthesis of a vinyl polymer which can mimic some of the functions of hemoglobin: oxygen and carbon dioxide carrying capacity, water solubility with hydrophobic domains and structural rigidity. The design of an effective model of hemoglobin requires insight into the structure/function relationships in the native protein.

### Hemoglobin Structure and Function

Hemoglobin is an elegant protein whose structure has evolved over hundreds of millions of years. The outstanding reviews and books concerning this widely studied protein are noted in several references.<sup>1,13-16</sup> The human hemoglobin molecule is composed of four



subunits each of which contains a heme group that is associated with a polypeptide with a molecular weight of approximately 16,000. The tetrameric units are of two types, two  $\alpha$  subunits which contain 141 amino acids and two  $\beta$  subunits of 146 amino acids. The exact sequence and folding of these residues has been identified<sup>17</sup> (Figure 1.1).

The structure of hemoglobin is described by the primary, secondary, tertiary and quaternary structure.<sup>18</sup> The primary structure of this protein is given by the twenty amino acids of varying hydrophilicity, hydrophobicity and charge. They are combined in a unique order to give proper chain folding and surface charge. Some residues are highly conserved in most species of globin,<sup>19</sup> and serve certain specific functions (Table 1.2). The heme group is not covalently bound to the polypeptide. It consists of an iron atom (charge of +2) surrounded by a highly conjugated porphyrin ring (Figure 1.2) with a net charge of -2. Normally, ferrous heme (uncharged) is irreversibly oxidized by oxygen, but when it is embedded in the folds of the globin molecule the iron group is protected from irreversible oxidation.

The secondary structure of hemoglobin is the helical arrangement of the polypeptide which is stabilized by intramolecular hydrogen bonding. Hemoglobin is nearly 70% helical with the helical segments labeled A through H (from the N-terminus to the C-terminus).<sup>20</sup> These are primarily  $\alpha$ -helices with 3.6 amino acid residues per turn. It is interesting to note that hydrophobic residues occur every three or four molecules along the chain which imparts hydrophobic and hydrophilic sidedness to the helix and is most important in determining chain

Figure 1.1. The structure of a  $\beta$ -subunit of human hemoglobin. Helical regions are denoted A to H and non-helical regions between them are denote AB, BC, etc. The iron of the heme group is coordinated to the F8-His and oxygen binds in the pocket between the heme group, Val E11 and the distal histidine E7.



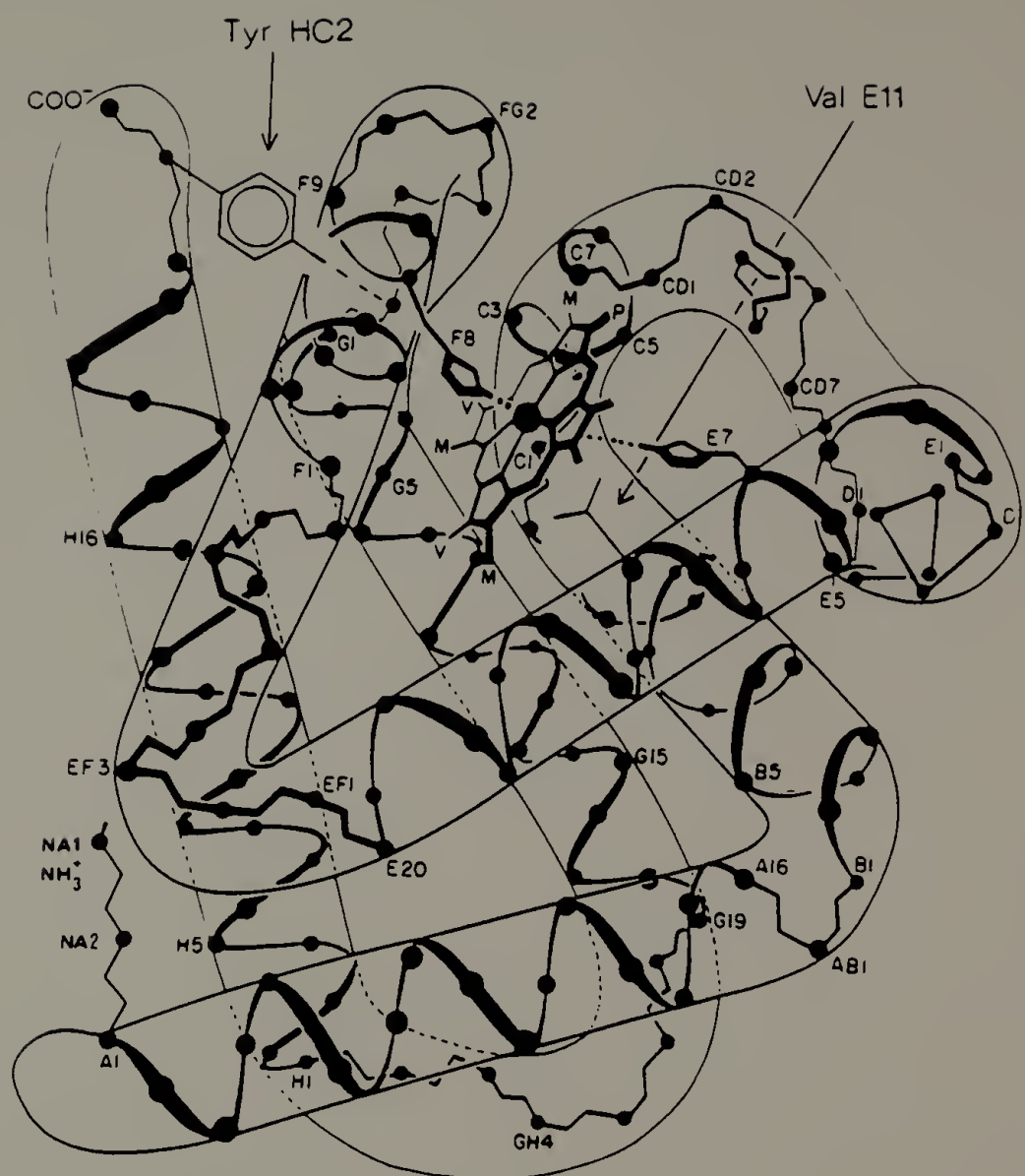


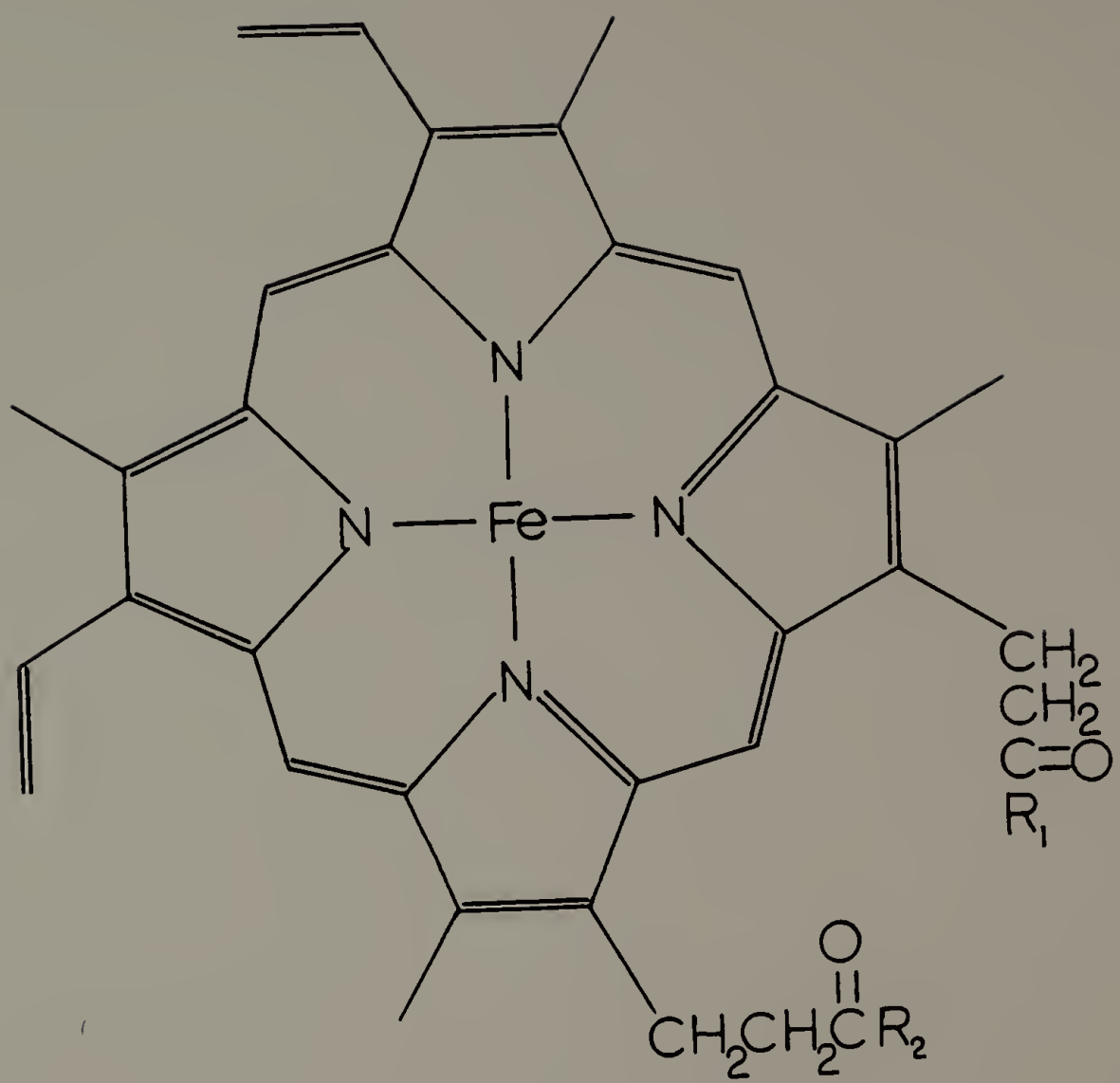
Table 1.2

Identities of Amino Acids in Hemoglobin and Myoglobin which  
Serve Specific Structure/Function Relationships<sup>a</sup>

Amino Acid	Position	Function
Val	NA1	Beginning of chain
Leu	NA2	Contact with H helix
Val	A8	H helix contact; hydrophobic cluster at bottom of heme pocket
Trp	A12	Hydrogen bond to E helix
Lys	A14	External salt bridges
Val	A15	In hydrophobic cluster at bottom of heme pocket, as a spacer between B and G helices
Gly	B6	Close contact with Gly E8 where helices cross
Leu	B10	In hydrophobic cluster at right of heme
Arg	B12	In hemoglobin, hydrogen bond to Phe GH5 C=O and to Gln H5 on neighboring subunit and salt bridge to Glu B8 of same subunit; in myoglobin, hydrogen bonds to water molecules
Pro	C2	Sharp turn between B and C helices
Thr	C4	Near heme
Phe	CD1	Packed against heme
Phe	CD4	In hydrophobic cluster at right of heme
Leu	CD7	In hydrophobic cluster at right of heme
Lys	E5	External salt bridges
His	E7	Interacts with sixth heme ligand
Gly	E8	Close contact with Gly B6 where helices cross
Val	E11	Packed against heme; in right hydrophobic cluster
Leu	F4	Packed against heme; in left hydrophobic cluster
His	F8	Fifth ligand to heme
Lys	FG2	Unknown
Leu	G16	Packed against A helix
Phe	GH5	In hydrophobic cluster at bottom of heme pocket, as a spacer between G and H helices
Lys	H10	External salt bridges
Lys	H22	External salt bridges
Tyr	H23	Hydrogen bond to C=O of Ile/Val to stabilize end of H helix

<sup>a</sup>See Ref. 1.

Figure 1.2. The structure of ferrous protoporphyrin IX where  
R = OH.

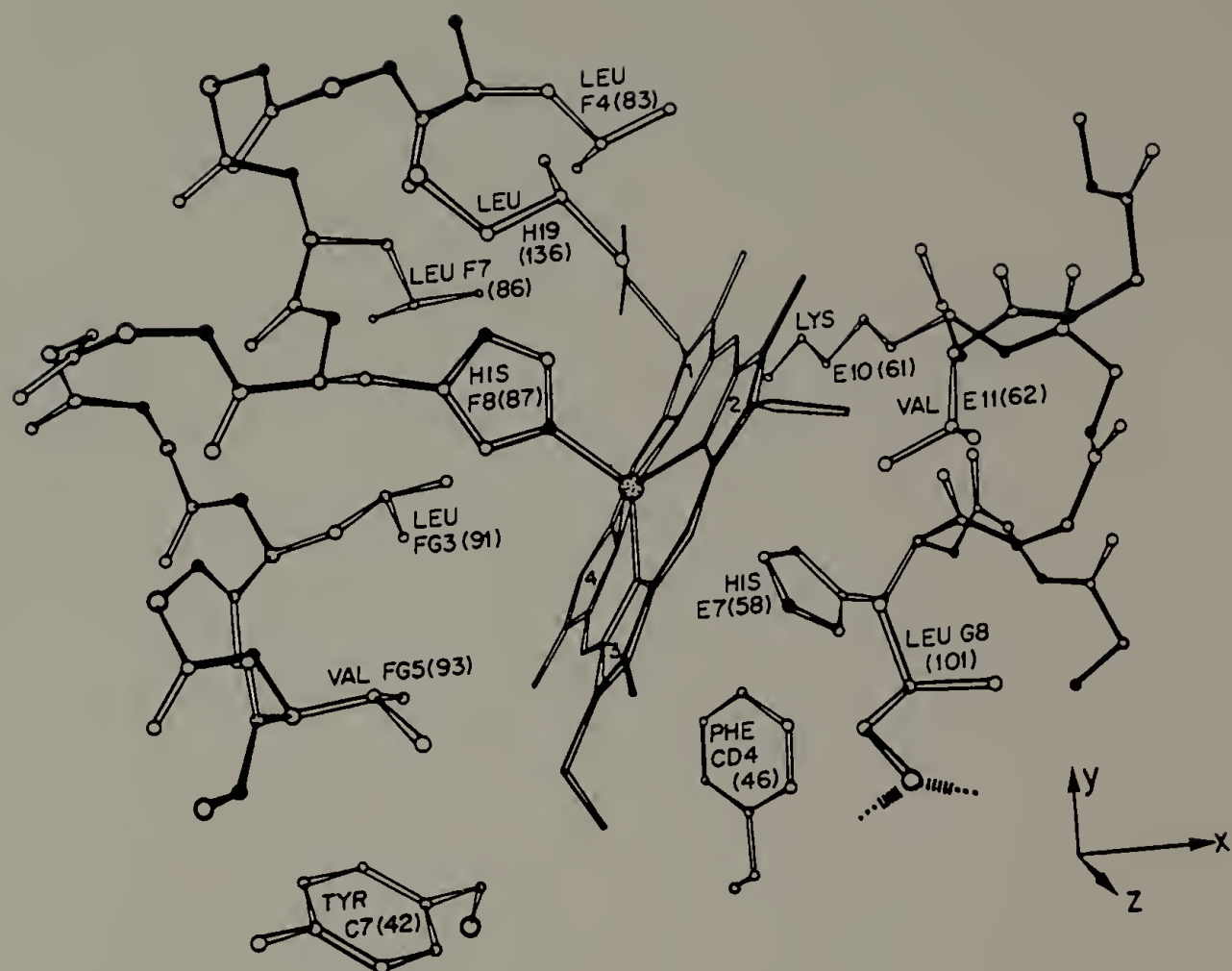


folding.

The way these helical segments are packed together to form the complete three-dimensional shape is called the tertiary structure. The heme group is surrounded by hydrophobic portions of the polypeptide chain to form approximately 60 van der Waals interactions with the periphery of the porphyrin ring<sup>21</sup> (Figure 1.3). The iron atom has a histidine moiety at its fifth coordination site. This proximal F8-His donates its negative charge and allows the heme to bind oxygen loosely.<sup>15</sup> Ferrous iron prefers an octahedral coordination structure and thus oxygen is the sixth ligand in oxyhemoglobin. A second histidine, His E7, on the distal side of the heme is too distant to coordinate directly with the iron but the N<sub>ε</sub> helps stabilize the bound oxygen.

The 2α and 2β subunits are held together by salt bridges, van der Waals forces and hydrogen bonds. Hemoglobin exhibits cooperativity in what Perutz has dubbed the "Matthew effect": "For to him who has will more be given, and he will have abundance; but from him who has not, even that which he has shall be taken away" (Matt. 13:12). The binding or loss of oxygen in one subunit dramatically facilitates binding/loss of oxygen in the other subunits. This is accomplished via a conformational change which triggers the breaking/formation of salt bridges and the changing of hydrogen bonds as well as van der Waals contacts. An extensive body of research is devoted to defining stereochemical changes that occur and the mathematical modeling of this process.<sup>22-26</sup>

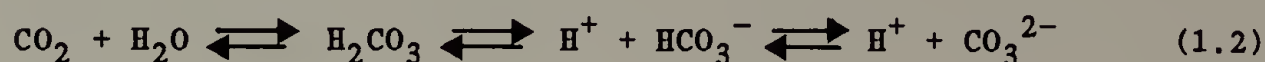
Figure 1.3. The heme group and its environment in the unliganded  $\alpha$ -chain. Solid bonds denote the polypeptide backbone. Only selected side chains are shown and the propionic acid groups are omitted for clarity.



Certain molecules, such as protons (Bohr effect),<sup>27</sup> carbon dioxide,<sup>28</sup> chloride ions<sup>29</sup> and 2,3-diphosphoglyceric acid (DPG),<sup>30</sup> cause the deoxygenated state of hemoglobin to be favored. Carbon dioxide is produced in the oxidation of carbohydrates to yield energy in the cell.



Carbon dioxide may react with water to form dissolved carbonates:



and 40% of the dissolved  $\text{CO}_2$  is transported by this mechanism. The remaining carbon dioxide is transported from the tissue to the lungs via the N-terminal amino groups on hemoglobin which are valines.<sup>31,32</sup> At a pH where these valine amino groups are unprotonated they will react with dissolved  $\text{CO}_2$  to form carbamates:



where  $K_a$  is the dissociation constant of the amine. Clearly, the  $\text{p}K_a$  of these amine groups must be sufficiently low to be uncharged at physiological pH (Table 1.3). The  $\text{p}K_a$  of the amino group is largely affected by the quaternary structure of the protein. It has been



Table 1.3

 $pK_a$  Values for Valine

---

	$pK_a$
deoxy Hb <sup>33</sup>	
Val 1 $\beta$	6.84
Val 1 $\alpha$	7.79
carbonmonoxy Hb	
Val 1 $\beta$	7.05
Val 1 $\alpha$	6.95
valine <sup>34</sup>	9.72

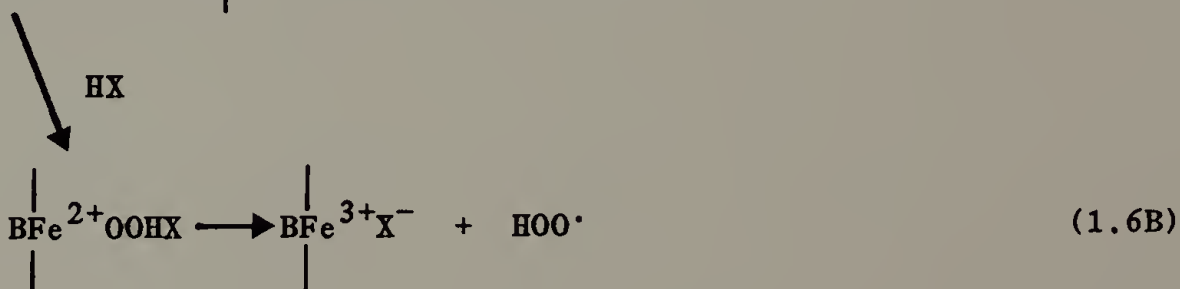
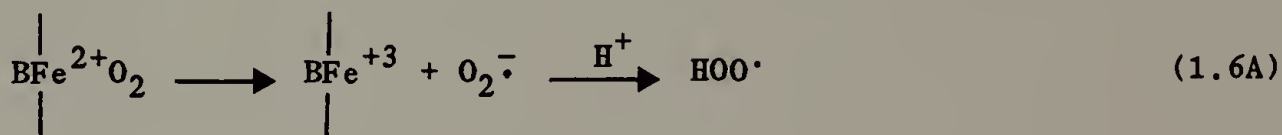
---

suggested that carbamate anions at the Val 1 $\beta$  site are stabilized through electrostatic interaction with the  $\epsilon$ -amino group of Lys 82 $\beta$ .<sup>32</sup> Val 1 $\alpha$  undergoes a greater change in  $pK_a$  upon deoxygenation which allows it to accept Bohr protons. The protonated Val 1 $\alpha$  would be stabilized by free chloride anions which could also interact with Arg 141 $\alpha$ .

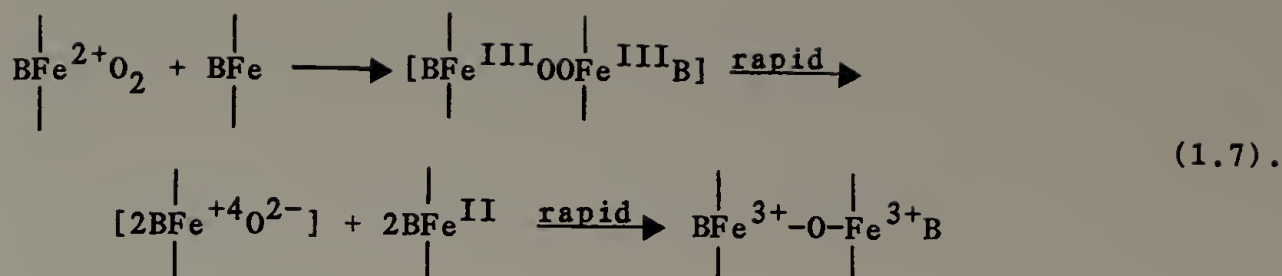
In hemoglobin the reaction of ferrous iron with oxygen is a reversible process:



where B = F8 His. This reversibility can be attributed to the presence of the proximal histidine and also to the nature of the globin. The protein provides a hydrophobic pocket which prevents autooxidation<sup>35,36</sup>



and also sterically hinders heme-heme contact to form the  $\mu$ -oxo dimer<sup>37,38</sup>



μ-oxo dimer

Hemoglobin is slowly oxidized to methemoglobin (metHb). The metHb is reduced by a reductase enzyme linked to the reduced form of nicotinamide adenine dinucleotide (NADH).<sup>39</sup> The rate of reduction is estimated to be 250 fold greater than the rate of oxidation.<sup>40</sup>

#### Hemoglobin Derivatives as Oxygen Carriers

Hemoglobin, free from stromal components, has been studied extensively as a blood substitute.<sup>10,41-44</sup> Pure hemoglobin solutions are rapidly eliminated from circulation by a renal route or through vascular walls with a  $t(1/2) = 85$  min.<sup>45</sup> Most of the current efforts involve chemical modification of the hemoglobin molecule. Hemoglobin has been crosslinked both inter- and intramolecularly, with many difunctional reagents and has shown improved vascular persistence ( $t(1/2) = 900$  min).<sup>46</sup> Hemoglobin has been covalently attached to modified detran and hydroxyethyl starch high polymers with an increase in circulating retention.<sup>47,48</sup> In the above cases, increase in vascular retention occurs concomitantly with an increase in the oxygen affinity of the bound hemoglobin rendering these solutions ineffective.

The connection of hemoglobin to a high polymer must be sufficiently

flexible to allow the cooperative conformational changes in the quaternary structure to occur. Hemoglobin which has been pyridoxylated with pyridoxal-5-phosphate before polymerization shows unaffected oxygen carrying capacity and some improvement in vascular retention.<sup>49</sup> Also polymers with a poly(vinyl pyrrolidone) linked hemoglobin<sup>50</sup> or an albumin linked hemoglobin<sup>51</sup> show promise as blood substitutes.

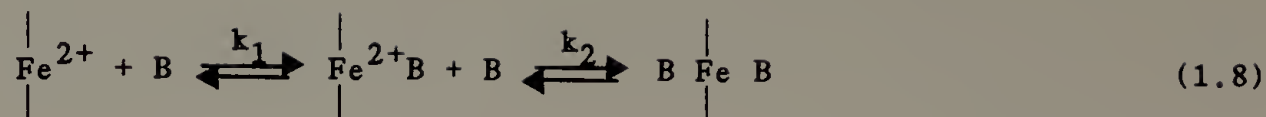
### Heme Derivatives as Hemoglobin Models

Excellent books concerning the physical and chemical behavior of iron porphyrins are available by Lever and Gray,<sup>52</sup> Smith,<sup>53</sup> Falk<sup>54</sup> and Dolphin.<sup>55</sup>

In contrast to the oxidative stability of hemoglobin, simple ferrous porphyrins are rapidly oxidized by oxygen via autooxidation (Equations 1.6A and B) or dimerization to form the  $\mu$ -oxo dimer (Equation 1.7). Hemoglobin is approximately  $10^8$  times more stable to iron oxidation than heme. The structure of a model compound which includes the heme moiety must somehow inhibit these oxidation reactions. The rate of dimerization may be lowered significantly by constructing a sterically hindered heme, by the use of low temperatures in experimental systems or by the attachment of a heme to a rigid surface.<sup>4</sup> A nonpolar or hydrophobic environment around a heme inhibits proton facilitated autooxidation.<sup>35</sup>

Another concern is that heme model compounds must have a five-coordinate structure. In the presence of strong nitrogen-donor ligands simple ferrous porphyrins have a preference for a six-coordinate

structure:

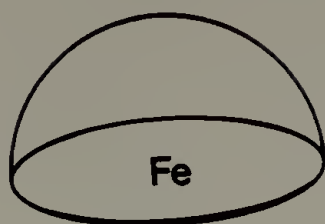


with  $k_2 > k_1$ . (For example, the binding constants of pyridine to Fe(II) tetraphenyl porphyrin have been found to be  $k_1 \simeq 1.5 \times 10^3 \text{ M}^{-1}$  and  $k_2 \simeq 1.9 \times 10^4 \text{ M}^{-1}$ ).<sup>56</sup> Nitrogen donor ligands as well as solvent molecules can effectively compete with oxygen binding at the sixth coordination site.<sup>57</sup>

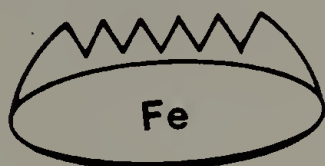
It has been shown that a Fe-Fe distance of  $4.4 \text{ \AA}$  is required for  $\mu$ -oxo dimer formation.<sup>58</sup> Several researchers have synthesized novel hemes bearing bulky groups on one face of the porphyrin to prevent dimerization in a solvent of a nitrogen donor base. 'Strapped' ferrous porphyrins have been synthesized which possess a difunctional moiety attached on opposite sides of the porphyrin to either the meso position<sup>59</sup> or to opposite pyrrole rings<sup>60,61</sup> (Figure 1.4A). In excess pyridine these compounds prefer a six-coordinate structure and have virtually no oxidative stability. Even in the case of a doubly strapped heme, formation of the  $\mu$ -oxo dimer has been observed.<sup>62</sup> In principle the strap provides a shearing strain to the ligand bound on the same side which promotes a five-coordinate deoxy structure. However, the affinity for gaseous oxygen or carbon monoxide decreases as the strap is tightened. Using this same principle, the oxidatively unstable 'crowned' heme has been synthesized by Chang<sup>63</sup> (Figure 1.4B). These 'strapped' and 'crowned' sterically hindered structures are not rigid

Figure 1.4. A schematic of the structure of novel heme derivatives.

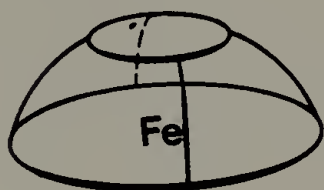
A) 'Strapped'



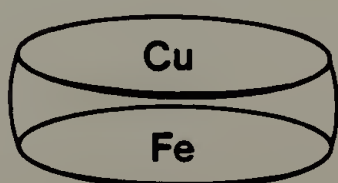
B) 'Crowned'



C) 'Capped'



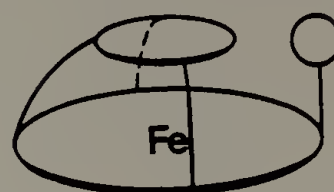
D) 'Cofacial diporphyrin'



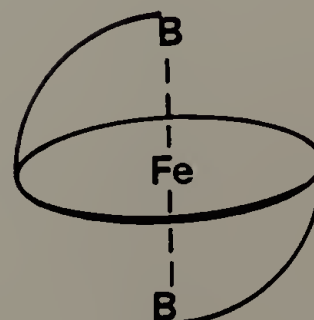
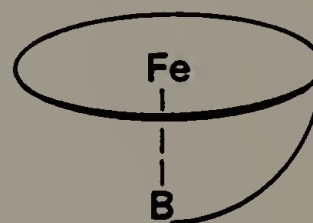
E) 'Picket fence'



F) 'Picket pocket'



G) 'Chelated'





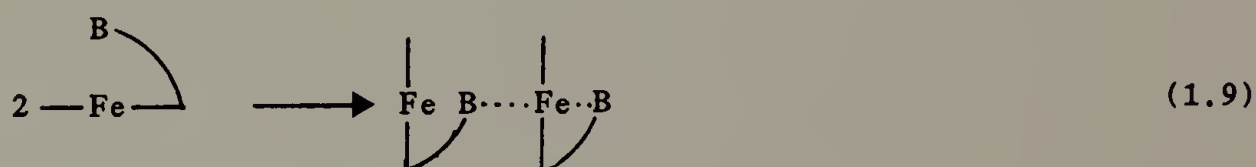
enough because they only have two arms for support. Baldwin et al.<sup>64</sup> designed a 'capped' heme which provides a cavity large enough for dioxygen binding without allowing a nitrogenous base to bind to the hindered side (Figure 1.4C). The oxygen and carbon dioxide affinities of the 'capped' models are lowered significantly. Oxidation was attributed to an equilibrium concentration of four-coordinate heme in solution. Chang and co-workers<sup>61</sup> have synthesized cofacial diporphyrins: one porphyrin contains an iron atom and the other an inert copper atom (Figure 1.4D). These complexes show no oxidation in benzene after twelve hours at room temperature.

The most stable sterically hindered models are Collman's 'picket fence' hemes and their subsequent derivatives<sup>65</sup> (Figure 1.4E). The 'picket fence' consists of four *o*-pivalamidophenyl groups attached at the meso positions on the porphyrin ring. These derivatives support reversible oxygenation in a wide variety of solvents at 25°C. Little oxidation is observed after 30 hours in dimethylformamide (DMF) solutions with 0.1 M  $\text{Et}_4\text{NCIO}_4$  suggesting that even high dielectric strength does not decrease the stability of the system. This system was further refined by the synthesis of a 'picket pocket' porphyrin<sup>66</sup> (Figure 1.4F) where a 'cap' is supported by three arms and a pivalamidophenyl group blocks the entrance to the pocket. In dry pure toluene with excess base (2-methylimidazole) these 'picket pocket' derivatives have a half life of 24 hours at 25°C.

The importance of the proximal and distal histidine in oxygen binding and oxidative stability was investigated by Traylor and co-

workers.<sup>67</sup> They synthesized a variety of hemes with either one or two imidazole groups bound covalently on an arm which would allow ligation of the base on the face of the iron porphyrin (Figure 1.4G). These 'chelated' hemes reversibly bind dioxygen but are rapidly oxidized at room temperature. Experiments were done at low temperature or with the very rapid flash photolysis and stopped-flow techniques. 'Chelated' hemes were synthesized which mimic the interaction of the histidines (F8 and E7) in both oxy- and deoxyhemoglobin.<sup>68</sup> This 'chelated' heme approach to provide the fifth ligand (the sixth being oxygen) and a high spin state has been used effectively by several other researchers.<sup>69</sup> Collman et al. have synthesized a 'tail-based picket fence' porphyrin as a model of the deoxy state of hemoglobin.<sup>70,71</sup>

Momenteau and coworkers<sup>72</sup> were the first to suggest that these five-coordinate heme models form dimers in solution,



which yield a four-coordinate and six-coordinate species. Collman<sup>71</sup> has further demonstrated that dimerization is favored by low temperatures and high concentrations of hemes. (At a concentration of approximately 1 mM and -25°C the 'tail-based picket fence' porphyrin is more than 50% dimerized). Traylor<sup>73</sup> argued against the dimerization in solution on the basis of <sup>1</sup>H-NMR chemical shifts. The model hemes discussed above have demonstrated both environmental as well as steric effects on

reversible oxygenation.

### Polymer Based Models of Hemoglobin

In hemoglobin the globin protects the heme from oxidation. One might suspect that a synthetic polymer might inhibit autooxidation as well as dimerization by providing a hydrophobic environment and shielding hemes from one another.

Simple hemes embedded in a solid matrix have shown greatly enhanced stability toward oxidation. In a seminal experiment, Wang<sup>74</sup> showed that heme diethylester surrounded by a matrix of amorphous poly(styrene) and 1-(2-phenylethyl)imidazole was stable for several days. Leal et al.<sup>75</sup> covalently linked ferrous tetraphenylporphyrin to a rigid silica gel support which inhibited autooxidation and provided a stable oxygen carrier. Collman and coworkers<sup>76</sup> synthesized copolymers of styrene and vinylimidazole that allowed reversible oxygenation of metalloporphyrins coordinated to the polymer in the solid state. The rate of oxygenation and ligand exchange reactions in these models depends on the gas permeability of the polymer matrix, which is significantly slower than in a homogeneous solution.<sup>77</sup>

As a result of the great oxidative stability of hemes embedded in synthetic polymers there has been considerable interest in the synthesis of a polymer bound metalloporphyrin which could form a stable oxygenated complex in homogeneous solution.<sup>78</sup> A polymer molecule generally has a random coiled conformation in solution where parts of the polymer may be shielded from others. Also the polymer chain might provide a

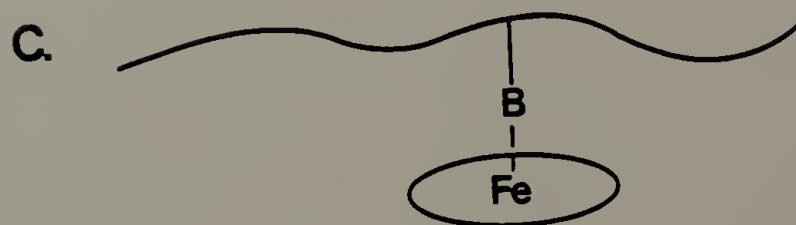
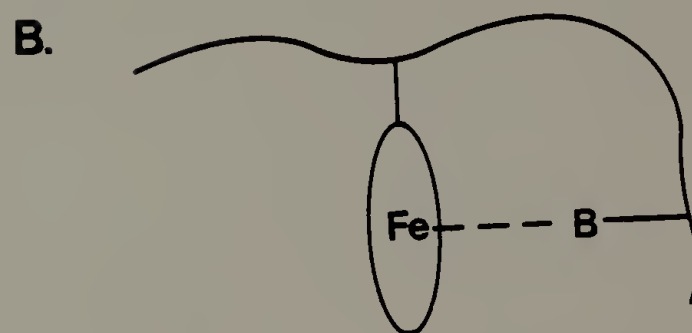
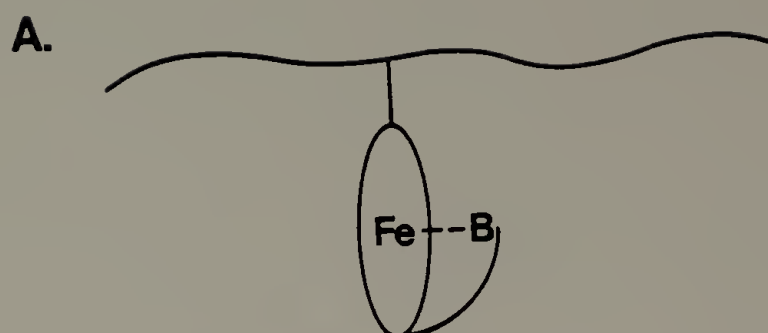
hydrophobic environment which would inhibit autooxidation. The attachment of a ferrous porphyrin to a polymer chain can be imagined in three ways: covalent attachment of the heme with an appended axial base, covalent attachment of the heme as well as the axial base to the polymer chain, or covalent bonding of the axial base followed by simple coordination of the heme group (Figure 1.5).

The first polymer bound heme to reversibly bind oxygen in solution was a heme complexed to poly(L-lysine) synthesized by Tsuchida and coworkers.<sup>79</sup> They reported reversible oxygenation with sigmoidal (cooperative) oxygen absorption which was attributed to the helical, rigid conformation of poly(L-lysine). Other polymeric ligands such as poly(4-vinylpyridine) showed no cooperativity. Soon after this work was published, Bayer and Holzbach<sup>80</sup> reported the synthesis of poly(ethylene oxide) containing a covalently bound histidylheme which reversibly oxygenated in aqueous media at room temperature. Tsuchida<sup>81</sup> could not repeat the results of the experiments of Bayer and Holzbach.

In 1977, Fuhrhop and coworkers<sup>82</sup> reported the synthesis of a terpolymer of styrene, 1-vinylimidazole and ferrous protoporphyrin IX dimethylester which was stable for weeks in the solid state but irreversibly oxidized after a few minutes in benzene at room temperature. Fuhrhop also suggested that the stability reported by Tsuchida was probably due to an excess of reducing agent (sodium hydrosulfite). Allcock et al.<sup>83</sup> reported that ferrous protoporphyrin IX complexed to water soluble poly(phosphazenes) failed to reversibly bind oxygen in the solid state.

Figure 1.5. Methods to attach heme groups to polymers.

- A. Covalent attachment of the heme with appended axial base
- B. Covalent attachment of heme and axial base to the polymer chain
- C. Coordination of a heme group to a covalently bound axial base.





Tsuchida and coworkers have been quite persistent in the pursuit of a polymer bound heme as a model of hemoglobin. Until 1982 they had synthesized a wide variety of polymeric hemes with no noteworthy success.<sup>84-87</sup> Recently they have reported the reversible oxygenation of ferrous protoporphyrin IX coordinated to poly(1-vinyl-2-methylimidazole) (PMI) in organic solvents containing 10 volume % water at  $-30^{\circ}\text{C}$ .<sup>88</sup> First-order kinetics were observed for the irreversible oxidation of the oxygenated species. Heme coordinated to copolymers of PMI-co-N,N-dimethylacrylamide and PMI-co-1-vinyl-2-pyrrolidone reversibly oxygenates in  $\text{H}_2\text{O}$ /ethylene glycol (1/1) at  $-30^{\circ}\text{C}$  ( $t(1/2) = 60$  min.) but hemes coordinated to ionic copolymers, PMI-co-methacrylic acid and PMI-co-1-vinyl-2-methyl-3-benzylimidazolium chloride, oxidize immediately. Tsuchida et al.<sup>89</sup> studied the physical properties of the PMI-heme complexes and concluded that these hemes are predominantly five-coordinate in solution. Viscometric studies in  $\text{H}_2\text{O}$ /ethylene glycol demonstrate that the heme-polymer complex has a compact shape which indicates a hydrophobic interaction of heme with the polymer ligand. Also Tsuchida<sup>81</sup> reported that poly(1-vinylpyrrolidone) with covalently bound mono-N-[3-(imidazol-1-yl)propyl amide or mono-N-[5-(2-methylimidazol-1-yl)pentyl amide reversibly oxygenates in  $\text{H}_2\text{O}$ /ethylene glycol at  $-30^{\circ}\text{C}$  with a half-life of one hour. Non-polymer bound heme analogs do not oxygenate under the same conditions. Tsuchida and coworkers most recent work involved incorporation of a heme group into liposomes<sup>90,91</sup> and heme complexation by cyclodextrin bound imidazole groups.<sup>92</sup> Both of these approaches seem hopeful. Tsuchida's research demonstrates the



promising possibilities for polymer bound hemes as oxygen carriers in solution.

### Research Strategy

The basic objective of this dissertation is the synthesis of a vinyl polymer which possesses some of the functions of hemoglobin. The model polymer should be water soluble and contain a five-coordinate heme group to carry oxygen as a function of the partial pressure dissolved in solution. In order to protect the heme from dimerization and subsequent oxidation, the concentration must be limited to less than one heme per polymer chain of a molecular weight of approximately 20,000, and the structure must be made rigid by intramolecular crosslinking.

Intramolecular crosslinking might limit the chain conformation and thus the possibility of heme-heme contact.<sup>82</sup> Intramolecular crosslinking in solution is favored by low polymer concentrations and moderate to high molecular weights as shown by Aharoni.<sup>93</sup> Approximately four crosslinks per polymer chain resulted in a reduction of the solution viscosity and a contraction of the polymer molecule. Aharoni's experiments demonstrate the methods required to obtain intramolecular crosslinking. More current work by Martin and Eichinger<sup>94,95</sup> gave a mathematical treatment of intramolecular crosslinking theory and the dimensions of these polymers were characterized by photon correlation spectroscopy.

The heme moiety must be dissolved in the hydrophobic domain of the polymer to inhibit autooxidation.<sup>78,89</sup> Polyelectrolytes with a very high hydrophobic content are known to form a tightly coiled structure in

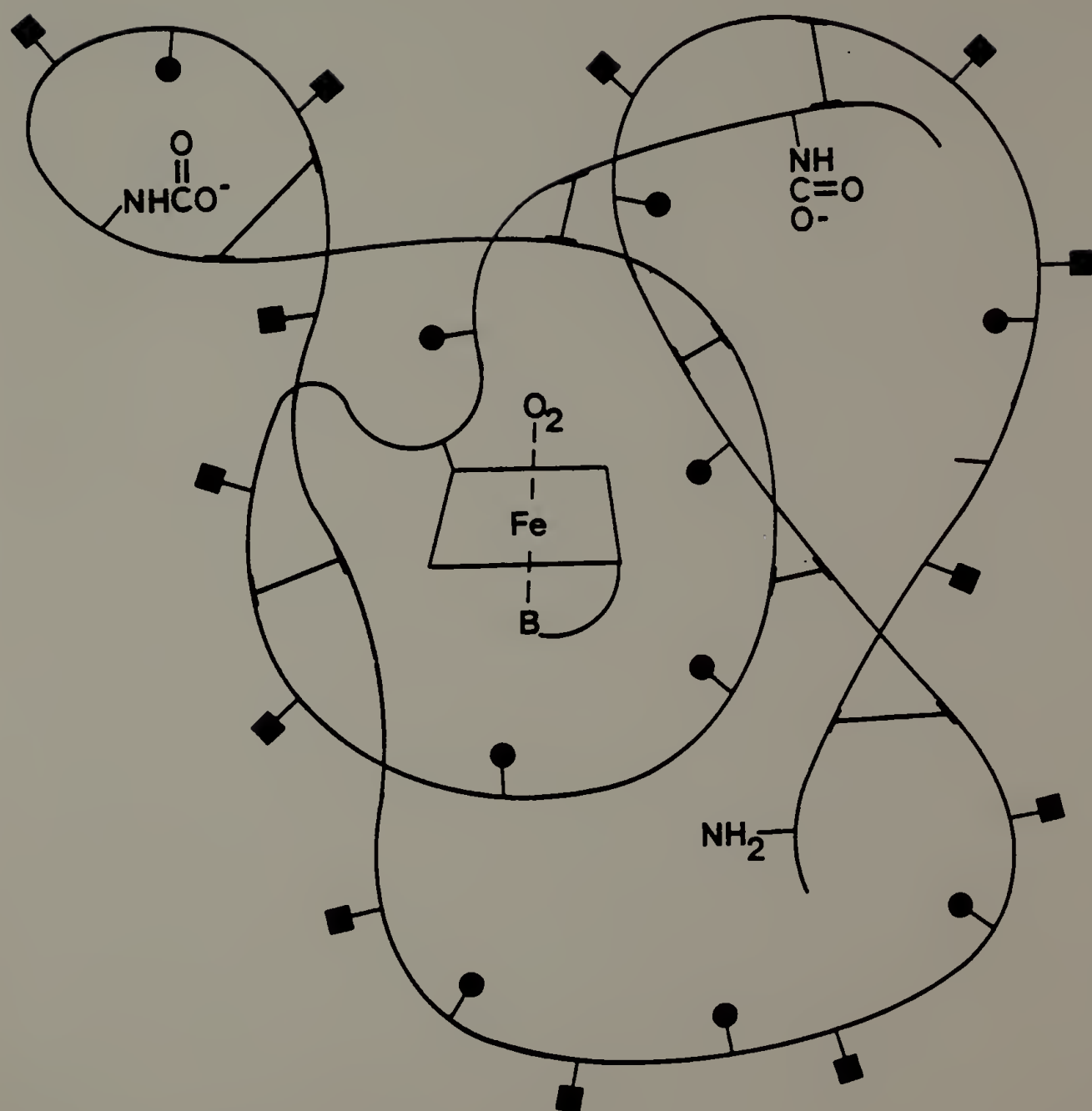
aqueous solution with both ionic repulsion and van der Waals forces being quite important in determining their conformation.<sup>96-99</sup> These polymers have soap-like properties and are capable of solubilizing water insoluble substances<sup>100</sup> which makes them promising carriers for hemes.

To model the capacity of hemoglobin to actively transport carbon dioxide one must include an amine functionality, with a  $pK_a$  of 7.4 or less which can react to form a carbamate. Hydrophobic domains in the hemoprotein lower the  $pK_a$  of the N-terminal valines.<sup>32</sup> Hydrophobic polymerizable amines are thought likely to be found in the hydrophobic domains of the model polymer and thus have lowered  $pK_a$  values.

By combining the above considerations one can envision the final model polymer (Figure 1.6). The polymer would be in a very compact state (near the theta dimension) with the water solubilizing groups exposed to the aqueous environment and with hydrophobic domains formed by aggregation of the hydrophobic elements. Both the five-coordinate heme group and the lipophilic amines would be solvated by these domains. When the polymer system is in the proper conformation, a copolymerized crosslinking agent could be activated to help limit mobility of the model structure.

Figure 1.6. A schematic of a heme-containing polymer which can mimic the functions of hemoglobin: (—) the polymer backbone; (●) water solubilizing group, (■) hydrophobic group, ( $\text{-NHCO}_2^-$ ) carbamate and (|—|) intramolecular crosslinking.

- ionic  
● hydrophobic  
—|— crosslink



### References

1. Dickerson, R.E.; Geis, I. Hemoglobin: Structure and Function, Evolution and Pathology, Benjamin/Cummings Pub. Co., Inc., Menlo Park, CA (1983).
2. Geyer, R.P. Fed. Proc., (1975), 34(6), 1525.
3. Baldwin, J.E.; Gill, B. Med. Lab. Sci., (1982), 39, 45.
4. Jones, R.D.; Summerville, D.A.; Basolo, F. Chem. Rev., (1979), 79(2), 139.
5. Clark, L.C.; Golland, F. Science, (1966), 152, 1755.
6. Yokoyama, K.; Yamanouchi, K.; Wantanabe, M.; Matsumoto, T.; Murashima, R.; Diamato, T.; Hamano, T.; Okamoto, H.; Suyama, T.; Wantanabe, R. Fed. Proc., (1975), 34, 1478.
7. Yokoyama, K.; Yamanouchi, K.; Ohyanagi, H.; Mitsuno, T. Chem. Pharm. Bull., (1978), 26, 956.
8. Long, D. Pathophysiology and Techniques Cardiopulmonary Bypass Vol. I, Utley, J.R., (ed.), Williams and Wilkins, Baltimore, (1982), pp. 12-23.
9. Clark, L. Pathophysiology of Shock, Anoxia and Ischemia, Cowley, R.A.; Trump, B.F., (eds.), Williams and Wilkins, Baltimore, (1982), pp. 507-522.
10. Geyer, R.P. (Chairman), Fed. Proc., (1975), 34, 1428-1530.
11. Riess, J.G.; LeBlanc, M. Pure Appl. Chem., (1982), 54(12), 2383.
12. Long, D.M.; Multer, F.K.; Greenburg, A.G.; Peskin, G.W.; Lasser, E.C.; Wickham, W.G.; Short, C.M. Surgery, (1978), 84, 104.
13. Antonini, E.; Brunori, M. Hemoglobin and Myoglobin in Their Reactions with Ligands, North Holland Pub. Co., Amsterdam, (1971).

14. Perutz, M.F. Annu. Rev. Biochem., (1979), 48, 327; Perutz, M.F. Scientific American, (1978), 239(6), 92.
15. Baldwin, J.M. Prog. Biophys. Mol. Biol., (1975), 29(3), 225.
16. Ho, Chien (ed.) Hemoglobin and Oxygen Binding, Elsevier, New York, (1982).
17. Perutz, M.F. Proc. Roy. Soc., (1969), B173, 113.
18. Lehninger, A.L. Biochemistry 2nd ed., Worth Pub., Inc., (1975).
19. Thompson, E.O.P. The Evaluation of Protein Sequence and Function, Sigman, D.S.; Brazier, M.B. (eds.), Academic Press, New York, (1980), p. 267.
20. Perutz, M.F. Nature, (1951), 167, 1053.
21. Perutz, M.F. Eur. J. Biochem., (1969), 8, 453.
22. Monod, J.; Wyman, J.; Changeux, J.P. J. Mol. Biol., (1965), 12, 88.
23. MacQuarrie, R.; Gibson, Q.H. J. Biol. Chem., (1972), 247, 5686.
24. Gelin, B.R.; Karplus, M. Proc. Natl. Acad. Sci. USA, (1977), 74, 801.
25. Perutz, M.F. Nature, (1970), 228, 726.
26. Imai, K.; Adair, G.S. Biochem. Biophys. Acta, (1970), 490, 456.
27. Kilmartin, J.V. Ann. N.Y. Acad. Sci., (1974), 241, 465.
28. Roughton, F.J.W. Handbook of Physiology, Section 3: Respiration, Fenn, W.O.; Rahn, W. (eds.), American Physiological Society, Washington, Vol. 1, 767.
29. O'Donnell, S.; Mandaro, R.; Schuster, T.M.; Arnone, A. J. Biol. Chem., (1979), 254, 12, 204.



30. Arnone, A. Nature, (1972), 237, 146; Arnone, A.; Perutz, M.F. Nature, (1974), 249, 34.
31. Kilmartin, J.V.; Rossi-Bernardi, L. Biochem. J., (1971), 124, 31.
32. Gurd, F.R.N.; Matthew, J.B.; Wittebort, R.J.; Morrow, J.S. Biophysics and Physiology of CO<sub>2</sub>, Bauer, C.; Gros, G.; Bartels, H. (eds.), Springer-Verlag, New York, (1980), 89.
33. Garner, M.H.; Bogardt, R.A. Jr.; Gurd, F.R.N. J. Biol. Chem., (1975), 250, 2398.
34. Weast, R.C. ed. CRC Handbook of Chemistry and Physics 56th, CRC Press, Cleveland, (1975), p. D149.
35. Wallace, W.J.; Caughey, W.S. Biochemical and Clinical Aspects of Oxygen, Academic Press, New York, (1979), 69.
36. Brunori, M.; Falcioni, G.; Fioretti, E.; Giordina, B.; Ratillo, E. Eur. J. Biochem., (1975), 53, 99.
37. Cohen, I.A.; Caughey, W.S. Biochemistry, (1968), 7, 636.
38. Hammod, C.J.; Wu, C.S. Adv. Chem. Ser., (1968), 77, 186.
39. Hsieh, H.-S.; Jaffe, E.R. The Red Blood Cell 2nd Ed., Surgenor, D.M. (ed.), Academic Press, New York, (1975), p. 799.
40. Scott, E.M. Hereditary Disorders of Erythrocyte Metabolism, Beutler, E. (ed.), Grune and Stratton, New York, (1968), p. 102.
41. DeVenuto, F. Vox. Sang., (1983), 44(3), 129.
42. DeVenuto, F.; Moores, W.Y.; Zegna, A.I.; Zuck, T.F. Transfusion, (1977), 17, 55
43. DeVenuto, F.; Zuck, T.F.; Zegna, A.I. Surg. Gynecol. Obstet., (1979), 148, 69.



44. Birndorf, N.I.; Lopas, H. J. Appl. Physiol., (1970), 29, 573.
45. Friedman, H.I.; DeVenuto, F.; Zuck, T.F.; Mellich, P.; Lollini, L. Surg. Form., (1977), 28, 3.
46. Mok, W.; Chen, D.E.; Mazur, A. Fed. Proc., (1975), 34, 1458.
47. Baldwin, J.E.; Gill, B.; Whitten, J.P.; Taegtmeyer, M. Tetrahedron, (1981), 37, 1723.
48. Cerny, L.C.; Stasiw, D.M.; Cerny, E.L.; Baldwin, J.E.; Gill, B. Clinical Hemorheology, (1982), 2, 355.
49. Sehgal, L.R.; Rosen, A.L.; Gould, S.A.; Sehgal, H.; Dalton, L.; Mayoral, J.; Moss, G. Fed. Proc., (1980), 39, 718.
50. Schmidt, K. Klin. Wochenschr., (1979), 1169.
51. Labrude, P.; Bonneaux, F.; Dellacherie, E.; Neel, J.; Vignerum, C. Ann. Pharm. Fr., (1979), 37, 291.
52. Lever, A.B.P.; Gray, H.B. (eds.) Physical Bioinorganic Chemistry Series (Iron Porphyrins, Part I and II), Addison-Wesley Pub. Co., Reading, MA, (1983).
53. Smith, K.M. Porphyrins and Metalloporphyrins, Elsevier Pub. Co., New York, (1975).
54. Falk, J.E. Porphyrins and Metalloporphyrins, Elsevier Pub. Co., New York, (1964).
55. Dolphin, D. (ed.) The Porphyrins, Academic Press, New York, 1978.
56. Brault, D.; Rougee, M. Biochemistry, (1974), 13, 4591.
57. Traylor, T.G.; Chang, C.K.; Geibel, J.; Berzinis, A.; Mincey, T.; Cannon, J. J. Am. Chem. Soc., (1979), 101, 6716.
58. Fleischer, E.B.; Srivastawa, T.S. J. Am. Chem. Soc., (1969), 91, 2403.

59. For a review: Baldwin, J.E.; Crossley, M.J.; Keese, T.; O'Rear (III), E.A.; Peters, M.K. Tetrahedron, (1982), 38(1), 27.
60. Traylor, T.G.; Mitchell, M.J.; Tsuchiya, S.; Campbell, D.H.; Styne, D.V.; Koga, N. J. Am. Chem. Soc., (1981), 103, 5235.
61. Ward, B.; Wang, C.B.; Chang, C.K. J. Am. Chem. Soc., (1981), 103, 5236.
62. Cruse, W.B.; Kennard, O.; Sheldrick, G.M.; Hamilton, A.D.; Hartley, S.G.; Battersby, A.R. J. Chem. Soc. Chem. Commun., (1980), 700.
63. Chang, C.K. J. Am. Chem. Soc., (1977), 99, 2819.
64. Almog, J.; Baldwin, J.E.; Crossley, M.; Debernardis, J.F.; Dyer, R.L.; Huff, J.R.; Peters, M.K. Tetrahedron, (1981), 37(21), 3589.
65. Collman, J.P.; Gagne, R.R.; Reed, C.A.; Halbert, T.R.; Lang, G.; Robinson, W.T. J. Am. Chem. Soc., (1975), 97, 1427.
66. Collman, J.P.; Brauman, J.I.; Collins, T.J.; Iverson, B.; Sessler, J.L. J. Am. Chem. Soc., (1981), 103(9), 2450.
67. For a review: Traylor, T.G. Acc. Chem. Res., (1981), 14, 102.
68. Geibel, J.; Cannon, J.; Campbell, D.; Traylor, T.G. J. Am. Chem. Soc., (1978), 100(11), 3575.
69. Tsuchida, E.; Nishide, H.; Sato, Y.; Kaneda, M. Bull. Chem. Soc. Jpn., (1982), 55, 1890.
70. Collman, J.P.; Brauman, J.I.; Doxsee, K.M.; Halbert, T.R. Proc. Natl. Acad. Sci., (1978), 75(2), 564.

71. Collman, J.P.; Brauman, J.I.; Doxsee, K.M; Halbert, T.R.;  
Bunnenburg, E.; Linder, R.E.; Lamar, G.N.; Del Gaudio, J.; Lang,  
G.; Spartalian, K. J. Am. Chem. Soc., (1980), 102(12), 4182.
72. Momenteau, M.; Rougee, M.; Loock, B. Eur. J. Biochem., (1976),  
71, 63.
73. Traylor, T.G.; Chang, C.K.; Geibel, J.; Berzinis, A.; Mincey,  
T.; Cannon, J. J. Am. Chem. Soc., (1979), 101(22), 6716.
74. Wang, J.H. Acc. Chem. Res., (1970), 3, 90.
75. Leal, O.; Anderson, D.L.; Bowman, R.G.; Basolo, F.; Birwell,  
Jr., R.L. J. Am. Chem. Soc., (1975), 97, 5125.
76. Collman, J.P.; Gagne, R.K.; Kouba, J.; Wahren, H.L. J. Am. Chem.  
Soc., (1974), 96, 6800.
77. Tsuchida, E.; Honda, K.; Hata, S. Bull. Chem. Soc. Jpn., (1976),  
49, 868.
78. For a review: Tsuchida, E. J. Macromol. Sci.-Chem., (1979),  
A(13)4, 545.
79. Tsuchida, E.; Hasegawa, E.; Kenji, H. Biochem. Biophys. Res.  
Commun., (1975), 67(3), 864.
80. Bayer, E.; Holzbach, G. Angew. Chem. Int. Ed. Engl., (1977),  
16(2), 117.
81. Tsuchida, E.; Nishide, H.; Sato, Y. J. Chem. Soc. Chem Commun.,  
(1982), 556.
82. Fuhrhop, J.-H.; Beseche, S.; Vogt, W.; Ernst, J.; Subramanian,  
J. Makromol. Chem., (1977), 178, 1621.
83. Allcock, H.R.; Greigger, P.A.; Gardner, J.E.; Schmutz, J.L. J.  
Am. Chem. Soc., (1979), 101(3), 606.

84. Hasegawa, E.; Kanayama, T.; Tsuchida, E. J. Polym. Sci.-Polym. Chem. Ed., (1977), 15, 3039.
85. Hasegawa, E.; Nemoto, J.-I.; Kanayama, T.; Tsuchida, E. Eur. Polym. J., (1978), 14, 123.
86. Tsuchida, E.; Hasegawa, E.; Kanayama, T. Macromolecules, (1978), 11(5), 947.
87. Nishide, H.; Shinohara, K.; Tsuchida, E. J. Polym. Sci.-Polym. Chem. Ed., (1981), 19, 1109.
88. Nishide, H.; Sekine, M.; Tsuchida, E. Polymer Journal, (1982), 14(8), 629.
89. Tsuchida, E.; Nishide, H.; Ohno, H. J. Inorg. Biochem., (1982), 17, 283.
90. Hasegawa, E.; Matsushita, Y.; Kaneda, M.; Ejima, K.; Tsuchida, E. Biochem. Biophys. Res. Commun., (1982), 105(4), 1416.
91. Tsuchida, E.; Nishide, H.; Sekine, M.; Yuasa, M.; Tetsutaro, I.; Ishimura, Y. Biochem. Biophys. Res. Commun., (1982), 109(3), 858.
92. Eshima, K.; Matsushita, Y.; Sekine, M.; Nishide, H.; Tsuchida, E. Nippon Kagaku Kaishi, (1983), 2, 214.
93. Aharoni, S.M. Angew. Makromol. Chem., (1977), 62, 115.
94. Martin, J.E.; Eichinger, B.E. Macromolecules, (1983), 16, 1345.
95. Martin, J.E.; Eichinger, B.E. Ibid., p. 1350.
96. Dubin, P.L.; Strauss, U.P. J. Phys. Chem., (1970), 74, 2842.
97. Dubin, P.L., Strauss, U.P. Polyelectrolytes and Their Applications; Rembaum, A; Selegny, E. (ed.), D. Reidel Pub. Co., Dordrecht, (1975), p. 3.

98. Muller, G.; Fenyo, J.-C.; Braud, C.; Selegny, E. Ibid., p. 15.
99. Wessling, R.A.; Pickelman, D.M. J. Dispersion Sci. Tech., (1981),  
2, 281.
100. Ito, K.; Ono, H.; Yamashita, Y. J. Colloid Sci., (1964), 19, 28.

## CHAPTER II

### MONOMER SYNTHESIS

The selection of monomers suitable for incorporation into a model of hemoglobin is complex. By classifying the monomer properties into five categories: hydrophobic, water solubilizing, heme, crosslinking agents and amines, one can choose promising monomer candidates as well as estimate the desired composition. All the monomers must have the same polymerizable group, a vinyl substituent, of relatively equal reactivity to ensure random placement in the polymer. Monomers must be soluble in the same solvent so that polymerization will be homogeneous. The most important requirement is that monomer units must not interact (e.g. ionic attraction or repulsion) with one another during polymerization, during subsequent chemical modification of the polymer, or in the final polymer model.

#### Experimental Procedure

The sources of chemicals used in synthesis are given below. Code: Aldrich (A), BioRad (B), a gift from duPont (D), a gift from Dow (DW), Eastman (E), Fisher (F), a gift from W.R. Grace (G), Polysciences (P), Sigma (S).

acrylonitrile	A
p-aminoacetophenone	A
2-aminoethyl methacrylate	DW
p-aminophenol	A,F



p-aminostyrene	P
Biobeads SX2	B
BOC-ON	A
2-bromoethylbenzene	A
chlorosulfonic acid	A,E
18-crown-6	A
decanol	A
dicyclohexylcarbodiimide	A
ethylbromide	A
hemin	S
1,6-hexanediamine	A
hexanol	A
2-hydroxyethyl methacrylate	A
imidazole	A
methacryloyl chloride	A
phosphorus pentachloride	A
potassium- <u>tert</u> -butoxide	A
Raney nickel #28	G
60-200 silica gel	F
sodium borohydride,	F
sodium methoxide	A
25% sodium methoxide	A
sodium styrenesulfonate	D
styrene	A
thin layer chromatography plates	E



thionyl chloride	A
p-toluenesulfonylchloride	A
triethylamine	A
trimethylchloride	A
4-vinylpyridine	A

### Purification

Chemicals were used as received unless specified below. Water was distilled and deionized. Methanol was refluxed over magnesium turnings, distilled under nitrogen and stored over molecular sieves.

Acrylonitrile was distilled under a nitrogen atmosphere and used immediately. Imidazole was recrystallized from ethanol. Pyridine and triethylamine were refluxed over potassium hydroxide for one hour, distilled under nitrogen and stored over 3 Å molecular sieves. 2-Aminoethyl methacrylate was a 35% aqueous solution as received from Dow. The water was removed in vacuo immediately before use and the white crystals in yellow slush were rinsed with acetonitrile until pure white and then dried in vacuo.

### Instrumentation

Melting points were measured with a Mel-temp (Laboratory Devices). Infrared spectra were obtained with a Perkin-Elmer 283. A Varian T-60 was used for the  $^1\text{H}$ -NMR and a CFT-20 for the  $^{13}\text{C}$ -NMR.

### Monomer Synthesis

p-(2-Bromoethyl)benzenesulfonylchloride. In a 1000 ml three neck round bottom flask, fitted with a thermometer and pressure equalizing

funnel, 1.0 Kg (8.58 mol) of chlorosulfonic acid was cooled to 5°C via an ice bath. 2-Bromoethylbenzene (151 ml, 1.11 mol) was added dropwise to maintain the temperature below 10°C. The mixture was stirred for an additional 4 hr and became a golden-amber color. The reaction mixture was transferred to a 1000 ml separatory funnel and slowly dripped into a 4 l beaker filled with ice to destroy excess chlorosulfonic acid. The whitish oily sulfonylchloride separated from solution and was allowed to stand overnight. Water was decanted off and the acid chloride was rinsed with water a second time. The acid chloride was dissolved in a sufficient quantity of diethyl ether to render it less dense than water and the water removed. The ether layer was dried over  $\text{MgSO}_4$  and the volume reduced in vacuo. Pure 2-bromoethylbenzenesulfonylchloride was crystallized from the ether solution at a lowered temperature to give a 66.4% yield (205 g, 0.790 mol) and was used without further purification.

Methyl p-(2-bromoethyl)benzenesulfonate. The sulfonylchloride (205 g, 0.790 mol) was redissolved in a minimum volume of anhydrous methanol (~ 1000 ml) and cooled to 5°C. Sodium methoxide (39.04 g, 0.708 mol) was added slowly with stirring keeping the temperature below 10°C. (Alternatively, a pre-prepared 25% solution of sodium methoxide in methanol was used.) After two hours, 400 ml of distilled water was added and the mixture was extracted with ether. Additional water was required to break emulsions which formed. The ether layer was dried over magnesium sulfate and filtered. The volume of ether was reduced and crystals of methyl p-(2-bromoethyl)benzenesulfonate were frozen out

of solution to give a yield of 93.0 g (0.33 mole, 47%). This compound was stored in the dark at 7°C and was stable for several months.  $^1\text{H-NMR}$  ( $\text{CDCl}_3$ ):  $\delta = 3.05 - 3.6$  ppm (m, 4H),  $\delta = 3.71$  ppm (s, 3H),  $\delta = 7.52$  ppm (d, 2H),  $\delta = 7.90$  ppm (d, 2H). (Appendix A.1).

Methyl p-vinylbenzenesulfonate. Methyl p-(2-bromo-ethyl)benzenesulfonate (10.0 g, 0.036 mol) was dissolved in 125 ml of anhydrous diethyl ether and 6.03 g (0.054 mol) of potassium tert-butoxide was added very slowly with stirring. The reaction was exothermic and a pink color noted. (In some experiments, when the ether was quite fresh, catalytic amounts of 18-crown-6 were added to start the reaction.) After 15 min the reaction was quenched with 125 ml of water. The ether layer was extracted with three 75 ml portions of water and dried over  $\text{MgSO}_4$ . The ether was removed in vacuo to yield 4.19 g (59.1%) of a yellow, cloudy oil. Polymeric impurities were removed on a Biobeads SX2 column in methylene chloride with a plug of 60-200 mesh silica gel at the top to remove polar impurities. Clear, colorless methyl p-vinylbenzenesulfonate was judged pure by the integration of the  $^1\text{H-NMR}$  spectrum.<sup>1</sup>  $^1\text{H-NMR}$  ( $\text{CDCl}_3$ ):  $\delta = 3.71$  ppm (s, 3H); vinyl ABX pattern;  $\delta_A = 5.37$  ppm (d, 1H),  $\delta_B = 5.81$  ppm (d, 1H),  $\delta_X = 6.70$  ppm (q, 1H);  $\delta = 7.50$  ppm (d, 2H);  $\delta = 7.85$  ppm (d, 2H); (Appendix A.2). Infrared spectrum (neat):  $1365, 1280\text{ cm}^{-1}$  ( $\text{RSO}_3\text{CH}_3$ ),  $1600\text{ cm}^{-1}$  (C=C stretch) (Appendix A.3). For  $^{13}\text{C-NMR}$  see Appendix A.4.

Analysis. Calculated for  $\text{C}_9\text{H}_{10}\text{SO}_3$  (198.24): C, 54.5; H, 5.1. Found: C, 55.2; H, 5.2.

p-Vinylbenzenesulfonylchloride. In a flame dried 500 ml round

bottom flask, 20.8 g (0.10 mol) of phosphorus pentachloride was cooled by an external ice bath and 17.32 g of sodium p-vinylbenzenesulfonate (0.084 mol) was added over a period of fifteen minutes. The mixture of solids was stirred mechanically and became a brownish, viscous liquid. The mixture was warmed slowly to room temperature and then heated gently on an oil bath to reflux at approximately 50°C for two hours. The reaction was cooled and then poured onto crushed ice to destroy unreacted  $\text{PCl}_5$ . The acid chloride was removed from the water slurry via ether extraction. The ether layer was thoroughly washed with distilled water, dried over  $\text{MgSO}_4$  and the ether removed in vacuo to yield 13.17 g (65%) of p-vinylbenzenesulfonylchloride. The acid chloride was converted to the methylester following the exact procedure used for p-(2-bromoethyl)benzenesulfonylchloride and had the same properties as methyl p-vinylbenzenesulfonate synthesized by dehydrobromination.

N-Ethyl-p-vinylpyridinium bromide. In a 500 ml round bottom flask, 100 ml of carbon tetrachloride, 20.5 ml of 4-vinylpyridine (0.19 mol) and 56 ml of bromoethane (0.75 mol) were combined and a pinkish powder precipitated from solution within minutes. The reaction was stirred at 40°C for 48 hr. The product was filtered, dried in vacuo and was quite hygroscopic.  $^1\text{H}$ -NMR of the product had no vinyl protons and had very broad resonances which corresponded to those of ethylpyridinium bromide (Sadtlir 21906 M):  $\delta = 1.5, 2.0, 4.4, 7.5$  and  $8.45$  ppm.

Ferric protoporphyrin IX dimethylester. Absolute distilled methanol (475 ml) was mixed with 25 ml of concentrated sulfuric acid in a one liter Erlenmeyer flask and allowed to cool. Hemin (0.50 g,  $7.67 \times 10^{-4}$



mol) was added but didn't dissolve. The mixture was stirred for 24 hr at  $-20^{\circ}\text{C}$  in the dark after which most of the hemin had dissolved. The reaction mixture was added to a 2 l separatory funnel with 200 ml of chloroform. Water was added until two immiscible layers formed (~ 400 ml). The chloroform layer was washed with 5 volumes of water, dried over  $\text{MgSO}_4$ , then removed in vacuo. The yield of hemin dimethylester was quantitative and moved with one spot purity by thin-layer chromatography (TLC) with an  $R_f$  of 0.83 in 9/1  $\text{CHCl}_3/\text{MeOH}$ . Infrared (KBr): 1735, 1435  $\text{cm}^{-1}$  (ester carbonyl), (Appendix A.5).

Analysis. Calculated for  $\text{C}_{36}\text{H}_{36}\text{N}_4\text{O}_4\text{FeCl}$  (679.79): C, 63.54; H, 5.29; N, 8.23; Fe, 8.20. Found: C, 63.32; H, 5.11; N, 8.20; Fe, 7.5.<sup>2</sup>

3-(1-Imidazolyl)propylamine. Acrylonitrile (25.0 ml, 0.38 mol) was refluxed under nitrogen to exclude oxygen in a 100 ml round bottom flask equipped with a magnetic stirrer. Imidazole (13.6 g, 0.20 mol) was added incrementally while the reflux temperature increased. After 6 hr of gentle reflux the unreacted acrylonitrile was removed in vacuo overnight. The remaining oil was mixed with 100 ml methanol and filtered to remove a faint cloudiness (presumably polyacrylonitrile).

The filtrate was mixed with 50 ml of methanol, 100 ml of concentrated ammonium hydroxide, and 8.0 g (wet weight) of Raney nickel. Hydrogenation was carried out at 45 p.s.i. for 3 hr and the loss was  $2\text{H}_2/\text{mol CN}$ . The catalyst was removed by filtration and the filtrate evaporated to dryness. The residual oil was distilled in vacuo at  $125^{\circ}\text{C}$  and stored under nitrogen.  $^1\text{H-NMR}$  ( $\text{CDCl}_3$ ):  $\delta = 1.85$  ppm (q, 2H),  $\delta =$

2.6 ppm (t, 2H),  $\delta$  = 4.0 ppm (t, 2H),  $\delta$  = 6.95 ppm (s, 1H),  $\delta$  = 7.03 ppm (s, 1H),  $\delta$  = 7.49 ppm (s, 1H), (Appendix A.6). Infrared spectrum see Appendix A.7.

Ferric protoporphyrin IX di-3-(1-imidazolyl)propylamide. Hemin (0.5 g,  $7.67 \times 10^{-4}$  mol) was added to a 25 ml Erlenmeyer flask and the atmosphere was purged with dry nitrogen in a glove bag. Pyridine (10 ml) was added to the hemin and the Erlenmeyer was cooled in an ice bath external to the glove bag. Trimethylacetylchloride ( $1.4 \times 10^{-3}$  mol) was added to the reaction mixture via a microliter syringe. Conversion to the dianhydride was followed by quenching aliquots of the reaction mixture with anhydrous methanol and chromatographing the product on TLC plates in 9/1  $\text{CHCl}_3/\text{MeOH}$ . Additional trimethylacetylchloride was added as necessary to complete the conversion to anhydride. 3-(1-Imidazolyl)propylamine ( $1.6 \times 10^{-3}$  mol) was added to the reaction mixture with stirring and it was allowed to stand overnight. The reaction flask was then taken from the glove bag and pyridine was removed in vacuo.

A silica gel column (45 x 3 cm) was packed in 9/1/0.1,  $\text{CHCl}_3/\text{MeOH}/\text{Et}_3\text{N}$ , and half the crude product was applied to the top in a minimum volume of solvent mixture. Fast eluting impurities were discarded and then the solvent was changed to 7.5/2.5/0.1 and the remaining material was collected. This procedure was repeated to yield 76% hemin di-3-(1-imidazolyl)propylamide which had one spot purity by TLC in 90/10,  $\text{CHCl}_3/\text{MeOH}$  with an  $R_f$  = 0.14. Hemin diamide does not move in 9/1/0.1  $\text{CHCl}_3/\text{MeOH}/\text{formic acid}$ . Infrared (KBr):  $1655 \text{ cm}^{-1}$  (amide

I),  $1545\text{ cm}^{-1}$  (amide II). (Appendix A.8).

Analysis. Calculated  $\text{C}_{46}\text{H}_{49}\text{N}_{10}\text{FeCl}$  (865.19): C, 65.20; H, 5.70; N, 16.17. Found: C, 62.13; H, 6.75; N, 11.98.

Ferric protoporphyrin IX mono-3-(1-imidazolyl)propylamidemonomethyl-ester.

Method I. The dianhydride of hemin was prepared as described for protohemin di-3-(1-imidazolyl)propylamide. An equimolar quantity of 3-(1-imidazolyl)propylamine (0.096 g,  $7.67 \times 10^{-4}$  mol) dissolved in pyridine (1/9) was added dropwise with stirring and allowed to stand 20 min. Conversion to monoamide ( $R_f = 0.43$ ) and diamide ( $R_f = 0.14$ ) was monitored by TLC in 9.0/1.0,  $\text{CHCl}_3/\text{MeOH}$ . The unreacted anhydride groups were esterified by the addition of 10 ml of anhydrous methanol. After 30 minutes volatiles were removed in vacuo and the crude product was dissolved in 100 ml of methanol with 1%  $\text{H}_2\text{SO}_4$  and allowed to stand for 2 hr at room temperature. Unreacted acid groups, formed by hydrolysis of the anhydride by traces of moisture in the reactants, were cleanly converted to the methyl ester derivative. The reaction mixture was poured into 300 ml of methylene chloride  $\text{CH}_2\text{Cl}_2$  and extracted with 100 ml of sodium chloride saturated water followed by 100 ml of sodium bicarbonate (sat) and finally 100 ml of NaCl (sat). The methylene chloride layer was dried over  $\text{MgSO}_4$  and then the solvent was removed in vacuo. Half the reaction mixture was layered on a silica gel column (45 x 3 cm) packed in 9/1/0.1,  $\text{CHCl}_3/\text{MeOH}/\text{Et}_3\text{N}$ . Hemin dimethylester eluted very rapidly. The solvent was changed to 8.5/1.5/0.1 and hemin monoester monoamide eluted with one spot purity.



Method II. To a 100 ml round bottom flask equipped with stirring bar was added 20 ml of pyridine and 0.5 g of hemin ( $7.67 \times 10^{-4}$  mol). The flask was cooled in ice and 1.0 g of dicyclohexylcarbodiimide (DCC) ( $4.8 \times 10^{-3}$  mol) was added in small amounts. Conversion to the carbodiimide adduct was followed by quenching aliquots in methanol for 0.5 hr. Development in 9/1,  $\text{CHCl}_3/\text{MeOH}$  gave the dimethylester ( $R_f = 0.83$ ) and a hemin-DCC adduct with an  $R_f = 0.17$ . Unreacted hemin doesn't move under these developing conditions.

A 10% solution of 3-(1-imidazolyl)propylamine (0.96 g,  $7.67 \times 10^{-4}$  mol) was added to the reaction mixture dropwise over 30 min with stirring. Conversion to the monoamide ( $R_f = 0.43$ ) and diamide ( $R_f = 0.14$ ) was followed as described above. Methanol (10 ml) was added and the solution was stirred for an additional 30 min. Then 5 ml of acetic acid was added and the mixture was allowed to stand overnight at room temperature. The crystals of N,N'-dicyclohexylurea were removed by filtration and the volatiles evaporated in vacuo. Purification was as described above to yield 0.189 g (31.8%).

Infrared (KBr):  $1730 \text{ cm}^{-1}$  (ester),  $1650 \text{ cm}^{-1}$  (amide I),  $1530 \text{ cm}^{-1}$  (amide II), (Appendix A.9).

Analysis. Calculated for  $\text{C}_{41}\text{H}_{43}\text{N}_7\text{O}_3\text{FeCl}$  (773.14): C, 63.69; 5.61; N, 12.67. Found: C, 62.31; H, 6.23; N, 11.86.

Ferric protoporphyrin IX mono-3-(1-imidazolyl)propylamide monodecyl-ester. The procedure for the synthesis of the hemin monoamide monodecylester was identical to that of the monoamide monomethylester up to the point of alcohol addition. Decyl alcohol (0.5 ml, 0.025 mol) was

added and the reaction mixture was stirred overnight. Then 5 ml of acetic acid was added and the mixture was stirred for 3 hr at room temperature. The N,N'-dicyclohexylurea crystals were removed by filtration and the volatiles evaporated in vacuo. The entire reaction mixture in the residual high boiling decanol was applied to a silica gel column (85 x 3 cm) in methylene chloride. The column was flushed with CH<sub>2</sub>Cl<sub>2</sub> to remove the decanol and then the solvent was gradually changed to 90/10, CH<sub>2</sub>Cl<sub>2</sub>/MeOH. The didecylester eluted first and the solvent was gradually changed to 7.5/2.5, CH<sub>2</sub>Cl<sub>2</sub>/MeOH. Hemin monoamide monodecylester had an  $R_f = 0.6$  in CH<sub>2</sub>Cl<sub>2</sub>/MeOH, 9/1 as compared with an  $R_f$  of 0.5 for hemin monoamide monomethylester. (A more significant difference in  $R_f$  was observed in CH<sub>2</sub>Cl<sub>2</sub>/MeOH, 30/1: for the didecylester the  $R_f = 0.74$  and for dimethylester  $R_f = 0.40$ .) The overall yield was 0.174 g (25.1%).

Analysis. Calculated for C<sub>50</sub>H<sub>61</sub>N<sub>7</sub>O<sub>3</sub>FeCl (898.94): C, 66.80; H, 6.79; N, 10.91. Found: C, 62.70; H, 7.24; N, 9.35.

Ferric protoporphyrin IX mono-3-(1-imidazolyl)propylamide monohexylester. The synthesis and purification of this hemin derivative was identical to that of the monoamide monodecylester. The TLC of the monoamide monohexylester was identical to that of the monoamide monomethylester. (The dihexylester moved with one spot in hexanol/CH<sub>2</sub>Cl<sub>2</sub>, 9/1 but the dimethylester had a broad tail.) The overall yield was 0.177 g (27.3%).

Analysis. Calculated for C<sub>46</sub>H<sub>56</sub>N<sub>7</sub>O<sub>3</sub>FeCl (843.28): C, 65.52; H, 6.33; N, 11.63. Found: C, 59.37; H, 7.16; N, 9.33.

N-tert-Butyloxycarbonyl-2-aminoethyl methacrylate. To a solution of 11.3 g (0.068 mol) of pure aminoethyl methacrylate in 30 ml of water was added 16.32 g (0.083 mol) of 2-(tert-butoxycarbonyloxyimino)-2-phenylacetonitrile (BOC-ON) in 30 ml of dioxane with stirring. Triethylamine (18 ml, 0.129 mol) was added dropwise over a half hour period. The reaction mixture was stirred at room temperature overnight. The solution was extracted with three 50 ml volumes of diethylether and the ether layer washed with two 75 ml portions of 1 M sodium hydroxide and then water. The ether was removed in vacuo and the product was recrystallized from aqueous methanol to yield 12.98 g (83%) of N-tert-butyloxycarbonyl-2-aminoethyl methacrylate with a melting point of 79-80.5°C. Infrared (KBr): 3390  $\text{cm}^{-1}$  NH stretch, 1720  $\text{cm}^{-1}$  (ester carbonyl), 1700  $\text{cm}^{-1}$  (carbamate C=O stretch), 1635  $\text{cm}^{-1}$  (vinyl conjugated with C=O), 1525  $\text{cm}^{-1}$  (amide II). (Appendix A.10).  $^1\text{H-NMR}$  ( $\text{CDCl}_3$ ):  $\delta$  = 1.51 ppm (s, 9H),  $\delta$  = 1.98 ppm (s, 3H),  $\delta$  = 3.48 ppm (t, 2H),  $\delta$  = 4.25 ppm (t, 2H),  $\delta$  = 5.60 ppm (s, 1H),  $\delta$  = 6.05 ppm (s, 1H) (Appendix A.11). For  $^{13}\text{C-NMR}$  see Appendix A.12.

Analysis. Calculated for  $\text{C}_{11}\text{H}_{19}\text{NO}_4$  (229.13): C, 57.66; H, 8.36; N, 6.11. Found: C, 57.54; H, 8.42; N, 6.05.

N-tert-Butyloxycarbonyl-1,6-diaminohexane·HCl. In a 1000 ml round bottom flask was placed 35.018 g (0.301 mol) of 1,6-hexanediamine in 200 ml of ethyl acetate. BOC-ON (25.010 g, 0.102 mol) dissolved in 100 ml of ethyl acetate was added dropwise over a 5 hr period and then the mixture was allowed to stir overnight. A solid yellow precipitate was removed by filtration and the solvent reduced in vacuo to a volume of

100 ml. Water (150 ml) was added and the solution was evaporated until white crystals of N,N'-tert-butyloxycarbonyl-1,6-diaminohexane precipitated. The solution was filtered to yield 3.41 g (0.011 mol) of the diblocked amine. Salt was added to the filtrate to saturate the solution which was then extracted with ethyl acetate. Ethyl acetate was removed in vacuo to yield a yellow oil. The oil was dissolved in water and titrated with 1M HCl to pH = 3.5. During the titration most of the yellow color disappeared. The product, in water, was then extracted with ethyl acetate until no color was observed in the ethyl acetate layer. The water layer was saturated with NaCl and the product oiled out and then crystallized. After filtration the mother liquor was again saturated with NaCl to yield a second crop. The crude t-BOC-amine was dissolved in 75 ml of hot ethanol and filtered to yield NaCl. Acetone was added very slowly and the solution decanted to remove the last traces of salt. Additional acetone was added until N-tert-butyloxycarbonyl-1,6-diaminohexane·HCl began to precipitate from solution. No cloud point was observed. The solution was cooled in ice to 3°C and then filtered to yield 10.95 g (0.042 mol, 41.7%) of shiny white plates; m.p. 162-163°C.

N-tert-Butyloxycarbonyl-N'-(2-methacrylyl)-1,6-diaminohexane. A suspension of 9.907 g (0.038 mol) of N-tert-butyloxycarbonyl-1,6-diaminohexane·HCl in 200 ml of methylene chloride was cooled in an ice bath and 1.6 ml (0.083 mol) of triethylamine was added. A solution of 3.95 ml (0.0403 mol) methacryloyl chloride in 50 ml of methylene chloride was added dropwise with stirring. After 30 min, the reaction



mixture was extracted three times with 100 ml of water and then the  $\text{CH}_2\text{Cl}_2$  layer was dried over  $\text{MgSO}_4$ . Methylene chloride was removed in vacuo to yield a waxy solid. The solid was recrystallized from a toluene/pentane mixture to yield 8.315 g (0.029 mol, 76.1%) of pure tert-butyloxycarbonyl-N'-(2-methylacrylyl)-1,6-diaminohexane; m.p. 61-62°C. Infrared (KBr): 3330, 3370  $\text{cm}^{-1}$  (NH stretch) 1690  $\text{cm}^{-1}$  (carbamate, C=O stretch), 1650  $\text{cm}^{-1}$  (amide I stretch), 1620  $\text{cm}^{-1}$  (vinyl conjugated with C=O), 1525  $\text{cm}^{-1}$  (amide II stretch), (Appendix A.13).  $^1\text{H}$ -NMR ( $\text{CDCl}_3$ ):  $\delta$  = 1.51 ppm (s, 9H),  $\delta$  = 1.98 ppm (s, 3H),  $\delta$  = 3.18 (m, 12H),  $\delta$  = 4.66 ppm (s, 1H),  $\delta$  = 5.33 ppm (s, 1H),  $\delta$  = 5.72 ppm (s, 1H), 6.12 ppm (s, 1H) see Appendix A.14. For  $^{13}\text{C}$ -NMR see Appendix A.15.

Analysis. Calculated for  $\text{C}_{15}\text{H}_{28}\text{N}_2\text{O}_3$  (284.40): C, 63.35; H, 9.92; N, 9.85. Found: C, 62.99; H, 10.01; N, 9.77.

p-Azidostyrene. In a 250 ml round bottom flask, 3.1 ml of HCl and 18 ml of water were combined and cooled in an ice bath. p-Aminostyrene (1.807 g, 0.016 mol) was added to yield a yellow solution. The amine was diazotized by the addition of sodium nitrite (1.452 g, 0.021 mol) in 12.5 ml of  $\text{H}_2\text{O}$  dropwise with stirring to maintain the temperature below 10°C. The reaction mixture was decolorized with 0.5 g of charcoal and filtered after 30 min. A solution of 1.803 g of sodium azide (0.277 mol) in 12.5 ml of water was added dropwise to the cold, stirred filtrate. Nitrogen was immediately evolved and a yellow precipitate formed. The mixture was stirred for hour and then allowed to warm up to room temperature overnight. An orange precipitate was filtered from solution and washed three times with 50 ml of 10% sodium carbonate

solution and then twice with 75 ml of water. The orange solid was only partially soluble in organic solvents and a vinyl group was just faintly evident by  $^1\text{H-NMR}$ . By infrared (KBr pellet) the azide band was clearly visible at  $2120\text{ cm}^{-1}$  and the solid decomposed with warming. Variations on this reaction sequence were not promising and thus were abandoned.

p-Azidoacetophenone. In a 300 ml round bottom flask, 6.72 ml of HCl and 40 ml of  $\text{H}_2\text{O}$  were cooled to  $5^\circ\text{C}$  and p-aminoacetophenone (5.00 g, 0.037 mol) was added. A solution of 3.082 g of  $\text{NaNO}_2$  (0.045 mol) in 25 ml of  $\text{H}_2\text{O}$  was added dropwise, maintaining the temperature below  $10^\circ\text{C}$ , to form the diazonium salt. After one hour, 4.035 g of  $\text{NaN}_3$  (0.062 mol) in 20 ml of  $\text{H}_2\text{O}$  was added dropwise and nitrogen was evolved. The reaction mixture was stirred for 1 hr at  $5^\circ\text{C}$  and then allowed to stand at room temperature overnight. The product was filtered from solution and washed with 10%  $\text{Na}_2\text{CO}_3$  and then water to yield 5.32 g of p-azidoacetophenone (89%). Infrared (KBr):  $2100\text{ cm}^{-1}$  ( $-\text{N}_3$  asymmetric stretch),  $1680\text{ cm}^{-1}$  (C=O stretch)  $1600\text{ cm}^{-1}$  (C=C stretch).  $^1\text{H-NMR}$  ( $\text{CDCl}_3$ ):  $\delta = 2.57\text{ ppm}$  (s, 3H,  $-\text{CH}_3$ ),  $\delta = 6.98\text{ ppm}$  (d, 2H, aromatic),  $\delta = 7.90\text{ ppm}$  (d, 2H, aromatic).

1-(p-Azidophenyl)ethanol. In a 100 ml beaker, 0.46 g of sodium borohydride (0.012 mol) was dissolved in 10 ml of 95% ethanol and 5.30 g of p-azidoacetophenone (0.033 mol) was dissolved in 40 ml of ethanol. The orangish-red solution was stirred for 15 min and then 3N HCl was added dropwise. HCl was added until hydrogen evolution ceased ( $\sim 4\text{ ml}$ ). The solution was diluted with 5 ml of  $\text{H}_2\text{O}$  and the ethanol removed in vacuo. The remaining water mixture was extracted twice with 50 ml of



chloroform and then the chloroform was washed with a 5% solution of sodium carbonate to yield a cherry red oil (4.09 g, 0.76%). Infrared (neat):  $3380\text{ cm}^{-1}$  (OH stretch),  $2120\text{ cm}^{-1}$  ( $\text{N}_3$  stretch)  $1610\text{ cm}^{-1}$  (C=C stretch).  $^1\text{H-NMR}$  ( $\text{CDCl}_3$ )  $\delta = 1.45\text{ ppm}$  (d, 3H,  $-\text{CH}_3$ ),  $\delta = 4.48\text{ ppm}$  (s, 1H, OH),  $\delta = 4.90\text{ ppm}$  (q, 1H,  $-\text{CH}^*\text{OHCH}_3$ ),  $\delta = 7.10\text{ ppm}$  (d, 2H, aromatic),  $\delta = 7.50\text{ ppm}$  (d, 2H, aromatic).

p-Azidostyrene. Attempts to dehydrate 1-(p-azidophenyl)ethanol were not successful. Reagents which were employed are listed below.

- (1) p-toluene sulfonylchloride/pyridine,  $25^\circ\text{C}$ , 18 hr
- (2) p-toluene sulfonylchloride/pyridine/KOH,  $40^\circ\text{C}$ , 28 hr
- (3) thionylchloride/pyridine,  $0^\circ\text{C}$ , 4 hr.

p-Azidostyrene was never observed by  $^1\text{H-NMR}$ . Products of the above reactions appeared to be quite complex.

2-Azidoethyl methacrylate. In a 125 ml Erlenmeyer flask was placed 2.90 ml of 2-hydroxyethyl methacrylate (0.023 mol), 25 ml of pyridine and 4.382 g of p-toluene sulfonylchloride (0.023 mol). This mixture was stirred at  $7^\circ\text{C}$  for 18 hr and crystals of pyridine hydrochloride were evident. Water was added to the solution and then the product was extracted into chloroform. The chloroform layer was washed twice with 50 ml of 5% HCl and then twice with 50 ml of  $\text{H}_2\text{O}$ . The chloroform layer was dried over  $\text{MgSO}_4$ , filtered and then solvent removed in vacuo to yield the crude tosyl ester. The ester was dissolved in 20 ml of ethanol and 1.796 g of  $\text{NaN}_3$  (0.027 mol) in 20 ml of  $\text{H}_2\text{O}$  was added. The reaction proceeded for 48 hr at which time 100 ml of  $\text{H}_2\text{O}$  was added and 2-azidoethyl methacrylate was extracted by two 35 ml volumes of

chloroform. The chloroform was dried over  $\text{MgSO}_4$ , filtered and then removed in vacuo to yield an impure oil. Infrared (neat):  $2120\text{ cm}^{-1}$  ( $\text{N}_3$  stretch),  $1720\text{ cm}^{-1}$  ( $\text{C}=\text{O}$  stretch),  $1640\text{ cm}^{-1}$  ( $\text{C}=\text{C}$  alkene stretch).  $^1\text{H}$ -NMR (neat) showed traces of both the desired product and the tosyl ester:  $\delta = 1.90\text{ ppm}$  (s, 3H,  $\text{C}=\text{C}-\text{CH}_3$ ),  $\delta = 2.42$  (s, aromatic- $\text{CH}_3$ ),  $\delta = 4.00\text{ ppm}$  (m, 4H,  $-\text{OCH}_2\text{CH}_2\text{N}_3$ ),  $\delta = 5.58$  (s, 1H, vinyl),  $\delta = 6.15$  (s, 1H, vinyl),  $\delta = 7.35, 7.80$  (two doublets for aromatic -H). From NMR the purity was estimated to be 55%.

p-Azidophenyl methacrylate. A solution of 34 ml of  $\text{HCl}$  in 100 ml of  $\text{H}_2\text{O}$  was cooled to  $5^\circ\text{C}$ . p-Aminophenol (20.0 g, 0.183 mol) was dissolved and the stirred amine solution was diazotized by the dropwise addition of 15.27 g of sodium nitrite (0.22 mol) in 140 ml of water. When the addition was complete, the solution was stirred for one hour with 1.0 g of activated charcoal. The charcoal was filtered off and 20.0 g of sodium azide (0.308 mol) in 110 ml of water was added dropwise. Nitrogen was evolved and a yellow solid precipitated. The suspension was stirred for one hour after azide addition was complete. The precipitate melted upon warming to room temperature. The reaction mixture was extracted with diethylether and the ether layer dried over  $\text{MgSO}_4$ . (An infrared spectrum of the isolated p-azidophenol has an OH stretch at  $3380\text{ cm}^{-1}$  and a  $\text{N}_3$  stretch at  $2110\text{ cm}^{-1}$ . See Appendix A.16.) To the filtered reddish solution was added 17.9 ml of methacryloyl chloride (0.18 mol), 25.1 ml of triethylamine (0.18 mol) and the mixture was stirred for 24 hr. The ether solution was then extracted with 1%  $\text{NaOH}$  until no green color remained in the water layer (approximately 5 x

50 ml) and then twice with water. The ether layer was dried over  $\text{MgSO}_4$ , filtered, and then crystals of p-azidophenyl methacrylate were frozen out of solution. The product was recrystallized in aqueous methanol to yield 14.0 g (58%) of shiny tan plates: m.p.  $56.5 - 57^\circ\text{C}$ , decompose  $155^\circ\text{C}$ . Infrared (KBr):  $2120\text{ cm}^{-1}$  ( $\text{N}_3$  stretch),  $1730\text{ cm}^{-1}$  ( $\text{C}=\text{O}$  stretch) (Appendix A.17).  $^1\text{H}$ -NMR ( $\text{CDCl}_3$ ):  $\delta = 2.10\text{ ppm}$  (s, 3H),  $\delta = 5.75\text{ ppm}$  (s, 1H),  $\delta = 6.35\text{ ppm}$  (s, 1H),  $\delta = 7.10\text{ ppm}$  (m, 4H) (Appendix A.18). See Appendix A.19 for  $^{13}\text{C}$ -NMR spectrum.

Analysis. Calculated for  $\text{C}_{10}\text{H}_9\text{N}_3\text{O}_2$  (203.20): C, 59.40; H, 4.48; N, 20.78. Found: C, 58.98; H, 4.22; N, 20.35.

### Results and Discussion

The vinyl monomers which were investigated are grouped into five categories below: hydrophobic, hydrophillic, hemes, amines and crosslinking agents.

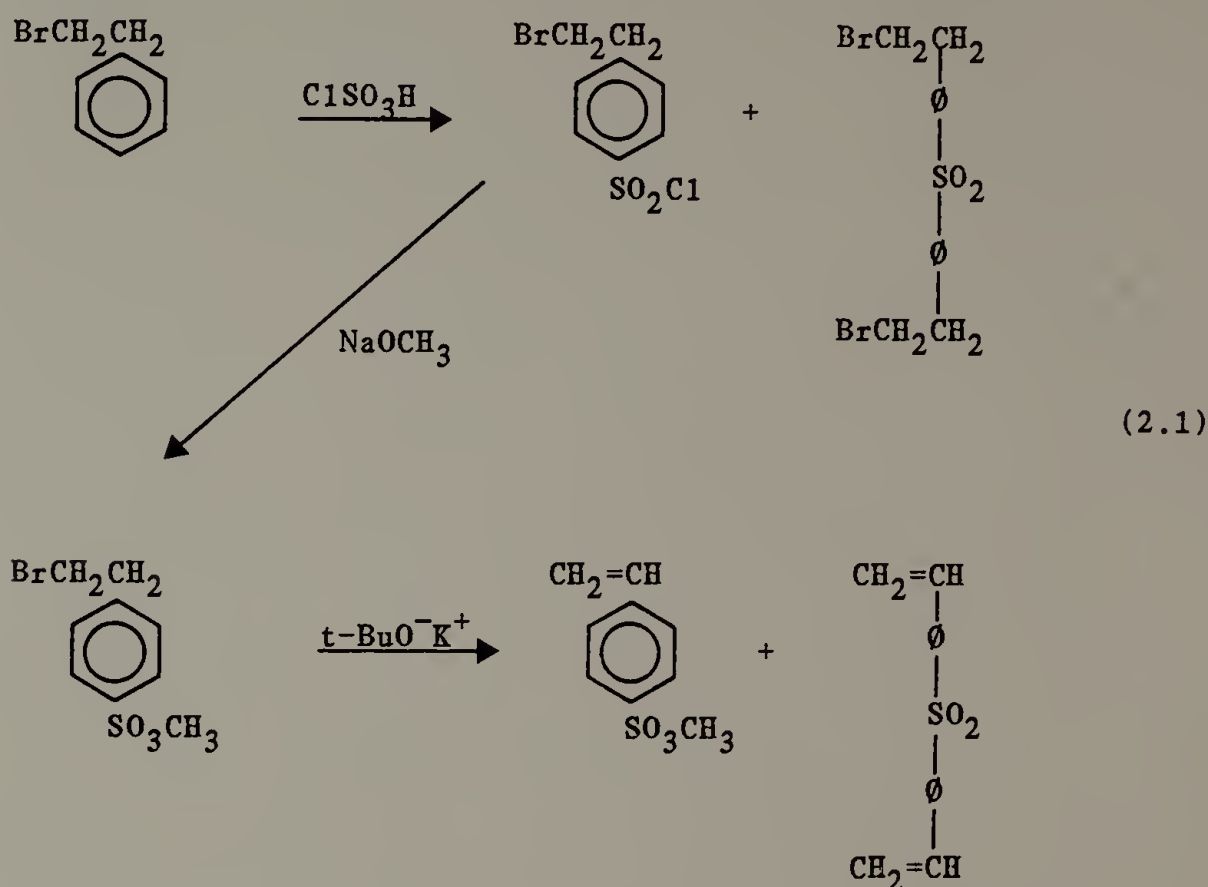
#### Hydrophobic Monomer

A single hydrophobic monomer was selected for study: styrene [S]. This commercially available vinyl monomer is resonance stabilized and forms random copolymers with methacrylates and styrene derivatives.<sup>3</sup> The necessary fraction of styrene in the model polymer was estimated to be 75-80 mol%.

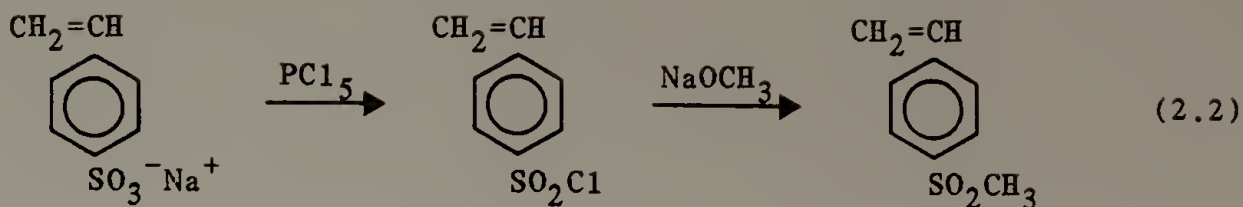
#### Hydrophillic Monomers

Sodium p-vinylbenzenesulfonate [ $\text{SS}^-$ ] was initially chosen to give water solubility. Preliminary work by L.C. Dickinson<sup>4</sup> showed that polymers containing 13 - 15% of the sodium sulfonate group could be

rendered water soluble using dialysis techniques.  $[SS^-]$  has a limited solubility in organic solvents and thus the easily hydrolyzed ester, methyl p-vinylbenzenesulfonate [MSS] was synthesized from bromoethylbenzene.<sup>5,6</sup> A difunctional sulfone impurity was formed by this reaction sequence which could not be removed by HPLC.<sup>7</sup>

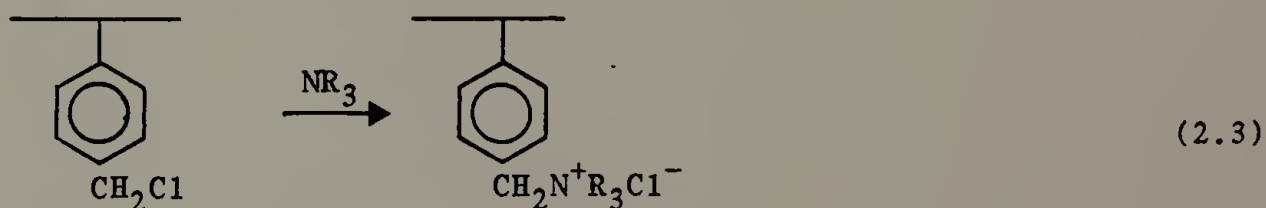


A second procedure adapted from Gritsai and Prib<sup>8</sup> by Vanzo was used for the synthesis of p-vinylbenzenesulfonylchloride. Synthesis of [MSS] from this intermediate was simple and the purity of the final product depended on the quality and age of the starting material.



The synthesis of alkylvinylpyridinium salts as a cationic solubilizing group was investigated.<sup>9</sup> It was observed that vinylpyridinium salts undergo spontaneous polymerization during monomer synthesis. This has been documented in the current literature.<sup>10</sup> Quaternization of the 4-vinylpyridine (4VP) groups after polymerization was successful but was abandoned due to possible simultaneous quaternization of covalently bound nitrogenous bases on the heme model compounds.<sup>11</sup>

Preliminary work on a third water solubilizing group was initiated. The benzylchloride group of a polymerized p-vinylbenzylchloride (VBC) monomer can be substituted by a tertiary amine to yield a quaternary ammonium complex (BVMA).<sup>11,12</sup>



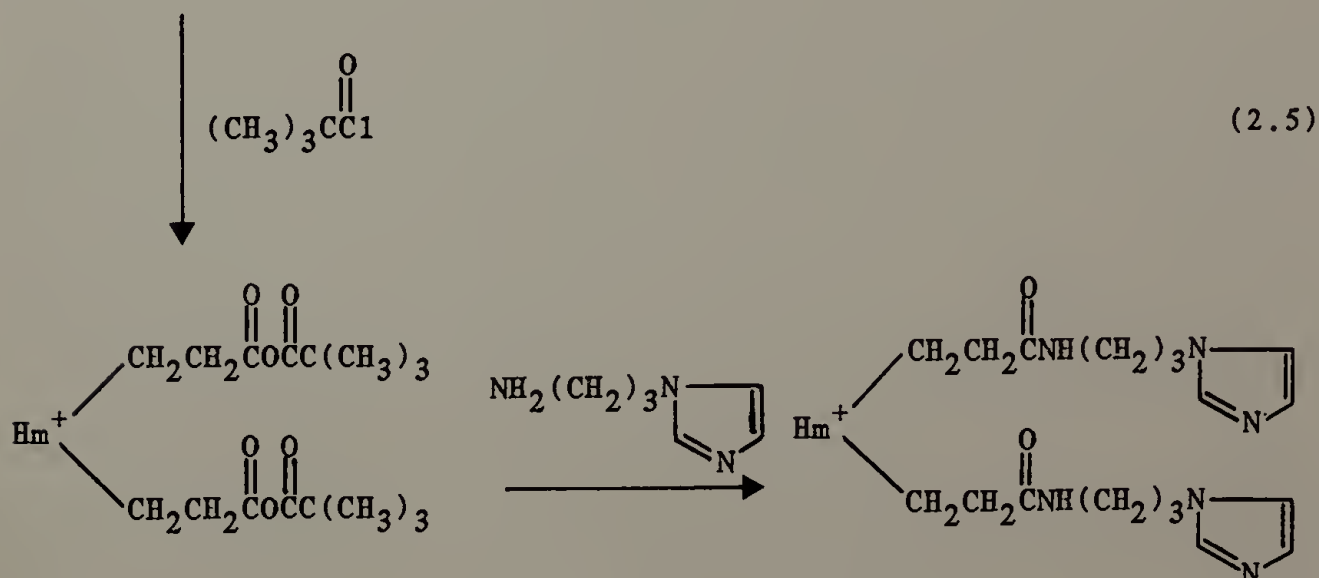
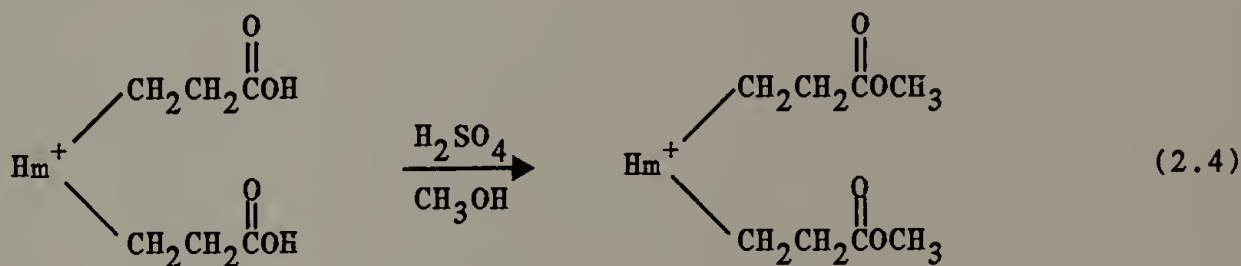
It is important to note the similarities between the anionic sulfonate and the cationic quaternary amine water solubilizing agents. The sulfonic acid moiety is unprotonated at virtually all pH values ( $\text{pK}_a = -6.56$  for p-toluenesulfonic acid, a chemically analogous acid).<sup>12</sup> The quaternary amines are permanent cations and do not contribute to the pH



of the resulting solution. Both sulfonate and quaternary amines require a counterion for neutralization of the ionic charge and the counterion may be exchanged by dialysis.

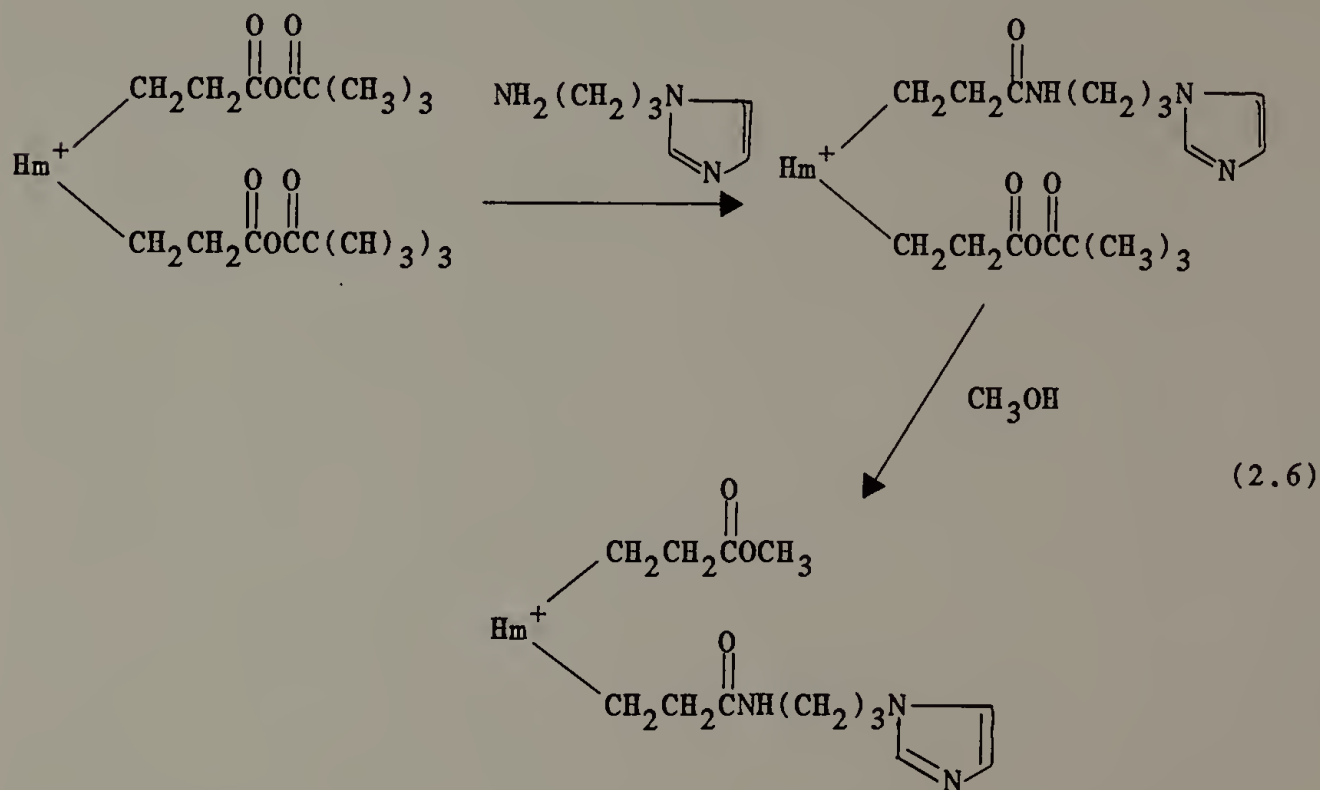
### Heme Model Compounds

Three heme model compounds were synthesized from naturally occurring ferric protoporphyrin IX (hemin): hemin dimethylester (HDME), hemin bis-3-(1-imidazolyl)propylamide (HDA) and hemin mono-3(1-imidazolyl)-propylamide monomethylester (HMEMA). Both HDME and HDA have no oxidative stability in organic solution, at lowered temperatures, or in the presence of carbon monoxide.<sup>14</sup> The synthesis of these two model compounds with high purity was facile and the ability of the polymer model to stabilize these hemes will be examined.





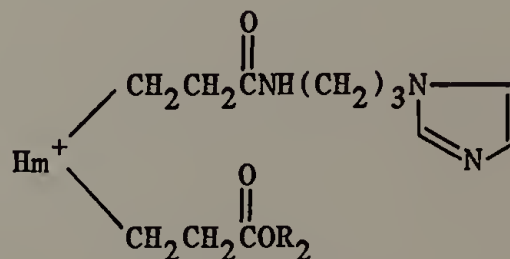
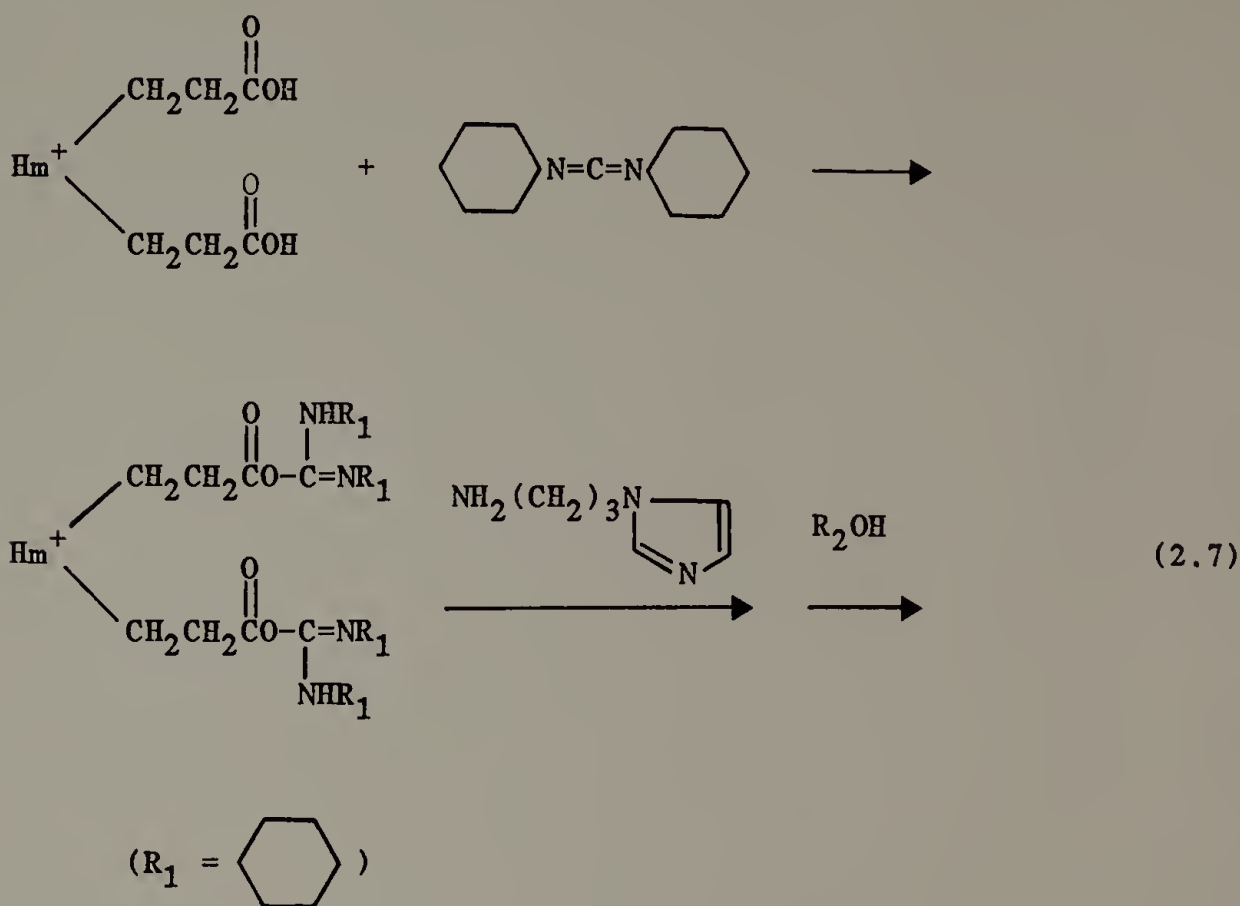
HMEMA reversibly binds oxygen with some stability in a variety of solvent systems at lowered temperatures.<sup>14,15</sup> Synthesis of HMEMA was accomplished by two different synthetic routes. First the dianhydride formed by the reaction of hemin with trimethylacetylchloride was carefully titrated with 3-(1-imidazolyl)propylamine to maximize monoamide formation and then methanol was added to convert the remaining anhydride groups to their corresponding methyl esters.



Purification of HMEMA was somewhat difficult due to the large number of reaction products: HMEMA, HDME, HDA, hemin monoester monoacid, hemin monoamide monoacid and hemin (diacid). Unfunctionalized acid groups resulted from moisture dissolved in the solvent system or atmospheric moisture. Reaction products were stirred in acidic methanol to complete the conversion to the three hemin monomers, HDME, HMEMA and HDA, with

column chromatography used to isolate pure HMEMA.

A new method to synthesize HMEMA using the peptide coupling agent, dicyclohexylcarbodiimide proved to have significantly less moisture sensitivity and gave a higher yield of HMEMA.



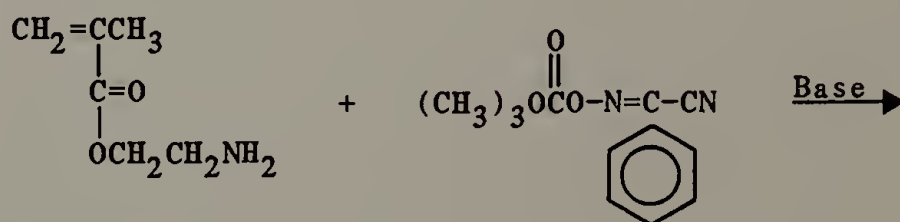
Oxidative stability of HMEMA before and after polymerization is a direct measure of the ability of a polymeric system to stabilize the oxygenated adduct.<sup>16</sup> In the final polymer 0.5 mol % HMEMA gives approximately one

heme per chain, assuming a DP = 200.

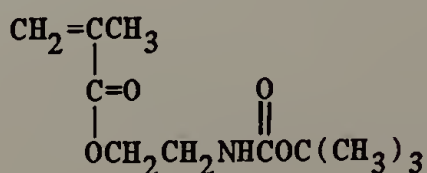
The above synthetic method allowed the synthesis of hemin mono-3-(1-imidazolyl)propylamide monodecylester (HMEMA-D) and hemin mono-3-(1-imidazolyl)propylamide monohexylester (HMEMA-H). By TLC, the polarity of these long chain esters is less than the methyl ester which suggests they are more hydrophobic. Attempts to synthesize a 20 carbon ester by this procedure were unsuccessful, probably due to the length of the long chain alcohol.

#### Amine Monomers

Initially 2-aminoethyl methacrylate [AEMA] was studied as a potential carbon dioxide carrier. Preliminary work by J. Gillis<sup>17</sup> showed the  $pK_a$  of copolymers of styrene and AEMA in water to be approximately 7.5. The free amine of AEMA was blocked using a BOC-ON reagent (2-(tert-butoxycarbonyloxyimino)-2-phenylacetonitrile)<sup>18</sup> to give solubility in a wide range of solvents and prevent reaction during polymerization or subsequent alteration of polymeric units.

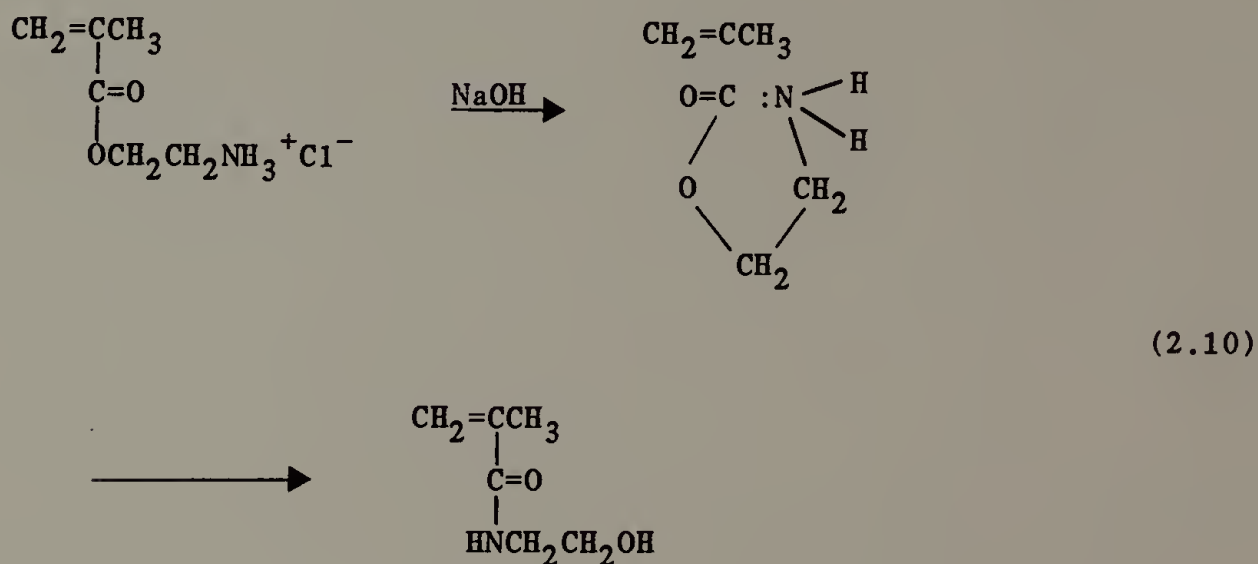


(2.9)



The t-butyloxycarbonyl group can be removed by a variety of gentle techniques.<sup>19,22</sup>

2-Aminoethyl methacrylate was abandoned when spectral evidence of the tautomerization to N-(2-hydroxyethyl)methacrylamide was observed by <sup>13</sup>C-NMR (Figure 2.1). The ester function is stable only in acidic solution and AEMA was received in solution at pH = 3.0. The rearrangement product is favored by formation of a five-membered ring intermediate as well as by the relative stability of the amide versus the ester.



The <sup>13</sup>C-spectra of AEMA shown in Figure 2.1 was taken one month after the solution was made basic. An internal pH standard, HEPES, was used to estimate the pH = 6.62.<sup>23</sup> Peaks attributed to pure AEMA as well as the rearrangement product are evident. The quantity of rearranged product was approximately equal to that of pure AEMA. Although Dow Chemical Co.<sup>24</sup> claims the rearrangement of poly(AEMA) is significantly

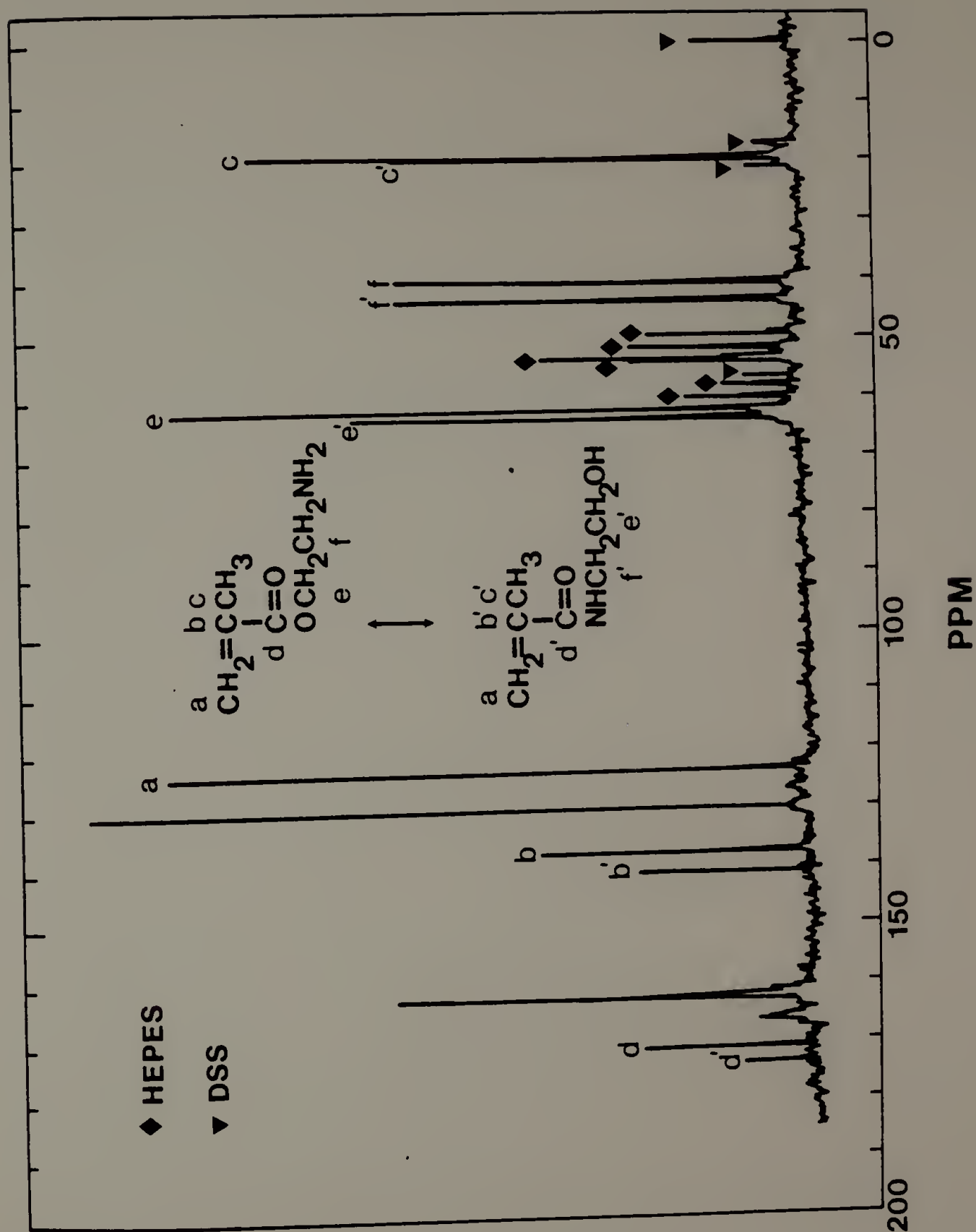
Figure 2.1.  $^{13}\text{C}$ -NMR of 2-aminoethyl methacrylate (AEMA) and its tautomer N-(2-hydroxyethyl)methacrylamide (HEMA).

Assignment: DSS,  $\blacktriangledown$  ; HEPES,  $\blacklozenge$  ;  $^{13}\text{CO}_2$ , 130.17 ppm;

$\text{H}_2\text{CO}_3 \rightleftharpoons \text{HCO}_3^- \rightleftharpoons \text{CO}_3^{2-}$ , 162.31 ppm;  $\text{RNHCO}_2^-$ ,

166.41 ppm;

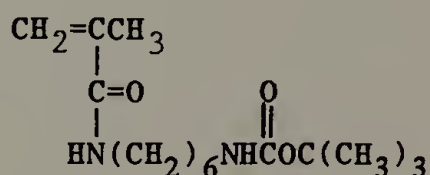
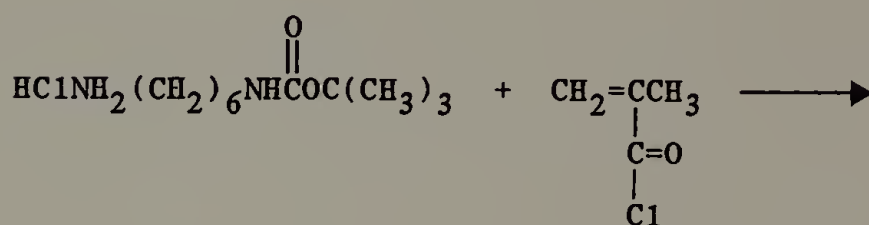
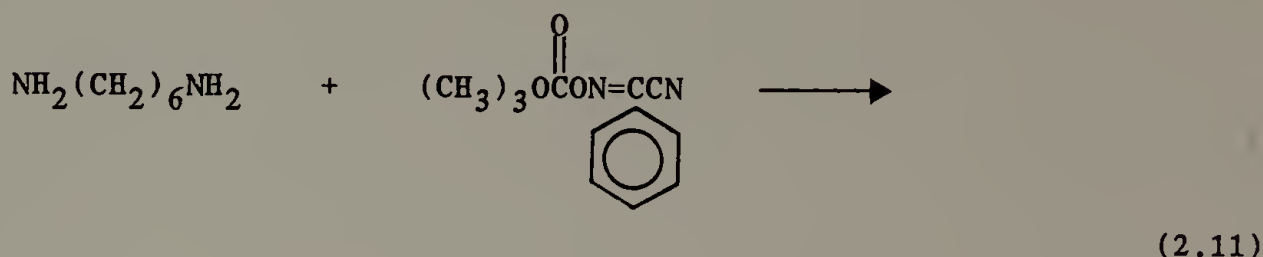
AEMA	a) = 123.67 ppm	HEMA	a') = 123.67 ppm
	b) = 137.50 ppm		b') = 141.25 ppm
	c) = 19.87 ppm		c') = 20.25 ppm
	d) = 171.09 ppm		d') = 173.79 ppm
	e) = 62.39 ppm		e') = 63.71 ppm
	f) = 41.02 ppm		f') = 44.00 ppm





slower than in the monomer, recently Ogata and coworkers<sup>25</sup> have studied copolymers containing AEMA which utilize the rearrangement mechanism as a proton pump in membrane systems.

A second, more hydrophobic, alkylamine, N-(2-methylacrylyl)-1,6-diaminohexane was synthesized in the blocked form (BNAHD) through a procedure adapted from Stahl et al.<sup>19</sup>

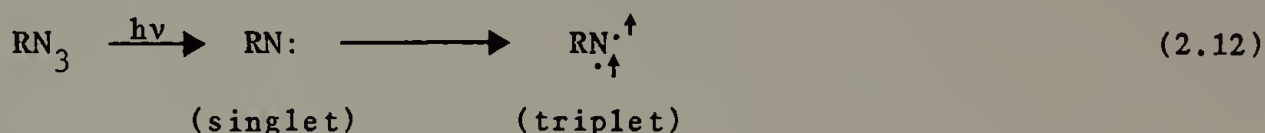


Elimination of difunctional impurities required careful purification of the intermediate, N-tert-butyloxycarbonyl-1,6-diaminohexane. It was estimated that 5 - 10 mol % amine would give sufficient carbon dioxide carrying capacity to the resulting polymer at physiological pH.

#### Photoactive Crosslinking Agents

The azide functionality was selected as a photoactive moiety that

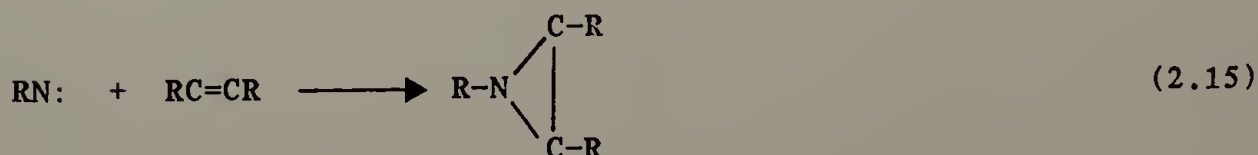
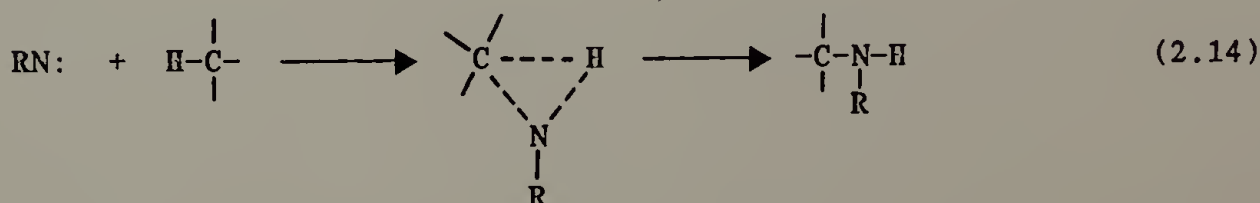
would be thermally stable under polymerization conditions and in ordinary light but extremely sensitive to ultraviolet light. The upper excited states of aromatic azides are those of the parent hydrocarbon. The molecule is excited to the  $n\pi^*$  state and decomposes to form a singlet nitrene or undergoes intersystem crossing to the triplet state.<sup>26</sup>



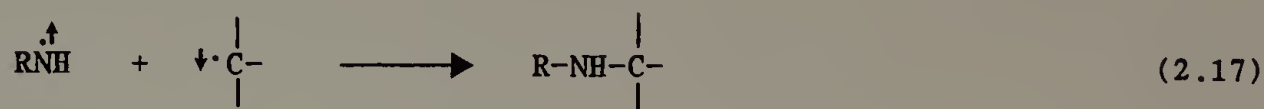
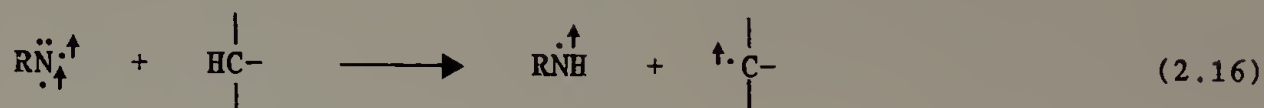
Nitrenes are relatively nonselective. Recombination is spin allowed for both the singlet and triplet state but is rarely observed due to low concentrations of free nitrene.



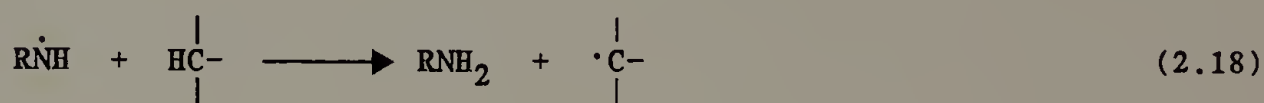
Singlet nitrenes can insert into carbon-hydrogen bonds or react by addition to double bonds.



Triplet nitrenes primarily react by hydrogen abstraction followed by combination (pseudo-insertion).

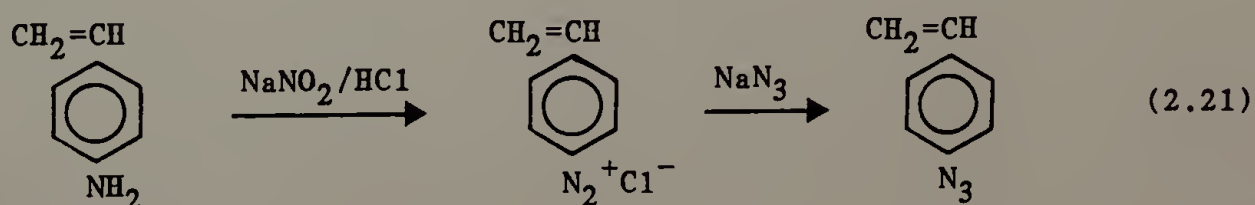


The time required for spin reversal before combination allows some of the radicals to diffuse away from one another before they can react.

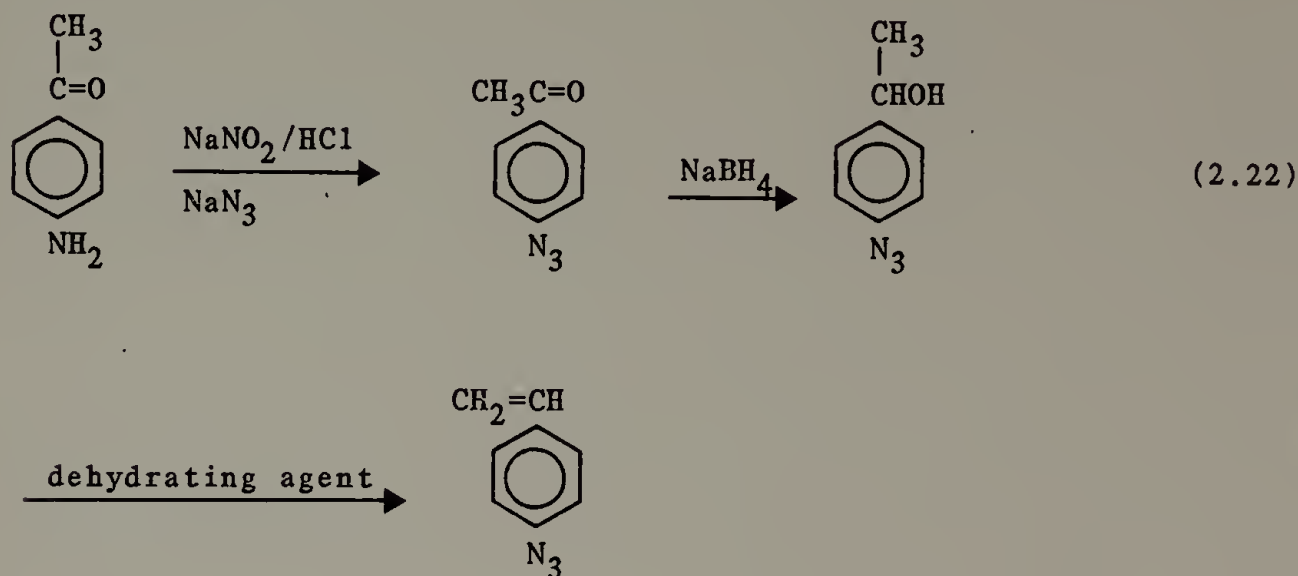


Reaction 2.18 does not yield a crosslinked product and reduces the efficiency of the crosslinking agent.

Initially, the synthesis of p-azidostyrene was attempted via the diazotization of p-aminostyrene followed with substitution by sodium azide.<sup>27</sup>

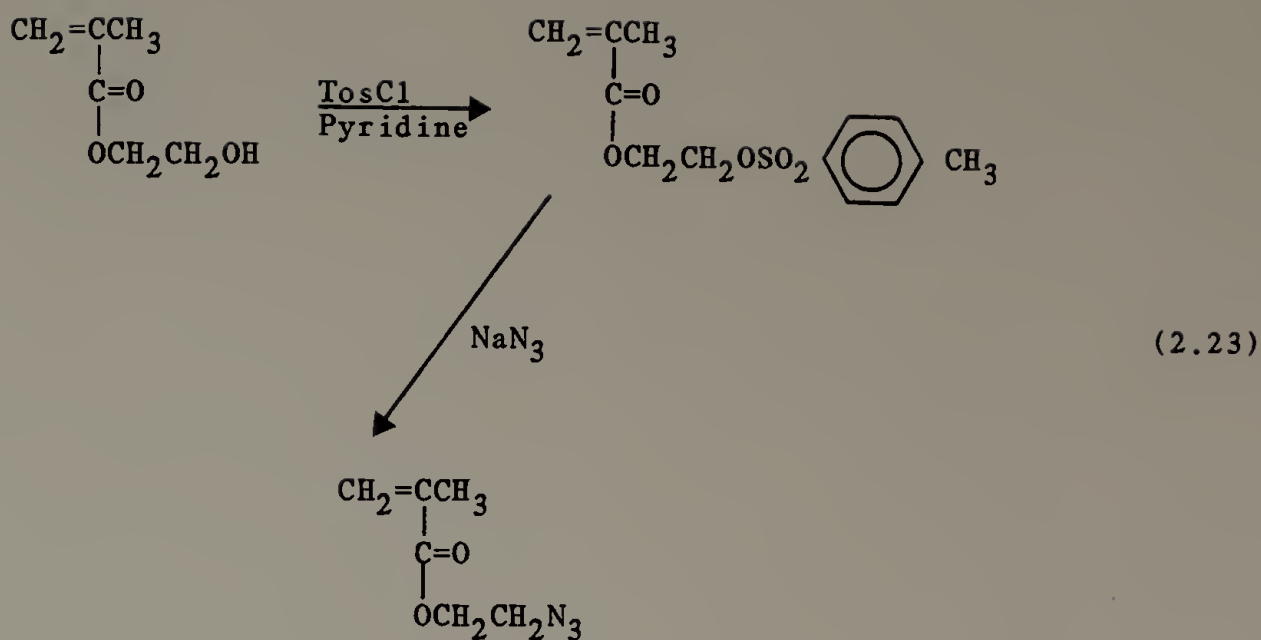


The reaction product was an intractable orange solid with the characteristic odor of an aromatic azide. A second method to synthesize p-azidostyrene from p-aminoacetophenone was also unsuccessful.<sup>27,28</sup>



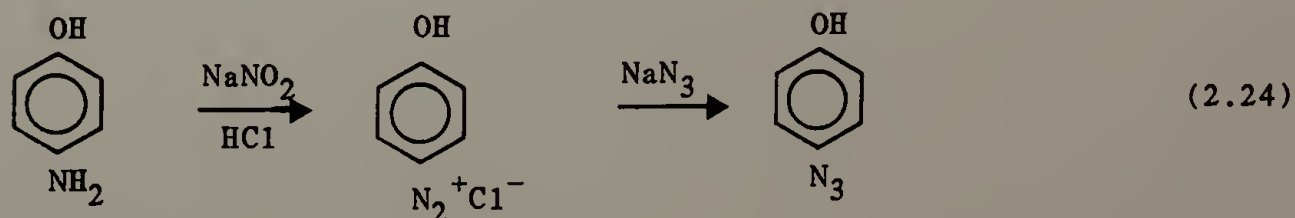
Attempts to dehydrate 1-(p-azidophenyl)ethanol by relatively mild techniques gave no reaction or polymeric products. Strong acids were unsuitable because they react to decompose the azide to its corresponding amine.

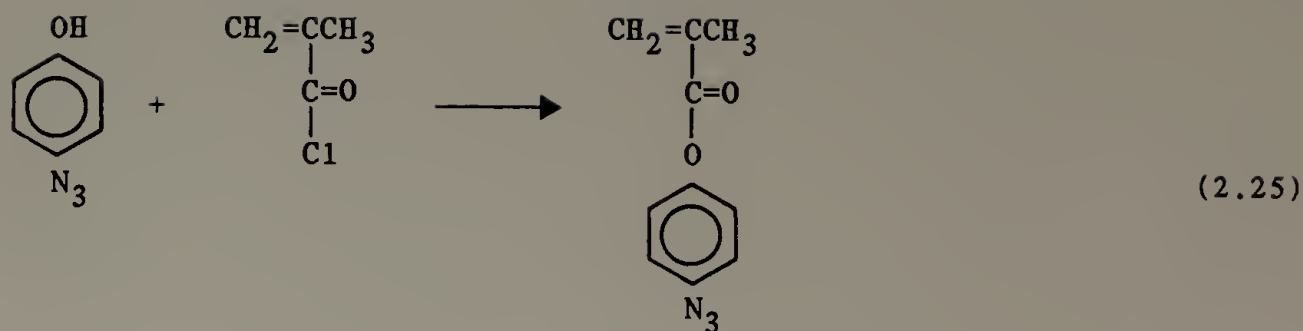
The method of Logothetis<sup>29</sup> was used to synthesize 2-azidoethyl methacrylate.<sup>28</sup>



Both  $^1\text{H}$ -NMR and infrared spectroscopy demonstrated that the second part of the reaction in Equation 2.23 is only 50% complete. The impure product can be purified on neutral alumina to yield pure azide. Alkyl azides are significantly less stable to shock and temperature than aromatic azides, thus further purification or characterization of this monomer was not pursued.

Finally the novel polymerizable azide, p-azidophenyl methacrylate (APMA) was synthesized in fairly good yield (58% overall) from p-aminophenol.

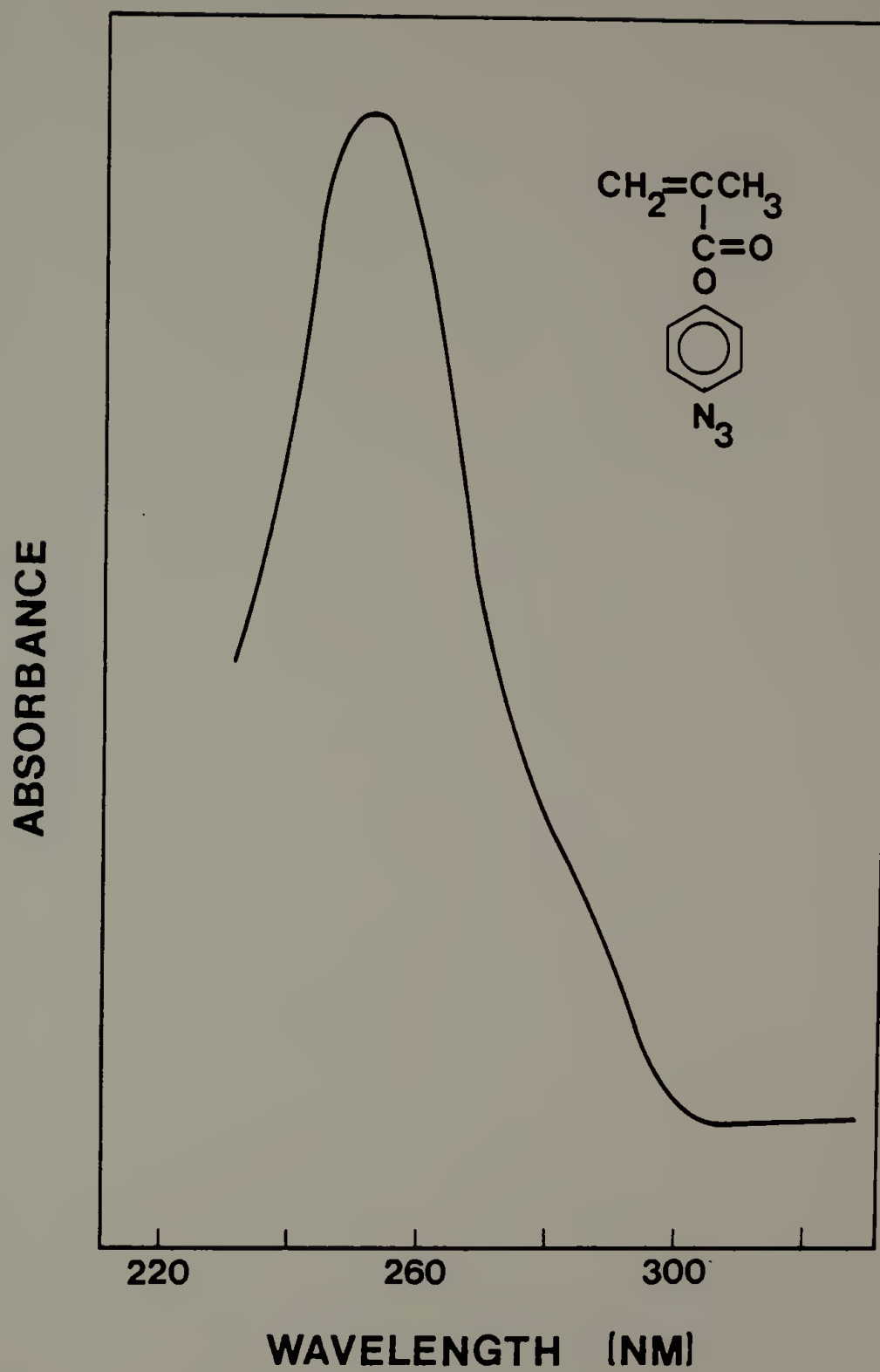




p-Azidophenol, a cherry red oil, was isolated for characterization, but the procedure was designed to avoid time consuming isolation steps, perhaps at the expense of the yield of APMA. APMA is thermally stable to 154°C, insensitive to shock and does not decompose in ordinary room light. Ultraviolet light at a wavelength of 250 nm readily decomposes APMA to the reactive nitrene species. The ultraviolet spectrum of the monomer is given in Figure 2.2. The above properties make APMA a good choice as a photoactive crosslinking agent and the model polymer is estimated to require 2 - 3% azide. The exact quantity can be adjusted after finding the efficiency of the crosslinking reaction in dilute, aqueous solution.



Figure 2.2. The ultraviolet spectrum of APMA:  $\lambda_{\text{max}} = 250 \text{ nm}$ ,  $\epsilon = 1.29 \times 10^4 \text{ M}^{-1} \text{ cm}^{-1}$ .



### References

1. Methyl p-vinylbenzenesulfonate can be distilled over  $\text{CuCl}_2$  under high vacuum. Private communication B. Vanzo, R.W. Lenz.
2. Iron analysis was routinely low even for hemin before the reaction. Best analysis results were obtained after combustion of sample followed by acid digestion at the boiling point for 5 hr.
3. The reactivity in polymerization is thoroughly discussed in Chapter III.
4. Private communication L.C. Dickinson (1979). These techniques are discussed in Chapter V.
5. Adapted from: Inskeep, G.E.; Deanin, R. J. Am. Chem. Soc., (1947), 69, 2237.
6. Adapted from: Spinner, I.H.; Ciric, J.; Graydon, W.F. Can. J. Chem., (1954), 32, 144.
7. Private communication B. Vanzo, R.W. Lenz.
8. Gritsai, N.I.; Prib, O.A. J. Org. Chem.-USSR, (1967), 3, 1554.
9. Kataoka, K.; Tsuruta, T. Makromol. Chem., (1978), 179, 1431.
10. Salamone, J.C.; Matimud, M.U.; Watterson, A.C.; Olson, A.P.; Ellis, E.J. J. Polym. Sci.: Polym. Chem. Ed., (1982), 20, 1153.
11. All chemical modification of polymers is described in Chapter V.
12. Wessling, R.A.; Pickelman, D.M. J. Dispersion Sci. Tech., (1981), 2, 281.
13. Buckingham, J. (ed.) Dictionary of Organic Compounds 5th Ed., 4, M00961 p. 3749, Chapman and Hall, New York (1982).
14. Traylor, T.G.; Chang, C.K.; Geibel, T.; Berzinis, A.; Mincey, T.; Cannon, J. J. Am. Chem. Soc., (1979), 101(22), 6716.

15. Tsuchida, E.; Nishide, H.; Sato, Y.; Kaneda, M. Bull. Chem. Soc. Jpn., (1982), 55, 1890.
16. These experiments are discussed in Chapter VI.
17. Gillis, J. Senior Honors Thesis, University of Massachusetts 1980.
18. Aldrich Technical Information, 19,337-2, 1976.
19. Stahl, G.L.; Walter, R.; Smith, C.W. J. Org. Chem., (1978), 43, 2285.
20. Lundt, B.F.; Johansen, N.L.; Volund, A.; Markussen, J. Int. J. Pept. Protein Res., (1978), 12, 258.
21. Lott, R.S.; Chauhan, V.S.; Stammer, C.H. J. Chem. Soc. Chem. Commun., (1979), 495.
22. Tsuji, T.; Kataoka, T.; Yoshioka, M.; Sendo, Y.; Nishitani, Y.; Hirai, S.; Maeda, T.; Nagata, W. Tetrahedron Lett., (1979), 2793.
23. Please see Chapter VIII for the experimental techniques used in obtaining this spectra.
24. Private communication, M. Fazio, Dow Chemical Co.
25. Ogata, N.; Yoshikaw, M. J. Synth. Org. Chem. Jpn., (1982), 40(10), 939.
26. For a review see: Patai, S. (ed.) The Chemistry of the Azido Group, Wiley Interscience, New York, 1971.
27. Smith, P.A.; Brown, B.B. J. Am. Chem. Soc., (1951), 73, 2440.
28. Roberts, R.M.; Gilbert, J.C.; Rodewalt, L.B.; Wingrove, A.S. Modern Experimental Organic Chemistry, Holt, Rinehart, Winston Inc., New York (1974), p. 319.
29. Logothetis, A.L. J. Am. Chem. Soc., (1965), 84(4), 749.

## C H A P T E R   I I I

### COPOLYMERIZATION

The synthesis of a vinyl polymer with five different comonomers requires an understanding of monomer and radical reactivity in order to make polymers of a desired composition. The determination of reactivity ratios is a simple way to characterize the reactivity of a pair of monomers. If one assumes that the reactivity of the propagating free radical only depends on the monomer unit at the end of the chain, then:



where  $PM_i \cdot$  represent the growing polymer chain and  $M_i$  are the unreacted monomers in solution. The rate of reaction of the two monomers with the growing radical is equal to the rate of incorporation into the polymer chain.

$$-\frac{d[M_1]}{dt} = k_{11}[PM_1 \cdot][M_1] + k_{21}[PM_2 \cdot][M_1] \quad (3.5)$$

$$-\frac{d[M_2]}{dt} = k_{12}[PM_1^\cdot][M_2] + k_{22}[PM_2^\cdot][M_2] \quad (3.6)$$

The reactivity ratios ( $r_1$ ,  $r_2$ ) are defined as the rate of homopropagation versus the rate of crosspropagation,

$$r_1 = \frac{k_{11}}{k_{12}} \quad \text{and} \quad r_2 = \frac{k_{22}}{k_{21}} \quad (3.7).$$

Assuming that under steady state conditions  $k_{21}[PM_2^\cdot][M_1] = k_{12}[PM_1^\cdot][M_2]$  and combining Equations 3.5, 3.6 and 3.7, one can obtain the familiar copolymerization equation:

$$\frac{d[M_1]}{d[M_2]} = \frac{[M_1](r_1[M_1] + [M_2])}{[M_2](r_2[M_2] + [M_1])} \quad (3.8).$$

After defining  $x = M_1/M_2$  and  $y = d[M_1]/d[M_2]$ , Equation 3.8 may be rewritten as

$$y = (x) \frac{1 + r_1 x}{r_2 + x} \quad (3.9).$$

Equation 3.9 was recast to a linearized form by Fineman and Ross<sup>1</sup> to give:

$$r_2 = r_1 x^{2/y} - \frac{x(y-1)}{y} \quad (3.10)$$

Plotting of appropriate quantities in Equation 3.10 gives  $r_1$  as the



slope and  $r_2$  as the intercept.

Fineman-Ross treatment of experimental data is unequally weighted and heavily influenced by data at low  $[M_2]$ . The calculated values of  $r_1$  and  $r_2$  may depend on the arbitrary assignment of  $[M_1]$  and inversion of the data (reassignment of  $[M_1] \longleftrightarrow [M_2]$ ) may not yield identical results.<sup>2,3</sup>

Another linear, more balanced method has been suggested by Yezrielev, Brokhina and Roshin,<sup>4</sup> but it lacks the capacity to treat the data by a simple graphical technique. Kelen and Tüdös<sup>5</sup> devised a new equation which offers a simple method for graphical determination which equally weights the experimental data. If

$$G = \frac{x(y-1)}{y} \quad \text{and} \quad F = x^2/y \quad (3.11)$$

then

$$\frac{G}{\alpha + F} = (r_1 + \frac{r_2}{\alpha}) \frac{F}{\alpha + F} - \frac{r_2}{\alpha} \quad (3.12)$$

where  $\alpha$  is a spacing parameter (a constant) which is used to give a good distribution of data. If  $\eta = G/\alpha + F$  and  $\xi = F/\alpha + F$ , then Equation 3.12 may be rewritten as follows:

$$\eta = r_1 \xi - \frac{r_2}{\alpha} (1 - \xi) \quad (3.13).$$

The value of  $\xi$  varies from  $\xi = 0$  to  $\xi = 1$ . A plot of  $\eta$  versus  $\xi$  gives a straight line with  $-r_2/\alpha$  and  $r_1$  equal to the intercepts at  $\xi = 0$  and  $\xi = 1$  respectively. The value of  $\alpha$  may be chosen from the smallest and largest values of  $F$ ,

$$\alpha = \sqrt{F_{\min} F_{\max}} \quad (3.14)$$

However, the best choice of  $\alpha$  depends on the judgement of the experimenter and does not influence the value of  $r_1$  and  $r_2$ .

In our model of hemoglobin, the composition of the polymer was estimated to be 65 - 75% styrene, 15 - 20% of a hydrophilic monomer, 0.5% of a heme monomer, 5 - 10% of an amine monomer and 2 - 3% azide. To assess polymer composition in a pentapolymer ten different sets of reactivity ratios would be needed. A change of one of the components would require the determination of four new pairs of reactivity ratios. The coreactivity of each component with styrene was studied because styrene is a major component in the model polymer. Ultimately this was all that was needed to estimate the composition of ter- and tetrapolymers.<sup>6</sup> The reactivity of heme monomers is treated separately in Chapter IV.

### Experimental Procedure

The source of monomers is given in Chapter II. p-Vinylbenzylchloride (VBC) was purchased from Polysciences and distilled at reduced pressure, under nitrogen before use. The initiator, 2,2'-azobis(2-

methylpropionitrile) (AIBN), was purchased from Aldrich and was recrystallized from methanol. Reagent grade dimethylformamide (DMF) was stirred over potassium hydroxide for 12 hr and then distilled over barium oxide, with a nitrogen atmosphere, at a pressure (5 - 10 mm) which allowed the DMF to boil between 45 - 70 °C. Pure solvent was stored over 3 Å and 4 Å molecular sieves, under a blanket of nitrogen, in the dark and remained odorless for at least two months.

All polymerizations were performed at 60°C using 0.3 - 1.0 mol % AIBN. DMF was selected as the reaction solvent because it is a good solvent for a wide range of polymers and monomers. Reaction vessels were either 25 ml Erlenmeyers sealed with a rubber septum or crown cap tubes with neoprene gaskets. Samples were degassed by two cycles of freeze, evacuation and thawing and then were blanketed with nitrogen. Reactions proceeded for approximately one hour and yields were less than 6%.

The polymers were purified by eluting each sample on a Biobeads SX2 column (30 x 2 cm) in benzene. (Biobeads SX2 have an exclusion volume of 2,000 Daltons, thus monomers and oligomers are retained by the pores and the polymer elutes cleanly.) Collected fractions (5 ml) were spotted on a TLC plate which was then developed in an iodine chamber. In general the polymer was found in fractions 4 - 6 and monomer in fractions 8 and higher. Polymer fractions were pooled in a tared, labeled flask and the benzene was removed in vacuo to yield a viscous liquid. Samples were frozen in crushed dry ice and the remaining benzene removed in vacuo over a 12 - 18 hr period. Freeze-dried

polymers were further dried at 60°C for 48 hr in vacuo.

Copolymers of styrene and methyl p-vinylbenzenesulfonate were not soluble in benzene at most MSS feeds and thus were precipitated first into methanol and then reprecipitated into petroleum ether. Copolymers were further dried at 60°C for 48 hr in vacuo.

Polymer composition was determined by elemental analysis for C, H and N.

The experimental details for each pair of reactivity ratios are given in Tables 3.1- 3.5.

### Results and Discussion

#### Copolymerization of [S]/[APMA]

Data for the analysis of  $r_1$  and  $r_2$  in the copolymerization of styrene and p-azidophenyl methacrylate is given in Table 3.6. A Fineman-Ross plot of the data is linear at low to moderate concentrations of APMA in the feed mixture (up to 40% APMA) with a slope = 1.80 and intercept = -0.083 (Figure 3.1). By examining the Fineman-Ross plot one finds that the spacing between points on both the x and y axis increases with increasing  $[M_1]$  and thus the slope and intercept are heavily weighted by  $[M_2]$ . It was observed that re-indexing  $[M_1] = S$  and  $[M_2] = APMA$  gave a curve that had a maximum and thus was meaningless.

The experimental data was replotted using Kelen-Tüdös's method and the curve has a maximum at  $\xi = 0.71$  (Figure 3.2). This corresponds to approximately 75% APMA in the copolymer. Non-linearity in the first-order Markov copolymerization equation (3.8) may be caused by failure in

Table 3.1

Experimental Parameters in the Copolymerization of p-Azidophenyl  
Methacrylate ( $M_1$ ) and Styrene ( $M_2$ )<sup>a,b</sup>

Sample Number (S/APMA)	$[M_1]$ (Feed Mol %)	% Conversion	$d[M_1]$ (Polymer Mol %)	$x$ ( $M_1/M_2$ )	$y$ ( $d[M_1]/d[M_2]$ )
99/1	1.0	2.14	9.2	0.010	0.102
90/10	10.4	3.63	41.4	0.117	0.706
80/20	19.2	2.70	51.5	0.237	1.060
70/30	30.3	3.49	60.1	0.435	1.504
60/40	39.2	3.59	65.8	0.644	1.921
50/50	49.9	3.52	70.9	0.997	2.436
40/60	58.4	4.60	73.4	1.404	2.764
25/75	73.1	5.15	77.7	2.715	3.494
10/90	89.5	--	86.1	8.515	6.174

<sup>a</sup>Reaction mixture contained 65 vol % DMF and 0.3 mol % AIBN.

<sup>b</sup>Reaction proceeded for 75 min.

Table 3.2

Experimental Parameters in the Copolymerization of N-tert-butoxy-carbonyl-2-aminoethyl methacrylate ( $M_1$ ) and Styrene ( $M_2$ )<sup>a,b</sup>

Sample Number (S/BAEMA)	$[M_1]$ (Feed Mol %)	% Conversion	$d[M_1]$ (Polymer Mol %)	$x$ ( $M_1/M_2$ )	$y$ ( $d[M_1]/d[M_2]$ )
99/1	1.0	1.37	6.0	0.010	0.639
80/20	20.0	6.82	43.4	0.250	0.715
70/30	30.0	2.76	53.6	0.437	1.149
60/40	39.2	2.56	63.0	0.646	1.703
50/50	50.0	3.57	68.0	1.000	2.119
40/60	58.5	1.37	78.3	1.409	3.614
30/70	68.3	3.94	78.0	2.150	3.540
10/90	89.5	5.88	89.7	8.500	8.737

<sup>a</sup>Reaction mixture contained 65 vol % DMF and 0.3 mol % AIBN.

<sup>b</sup>Reaction proceeded for 60 min.



Table 3.3

Experimental Parameters in the Copolymerization of N-tert-butyloxy-carbonyl-N'-(2-methacrylyl)-1,6-diaminohexane ( $M_1$ ) and Styrene ( $M_2$ )<sup>a,b</sup>

Sample Number (S/BNAHD)	$[M_1]$ (Feed Mol %)	% Conversion	$d[M_1]$ (Polymer Mol %)	$\bar{x}$ ( $M_1/M_2$ )	$\bar{y}$ ( $d[M_1]/d[M_2]$ )
90/10	9.0	3.11	13.4	0.099	0.155
80/20	18.0	2.26	21.1	0.219	0.284
70/30	26.8	1.73	36.7	0.366	0.531
50/50	50.4	1.18	61.6	1.015	1.604
40/60	57.1	1.21	63.6	1.333	1.745
25/75	75.0	0.27	90.1	3.008	9.070
10/90	90.1	0.46	91.7	9.140	11.010

<sup>a</sup>Reaction mixture contained 65 vol % DMF and 1.0 mol % AIBN.

<sup>b</sup>Reaction proceeded for 60 min.

Table 3.4

Experimental Parameters in the Copolymerization of Styrene ( $M_1$ )  
and Methyl p-vinylbenzenesulfonate ( $M_2$ )<sup>a</sup>

Sample Number (S/MSS)	$[M_2]$ (Feed Mol %)	% Conversion	$d[M_2]$ (Polymer Mol %)	$\bar{x}$ ( $M_1/M_2$ )	$\bar{y}$ ( $d[M_1]/d[M_2]$ )
99/1 <sup>b</sup>	1.0	4.14	8.2	97.96	11.13
90/10 <sup>b</sup>	10.7	1.88	50.6	8.34	0.977
82/18 <sup>c</sup>	18.1	5.39	59.0	4.53	0.696
76/24 <sup>c</sup>	24.7	0.55	63.3	3.05	0.579

<sup>a</sup>Reaction mixture contained 75 vol % DMF and 1.0 mol % AIBN.

<sup>b</sup>Reaction proceeded for 60 min.

<sup>c</sup>Reaction proceeded for 40 min.

Table 3.5

Experimental Parameters in the Copolymerization of p-Vinylbenzyl-  
chloride ( $M_1$ ) and Styrene ( $M_2$ )<sup>a,b</sup>

Sample Number (S/VBC)	$[M_1]$ (Feed Mol %)	% Conversion	$d[M_1]$ (Polymer Mol %)	$x$ ( $M_1/M_2$ )	$y$ ( $d[M_1]/d[M_2]$ )
90/10	10.0	5.08	22.5	0.111	0.291
80/20	20.0	4.52	34.8	0.250	0.533
70/30	30.0	4.42	44.3	0.429	0.797
60/40	40.0	5.04	54.3	0.667	1.188
50/50	50.0	6.08	60.7	1.000	1.547
40/60	60.0	5.77	72.6	1.491	2.644

<sup>a</sup>Reaction mixture contained 35 vol % DMF and 0.3 mol % AIBN.

<sup>b</sup>Reaction proceeded for 60 min.

Table 3.6

Data for Reactivity Ratio Analysis with  $M_1 = \text{APMA}$ , $M_2 = \text{Styrene}$  and  $\alpha = 0.2$ 

Sample Number (S/APMA)	F	G	$\xi$	$\eta$
99/1	0.0001	-0.0918	0.0005	-0.450
90/10	0.0192	-0.0481	0.0876	-0.014
80/20	0.0529	0.0134	0.2092	0.053
70/30	0.1258	0.1458	0.3860	0.448
60/40	0.2157	0.3085	0.519	0.742
50/50	0.4082	0.5878	0.617	0.966
40/60	0.7134	0.8960	0.781	0.981
25/75 <sup>a</sup>	0.1097	1.938	0.913	0.839
10/90 <sup>a</sup>	11.744	7.136	0.983	0.597

<sup>a</sup>Data not included in Figure 3.1 to show linear region with more detail.  
Curvature continues smoothly.

Figure 3.1. A Fineman-Ross plot for the copolymerization of APMA ( $M_1$ ) and styrene ( $M_2$ ): slope = 1.80, intercept = -0.083.

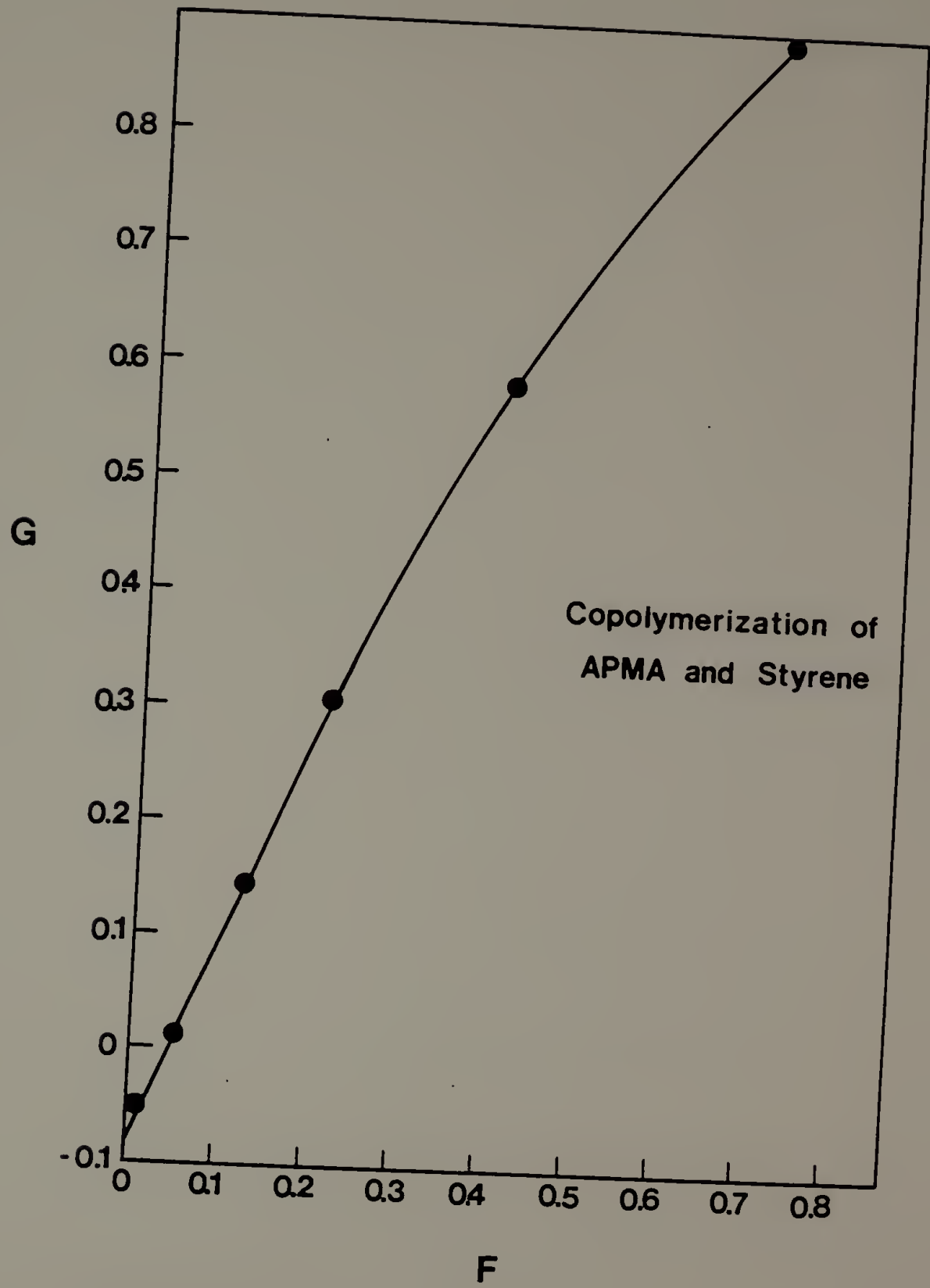
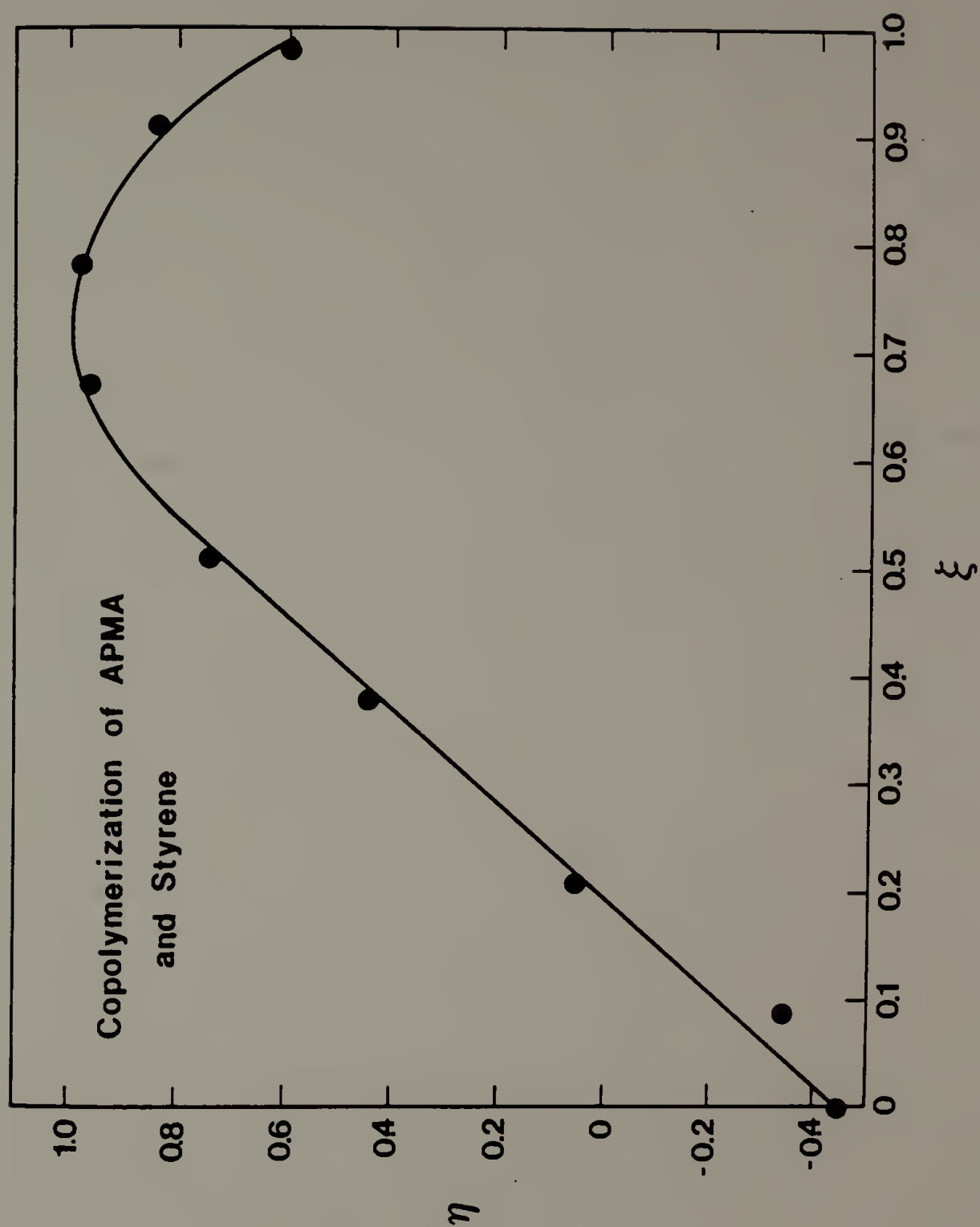




Figure 3.2. A Kelen-Tüdös plot for the copolymerization of APMA ( $M_1$ ) and styrene ( $M_2$ ),  $\alpha = 0.22$ .



the assumption that radical reactivity is determined by the identity of the last unit on the growing chain or in treating the propagation reaction as an irreversible process.

Second-order Markovian behavior is manifested in radical copolymerizations where monomers contain highly bulky or polar substituents. One must consider the effect of the penultimate unit on the propagation of the growing chain thus there are four different radicals:  $PM_1M_1^\cdot$ ,  $PM_1M_2^\cdot$ ,  $PM_2M_2^\cdot$  and  $PM_2M_1^\cdot$ , eight rate constants:  $k_{111}$ ,  $k_{112}$ ,  $k_{221}$ ,  $k_{222}$ ,  $k_{211}$ ,  $k_{212}$ ,  $k_{121}$ , and  $k_{122}$ , with four reactivity ratios  $r_1 = k_{111}/k_{112}$ ,  $r_2 = k_{222}/k_{221}$ ,  $r_1' = k_{211}/k_{212}$  and  $r_2' = k_{122}/k_{121}$ .<sup>8-10</sup>

The 'penultimate effect' for styrene copolymerized with bulky methacrylates has been studied by Rounsfell and Pittman.<sup>11</sup> They attributed the penultimate effect to the steric crowding of the methacrylates and  $r_1'$  was larger than  $r_1$  ( $[M_1] = 2,3,4$ -trimethyl-3-pentylmethacrylate). When styrene was the penultimate unit the reactivity of  $[M_1]$  and  $[M_2]$  was determined by their polarity and resonance stabilization. However, when  $[M_1]$  was the penultimate unit and styrene the terminal unit the polymer radical preferred to add styrene. This effect was even more pronounced when both the penultimate and terminal unit were the bulky methacrylates.

The conclusions of Rounsfell and Pittman suggest that a steric penultimate effect is a good explanation for the curvature observed in Figures 3.1 and 3.2. At high APMA feeds less APMA is incorporated into the copolymer than one would predict from the data at low feeds. At low

APMA feeds,  $r_2 = 0.083$ , styrene prefers crosspropagation by a factor of 12 and APMA prefers homopropagation by a factor of 1.8.

It is interesting to examine the statistical sequence length of a sample which has first-order Markovian behavior but is near the critical region where curvature begins. If one defines the number average sequence length  $\bar{n}$  as follows:<sup>12</sup>

$$\bar{n}_i = \frac{r_i[M_i] + [M_j]}{[M_j]} \quad (3.15)$$

then  $\bar{n}_1 = 2.16$  and  $\bar{n}_2 = 1.13$  for S40/60APMA. The next sample, S50/50APMA has  $\bar{n}_1 = 2.79$  and  $\bar{n}_2 = 1.08$ . Clearly the curvature begins where three consecutive APMA units are added to the polymer chain ( $\bar{n}_1 = 3$ ).

Fortuitously, the use of APMA as a photocrosslinking agent requires no more than 2 - 3% APMA in the model polymer thus the linear region of the Kelen-Tüdös and Fineman-Ross plots allows the estimation of  $r_1$  and  $r_2$ . For the copolymerization of S[M<sub>2</sub>]/APMA[M<sub>1</sub>],  $r_1 = 1.80$  and  $r_2 = 0.083$  with an error of approximately 10%.

#### Copolymerization of S/BAEMA

Data for the analysis of  $r_1$  and  $r_2$  in the copolymerization of styrene and N-tert-butyloxycarbonyl-2-aminoethyl methacrylate is given in Table 3.7. The Fineman-Ross plot appears to be fairly linear but the point S10/90BAEMA was omitted to give greater accuracy at low BAEMA feeds (Figure 3.3). Re-indexing of the monomers (i.e. S = [M<sub>1</sub>], BAEMA = [M<sub>2</sub>]) yields a curve with a maximum which again illustrates problems

Table 3.7

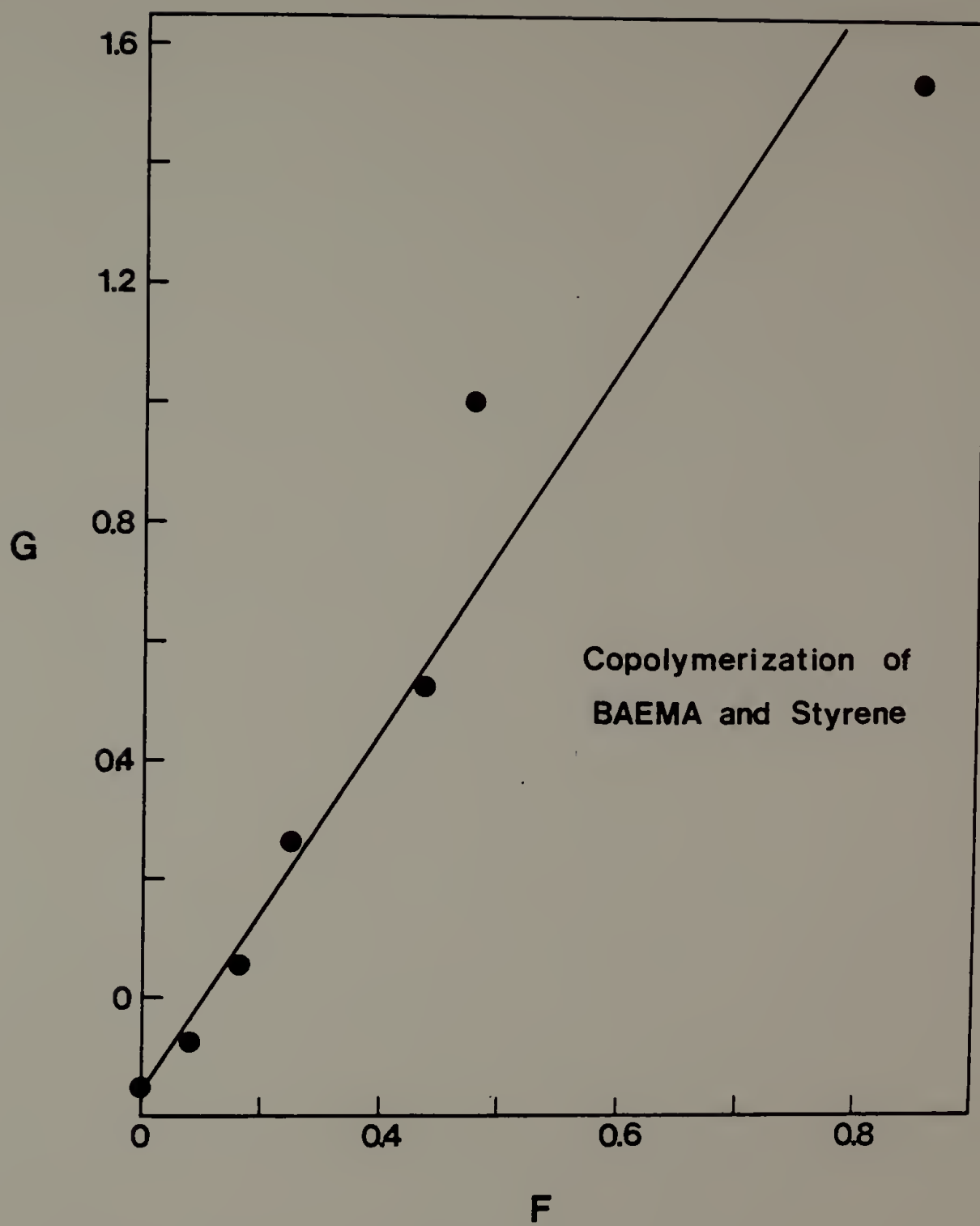
Data for Reactivity Ratio Analysis with  $M_1 = \text{BAEMA}$ , $M_2 = \text{Styrene}$  and  $\alpha = 0.55$ 

Sample Number (S/BAEMA)	F	G	$\xi$	$\eta$
99/1	0.0017	-0.1522	0.003	-0.276
80/20	0.0815	-0.0760	0.129	-0.120
70/30	0.1659	0.0567	0.232	0.079
60/40	0.2449	0.2665	0.308	0.335
50/50	0.4719	0.5280	0.462	0.517
40/60	0.5493	1.019	0.500	0.927
30/70	1.3024	1.544	0.703	0.833
10/90 <sup>a</sup>	8.2690	7.522	0.938	0.853

<sup>a</sup>Point omitted from Fineman-Ross plot to give detail at points of low BAEMA feed.

Figure 3.3. A Fineman-Ross plot for the copolymerization of BAEMA ( $M_1$ ) and styrene ( $M_2$ ): slope = 1.316, intercept = -0.15.





with the Fineman-Ross method. The slope and intercept give an  $r_1 = 1.32$  and  $r_2 = 0.15$  in the linear region of the data.

The Kelen-Tüdös plot is linear from 0 - 50% BAEMA in the feed (to approximately 78% in the polymer) but then it curves (Figure 3.4). The curvature is evidence for a penultimate effect caused by the bulky methacrylate monomer, BAEMA. Calculating the statistical sequence length for S50/50BAEMA near the region of curvature yields  $\bar{n}_1 = 2.32$  (BAEMA) and  $\bar{n}_2 = 1.12$  (S). At approximately 70% BAEMA in the feed,  $\bar{n}_1 = 3.84$  and  $\bar{n}_2 = 1.07$ . The curvature begins where one would predict three methacrylate units to be added in a row.

The model of hemoglobin was estimated to require 5 - 10% of the amine monomer thus the curvature was not problematic for our purposes.

#### Copolymerization of S/BNAHD

Data for the reactivity ratio plots of styrene and N-tert-butyloxycarbonyl-N'-(2-methacrylyl)-1,6-diaminohexane is given in Table 3.8. A Kelen-Tüdös plot of the data is linear with an intercept of  $r_2/\alpha = -0.85$  at  $\xi = 0$  and  $r_1 = 1.17$  at  $\xi = 1$  (Figure 3.5). This gives  $r_1 = 1.17$  and  $r_2 = 0.62$  where  $\alpha = 0.69$ .

The copolymerizability of BNAHD and styrene can be compared to BAEMA/styrene. At low methacrylyl derivative feeds, the reactivities of BNAHD and BAEMA are very similar. The differences can be attributed to the amide versus ester functionality in conjugation with the vinyl group. BAEMA is a slightly more reactive monomer than BNAHD. At high feeds, BNAHD does not exhibit any penultimate effects. Probably, the hexane unit between the amide and the t-butyloxycarbonyl group prevents

Figure 3.4. A Kelen-Tüdös plot for the copolymerization of BAEMA  
( $M_1$ ) and styrene ( $M_2$ ),  $\alpha = 0.55$ .

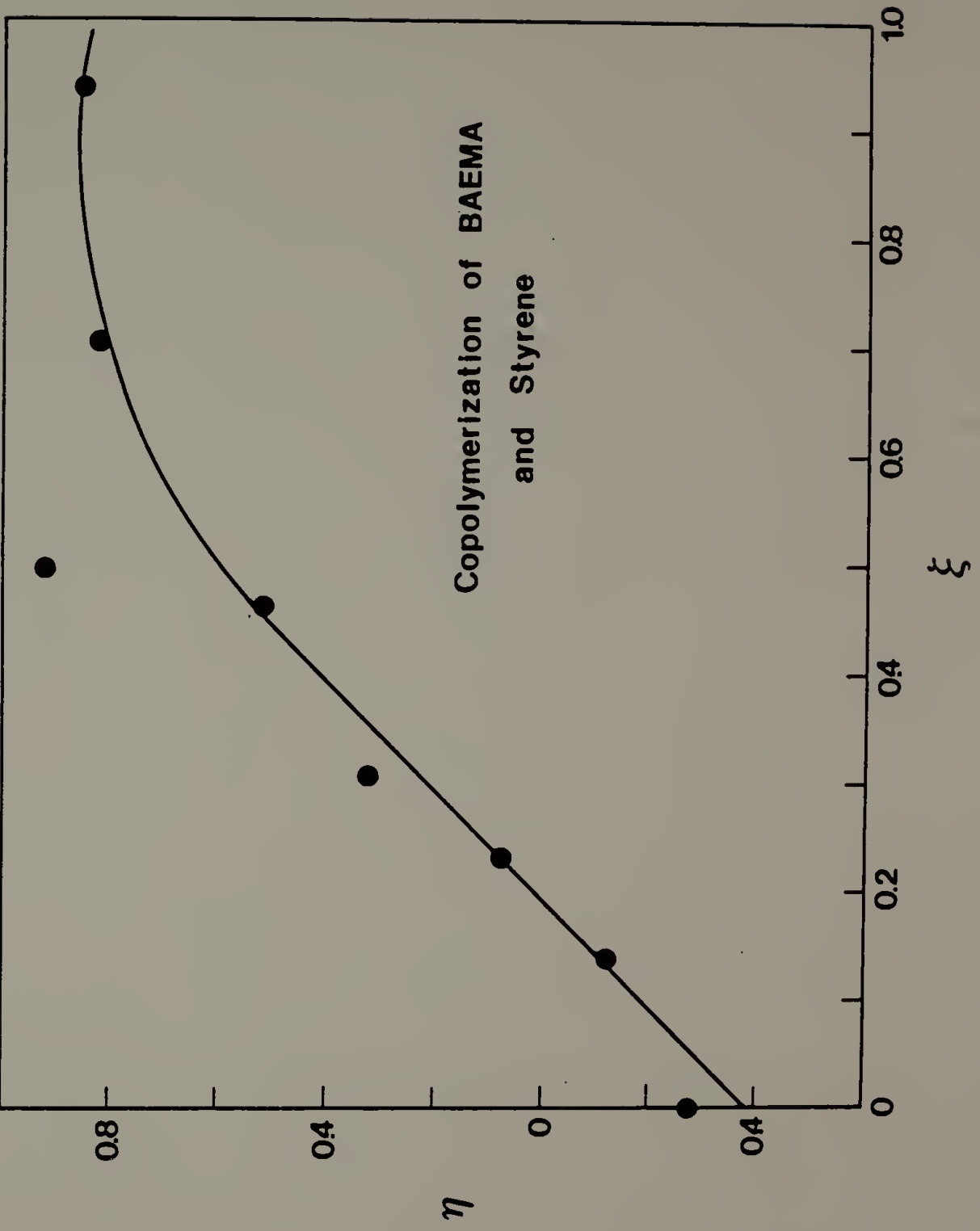


Table 3.8

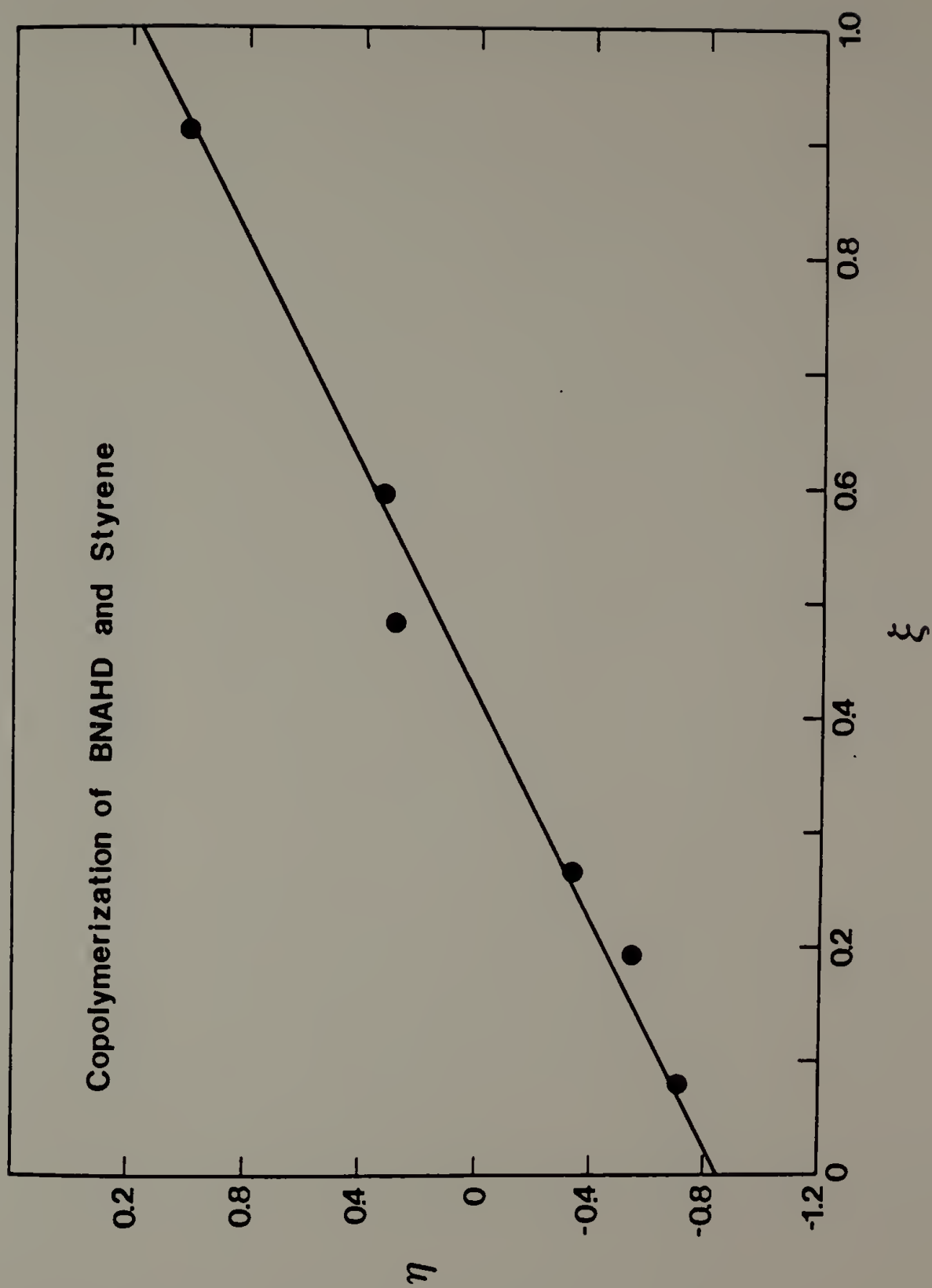
Data for Reactivity Ratio Analysis with  $M_1 = \text{BNAHD}$ , $M_2 = \text{Styrene}$  and  $\alpha = 0.69$ 

Sample Number (S/BNAHD)	F	G	$\xi$	$\eta$
90/10	0.064	-0.541	0.084	-0.717
80/20	0.169	-0.551	0.196	-0.551
70/30	0.252	-0.323	0.267	-0.342
50/50	0.642	0.382	0.481	0.287
60/40	1.018	0.569	0.595	0.333
25/75 <sup>a</sup>	0.998	2.676	0.590	1.584
10/90	7.535	8.309	0.916	1.010

<sup>a</sup>Data omitted from plot in Figure 3.5

Figure 3.5. A Kelen-Tüdös plot for the copolymerization of BNAHD ( $M_1$ ) and styrene ( $M_2$ ),  $\alpha = 0.69$ .





the blocking groups from being crowded together and causing steric hindrance in the polymerization process.

#### Copolymerization of S/MSS

The copolymerization of styrene and methyl p-vinylbenzenesulfonate was quite difficult experimentally: methyl p-vinylbenzenesulfonate was difficult to prepare in pure form. Copolymers were not soluble in benzene and thus had to be purified by reprecipitation. Polymers with modest amounts of MSS (40%) were only soluble in DMF. DMF, a strongly solvating, high boiling solvent, didn't allow the polymers to precipitate cleanly and was difficult to remove in vacuo. These copolymers had detectable quantities of nitrogen by elemental analysis (up to 2% N) which was attributed to residues of DMF trapped during precipitation of the copolymers. Thus only feed ratios up to 25% MSS were reliable for reactivity ratio analysis. Data for the calculation of reactivity ratios is given in Table 3.9.

A Fineman-Ross plot of the data is given in Figure 3.6. The data is linear with  $r_1 = 0.037$  and  $r_2 = 2.89$ . A Kelen-Tüdös plot (Figure 3.7) shows two possible lines for the reactivity ratios. Including the point S99/1MSS yields a line with  $r_1 = 0.10$  and  $r_2 = 4.12$ . Excluding this point,  $r_1 = 0.04$  and  $r_2 = 2.85$ . With such a small number of points at only one end of the scale of composition there is significant uncertainty in the reactivity ratio data. Errors in the concentration of MSS in the S99/1MSS sample feed could have caused significant deviation in the resulting polymer composition, especially since MSS is much more reactive than styrene. The reactivity ratios are estimated to

Table 3.9

Data for Reactivity Ratio Analysis with  $M_2 = \text{Styrene}$ , $M_2 = \text{MSS}$  and  $\alpha = 25$ 

Sample Number (S/MSS)	F	G	$\xi$	$\eta$
99/1 <sup>a</sup>	862.21	89.16	0.973	0.100
90/10	71.36	-0.196	0.740	-0.002
82/28	29.44	-1.976	0.540	-0.036
76/24	16.08	-2.215	0.342	-0.054

<sup>a</sup>Data omitted from Fineman-Ross plot.

Figure 3.6. A Fineman-Ross plot for the copolymerization of styrene ( $M_1$ ) and MSS ( $M_2$ ): slope = 0.037, intercept = -2.89.

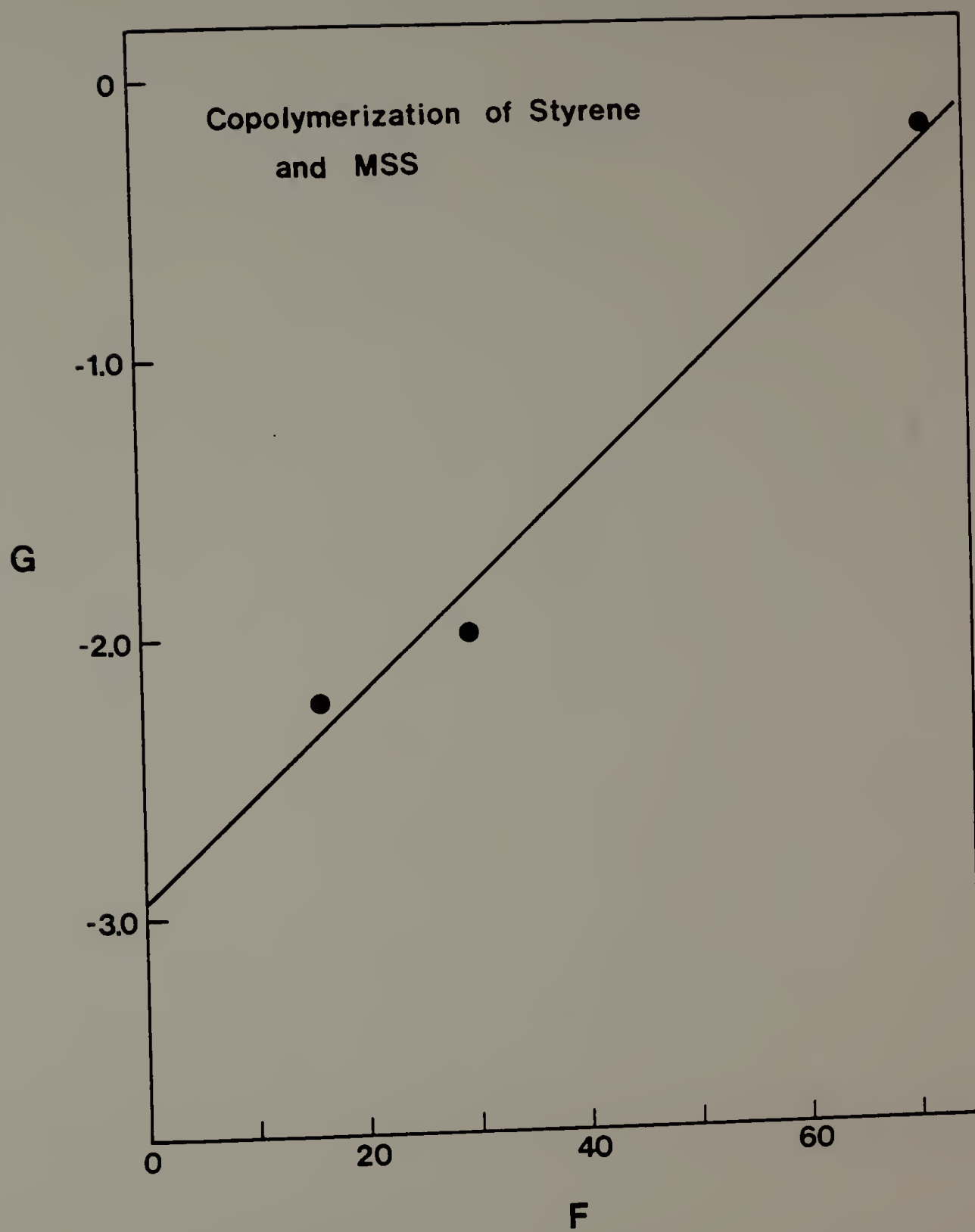
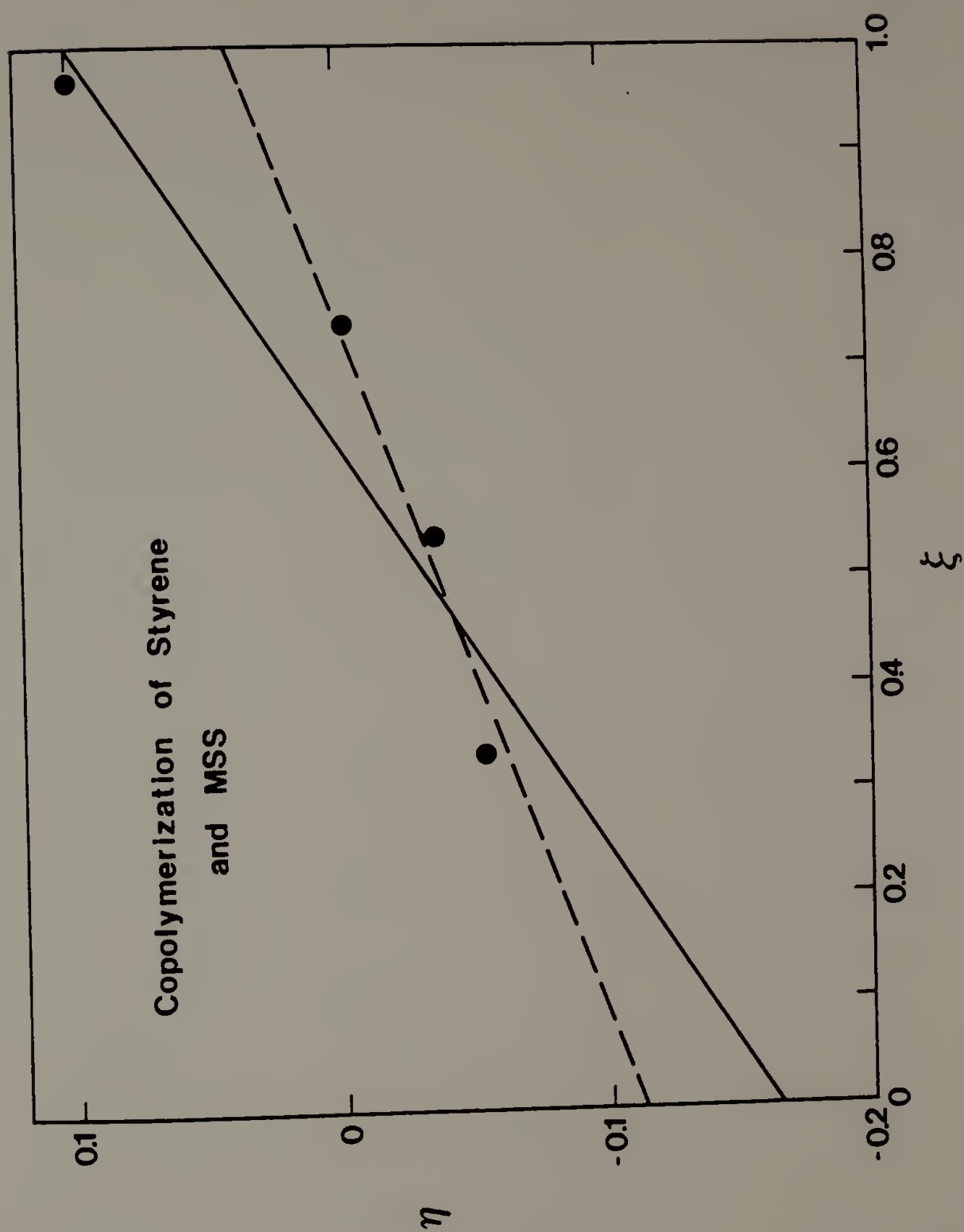


Figure 3.7. A Kelen-Tüdös plot for the copolymerization of styrene ( $M_1$ ) and MSS ( $M_2$ ),  $\alpha = 25.0$ .





be  $r_1 = 0.1 \pm 0.05$  and  $r_2 = 2.90 \pm 1.2$ . Vanzo and Lenz<sup>14</sup> determined the reactivity ratios in bulk and reported  $r_1 = 0.30$  and  $r_2 = 1.4$ . The difference in  $r_1$  and  $r_2$  values might be due to a solvent effect or impurities in the [MSS].

#### Copolymerization of S/VBC

The copolymerization of styrene and p-vinylbenzylchloride was trouble-free and data for reactivity ratio calculations is shown in Table 3.10. A Kelen-Tüdös plot yields  $-r_2/\alpha = 1.85$  at  $\xi = 0$  ( $\alpha = 0.19$ ) and  $r_1 = 1.20$  at  $\xi = 1.0$  (Figure 3.8). Thus  $r_1 = 1.20$  and  $r_2 = 0.35$ .

#### Conclusions

A summary of the monomer reactivities obtained experimentally as well as those useful in later parts of this dissertation are given in Table 3.11. The Alfrey-Price<sup>15</sup> parameters have been calculated from the reactivity ratios.

$$r_1 = Q_1/Q_2 \exp[-e_1(e_1 - e_2)] \quad (3.16)$$

$$r_2 = Q_2/Q_1 \exp[-e_2(e_2 - e_1)] \quad (3.17)$$

In Equations 3.16 and 3.17,  $Q_i$  is a measure of the reactivity of the monomer and primarily describes resonance effects,  $e$  defines the polarity of the monomer and radical. Styrene is an arbitrary reference for the system with  $Q = 1$  and  $e = -0.80$ . The  $Q - e$  scheme is a qualitative basis to compare monomers and is semi-quantitative when

Table 3.10

Data for Reactivity Ratio Analysis  $M_1 = \text{VBC}$ , $M_2 = \text{Styrene}$  and  $\alpha = 0.19$ 

Sample Number (S/VBC)	F	G	$\xi$	$\eta$
90/10	0.042	-0.271	0.184	-1.171
80/20	0.117	-0.219	0.383	-0.716
70/30	0.231	-0.109	0.550	-0.195
60/40	0.374	0.156	0.665	0.276
50/50	0.646	0.354	0.774	0.345
40/60	0.841	0.927	0.817	0.901

Figure 3.8. A Kelen-Tüdő's plot for the copolymerization of VBC ( $M_1$ ) and styrene ( $M_2$ ),  $\alpha = 0.19$ .

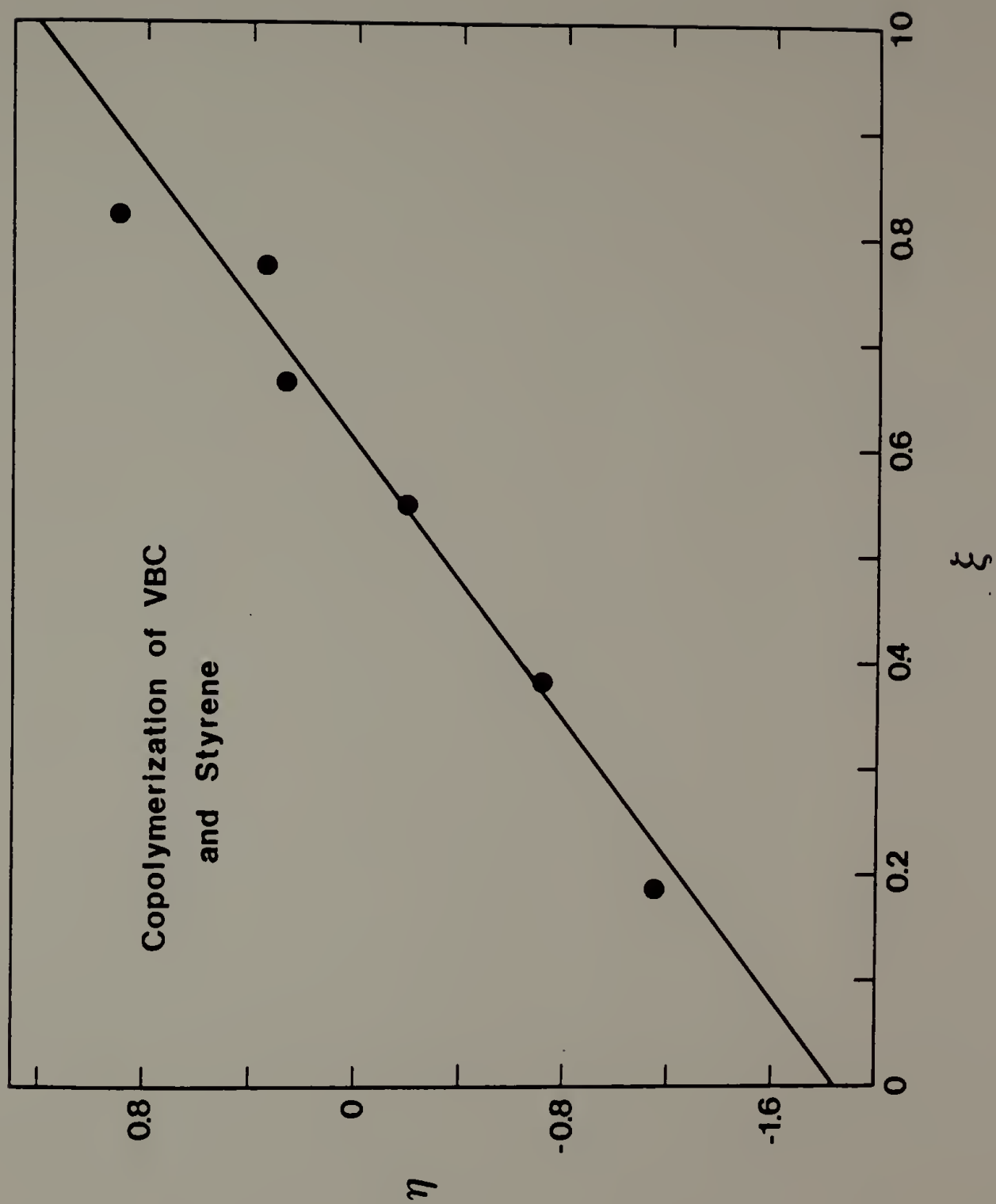


Table 3.11  
Summary of Monomer Reactivity

Monomer Pair ( $M_1/M_2$ )	$r_1$	$r_2$	Q	e
S/APMA <sup>a</sup>	0.083	1.8	3.74	0.55
S/BAEMA <sup>a</sup>	0.15	1.32	2.38	0.47
S/BNAHD	0.62	1.17	1.03	-0.23
S/MSS	0.1	2.7	---	---
S/VBC <sup>b</sup>	0.35	1.20	1.36	0.13
-----				
S/4VP <sup>b,16</sup>	0.54	0.70	1.00	-0.28
S/HDME <sup>17</sup>	0.012	78.6	70.0	-0.6
S/MMA <sup>b,16</sup>	0.52	0.46	0.74	0.40

<sup>a</sup>Deviation due to penultimate effect at high  $[M_2]$  feed.

<sup>b</sup>4VP, 4-vinylpyridine; VBC p-vinylbenzylchloride; MMA, methyl methacrylate.

styrene is the comonomer.

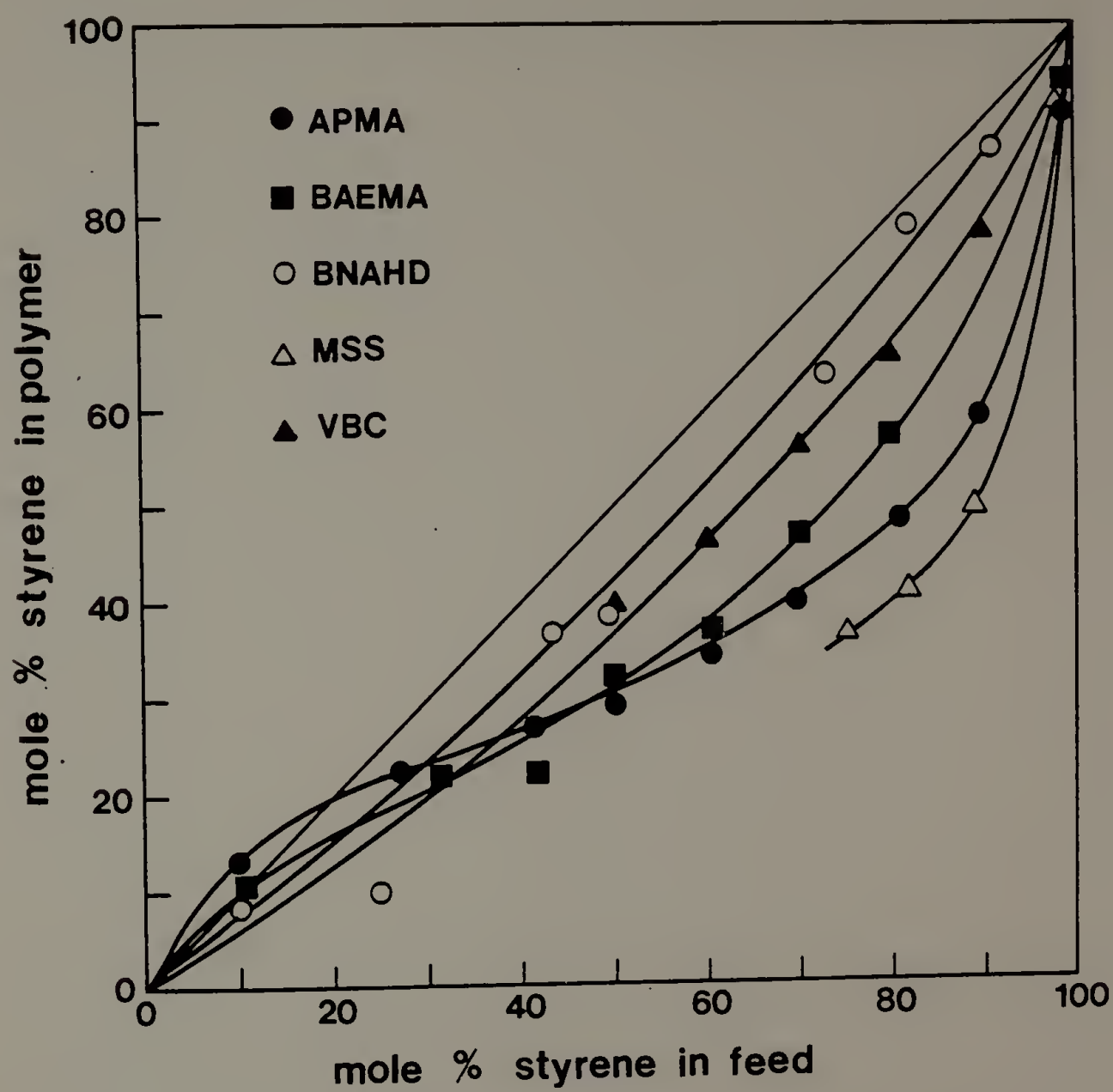
A plot of the feed of styrene in a reaction mixture versus the resultant copolymer composition demonstrates that styrene was the less reactive monomer in all the systems studied (Figure 3.9). In general methacrylates are more reactive than styrene because the highly electronegative carboalkoxy group causes the double bond to be relatively positive in character.<sup>18</sup> Although one would expect a methyl group to decrease the polarity of the double bond, methacrylates are more reactive than acrylates due to hyperconjugation of the methyl hydrogens. The higher reactivity of MSS and VBC could be due to enhanced resonance stabilization of the free radical.

Random placement of a monomer in the polymer chain occurs when the reactivity ratios are between 0.5 - 2.0. The reactivity of styrene in the monomer pairs studied is significantly less than the ideal value for random placement and in several pairs one would predict that styrene would prefer alternating placement in the polymer chain. Fortunately, the quantity of the other monomers in the feed to give the desired composition is quite small and styrene is the bulk of the feed mixture, 85 - 95%.

A particular concern is that heme groups have a random placement in the polymer chain to prevent dimerization to the  $\mu$ -oxo dimer. From Nishide's<sup>17</sup> estimate of the reactivity of the S/HDME monomer pair, (Table 3.11), the preference for homopolymerization of HDME is clear and adjacent hemes are an undesirable possibility. If  $[HDME] = [S]/1000$ , then one would predict  $\bar{n}_{HDME} = 1.079$  and  $\bar{n}_S = 13.18$  according to

Figure 3.9. Dependence of the copolymer composition,  $d[M_1]$ , on the mole percent styrene in the feed: (●) APMA; (■) BAEMA; (○) BNAHD; (△) MSS; (▲) VBC.





Equation 3.15. And, probability theory<sup>12</sup> predicts that two hemes would be found adjacent to one another in the polymer chain,  $P_{11}$ ;

$$P_{11} = \frac{r_1}{r_1 + [M_2]/[M_1]} = 0.07 \quad (3.16)$$

only 7.0% of the time. Thus, low concentrations of highly reactive monomers give more nearly random placement in the polymer chain.

The error in determining the reactivity ratios was no more than 10% with the exception of the copolymerization of S/MSS. Very accurate assessment of  $r_1$  and  $r_2$  required careful measurement of reactant feed and polymer yield. Yields had to be below 5% to make the assumption that the feed composition did not drift as monomers were incorporated into the polymer. Polymers had to be dried carefully to remove solvent and prevent anomalous results by elemental analysis. DMF is very difficult to use for reprecipitation of polymers and thus the Biobeads SX2 column had the advantage of cleanly removing unreacted monomers, initiators as well as the DMF solvent. Benzene was easy to remove from the polymers by freeze drying and values of carbon and nitrogen analysis were in good agreement. In general, carbon analysis gave greater accuracy for the determination of composition because the range of values differed by 30 - 34% carbon where nitrogen only varied by 6 - 20%.

### References

1. Fineman, M; Ross, S.D. J. Polym. Sci., (1950), 5, 259.
2. Tidwell, P.W.; Mortimer, G.A. J. Polym. Sci., (1965), A3, 369.
3. Tidwell, P.W.; Mortimer, G.A. J. Macromol. Sci.-Revs. Macromol. Chem., (1970), C4, 281.
4. Yezrielev, A.J.; Brokhina, E.L.; Roshin, Y.S. Vysokomol. Soedin, (1969), A(11), 1670.
5. Kelen, T.; Tüdő's, F. J. Macromol. Sci.-Chem., (1975), A9(1), 1.
6. A complete explanation is given in Chapter V.
7. General procedure from: Ito, T.; Otsu, T. J. Macromol. Sci.-Chem., (1969), A3(2), 177.
8. Mertz, E.; Alfrey, T.; Goldfinger, G. J. Polym. Sci., (1976), 1, 75.
9. Ham, G.E. J. Polym. Sci., (1960), 45, 169, 177, 183.
10. Ham, G.E. (ed.) Copolymerization, Interscience, New York (1964) p. 9.
11. Rounsfe'll, T.D.; Pittman, C.U. Jr. J. Macromol. Sci.-Chem., (1979), A13(2), 153.
12. Odian, G. Principles of Polymerization 2nd Ed., Wiley-Interscience Pub., New York, (1981), p.428.
13. For an estimation of the errors in the Kelen-Tüdő's method as well as guidelines for obtaining good experimental results: McFarlane, R.C.; Reilly, P.M.; O'Driscoll, K.F. J. Polym. Sci.-Polym. Chem. Ed., (1980), 18, 251, and references therein.

14. Vanzo, B.; Lenz, R.W. Private communication. Highly pure MSS was used and samples were only precipitated once. Reaction times were adjusted to give less than 10% yield. Composition was found by analysis for sulfur.
15. Alfrey, T. Jr.; Price, C.C. J. Polym. Sci., (1947), 2, 101; Reference 10, Chapter II.
16. Tanikado, T. J. Polym. Sci., (1960), 43, 489.
17. Nishide, H.; Shinohara, K.; Tsuchida, E. J. Polym. Sci.-Polym. Chem. Ed., (1981), 19, 1109.
18. Reference 10, p. 449.

C H A P T E R   I V

COPOLYMERIZATION OF STYRENE WITH FERROUS AND  
FERRIC PROTOPORPHYRIN IX DERIVATIVES AND THE  
EFFECT OF LIGAND COMPLEXATION<sup>1</sup>

Incorporation of a heme unit into the backbone of the polymer chain enhances polymer-heme interactions, which may provide the hydrophobic, sterically protected environment necessary to prevent oxidation of ferrous iron. Lautsch et al.<sup>2,3</sup> reported the first radical polymerization of protoporphyrin IX through the 2,4-vinyl groups. Protoporphyrins have been copolymerized with a variety of monomers with iron insertion subsequent to polymerization. The synthesis of these copolymers is difficult and strongly acidic conditions are necessary for iron insertion. Nishide and coworkers<sup>4</sup> attempted to define the polymerizability of hemin dimethylester (HDME) and concluded that HDME acts as a chain terminator in copolymerization with styrene but may be incorporated in the polymer chain when vinylimidazole is a termonomer. They proposed that termination occurs through a radical transfer from the vinyl group to the central iron atom. Castro et al.<sup>6</sup> have shown that free radical polymerization initiators undergo redox reactions with iron octaethylprophyrin in both the Fe(II) and Fe(III) states.

It appears that iron porphyrins can act as inhibitors of free radical polymerization; however, the mechanism of termination is unclear. The central objective of this chapter is to resolve the apparently conflicting observations of Nishide and Castro and propose a means to eliminate the termination reaction. The results presented show

the role of iron protoporphyrin derivatives as comonomers or retarders in free radical polymerization as a function of the number and type of axial ligand on the iron and the oxidation state.

### Experimental Procedure

Initiators, monomers and solvents were synthesized and purified as described in Chapters II and III.

#### Polymerizations

The same general copolymerization procedure was used throughout this work and is given below in detail for styrene and hemin dimethylester. Any variations in this procedure, methods of ligand addition, and oxidation or reduction are given subsequently.

In a polymerization tube with a side arm were placed 9.0 ml of styrene (0.078 mol), 18.0 ml of DMF, 0.045 g of AIBN ( $7.8 \times 10^{-4}$  mol), and 0.075 g of HDME ( $1.1 \times 10^{-4}$  mol). This tube was sealed with a crown cap and neoprene gasket and degassed by four cycles of freezing and evacuation followed by thawing. The vessel was filled with nitrogen and placed in a bath at 60°C. An aliquot was removed from the mixture by syringe at 1 hr intervals under a steady nitrogen stream. A 2.0 ml volume of this aliquot was eluted through a Biobeads SX2 column in benzene, which cleanly separated the copolymer from the unreacted monomers. This column purification method yielded ligand-free, oxidized iron prophyrin/styrene copolymers. The polymer fraction was freeze dried in a preweighed flask and then further dried at 60°C in vacuo for 48 hr.



Polymer composition was determined by UV/visible spectroscopy using a Cary 14 recording spectrophotometer. Two methods, which gave consistent results, were used. If sufficient polymer was obtained for accurate weighing, hemin content was found by Beer's law. Polymerization of the porphyrin vinyl group causes a shift in the Soret maximum from 388 to 383 nm for HDME (Figure 4.1). Extinction coefficients,  $\epsilon$ , were determined by weighing for the monomers and assumed to be equivalent with those in the polymer, with  $\epsilon_{388}(\text{Fe}^{\text{III}}\text{HDME}) = 90,000 \text{ M}^{-1} \text{ cm}^{-1}$  and  $\epsilon_{409}(\text{Fe}^{\text{III}}\text{HDA}) = 47,800 \text{ M}^{-1} \text{ cm}^{-1}$ . Alternatively, the ratio of hemin to styrene in the copolymer was determined from the ratio of absorbances, with  $\epsilon_{269}(\text{polystyrene}) = 186 \text{ M}^{-1} \text{ cm}^{-1}$ .

Molecular weight was determined with a Waters Model 201 gel permeation chromatograph calibrated with poly(styrene) standards, with either tetrahydrofuran or chloroform solvent.

Copolymerizations are coded below in a S/HDME-XN format, where S/H designates styrene/hemin copolymer, DME or DA refer to the hemin derivative, X is the ligand, and N is the time, in hours, at which an aliquot was taken.

S/Fe<sup>II</sup>HDME. The S/Fe<sup>III</sup>HDME reaction mixture was titrated with aqueous dithionite to the reduced species, indicated by a visible shift from 570 to 552 nm (Figure 4.2).

S/Fe<sup>III</sup>HDME·(CN)<sub>2</sub><sup>-1</sup>. The S/Fe<sup>III</sup>HDME reaction mixture was titrated with either concentrated aqueous KCN (using the  $\lambda_{\text{max}} = 431 \text{ nm}$  absorption band for the dicyanide complex) or a filtered solution of 0.59 g of 18-crown-6 (Aldrich), 0.13 g of KCN, and 10.0 ml of DMF.



Figure 4.1. Visible spectra of ferric HDME in  $\text{CHCl}_3$ ,  $-\cdot-$  ( $\lambda_{\text{max}} = 388 \text{ nm}$ );  $(\text{CN})_2^{-1}$  derivative in DMF/styrene solvent,  $\text{—}$  ( $\lambda_{\text{max}} = 431 \text{ nm}$ ); 1-methylimidazole ligand 230 fold excess in  $\text{CHCl}_3$ ,  $\text{-----}$  ( $\lambda_{\text{max}} = 407 \text{ nm}$ ). Concentration of each species is different.

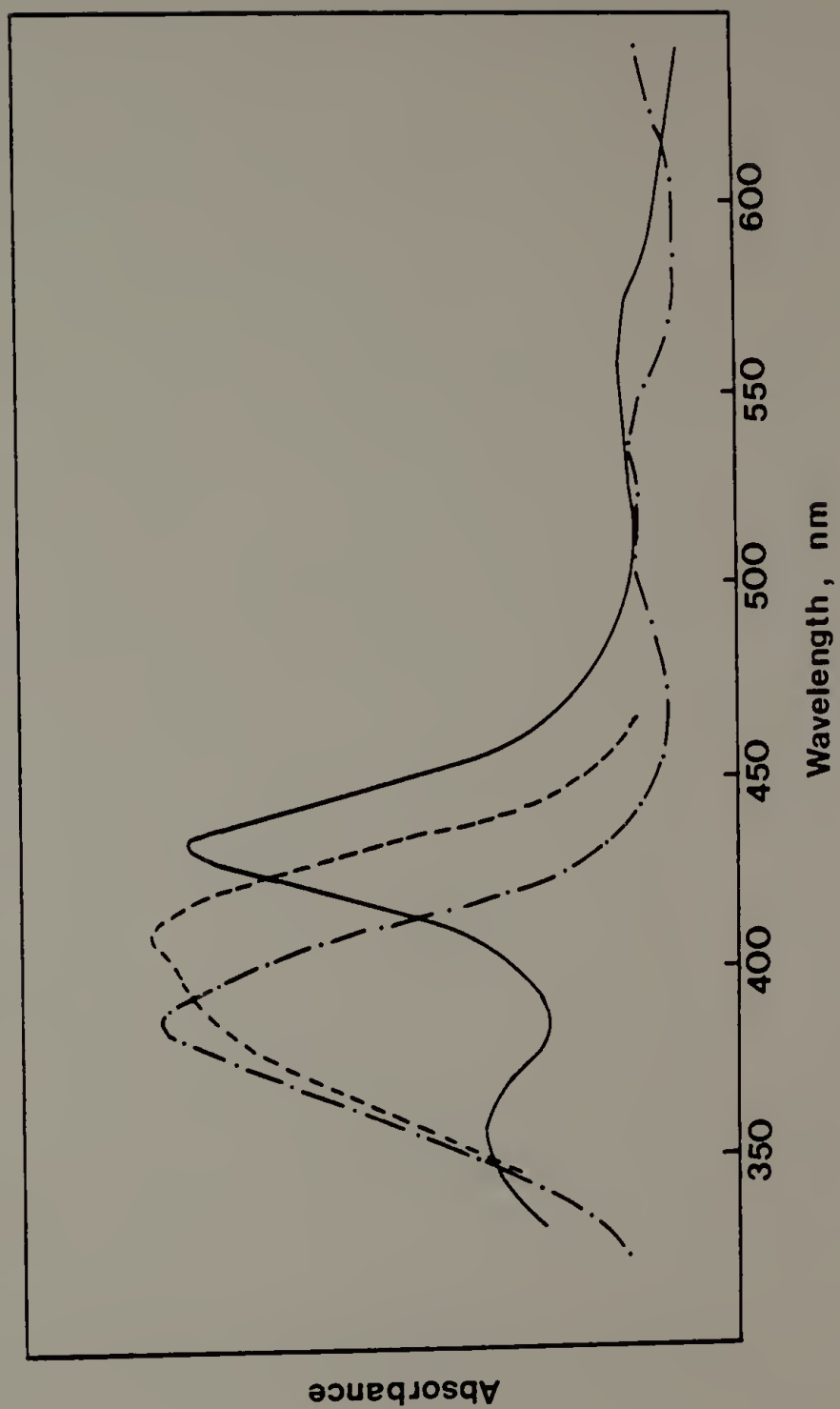
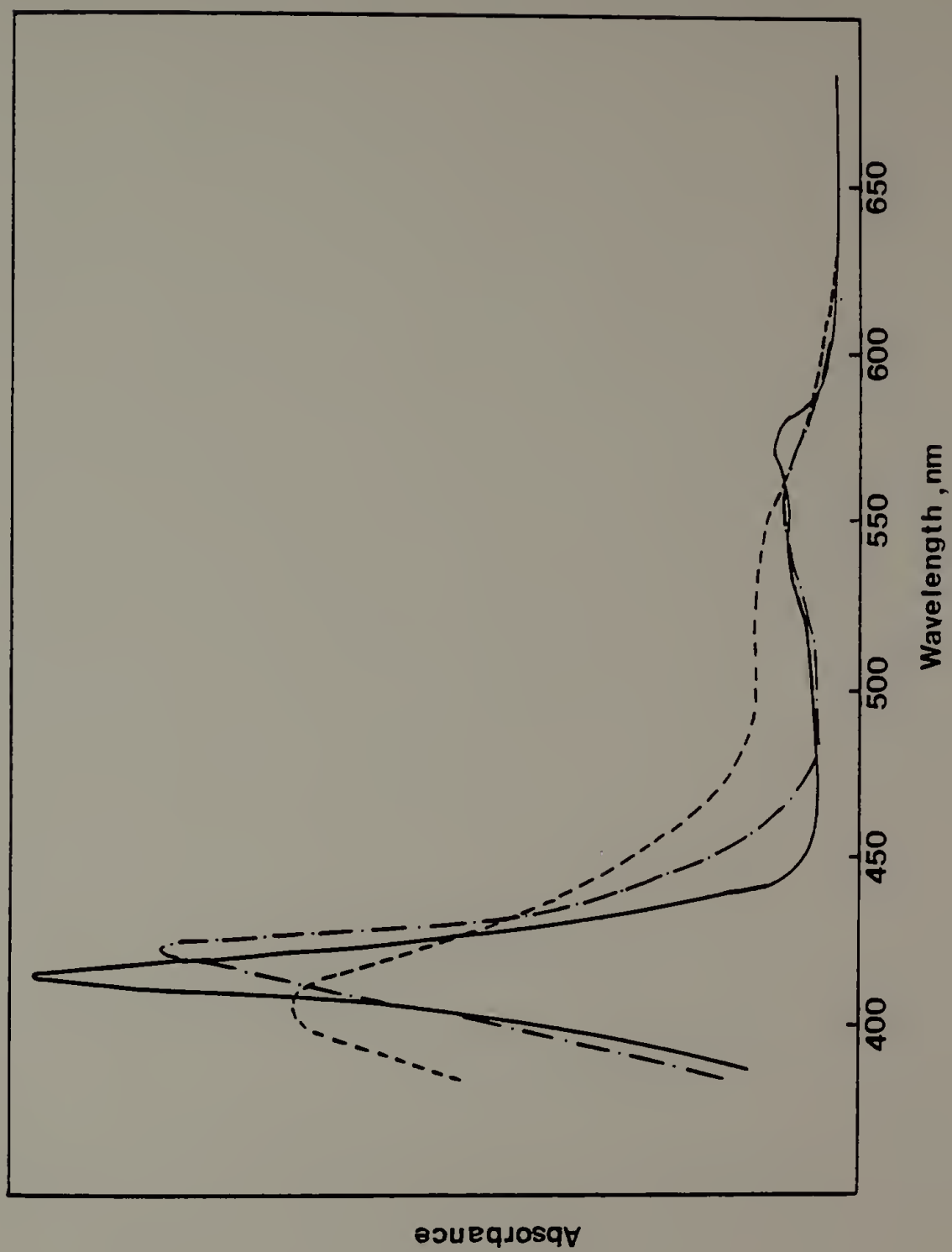


Figure 4.2. Visible spectra of ferrous HDME in DMF,  $-\cdot-$  ( $\lambda_{\text{max}} = 423 \text{ nm}$ ); with CO added in  $\text{CHCl}_3$ ,  $---$  ( $\lambda_{\text{max}} = 411 \text{ nm}$ ); S/HDME $\cdot$ (IM) $_2$  reaction mixture in DMF,  $-----$  ( $\lambda_{\text{max}} = 408$ ) after 24 hr. Concentration of each species is different.



Additional DMF was added after the end point was reached to give a total volume of 18.0 ml. Both methods gave cyanide derivatives that behaved identically in copolymerization (Figure 4.1).

S/Fe<sup>III</sup>HDME·(IM)<sub>2</sub>. To the S/Fe<sup>III</sup>HDME reaction mixture was added a 230-fold excess of 1-methylimidazole (IM). Visible spectra of the initial reaction mixture ( $\lambda_{\text{max}}$ [HDME·(IM)<sub>2</sub>] = 407 nm) showed the HDME to be approximately 50% unligated, but with progression of the polymerization all iron porphyrins became six-coordinated, with a color change from brown to red, indicative of the formation of Fe<sup>II</sup>HDME·(IM)<sub>2</sub>. The red color was lost upon exposure to air (Figures 4.1 and 4.2).

S/Fe<sup>II</sup>HDME·CO. Carbon monoxide was bubbled through the S/Fe<sup>II</sup>HDME reaction mixture to yield a cherry red solution ( $\lambda_{\text{max}}$  = 411 nm) (Figure 4.2).

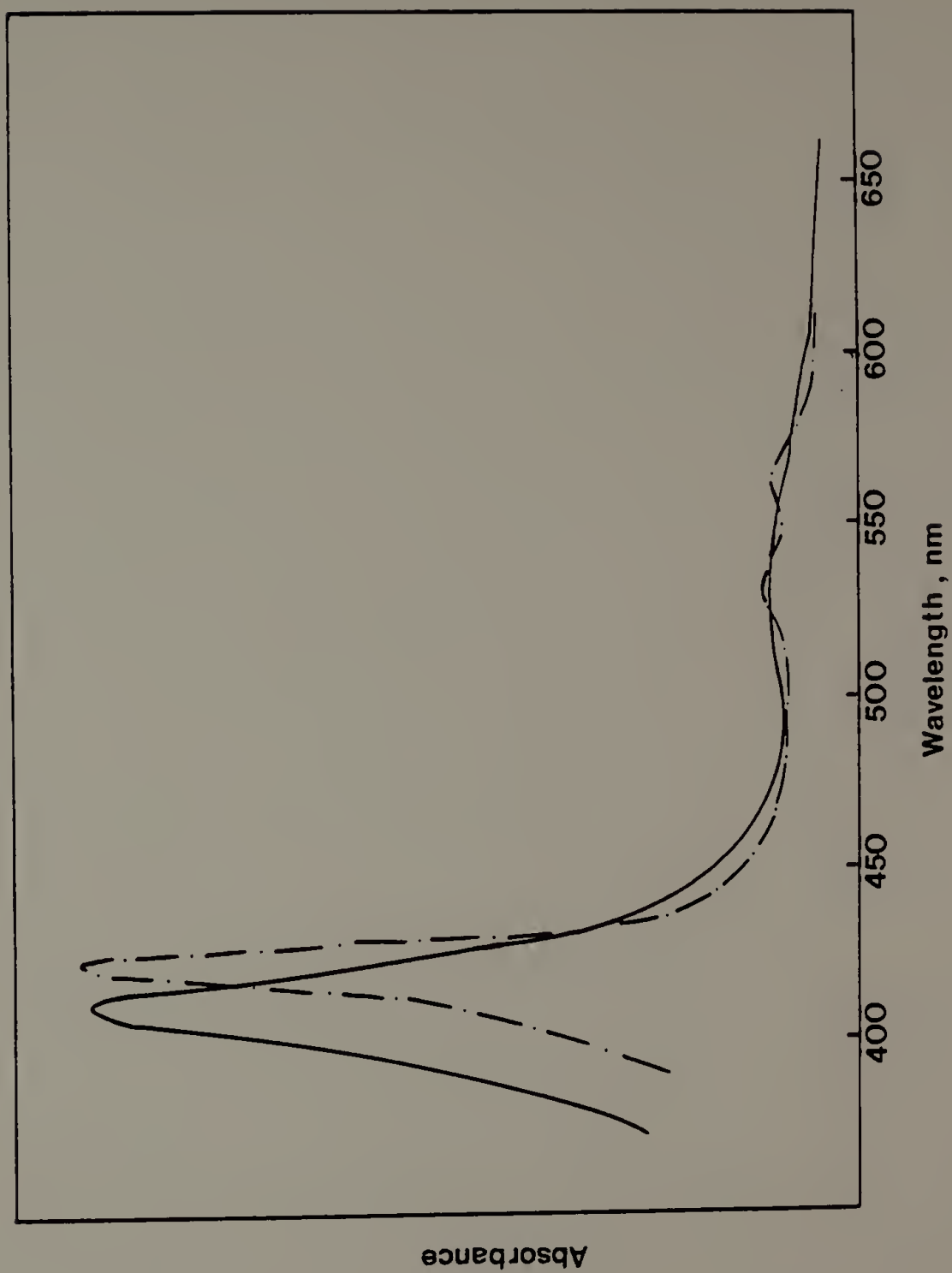
S/Fe<sup>III</sup>HDA. Polymerization was identical with that of S/Fe<sup>III</sup>HDME except that an equimolar quantity of HDA replaced the HDME ( $\lambda_{\text{max}}$  = 409 nm) (Figure 4.3).

S/Fe<sup>II</sup>HDA·CO. To the S/HDA reaction mixture was added 100  $\mu$ l of acetic acid, aqueous dithionite and then the mixture was saturated with CO ( $\lambda_{\text{max}}$  = 419 nm) (Figure 4.3).

S. Styrene was homopolymerized for reference purposes; the procedure for copolymerization was followed except for omission of the iron porphyrin monomer.

A series of S/HDME·CO polymers with varying HDME contents was prepared as follows: 2.76 ml of styrene (0.024 mol), 0.0394 g of AIBN (0.00024 mol), and 0.5 ml of DMF and HDME with a HDME/S  $\times 10^4$  molar

Figure 4.3. Visible spectra of ferric HDA, — (  $\lambda_{\text{max}}$  = 409 nm); and ferrous HDA·CO in the polymerization mixture, -·- (  $\lambda_{\text{max}}$  = 419 nm). Concentration of each species is different.





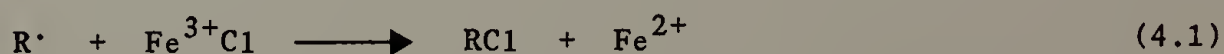
ratio equal to 0, 2.5, 5, 7.5, and 10. Each sample was degassed and a constant volume of concentrated aqueous sodium dithionite added. After thorough flushing with carbon monoxide, the cherry red reaction mixtures were placed in a 60°C bath for 6 hr. Polymers were precipitated into methanol three times and dried at 60°C in vacuo for 48 hr.

## Results and Discussion

### Polymerization and Polymer Composition

Polymerization yield as a function of time for the formation of poly(styrene) in the presence and absence of HDME is shown in Figure 4.4. The presence of iron prophyrin in either the Fe(II) or Fe(III) state retards the polymerization rate significantly, with very little polymer being formed within 4 hr. In the absence of iron porphyrins, styrene has a very rapid rate of polymerization. Initially, Fe<sup>III</sup><sub>HDME</sub> is incorporated almost threefold faster than Fe<sup>II</sup><sub>HDME</sub> and the iron porphyrin is enriched in the polymer about eightfold over the feed composition.

The retardation effect may be explained on the basis of the mechanism proposed by Castro<sup>6</sup> for the reaction of hemin derivatives with free radicals. For Fe(III) porphyrins, axial inner-sphere reduction to Fe(II) is followed by radical-ligand combination:

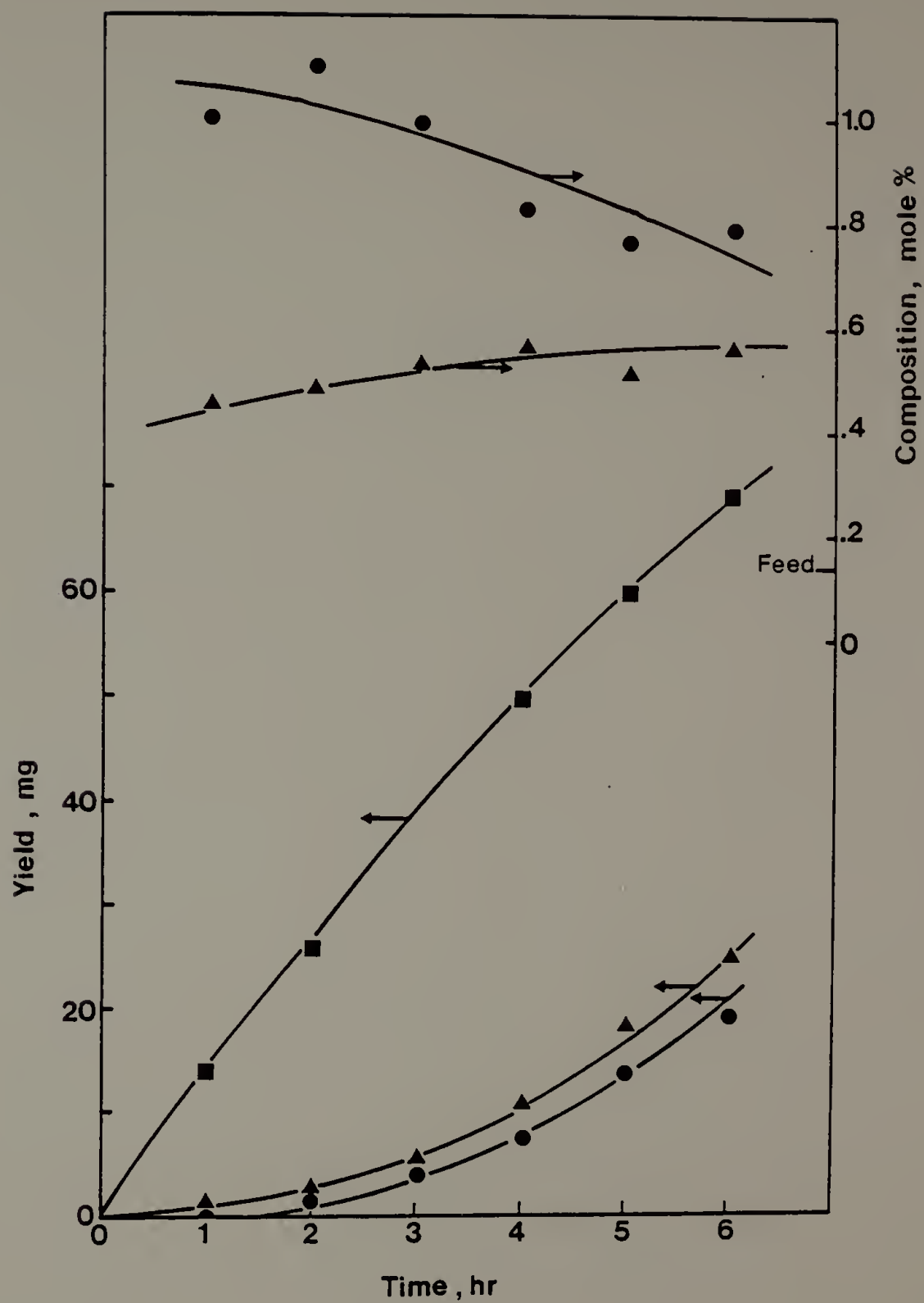


On the other hand, Fe(II) porphyrins were found to be oxidized:

Figure 4.4. Polymer yield versus time for (■) polystyrene,

(▲) S/HDME (Fe II), (●) S/HDME (Fe III).

Reaction conditions were identical and are given in the text. No strong ligands are present. Inset is mol % heme in polymer as a function of time for S/HDME (Fe II) and S/HDME (Fe III).





Reactions 1 and 2 allow iron to cycle between its two oxidation states until the source of radicals is consumed. The radical concentration and its relation to the retardation of polymerization are discussed below. The high reactivity of the porphyrin vinyl group causes the observed iron porphyrin enrichment in the copolymer. This enhanced reactivity may be attributed to the resonance-stabilized nature of the porphyrin macrocycle in conjugation with the vinyl groups. This is supported by Nishide's observation that porphyrin vinyl groups do not copolymerize with unconjugated monomers.<sup>5</sup>

If reactions 1 and 2 had very high rates, then HDME would completely prevent polymerization. It appears that polymerization is competitive with these modes of chain termination; thus these four-coordinate iron protoporphyrins act as retarders rather than as inhibitors. This picture is consistent with the results of Nishide et al.,<sup>5</sup> who copolymerized styrene with  $Fe^{III}$ HDME in varying amounts. They found a decrease in molecular weight with increasing iron protoporphyrin concentration, which would be expected for an iron protoporphyrin behaving as a chain-terminating agent in the polymerization.

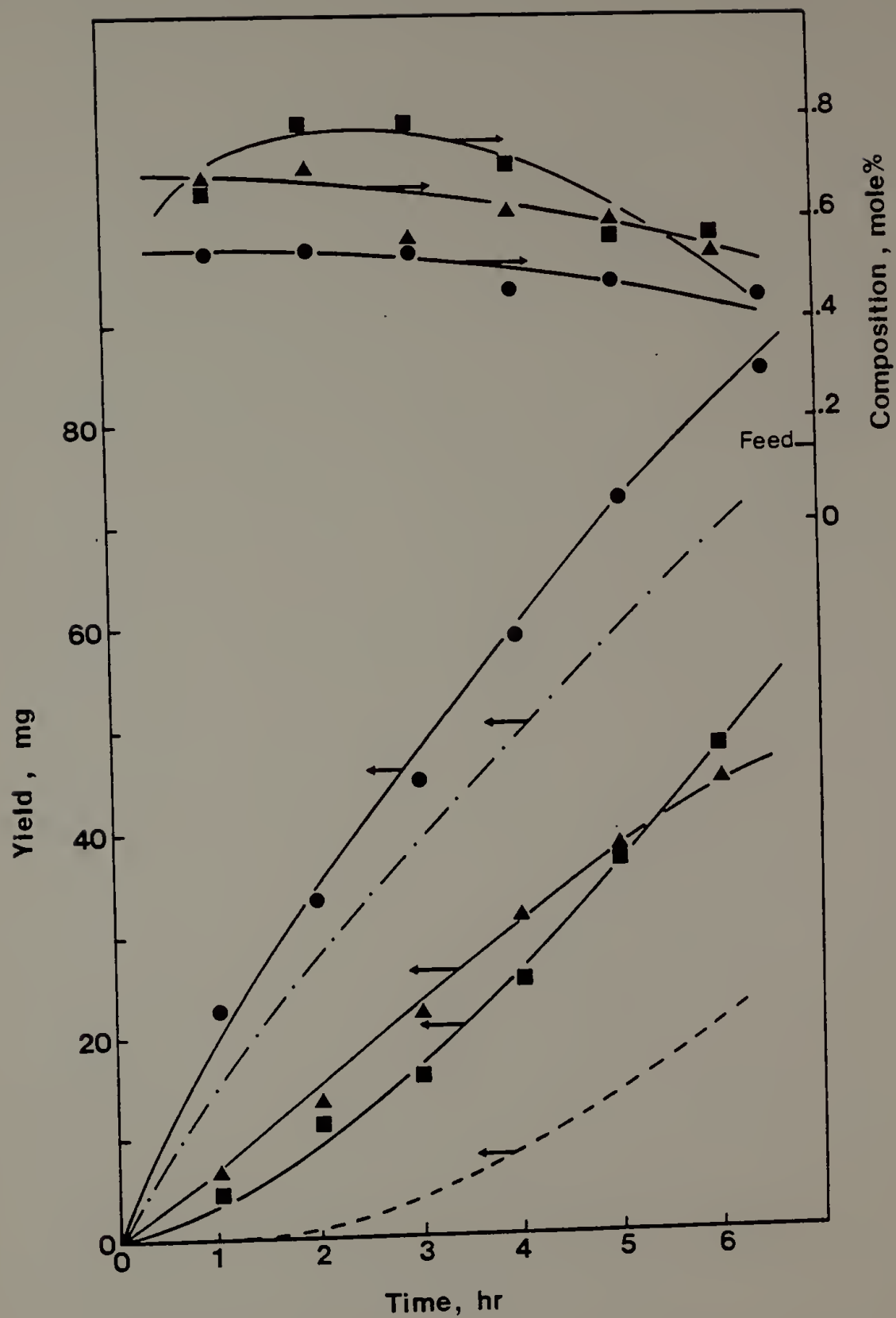
If the retardation of free radical polymerization by iron protoporphyrins occurs through the proposed inner-sphere mechanism, strong ligands in the fifth and sixth coordination positions should eliminate the retardation by blocking direct access to the iron atom. We have chosen to study copolymerization of styrene with  $Fe^{III}$ HDME with

cyanide and 1-methylimidazole ligands and copolymerization of styrene with  $\text{Fe}^{\text{II}}\text{HDME}\cdot\text{CO}$ . For these cases polymer yield and hemin content in polymer as a function of time are shown in Figure 4.5 and compared with the yield of polystyrene in the absence of any iron porphyrin complex. All three cases show a dramatic increase in copolymerization rate compared to the rate for iron protoporphyrins without strong ligands. Cyanide eliminates the retardation and greatly increases the initial polymerization rate to about half of that for styrene homopolymerization.  $\text{S}/\text{Fe}^{\text{II}}\text{HDME}\cdot\text{CO}$  shows no sign of retardation and even has a slightly higher rate of polymerization than styrene alone. Initially, the  $\text{S}/\text{Fe}^{\text{III}}\text{HDME}\cdot(\text{IM})_2$  case behaves similarly to the  $\text{S}/\text{Fe}^{\text{III}}\text{HDME}\cdot(\text{CN})_2^-$  case except the former polymerization rate curve has a concave-upward shape with respect to the x axis, as in the  $\text{S}/\text{Fe}^{\text{III}}\text{HDME}$  curve, which suggests that there is some four-coordinate hemin present. This is supported by the optical spectra of the initial reaction mixture. As the  $\text{Fe}(\text{III})$  is converted to  $\text{Fe}(\text{II})$ , the binding of imidazole to the hemin is presumably more complete and the slope of the curve becomes identical with that for  $\text{S}/\text{HDME}\cdot\text{CO}$ .

The change in slope of the  $\text{S}/\text{HDME}\cdot(\text{IM})_2$  curve occurs after about 3.5 hr. If one assumes each radical is terminated by contact with an iron, then the moles of radicals generated over this time period should equal the moles of  $\text{Fe}^{\text{III}}\text{HDME}$ . The expression for the rate of initiation is

$$R_i = 2fk_d[\text{I}] \quad (4.3)$$

Figure 4.5. Polymer yield versus time for various ligated HDME monomers copolymerized with styrene under identical reaction conditions: (---) polystyrene; (-----) S/Fe<sup>III</sup> HDME; (●) S/HDME·CO; (▲) S/HDME·(CN)<sub>2</sub><sup>-1</sup>; (■) S/HDME·(IM)<sub>2</sub>. Inset is mol % HDME in copolymers as a function of time.





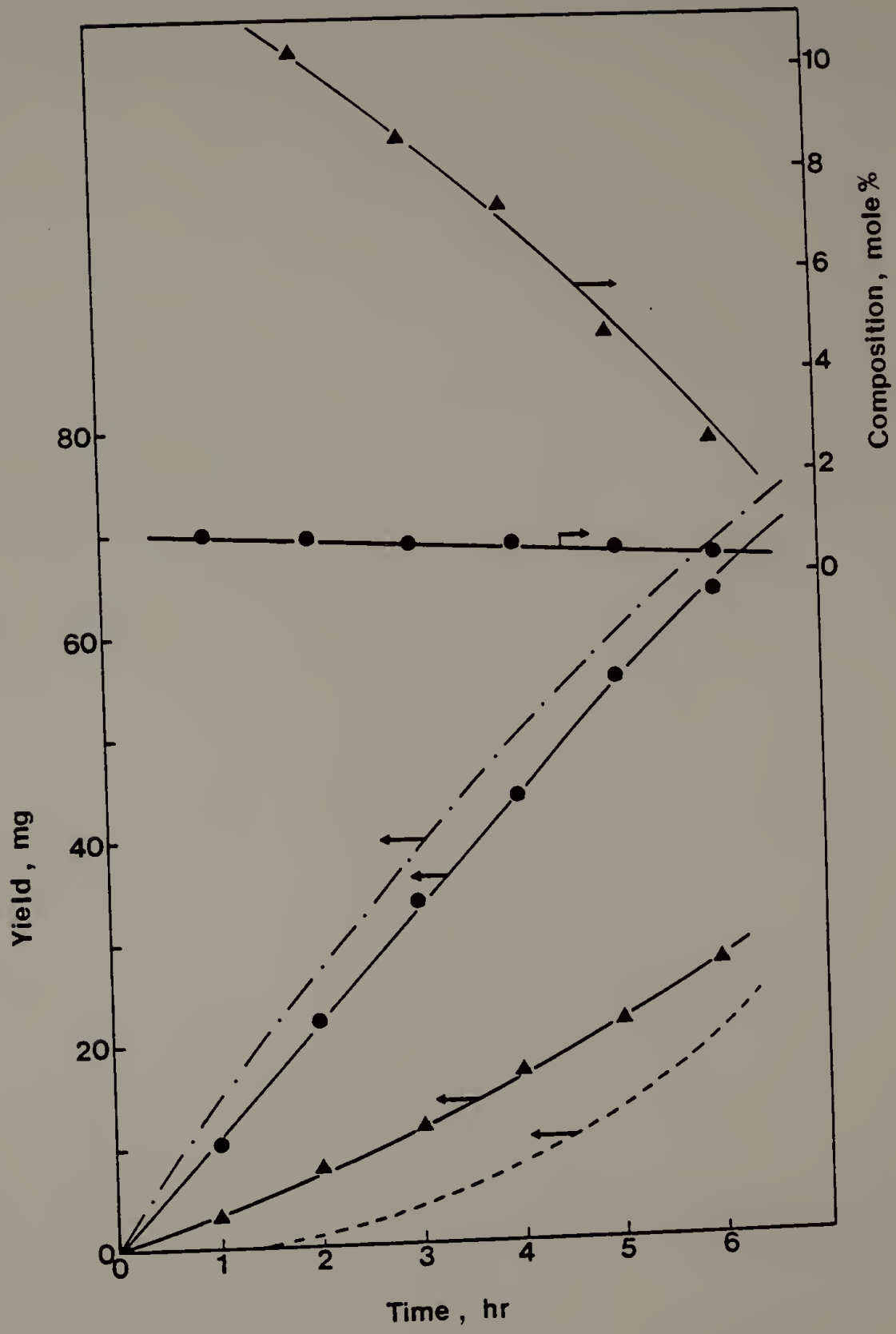
where  $k_d = 8.5 \times 10^{-6} \text{ s}^{-1}$ ,<sup>7</sup>  $f = 0.7$ ,<sup>8</sup> and  $[I] = 2.89 \times 10^{-2} \text{ M}$ . Then  $R_i = 3.93 \times 10^{-7} \text{ M s}^{-1}$  and  $R_i t = 4.2 \times 10^{-3} \text{ M}$  at  $t = 3 \text{ hr}$  as compared to the total amount of HDME in the reaction mixture of  $4.07 \times 10^{-3} \text{ M}$ .

Therefore the total number of radicals generated is approximately equal to the number of hemins that are reduced by reaction with these radicals after 3 hr. The rate of polymerization does not have a dependence on the type of ligand for a given oxidation state. One would expect the polymeric product of the  $S/\text{HDME}^{\cdot}(\text{IM})_2$  reaction to have a larger range of molecular weights due to the steadily decreasing amount of chain-transfer agent (i.e., unchelated iron) present as will be discussed later.

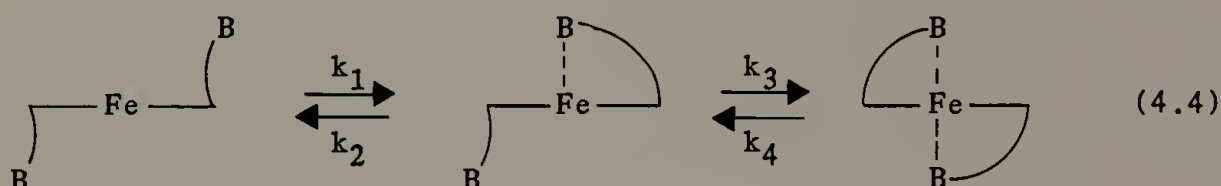
The composition versus time data given in Figure 4.5 show a significant enrichment of iron porphyrin in the copolymer, as seen previously, with no apparent effect of ligand on the reactivity of HDME. The percent HDME in the polymer decreases slowly over time due to depletion of the iron protoporphyrin from the reaction mixture. In the  $(\text{CN})_2^-$  case, 9% of the total hemin has been consumed after 2 hr and 27% has been consumed after 6 hr.

$\text{Fe(II)}$  protoporphyrin IX bis-3-(1-imidazolyl)propylamide (HDA) is a promising monomer in the synthesis of a polymer that may bind oxygen reversibly and also is interesting in this investigation because two strong ligands are covalently bound to the macrocycle.<sup>9,10</sup> The results for copolymerization of styrene and HDA are shown in Figure 4.6. The polymerization rate for  $S/\text{Fe}^{\text{III}}\text{HDA}$ , though linear and thus not showing typical retardation behavior of the four-coordinate hemins, is markedly

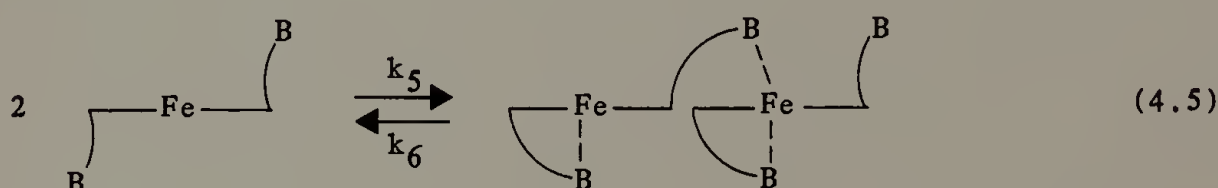
Figure 4.6. Polymer yield versus time for copolymers of styrene and iron protoporphyrin IX bis-3-(1-imidazolyl)-propylamide: (-·-) polystyrene; (-----) S/Fe<sup>III</sup><sub>HDME</sub>; (▲) S/HDA; (●) S/HDA·CO. Inset is mol % HDA in copolymers as a function of time.



depressed compared to the rate with cyanide or carbon monoxide as ligands. Furthermore, the initial incorporation of HDA into the polymer is at least tenfold greater than for any of the other hemin complexes we have studied. This enrichment could be attributed to equilibria found in hemins with two attached bases, which would raise the effective concentration of hemins in the vicinity of a hemin already attached to the polymer chain. According to Momenteau and co-workers,<sup>11</sup> an iron porphyrin with covalently bound axial bases has several potential equilibria:



In solution other possible interactions exist:



Thus HDA could exist in aggregates in solution or at the growing end of a polymer chain. Through such equilibria the porphyrin vinyl groups would be held in close proximity to the growing chain end and thus polymerization may be sterically assisted. During purification of the S/HDA·24 sample on the Biobeads SX2 column, we observed that the HDA monomer is completely consumed after 24 hr and the copolymer composition is equal to the maximum theoretical hemin enrichment for the yield

obtained. This explains the sharp linear decline of heme enrichment shown in Figure 4.6. The depression of the yield versus time curve implies the heme radical on the polymer terminus is less reactive than a styryl radical.

When an imidazolyl ligand of  $\text{Fe}^{\text{II}}\text{HDA}$  is replaced by carbon monoxide, the polymerization is very similar to that for  $\text{HDME}\cdot\text{CO}$ . The rate of polymerization is nearly that of pure polystyrene and the polymer HDA content is about the same as found for the other iron porphyrin derivatives studied in this work.

#### Molecular Weight Studies

Owing to the large number of samples and small yield of polymer for some cases, samples taken at 6 hr were selected for molecular weight study. Table 4.1A compares the molecular weight of pure polystyrene to the various ligated iron porphyrin/styrene copolymers synthesized under identical conditions.

The lower molecular weight for copolymer systems than for pure polystyrene could be explained by the presence of chain-transfer agents such as water during ligand addition, however, the polydispersity should be about the same for each case. For  $\text{S}/\text{HDME}\cdot(\text{IM})_2$  the polydispersity is 2 times greater than for the other polymerizations. This supports our hypothesis, presented above, that the  $\text{Fe}^{\text{III}}\text{HDME}$  acts as a chain-transfer agent or retarder. As the  $\text{Fe}(\text{III})$  is reduced to  $\text{Fe}(\text{II})$  the ligand binds, the chain-transfer agent is consumed, and the molecular weight increases.

We studied the molecular weight of the samples from the  $\text{S}/\text{HDME}\cdot\text{CO}$

Table 4.1  
Molecular Weight Data for Styrene/Iron Porphyrin Copolymers

Determined by Gel Permeation Chromatography in THF

Sample	$M_n$	$M_w$	$M_w/M_n$	Hemins/Chain	Mol % Hemin
A. Molecular Weight of Polystyrene vs. Molecular Weights of S/HDME·X Copolymer					
PS·6	16,300	39,500	2.43	--	--
S/HDME·CO6	13,900	30,000	2.12	0.56	0.44
S/HDME·CN6	10,400	25,900	2.49	0.54	0.53
S/HDME·IM6	4,300	19,900	4.62	0.26	0.56
B. Molecular Weights of S/HDME·CO Copolymers					
S/HDME·CO4	13,900	30,000	2.16	0.56	0.45
S/HDME·CO6	14,900	32,000	2.21	0.64	0.44
S/HDME·CO24	15,600	41,800	2.67	0.46	0.31
C. Molecular Weights of S/HDA and S/HDA·CO Copolymers					
S/HDA·6	6,400	18,000	2.81	1.35	2.62
S/HDA·24	12,200	15,900	2.12	0.75	0.67
S/HDA·CO4	10,200	24,800	2.42	0.69	0.61
S/HDA·CO6	9,800	24,000	2.46	0.48	0.44

polymerization to see if there was any change in molecular weight with time and decreasing heme content. The results are given in Table 4.1B. The molecular weight appears to increase very slightly with time with a concurrent increase in the polydispersity index. There is about one heme group per two polymer chains.

It is imperative for our future work to know whether iron porphyrins are incorporated only on the chain terminus, in the middle of a chain, or both. If iron porphyrins are chain terminators one would expect that increasing the monomer feed of HDME would significantly affect the molecular weight. A series of S/HDME·CO polymers of varying heme concentration showed no change in molecular weight with increasing heme concentration (Table 4.2). Thus we can conclude that HDME·CO is incorporated into the polymer backbone. If the feed concentration was increased to a S/HDME ratio of  $19.8 \times 10^{-4}$ , one would expect more than one heme to be incorporated per polymer chain under these experimental conditions.

The molecular weights of the S/HDA·CO copolymers, shown in Table 4.1C, are comparable to those of the other copolymers formed in the presence of six-coordinate iron porphyrins. However, the S/HDA copolymers show an increase in molecular weight with decreasing HDA feed concentration (increasing reaction time). Earlier samples in the S/HDA copolymerization have a very high weight fraction of HDA in the copolymer and a large number of hemins per chain.

### Conclusions

Iron protoporphyrins without strong axial ligands, such as HDME in



Table 4.2

Molecular Weight Data for S/HDME·CO Copolymers with Varying Heme Concentrations Determined by Gel Permeation Chromatography in Chloroform

Feed HDME/S $\times 10^4$	Polymer HDME/S $\times 10^4$	$M_n$	$M_w$	$M_w/M_n$	Hemes/Chain
0	0	32,800	65,000	1.98	---
2.5	4.6	30,800	66,200	2.15	0.136
5	8.6	28,900	64,600	2.24	0.237
7.5	13.4	30,400	65,400	2.15	0.388
10	17.5	30,800	77,500	2.52	0.507

the Fe(II) and Fe(III) state, appear to retard polymerization through reactions of a radical with the iron atom via redox reactions. The retardation is seen in the very slow rate of conversion for these copolymers in comparison with pure poly(styrene). Ligands such as carbon monoxide, cyanide, and 1-methylimidazole prevent the reaction of a radical with the central iron and allow polymerization to proceed in the usual manner. The molecular weight of a heme/styrene copolymer with a carbon monoxide ligand remains constant, despite varying heme concentration, which suggests that heme is not a chain-terminating agent and is incorporated in the polymer chain.

Protoporphyrins are very reactive vinyl monomers owing to the conjugation with the porphyrin ring. This may be seen in the considerable enrichment of iron porphyrin in the polymer composition from the monomer feed. Thus one would expect a relatively slow rate of polymerization. This is seen in the S/HDA case, where the polymer is composed of a significant amount of hemin and the rate of conversion is slower than those polymerizations where the iron porphyrin enrichment is less significant. Also it appears that Fe(III) hemins polymerize more slowly and are more reactive monomers than Fe(II) hemes, possibly due to the greater resonance stabilization of the radical. This is observed in comparing the slower rate of conversion of S/HDME $\cdot$ (CN) $^-_2$  to those of S/HDME $\cdot$ CO and S/Fe $^{II}$ HDME $\cdot$ (IM) $_2$ .

We have postulated a mechanism of hemin enrichment observed in the S/HDA polymerization whereby the axial basis of the HDA, in solution or at the end of a polymer chain, may bind to nearby hemins. The physical

proximity of these monomers results in an increased probability of hemin-hemin polymerization over hemin-styrene copolymerization. We have shown that when one of these ligands is displaced, as in the  $S/Fe^{II}HDA \cdot CO$  polymerization, the reaction proceeds as a usual styrene-heme copolymerization.

### References

1. Finkenaur, A.L.; Dickinson, L.C.; Chien, J.C.W. Macromolecules, (1983), 16, 728.
2. Lautsch, W.; Broser, W.; Doring, U.; Zochke, H. Naturwissenschaften, (1951), 38, 210.
3. Lautsch, W.; Broser, W.; Bredermann, W.; Grichtel, H. J. Polym. Sci., (1955), 42, 479.
4. Tsuchida, E. J. Macromol. Sci. Chem., (1979), A13(4), 545.
5. Nishide, H.; Shinohara, K.; Tsuchida, E. J. Polym. Sci. Polym. Chem. Ed., (1981), 19, 1109.
6. Castro, C.E.; Robertson, C.; Davis, H. Bioorg. Chem., (1974), 3, 343.
7. Brandrup, T.; Immergut, E.H. (ed.) Polymer Handbook, Interscience, New York, 1975.
8. Amett, L.M.; Peterson, J.J. J. Am. Chem. Soc., (1952), 74, 2031.
9. Traylor, T.G.; Chang, C.K.; Geibel, J.; Berzinis, A.; Mincey, T.; Cannon, J. J. Am. Chem. Soc., (1979), 101, 6716.
10. Chang, C.K.; Traylor, T.G. Proc. Nat. Acad. Sci., U.S.A., (1973), 70, 2674.
11. Momenteau, M.; Rougee, M.; Loock, B. Eur. J. Biochem., (1976), 71, 63.

## CHAPTER V

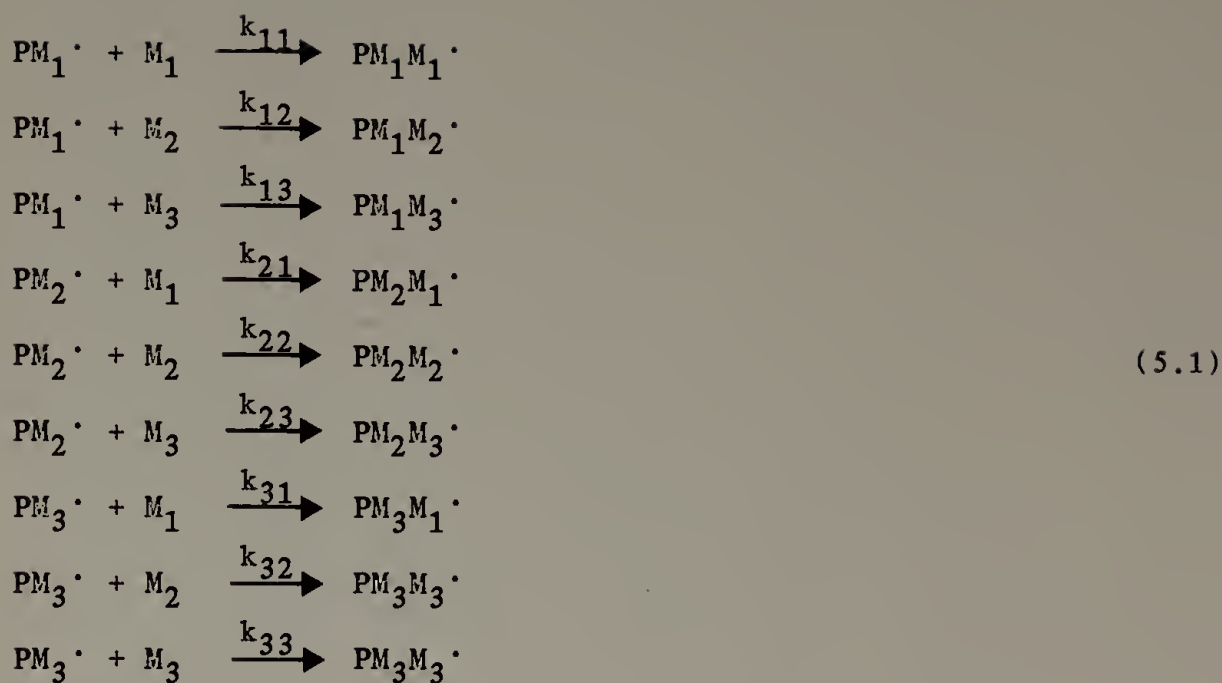
### TAILORING THE COMPOSITION, PHYSICAL AND CHEMICAL

#### PROPERTIES OF MODEL POLYMERS

The synthesis of a vinyl pentapolymer which can mimic the functions of hemoglobin is a complex task. Scientific logic demands that one begin by making smaller models, such as terpolymers, which mimic two or more of the five functions. For example: to study oxygenation in an aqueous solution the polymer should be water soluble  $[SS^-]$  with hydrophobic domains  $[S]$  and contain a small amount of heme  $[HMEMA]$  as an oxygen carrier. This terpolymer need not contain a carrier of carbon dioxide or a crosslinking agent. Then, to assess the effectiveness of the crosslinking agent  $[APMA]$ , a tetrapolymer of  $S/SS^-/APMA/HMEMA$  could be synthesized, photocrosslinked and the oxygenation/oxidation stability compared with  $S/SS^-/HMEMA$ . A model polymer for the study of carbon dioxide uptake requires three functions: water solubility, hydrophobic domains and an amine functionality. These simple terpolymers allow a quantitative evaluation of the composition, physical and chemical behavior of the functional units.

#### Composition

The composition of a terpolymer can be predicted using terpolymerization theory.<sup>1</sup> There are nine propagation reactions:



and six monomer reactivity ratios:

$$r_{12} = k_{11}/k_{12}, \quad r_{13} = k_{11}/k_{13}, \quad r_{21} = k_{22}/k_{21}, \tag{5.2}.$$

$$r_{23} = k_{22}/k_{23}, \quad r_{31} = k_{33}/k_{31} \quad \text{and} \quad r_{32} = k_{33}/k_{32}$$

The rates of disappearance of the three monomers are given by

$$\begin{aligned}
-\frac{d[\text{M}_1]}{dt} &= k_{11}[\text{PM}_1^\cdot][\text{M}_1] + k_{21}[\text{PM}_2^\cdot][\text{M}_1] + k_{31}[\text{PM}_3^\cdot][\text{M}_1] \\
-\frac{d[\text{M}_2]}{dt} &= k_{12}[\text{PM}_1^\cdot][\text{M}_2] + k_{22}[\text{PM}_2^\cdot][\text{M}_2] + k_{32}[\text{PM}_3^\cdot][\text{M}_2] \\
-\frac{d[\text{M}_3]}{dt} &= k_{13}[\text{PM}_1^\cdot][\text{M}_3] + k_{23}[\text{PM}_2^\cdot][\text{M}_3] + k_{33}[\text{PM}_3^\cdot][\text{M}_3]
\end{aligned} \tag{5.3}.$$

At a steady state, one assumes

$$k_{12}[PM_1^{\cdot}][M_2] + k_{13}[PM_1^{\cdot}][M_3] = k_{21}[PM_2^{\cdot}][M_1] + k_{31}[PM_3^{\cdot}][M_1]$$

$$k_{21}[PM_2^{\cdot}][M_1] + k_{23}[PM_2^{\cdot}][M_3] = k_{12}[PM_1^{\cdot}][M_2] + k_{32}[PM_3^{\cdot}][M_2] \quad (5.4).$$

$$k_{31}[PM_3^{\cdot}][M_1] + k_{32}[PM_3^{\cdot}][M_2] = k_{13}[PM_1^{\cdot}][M_3] + k_{23}[PM_2^{\cdot}][M_3]$$

Combination of Equations 5.3 and 5.4 yields the terpolymer composition

$$\begin{aligned} d[M_1]:d[M_2]:d[M_3] = \\ [M_1] \left\{ \frac{[M_1]}{r_{31}r_{21}} + \frac{[M_2]}{r_{21}r_{32}} + \frac{[M_3]}{r_{31}r_{23}} \right\} \left\{ [M_1] + \frac{[M_2]}{r_{12}} + \frac{[M_3]}{r_{13}} \right\} \\ : [M_2] \left\{ \frac{[M_1]}{r_{12}r_{31}} + \frac{[M_2]}{r_{12}r_{32}} + \frac{[M_3]}{r_{32}r_{13}} \right\} \left\{ [M_2] + \frac{[M_1]}{r_{21}} + \frac{[M_3]}{r_{23}} \right\} \quad (5.5). \\ : [M_3] \left\{ \frac{[M_1]}{r_{13}r_{21}} + \frac{[M_2]}{r_{23}r_{12}} + \frac{[M_3]}{r_{13}r_{23}} \right\} \left\{ [M_3] + \frac{[M_1]}{r_{31}} + \frac{[M_2]}{r_{32}} \right\} \end{aligned}$$

A simpler expression has been obtained using different steady state assumptions:<sup>2</sup>

$$k_{12}[PM_1^{\cdot}][M_2] = k_{21}[PM_2^{\cdot}][M_1]$$

$$k_{23}[PM_2^{\cdot}][M_3] = k_{32}[PM_3^{\cdot}][M_2] \quad (5.6)$$

$$k_{31}[PM_3^{\cdot}][M_1] = k_{13}[PM_1^{\cdot}][M_3]$$



which yield the terpolymer composition

$$\begin{aligned}
 d[M_1]:d[M_2]:d[M_3] &= [M_1]\left\{[M_1] + \frac{[M_2]}{r_{12}} + \frac{[M_3]}{r_{13}}\right\} \\
 &: [M_2] \frac{r_{21}}{r_{12}} \left\{ \frac{[M_1]}{r_{21}} + [M_2] + \frac{[M_3]}{r_{23}} \right\} \\
 &: [M_3] \frac{r_{31}}{r_{13}} \left\{ \frac{[M_1]}{r_{31}} + \frac{[M_2]}{r_{32}} + [M_3] \right\}
 \end{aligned} \tag{5.7}$$

Although the steady state assumptions in Equations 5.4 have received more widespread application, agreement between Equations 5.5 and 5.7 is quite good and both predict terpolymer composition with accuracy.<sup>3,4</sup> Wallings and Briggs<sup>3</sup> suggested that the greatest source of error was caused by inaccuracies in reactivity ratios, especially when they have small values. Kelen et al.<sup>5</sup> have proposed a graphical representation of the ternary systems which is similar to the customary binary representation shown in Figure 3.11. This method has no particular advantage over the mathematical ones given in Equations 5.5 and 5.7. Wallings and Briggs<sup>3</sup> also extended the usefulness of Equations 5.1 - 5.5 to include polymers of N components in the feed mixture. Despite the obvious usefulness of multicomponent polymers, only a small amount of research on these systems is evident in the current literature.

#### Chemical and Physical Properties

This chapter will discuss the experimental techniques required to chemically tailor the desired physical properties into the polymer.

(The rationale for chemical modifications of the polymer is described in Chapter III). Several monomers in the system were blocked with an easily hydrolyzed substituent to give greater solubility in the polymerization solvent, DMF, and to prevent chemical reactions in the subsequent polymer modification steps. Techniques to remove these blocking groups were quick and quantitative. Two monomers, 4-vinylpyridine (4VP) and p-vinylbenzylchloride (VBC) were polymerized and then functionalized while on the polymer chain to give cationic water solubilizing groups. Polymers were further modified by the photolysis of the aromatic azide, p-azidophenylmethacrylate (APMA). Model polymers have been modified by at least one and usually two of the chemical methods described above.

### Molecular Weight

Molecular weight is an important physical property of the polymer system. The kinetic chain length,  $\nu$ , of a polymer is defined by

$$\nu = \frac{R_p}{R_i} = \frac{R_p}{R_t} \quad (5.8)$$

where  $R_p$ ,  $R_i$  and  $R_t$  are the rates of propagation, initiation and termination respectively. The kinetic chain length is the number of monomer units polymerized per initiating radical. For polymerization of monomer  $[M]$ , which was initiated by thermal homolysis of the initiator,  $[I]$ ,

$$v = \frac{k_p [M]}{2(fk_d k_t [I])} \quad (5.9)$$

where  $k_p$ ,  $k_t$ ,  $k_d$  are the rate constants for propagation, termination and catalyst dissociation and  $f$ , the initiator efficiency, is a measure of radical wastage owing to the cage effect. The values for  $k_p$ ,  $k_t$ ,  $k_d$  and  $f$  are known for a variety of monomer systems and initiators.<sup>6</sup> According to Equation 5.9, the kinetic chain length is proportional to the monomer concentration and inversely proportional to the initiator concentration, thus molecular weight can be selectively controlled.

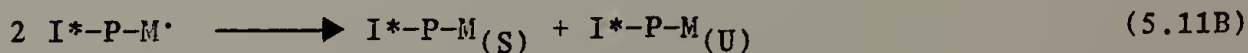
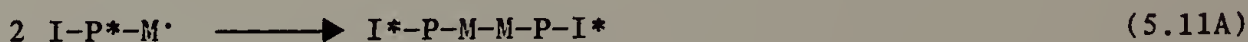
There are many experimental techniques for molecular weight determination including the measurement of colligative properties (e.g. osmotic pressure, vapor-phase osmometry), the study of hydrodynamic radius (e.g. intrinsic viscosity, gel permeation chromatography), light scattering techniques or end group analysis (titration, radioactive endgroup tagging).<sup>7</sup> Each technique has a range of molecular weights which can be determined with good accuracy and it is wise to know the assumptions made in each.

Gel permeation chromatography (GPC) is a widely used technique which yields  $\bar{M}_n$ ,  $\bar{M}_w$  and the polydispersity,  $\bar{M}_w/\bar{M}_n$ , with experimental ease. A gel permeation chromatograph is calibrated for the elution volume required to elute a monodisperse polymer standard, generally polystyrene, whose molecular weight has been determined using a separate absolute method. A calibration curve is constructed for the elution volume versus  $\log(\text{molecular weight})$ . Generalization of the calibration curve can be done if the constants  $K$  and  $a$  in the Mark-Houwink equation,

$$[\eta] = KM^a \quad (5.10),$$

are known.<sup>8</sup> Then one can plot elution volume versus  $\log(\text{molecular weight}) \times [\eta]$  to obtain a universal calibration curve. For our terpolymer,  $K$  and  $a$  are unknown thus the absolute method can't be used. Comparing a terpolymer with a polystyrene calibration curve to find the molecular weight assumes the hydrodynamic volume of the terpolymer dissolved in the solvent is equal to the hydrodynamic volume of polystyrene of the same molecular weight.

Use of a second technique to study the molecular weight of a terpolymer gives more confidence in GPC experimental data. Isotopic labelling of an initiator ( $^{14}\text{C}$ -AIBN) allows radioactive tagging of the end of a polymer chain and thus the exact determination of  $\bar{M}_n$ . The mode of termination, i.e. the extent of combination (Equation 5.11A) versus disproportionation (Equation 5.11B), determines the number of initiator fragments per molecule:



where (S) stands for a saturated and (U) an unsaturated end group. The mechanism of termination in the terpolymer must be known or assumed from experimental data otherwise  $\bar{M}_n$  can be in error by a factor of two.

The results of GPC analysis and radioisotopic endgroup labelling are

compared for a terpolymer of S/MSS/BNAHD and the implication for other molecular weight determinations is discussed in this chapter.

### Experimental Procedure

#### Materials

Bromoethane and a 25% solution of trimethylamine in  $H_2O$  were purchased from Aldrich. Dialysis tubing was Spectra/Por 2 purchased from Fisher.

Radioisotopically labelled  $^{14}C$ -AIBN was custom synthesized by ICN Pharmaceuticals and was received as 10 mCi  $^{14}C$ -AIBN in 10.0 ml of benzene. The hot stock solution was diluted as follows: 140 g of AIBN and 10 mCi of  $^{14}C$ -AIBN in benzene were dissolved in 900 ml of methanol with gentle heating. The methanol was cooled in powdered  $CO_2$  and the AIBN crystallized from solution. The supernatant was decanted and 800 ml of methanol was added. The crystals of AIBN redissolved after warming and the solution was again cooled in powdered  $CO_2$ . Needles of AIBN were filtered from solution, air dried 45 min (yield 105 g) and then dried in vacuo for 90 min. The specific activity was found by diluting 0.004 g of  $^{14}C$ -AIBN in 10 ml of toluene. A 50  $\mu$ l sample was dissolved in 5 ml of Biofluor (New England Nuclear) and counted to give a specific activity 5.52 mCi/mol.<sup>9</sup>

#### Instrumentation

A Waters Model 201 gel permeation chromatograph calibrated with polystyrene standards in tetrahydrofuran was used to measure the molecular weights. Infrared spectra were obtained with a Perkin-Elmer 283 and visible spectra with a Beckman Acta MVI spectrophotometer.



Scintillation counting was done with a Beckman LS100C. The efficiency of counting was determined using a  $^{14}\text{C}$ -toluene standard from New England Nuclear.

### Polymerization

Polymerization techniques were described in Chapter III. Exact reaction parameters are given in Table 5.1. Samples are denoted by the monomer content in decreasing concentration in the feed from left to right. Analysis of polymer composition is given in Table 5.2.

Abbreviations are as follows: styrene [S], p-azidophenyl methacrylate [APMA], N-(t-butyloxycarbonyl)-2-aminoethyl methacrylate [BAEMA], N-t-(butyloxycarbonyl)-N'-(2-methacrylyl)-1,6-diaminohexane [BNAHD], methyl p-vinylbenzenesulfonate [MSS] and 4-vinylpyridine [4VP]. The yield in all the polymerizations was kept below 10%. Specific details for a few unusual polymerizations are given below.

$^{14}\text{C}$ -AIBN Labelled S/MSS/BNAHD (88/4/8). A stock reaction solution containing 0.13 mol of S,  $6.6 \times 10^{-3}$  mol of MSS,  $1.4 \times 10^{-2}$  mol of BNAHD and 7.5 ml of DMF was prepared. A 2 ml aliquot was removed from the reaction mixture and  $6.17 \times 10^{-4}$  mol of AIBN was added to the stock solution which was then degassed and polymerized normally. In a clean Erlenmeyer flask  $4.75 \times 10^{-5}$  mol of  $^{14}\text{C}$ -AIBN was weighed out by difference and the 2 ml of stock solution added. ( $^{14}\text{C}$ -AIBN was handled in the hood using poly(vinylchloride) over neoprene gloves. An estimate of the desired weight of  $^{14}\text{C}$ -AIBN was added to the reaction flask which was then stoppered and weighed. This process was repeated to give the exact quantity and then this value was used to calculate the weight of

Table 5.1

Experimental Parameters for Terpolymerization

Sample	$[M_1]/[M_2]/[M_3]$ Feed (Molar Ratio)	$[M_1]$ (mol) ( $\times 10^{-1}$ )	$[M_2]$ (mol) ( $\times 10^{-4}$ )	$[M_3]$ (mol) ( $\times 10^{-4}$ )	$[AIBN]$ (mol) ( $\times 10^{-4}$ )	$[DMF]$ (ml)	[Time] (min)	Purification <sup>a</sup>
S/APMA/BAEMA	98/1/1	0.145	1.5	1.5	0.487	3.1	60	Biobeads SX2
S/MSS/APMA	98/1/1	0.145	1.5	1.5	0.487	3.0	60	Biobeads SX2
	97/2/0.8	1.94	40	16	19.0	22	60	1) Isopropanol
	97.3/2.5/0.25	6.80	175	18	70.0	80 ml	75	2) Methanol MeOH
S/MSS/BAEMA	98/1/1	0.145	1.5	1.5	0.487	3.0	60	Biobeads SX2
	97.1/2/0.9	1.94	40	32	19	22	60	Isopropanol
S/4VP/BNAHD	72/20/8	0.72	200	80	3.0	5	60	1) Acetone
	41/50/9	0.41	500	90	3.0	5	60	2) Skelly B 1) Acetone 2) Skelly B
S/MSS/BNAHD	88/4/8	1.30	66	140	6.17	7.5	60	Methanol
	<sup>14</sup> C-AIBN <sup>b</sup>				0.475		60	Biobeads SX2

<sup>a</sup>When a solvent is specified, the reaction mixture was precipitated into that solvent, redissolved in  $CH_2Cl_2$  and then reprecipitated two more times.

<sup>b</sup>A 2 ml aliquot of S88/MSS4/BNAHD8 was removed and radioactive AIBN added. The protocol is given in the text.



Table 5.2

Composition of Terpolymers from Table 5.1

Sample [M <sub>1</sub> ]/[M <sub>2</sub> ]/[M <sub>3</sub> ]	Feed (Molar Ratio) [M <sub>1</sub> ]/[M <sub>2</sub> ]/[M <sub>3</sub> ]	% C	% H	% N	Polymer (Molar Ratio) [M <sub>1</sub> ]/[M <sub>2</sub> ]/[M <sub>3</sub> ]
S/APMA/BAEMA	98/1/1	87.44	7.52	1.86	85.8/6.8/7.4
S/MSS/APMA	98/1/1	86.54	7.23	1.63	84.93/7.19/7.89
	97/2/0.8	85.88	7.43	1.15	82.2/12.1/5.6
	97.3/2.5/0.25	86.48	7.22	0.42	84.5/13.5/2
S/MSS/BAEMA	98/1/1	87.45	7.47	0.41	86.7/6.6/6.72
	97.1/2/0.9	86.27	7.56	0.32	83.6/11.7/5.24
S/4VP/BNAHD	72/20/8	84.62	7.55	4.70	60.9/23.5/15.5
	41/50/8	81.44	7.62	8.00	35.4/47.3/17.3
S/MSS/BNAED	88/4/8	78.28	6.86	0.66	61.3/32/6.7

unlabelled AIBN added to the stock solution.) The  $^{14}\text{C}$ -containing reaction mixture was degassed using a double trap system and then reacted normally. A separate Biobeads SX2 column was set up for  $^{14}\text{C}$  work only and the polymer was purified and dried as described in Chapter III, but using a double trap system to prevent  $^{14}\text{C}$  contamination of vacuum line and pump. All wastes were discarded via Environmental Health and Safety. A 0.01 g sample of polymer was dissolved in 2.1 ml toluene and 5.0 ml Biofluor was added. The sample was counted and the molecular weight,  $\bar{M}_n$ , of the polymer calculated.

S/MSS/APMA/HMEMA (95/4/0.3/0.04). The following reactants: 0.0173 mol of S, 0.0073 mol of MSS,  $4.97 \times 10^{-4}$  mol of APMA,  $6.5 \times 10^{-5}$  mol of HMEMA, and  $5.42 \times 10^{-4}$  mol of AIBN were combined in 6 ml of DMF. The polymerization mixture was degassed in a crown cap tube with a neoprene gasket. The atmosphere was flushed with carbon monoxide and then 0.5 ml of a stock solution of reducing agent was added to yield a cherry red solution. (Reducing agent: 0.057 g of sodium dithionite and 0.20 g of 18-crown-6 were combined and degassed. Methanol, 5 ml, was degassed and then added to the solids under a nitrogen stream. After stirring for 0.5 hr all the solids had dissolved.) The reactants were polymerized for 105 minutes at  $60^\circ\text{C}$  and then the reaction mixture was precipitated into methanol. The polymer was filtered from solution, reprecipitated, filtered again and then dried to yield 1.18 g (6.1%) of a fluffy brown polymer. Analysis: C, 83.19; H, 7.18; N, 0.58.

S/APMA (9/1). In a 25 ml Erlenmeyer, 0.015 mol of S, 0.0015 mol of APMA,  $6.1 \times 10^{-5}$  mol of AIBN and 5 ml of toluene were combined and

degassed. Polymerization proceeded for 15 hr at 60° and the polymer was purified by reprecipitation into Skelly B and then isopropanol.

Elemental analysis results gave 32% APMA in the copolymer: C, 81.86; H, 7.14; N, 5.73.

#### Chemical Modification of Polymers

Reactions described below are representative of the methods used to chemically alter the polymer structure.

Hydrolysis of Methylsulfonate. A polymer of S/MSS/APMA with a composition of 84.5/13.5/2, 3.049 g, was dissolved in 20 ml of DMF. Sodium hydroxide, 2 ml of a 1% solution, was added dropwise. The solution was cloudy and gradually became clear with time. After 90 minutes a drop of the polymer/DMF solution was mixed with a large volume of water and no precipitate was observed. The solution was placed in a dialysis tube and dialyzed against 2000 ml distilled water for 36 hr. The distilled water was changed often. The polymer solution of S/SS<sup>-</sup>/APMA in water had a clear yellow color and soap-like properties (i.e. the capacity to solvate water insoluble substances).

The methylsulfonate group was quite unstable to hydrolysis. Samples allowed to stand in impure DMF were water soluble after 2-3 days, presumably due to ester hydrolysis by methylamine impurities in the DMF. Old unhydrolyzed polymer samples were observed to have a water soluble fraction. (After long times these polymers have a milky appearance when dissolved in nonpolar organic solvents). The methylsulfonate group was always removed before the t-BOC protecting group to avoid methylation of the amine functionality.

Quaternization of Polymerized 4-Vinylpyridine. A sample of S/4VP-/BNAHD with a final composition of 60.9/23.5/15.5, 1.086 g, was dissolved in 20 ml of methylene chloride. It was calculated that 0.233 g of the polymer corresponded to 4-vinylpyridine units (0.002 mol). A ten fold excess of bromoethane (0.02 mol, 1.64 ml) was added and the mixture was refluxed. Aliquots were dried on NaCl plates and infrared spectra were obtained as a function of time. When the reaction mixture became cloudy (3 hr) 10 ml of methanol was added to maintain polymer solubility. The reaction was monitored over several days and was judged complete after 70 hr. A peak at  $1640\text{ cm}^{-1}$  characteristic of the pyridinium C=C stretch and a peak at  $1420\text{ cm}^{-1}$  of the pyridine C=N stretch were used to evaluate the extent of reaction with the C-H stretch at  $2940\text{ cm}^{-1}$  used as a standard. Samples, after quaternization, are denoted 4VPQ. Bromoethane and methylenechloride were removed in vacuo and the polymer solution in methanol was precipitated into diethyl ether to yield a hydroscopic polymer, S/4VPQ/BNAHD.

Ammonium Derivatives of Polymerized p-Vinylbenzenechloride. A copolymer of S/VBC synthesized for reactivity ratio analysis (Chapter III), 0.3763 g, of a polymer which contained 22.5 mol % VBC ( $7.35 \times 10^{-4}$  mol) was dissolved in 2.1 ml of tetrahydrofuran. A 2:1 molar excess of an aqueous 25% solution of trimethylamine (3.28 ml) was added and the mixture was refluxed at  $55^{\circ}\text{C}$ . Water was added as necessary to maintain a homogeneous solution. Aliquots of the reaction mixture were thoroughly dried in vacuo, redissolved in methanol and a film was cast on NaCl plates. Infrared spectra obtained before and during the

reaction were used to monitor the extent of substitution on the VBC unit. A peak at  $1275\text{ cm}^{-1}$  ( $\text{CH}_2$  wagging for  $-\text{CH}_2\text{Cl}$ ) characteristic of the unreacted VBC moiety disappeared after three hours. Tetrahydrofuran was removed in vacuo and the water soluble polymer was dialyzed against distilled water to yield a clear solution of S/VBCQ in water.

Removal of the t-Butyloxycarbonyl Protecting Group. S/4VPQ/BNAHD, with a composition of 60.9/23.5/15.5, (1.26 g) was dissolved in 20 ml of methanol and 2.5 ml of HCl was added. (DMF was sometimes substituted for methanol.) The mixture was warmed to  $35^\circ\text{C}$  for 24 hr. The polymer solution was dialyzed against distilled water and appeared to precipitate and then redissolve. (This was not observed for the S/4VPQ/BNAHD (35.4/47.3/17.3) sample which dissolved directly in water.) The dialysis was continued for 48 hr to yield a pure aqueous solution of S/4VPQ/NAHD, 60.9/23.5/15.5.

To insure that the quaternization reaction did not quaternize the blocked amine and that all the blocking groups had been removed by acidic treatment an aliquot of the S/4VPQ/NAHD sample was analyzed for free amines.<sup>10</sup> The aliquot was dried in vacuo to a constant weight of 0.0333 g which was then dissolved in 25 ml of methanol and 10 ml of freshly prepared 1% benzoquinone solution (wt/vol) in methanol. The sealed sample was incubated, in the dark, at  $60^\circ\text{C}$  for 5 hr. The extinction coefficient determined for the reaction of polymerized AEMA with benzoquinone of  $2.02\text{ l g}^{-1}\text{ cm}^{-1}$  ( $260.6\text{ M}^{-1}\text{ cm}^{-1}$ )<sup>11</sup> at 510 nm was assumed correct for polymerized NAHD. From an absorbance of 0.255 the weight fraction of NAHD was found to be 18.95%. By elemental analysis,



the weight fraction of NAHD was 21.48%.

Thermolysis of Polymerized p-Azidophenylmethacrylate. A small amount of S/APMA (9/1 feed) was wetted with tetrahydrofuran in a micro-testtube. The polymer was placed in an oil bath at 157°C and decomposed immediately with nitrogen evolution to yield a crosslinked matrix which could be swollen by THF.

Photolysis of S/APMA in Organic Solvents. In 15 cm quartz tubes with a diameter of 3 mm was placed 0.025 g of S/APMA in 0.5 ml of a solvent: tetrahydrofuran, benzene or ethyl acetate. The polymer solutions were irradiated by a low pressure mercury lamp with an output at 254 nm. All the samples gelled within 60 min. A solution of 0.15 g polymer in 0.25 ml tetrahydrofuran was flushed through an infrared cell with a 0.5 mm teflon spacer. The sample was photolyzed at 254 nm and the infrared spectrum studied as a function of time. A decrease in the  $\text{-N}_3$  stretching band at  $2120\text{ cm}^{-1}$  was evident but not large even though the sample had gelled. The extinction of the copolymer was determined to be  $1.89 \times 10^4\text{ ml g}^{-1}\text{ cm}^{-1}$  ( $\lambda = 252\text{ nm}$ ). This relatively insignificant loss of  $\text{-N}_3$  was explained because the high absorptivity of the matrix prevented the light at 254 nm from passing through the sample. At 0.01 cm the light had been reduced to 1/1000 the original intensity. These results suggested the need for well-mixed dilute solutions.

Photolysis of S/SS<sup>-</sup>/APMA in Aqueous Solution. A sample of a solution of S/SS<sup>-</sup>/APMA (84.5/13.5/2), 5 ml of a 2.86 wt % solution in water, was placed in a quartz tube. A glass rod, with a diameter

approximately 4 mm smaller than the internal diameter of the quartz tube, was suspended in the center of the tube to give a thin layer of solution. The solution was irradiated for 6 hr at 254 nm and was mixed once to obtain uniform irradiation. The aqueous solution of the azide terpolymer yellowed and bubbles were observed on the walls of the test tube. A sample was removed and dried in vacuo and then cast from methanol onto a NaCl plate. The characteristic  $\text{-N}_3$  stretch at  $2120\text{ cm}^{-1}$  had completely disappeared indicating complete photolysis of the azide group. Interestingly, the solution did not gel immediately but gelled after standing undisturbed for one week. This phenomenon will be discussed in Chapter VII.

## Results and Discussion

### Composition

According to Equation 5.7, three pairs of reactivity ratios are required to predict the composition of a terpolymer. For the model system ten different monomers have been selected:

- 1) hydrophobic (S)
- 2) water solubilizing ( $\text{SS}^-$ ), (4VPQ), (VBCQ)
- 3) amine (BAEMA), (BNAHD)
- 4) heme (HDME), (HDA), (HMEMA)
- 5) photocrosslinking (APMA)

The number of possible monomer combinations for terpolymers or tetrapolymer synthesis presents a huge task for the experimentalist. Substitution of one monomer in the five categories would require



experimental determination of four new pairs of reactivity ratios.

In the model of hemoglobin, styrene was estimated to compose the bulk of the pentapolymer. It has also been shown that styrene is less reactive than all of the other monomers and thus a high feed percentage of styrene is necessary to have a moderate percentage of styrene in the polymer. These facts can be used to an advantage. If one assumes that  $r_{32} \approx r_{23} = 1$ , that is monomers 2 and 3 have essentially no preference for homopropagation versus crosspropagation, and  $[M_1] \gg [M_2], [M_3]$  then Equation 5.7 can be simplified to:

$$d[M_1]:d[M_2]:d[M_3] = [M_1]\left\{[M_1] + \frac{[M_2]}{r_{12}} + \frac{[M_3]}{r_{13}}\right\}:$$

$$[M_2] \frac{r_{21}}{r_{12}} \left\{\frac{[M_1]}{r_{21}} + [M_2] + [M_3]\right\}: \quad (5.12)$$

$$[M_3] \frac{r_{31}}{r_{13}} \left\{\frac{[M_1]}{r_{31}} + [M_2] + [M_3]\right\}$$

Equation 5.12 predicts the terpolymer polymer composition by determining the reactivity of each monomer with styrene, ( $M_1$ ).

The actual polymer composition is determined by elemental analysis. The weight percent of an element,  $W_E$ , reported in the elemental analysis of a terpolymer is given by the following expression:

$$W_E = x_1 W_{1,E} + x_2 W_{2,E} + x_3 W_{3,E} \quad (5.13)$$

where  $x_i$  ( $i = 1, 2, 3$ ) is the mole fraction of the monomers in the terpolymer and  $W_{i,E}$  is the weight percent of a particular element in a

monomer. The weight percent of each element is obtained from the chemical formula for the monomer. These appear in Table 5.3.

The analysis for carbon and nitrogen is sufficient to determine the mole fraction of monomers in the terpolymer since

$$x_1 + x_2 + x_3 = 1 \quad (5.14)$$

Equation 5.13 can be expressed as follows:

$$W_E = (1 - x_2 - x_3)W_{1,E} + x_2W_{2,E} + x_3W_{3,E} \quad (5.15).$$

For a terpolymer S/APMA/BAEMA with a feed ratio of 98/1/1 the weight percent carbon from elemental analysis is

$$W_C = 87.44 = (1 - x_2 - x_3)(0.9226) + x_2(0.5911) + x_3(0.5763) \quad (5.16)$$

and the weight percent nitrogen is

$$W_N = 1.86 = x_2(0.2067) + x_3(0.061) \quad (5.17)$$

Solving Equations 5.16 and 5.17 simultaneously yields a molar ratio,  $x_1/x_2/x_3$ , of 85.8/6.8/7.4. (See Tables 5.2 and 5.3 for details.)

The type of analysis used depends on the monomer units in the polymer. The larger the difference in the weight percent values, the more accurate will be the estimate of composition. (For example:

Table 5.3  
Theoretical Values for Elemental Analysis

Monomer	Formula	Weight % C	Weight % H	Weight % N	Weight % O	Weight % S/Cl
Styrene	$C_8H_8$	92.26	7.74	---	---	----
APMA	$C_{10}H_9N_3O_2$	59.11	4.46	20.67	15.75	----
BAEMA	$C_{11}H_{19}NO_4$	57.63	8.35	6.1	27.91	----
MSS	$C_9H_{10}SO_3$	54.53	5.08	---	24.21	16.17 (S)
BNAHD	$C_{15}H_{28}N_2O_3$	63.35	9.92	9.85	16.87	----
4VP	$C_7H_7N$	79.96	6.77	13.32	---	----
VBC	$C_9H_9Cl$	70.83	5.94	---	---	23.23 (Cl)

analysis for carbon content in S/MSS copolymer will give better accuracy in copolymer composition than analysis for sulfur). Quite often the weight percent oxygen (determined by difference) can be used to double check the results of the calculations.

The assumptions in the terpolymerization composition equation (Equation 5.12) have been shown to be quite good experimentally (Table 5.4). (Reactivity ratios, used in the calculations, are given in Table 3.11). The largest error, observed in predicting MSS ( $M_2$ ) composition in the polymer, has two sources: error in the reactivity ratios, especially in  $r_{12}$  where the value was estimated to be  $r_{12} = 0.1 \pm 0.05$ , can cause significant deviation in the predicted polymer composition. (e.g. for system 2, S/MSS/APMA; if  $r_{12} = 0.5$  then Equation 5.12 predicts 77.6/15.21/7.17). Obviously our choice of  $r_{12}$  for MSS is fairly accurate, because agreement between experiment and predicted composition in most systems is good. Variance in the purity of MSS causes polymer composition to vary from experiment to experiment. This source of error becomes more important when the concentration of MSS in the feed is increased.

Systems 7 and 8 are interesting because  $M_1 \geq M_2 > M_3$  however, Equation 5.12 predicts the polymer composition with accuracy. The reactivity ratios ( $r_{12} = 0.54$ ,  $r_{21} = 0.70$ ,<sup>12</sup>  $r_{13} = 0.62$ ,  $r_{31} = 1.17$ <sup>13</sup>) for 4VP and BNAHD with styrene are within the range of ideal behavior ( $r_1, r_2 = 0.5 - 2.0$ ). The assumption that  $r_{32} = r_{23} = 1$  must be fairly good for this terpolymer system. From the observed enrichment of BNAHD over that which was predicted one can conclude that BNAHD is slightly

Table 5.4

A Comparison of Experimentally Determined Polymer Composition and That Predicted from Equation 5.12

System	Feed Composition		Polymer Composition	
	Monomer	Mol %	Found	Predicted
1	S	98	85.8	86.4
	APMA	1	6.8	8.5
	BAEMA	1	7.4	5.1
2	S	98	86.7	83.9
	MSS	1	6.6	7.4
	APMA	1	6.72	8.7
3	S	97	82.2	79.9
	MSS	2	12.1	13.7
	APMA	0.8	5.6	6.4
4	S	97.3	84.5	80.6
	MSS	2.5	13.5	17.4
	APMA	0.25	2.0	2.0
5	S	98	86.7	86.8
	MSS	1	6.6	8.0
	BAEMA	1	6.7	5.2
6	S	97.1	83.6	81.5
	MSS	2	11.7	14.4
	BAEMA	0.9	5.24	4.1
7	S	72	60.9	64.9
	4VP	20	23.5	25.1
	BNAHD	8	15.5	10.0
8	S	41	35.4	39.7
	4VP	50	47.3	49.8
	BNAHD	8	17.3	10.5
9	S	88	61.3	66.6
	MSS	4	32	26.4
	BNAHD	8	6.7	7.1
10	S	95.7	84.1	74.1
	MSS	4	13.1	24.1
	APMA	0.26	2.7	1.8
	HMEMA	0.036	0.16	0.14

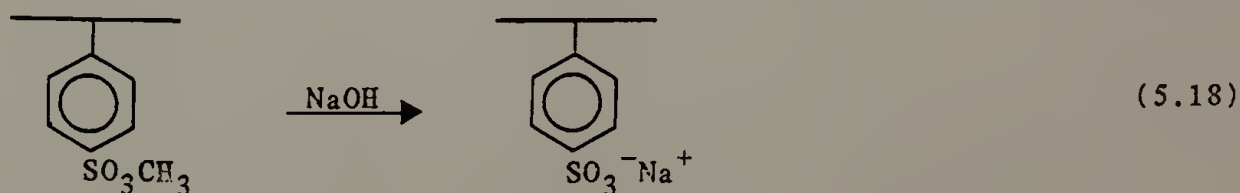
more reactive than 4VP and the polymer feed can be altered accordingly.

The prediction of the composition of a heme containing tetrapolymer (system 10, Table 5.4) is treated in two parts. From the results of Chapter IV, it is estimated that hemes are enriched 3 - 5 times their feed composition in the polymer. Thus, a feed of 0.036 mol % HMEMA in reaction mixture gives 0.11 - 0.18 mol % heme in the polymer. The rest of the polymer composition is estimated using Equation 5.12 and ignoring the contribution of heme reactivity to the polymerization process. The error in predicting the composition of the S/MSS/APMA/HMEMA tetrapolymer is attributed to impurities in the MSS monomer.

As a result of the above work, the synthesis of a ter- or tetrapolymer of a select composition is possible with a minimum of trial and error experiments. This technique requires the reactivity of styrene with each new monomer be studied which greatly reduces experimental labor. Obviously, a change in the identity of the hydrophobic monomer would necessitate a larger number of reactivity ratio studies.

#### Chemical Modification of Polymers

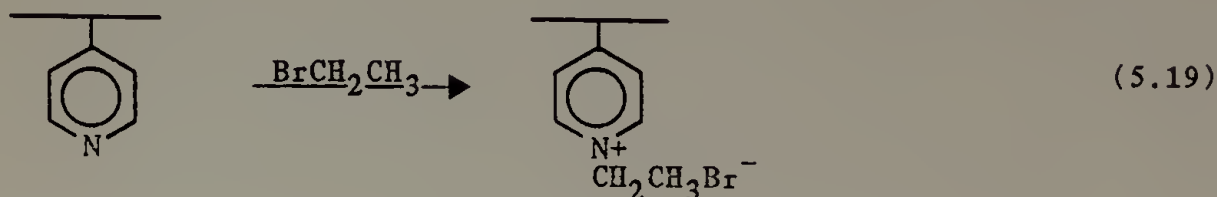
Water Solubility. All of the hydrophyllic monomers were polymerized in a non-ionic form. Methyl p-vinylbenzenesulfonate is easily hydrolyzed by dilute quantities of base such as sodium hydroxide, triethylamine and even methylamine impurities in dimethylformamide.





The counterion can be exchanged by dialysis against a salt solution of the desired counterion.

The quaternization of polymerized 4-vinylpyridine is a slow process.<sup>14</sup>



The reaction temperature is limited to 40°C by the reflux temperature of the reaction solvent. The quaternization was followed by infrared spectroscopy using the appearance of a peak for the pyridinium C=C stretch at 1640 cm<sup>-1</sup> and the disappearance of a peak for the pyridine C=N stretch at 1420 cm<sup>-1</sup> relative to the constant intensity of the C-H stretch at 2940 cm<sup>-1</sup> (Figure 5.1 and 5.2). The reaction is complete after approximately 75 hr. The quaternized terpolymers of S/4VPQ/BNAHD were characterized for hydrophobic domains and the capacity to carry carbon dioxide as a function of pH. The physical properties of the 4VPQ cationic solubilizing group can be generalized to other systems. Unfortunately, the chemical method can quaternize the imidazole nitrogen on HMEMA and thus prevent its coordination to the heme iron group. Chemical modification of a single polymer unit must not alter other functional units in the polymer.

p-Vinylbenzylchloride (VBC) was selected due to its widespread use in the manufacture of anion exchange resins. Polymerized VBC reacts by nucleophilic substitution with trialkylamines to form a water soluble



Figure 5.1. Infrared spectra of S/4VP/BNAHD (60.9/23.5/15.5) before (A) and after (B) quaternization of the pyridine group with bromoethane. Note the pyridine C=N stretch at  $1420\text{ cm}^{-1}$  present before quaternization is not present in spectrum B and a new peak for the pyridinium C=C stretch is evident at  $1640\text{ cm}^{-1}$ .

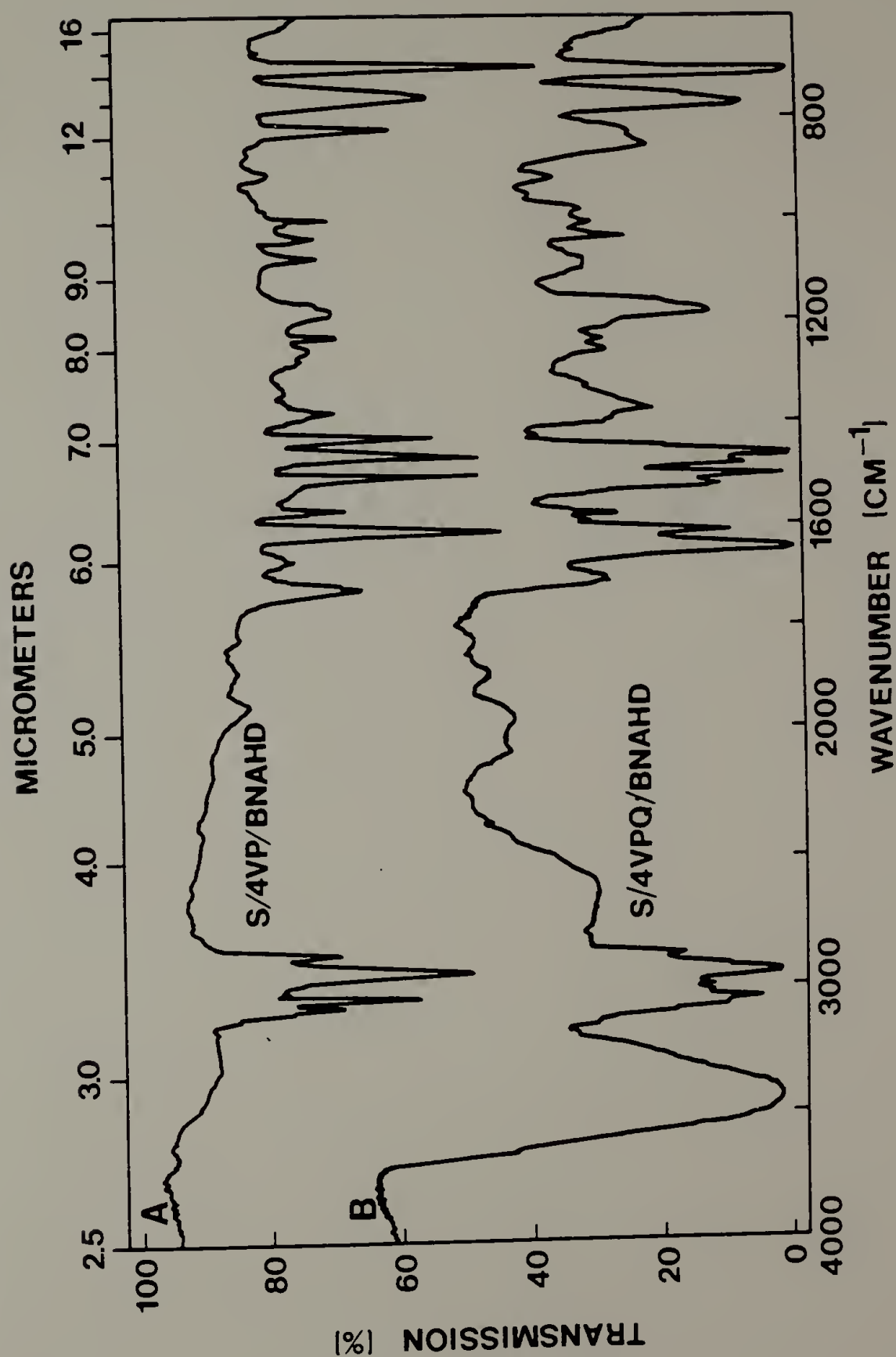
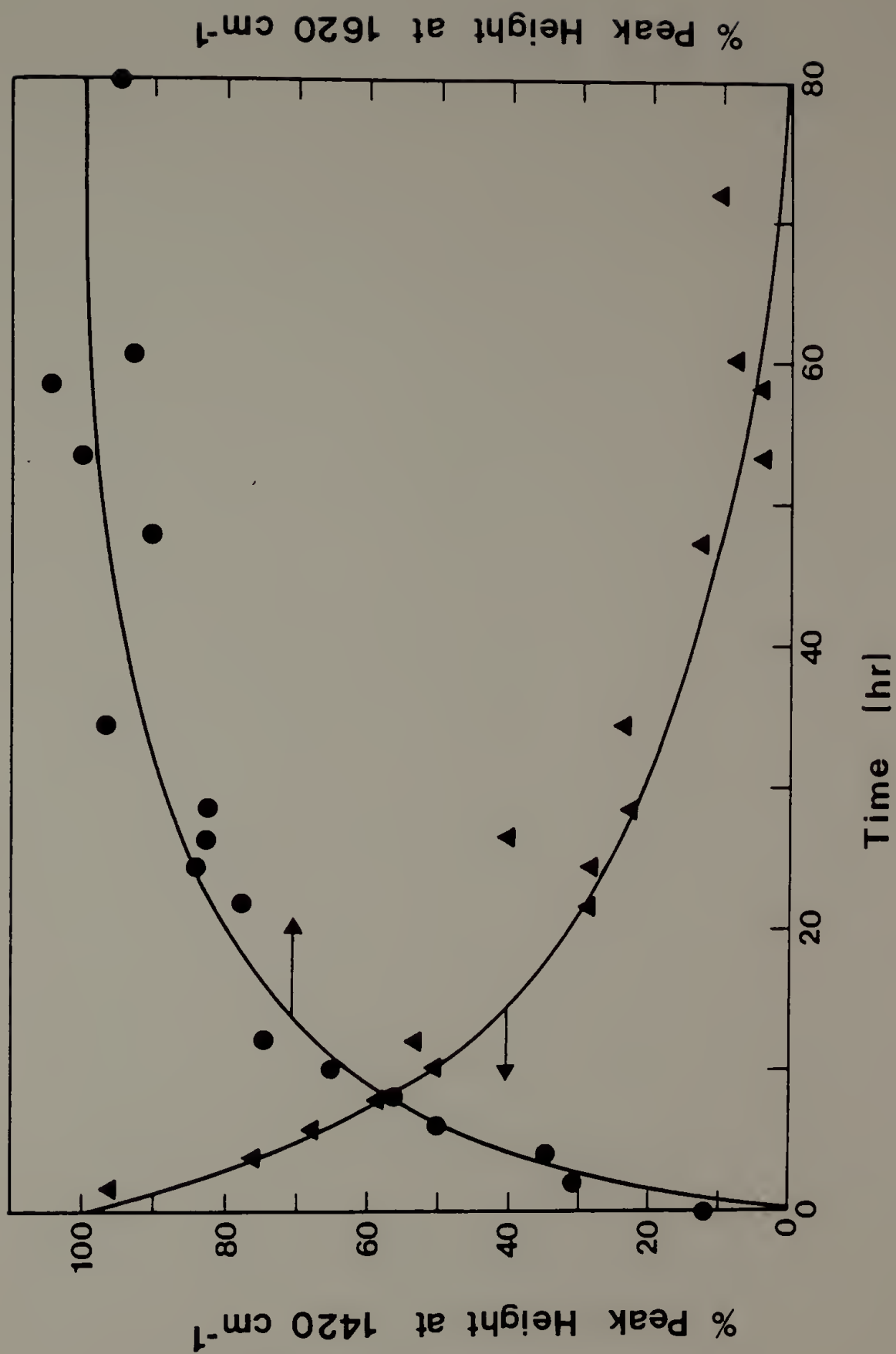


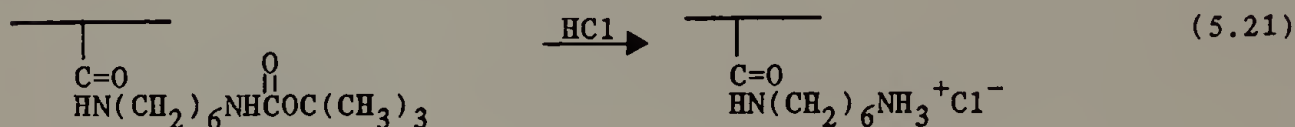
Figure 5.2. The relative peak heights observed by infrared spectroscopy during quaternization of S/4VP/BNAHD as a function of time (●) pyridine C=N stretch at  $1420\text{ cm}^{-1}$ , (▲) pyridinium C=C stretch at  $1640\text{ cm}^{-1}$ . The reaction was complete after 70 hr.



group.<sup>15</sup>

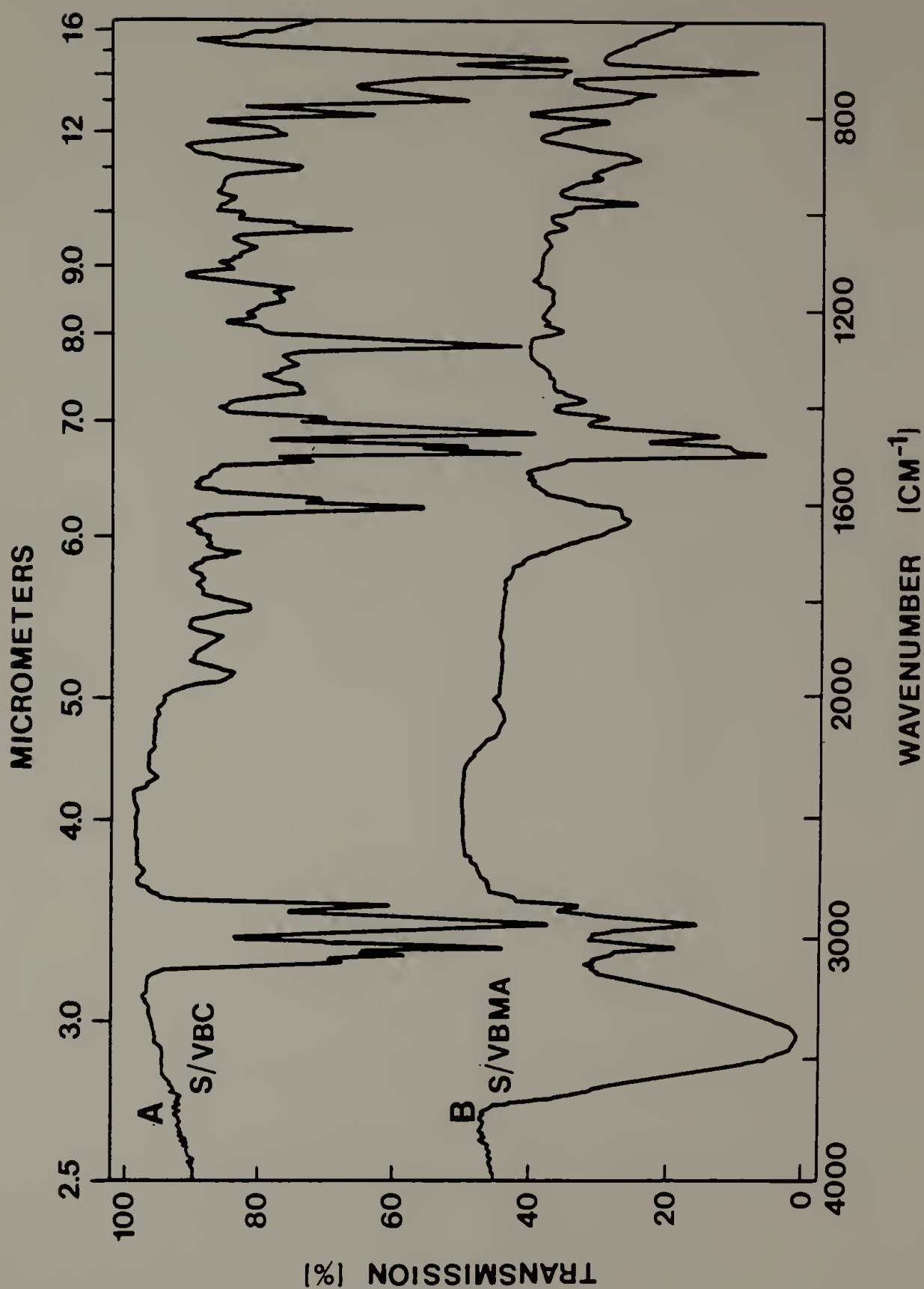
This reaction was complete for a copolymer of S/VBC with 22.5 mol % VBC after three hours as shown by infrared spectroscopy. A comparison of the spectra before and after the reaction is given in Figure 5.3. The clear aqueous polymer solution has soap-like properties.

Removal of the t-Butyloxycarbonyl Protecting Group. The procedure to cleave the t-butyloxycarbonyl (t-BOC) protecting group (Stahl et al.)<sup>16</sup> was acid hydrolysis.



The time of the reaction was lengthened to insure complete cleavage of the polymer bound t-BOC groups which presumably react more slowly than the monomeric analog. Polymers containing the azide moiety are sensitive to the presence of HCl used for cleavage of the t-BOC group and thus more gentle methods would be required to hydrolyze the t-BOC group when APMA and t-BOC-amines are incorporated in the same polymer.<sup>17</sup> The procedure worked equally well for unblocking BAEMA. Benson's test<sup>10</sup> for free amines was used to determine the extent of cleavage of the t-BOC group. It was assumed that the extinction coefficient for the AEMA-

Figure 5.3. The infrared spectra of S/VBC (22.5% VBC) before (A) and after (B) quaternization. A peak at  $1275\text{ cm}^{-1}$  characteristic of  $\text{CH}_2$  wagging in  $-\text{CH}_2\text{Cl}$  observed in (A) completely disappears after three hours using the procedure given in the text.

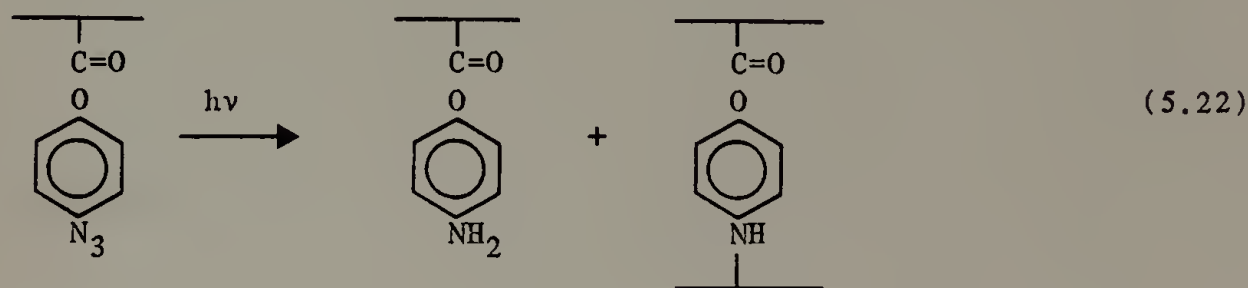




benzoquinone adduct<sup>11</sup> at 510 nm was identical to that for the NADH-benzoquinone adduct. The results from Benson's test gave concentrations of free amine equal to 88.2% of the amine content determined by elemental analysis before cleavage of the t-BOC group. This result verifies that at least 88% of the t-BOC groups have been removed by acidic treatment.

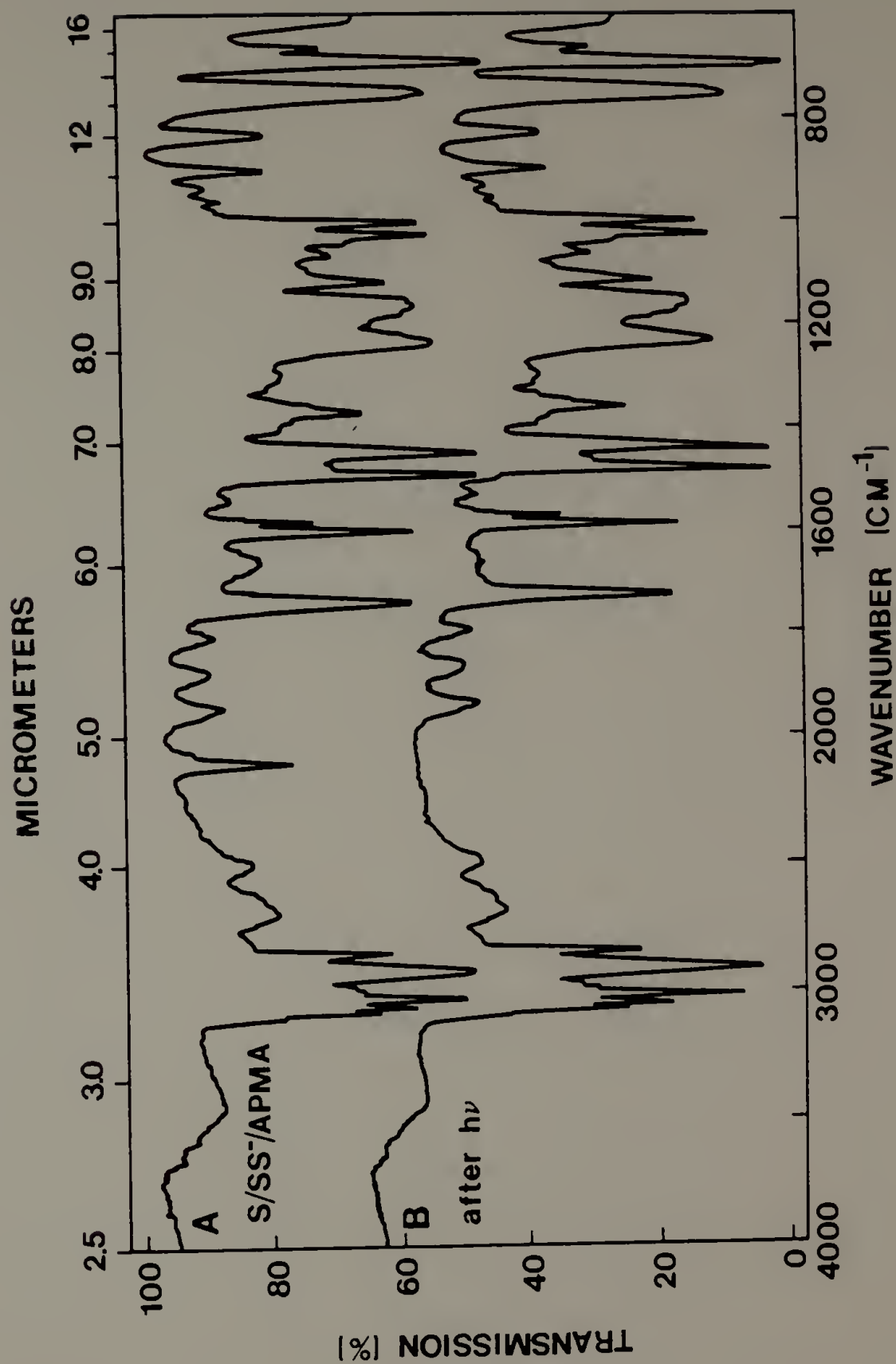
#### Photolysis of the Azide Group

Polymerized p-azidophenyl methacrylate was photolyzed at 254 nm to yield both primary and secondary amines:



An infrared spectrum before and after photolysis shows complete disappearance of the  $\text{-N}_3$  stretch with no other obvious change in the spectrum (Figure 5.4). Photolysis of a copolymer of S/APMA containing 30 mol % APMA in a 5.0 wt % solution in organic solvent yields a crosslinked matrix after a short period of irradiation. This is evidence for secondary amine formation. The efficiency of the crosslinking reaction was not studied. In dilute aqueous solution, it was presumed that polymers are highly coiled with the hydrophobic azide units on the interior of the polymers. Photolysis of a 2.8 weight % solution of S/SS<sup>-</sup>/APMA (84.5/13.5/2) did not result in a network

Figure 5.4. The infrared spectra of S/SS<sup>-</sup>/APMA before (A) and after (B) photolysis of the azide group. Note that after photolysis the -N<sub>3</sub> stretch at 2120 cm<sup>-1</sup> has completely disappeared.



structure. After this solution was allowed to stand for a length of time it gelled. This means that the irradiated solution is in a meso-state and the polymer chains are rearranging to form a thermodynamically preferred state. The terpolymer, S/SS<sup>-</sup>/APMA, is very close to the theta dimension: the solution has a turbid appearance and if the solution is frozen or shaken vigorously the polymer precipitates and will not redissolve in water. Gelation of S/SS<sup>-</sup>/APMA after irradiation could be due to two phenomena. The number of conformations of the terpolymer is limited by intramolecular crosslinks causing gelation due to aggregation of the hydrophobic domains and/or there is some ionic aggregation of sulfonate anions and protonated primary and secondary amines formed by the photolysis reaction. This will be discussed more thoroughly in Chapter VII.

#### Molecular Weight Studies

The molecular weight of four polymers determined by gel permeation chromatography is given in Table 5.5. The influence of the monomer concentration, initiator concentration and monomer purity is evident. As the volume % solvent and the initiator concentration in the reaction mixture are decreased, the molecular weight of the resulting polymer is increased. System 7, S/4VP/BNADH, appears to be an anomaly: comparison of system 7 with system 10, where [AIBN] is nearly equal and system 10 has a lower vol % solvent suggests that system 7 should have a lower molecular weight than system 10 however it does not. The likely cause is MSS in system 10, it is a difficult monomer to synthesize in a pure form. The impurities in MSS probably lower the molecular weights

Table 5.5  
Molecular Weights of Select Polymers Determined by  
Gel Permeation Chromatography in Tetrahydrofuran

System	Polymer	Composition	Vol % Solvent	[AIBN] mol %	$\bar{M}_n$	$\bar{M}_w$	$\bar{M}_w/\bar{M}_n$
10	S/MSS/APMA/HMEMA	84.1/13.1/2.7/0.16	22.2	0.29	45,900	104,800	2.28
7	S/4VP/BNAND	60.9/23.5/15.5	31.3	0.30	54,900	114,300	2.08
9	S/MSS/BNAND <sup>a</sup>	61.3/32/6.7	27.0	0.44	26,800	62,300	2.32
4	S/MSS/APMA	84.5/13.5/2	50.0	1.0	19,700	44,600	2.62

<sup>a</sup>Comparative  $\bar{M}_n$  (= 32,600) determined by <sup>14</sup>C-AIBN labelling.

observed in systems 10, 4 and 9 below the theoretical value. Purity of reactants is an important factor in determining the molecular weight. The choice of solvent affects the rate of initiation and thus the molecular weight (Equation 5.8 and 5.9). The rate of initiation at a constant initiator concentration is higher in DMF than in other media (e.g. bulk, acetone) except for feeds very rich in styrene (95 - 100%).<sup>18</sup> These results show the molecular weight of a terpolymer may be tailored to the desired value by the choice of solvent, monomer concentration, initiator concentration, and impurities or chain terminating agents.

The value of  $\bar{M}_n$  for S/MSS/BNAHD (system 9) was also determined by radioisotopic labelling of the polymer endgroups. Bonta and coworkers<sup>18</sup> have studied the mechanism of termination in the copolymerization of styrene and methyl methacrylate (MMA) and have shown that the mechanism of termination is primarily by combination (Equation 5.11A) for 0 - 60% MMA in the feed mixture. For pure MMA, the fraction of polymer radicals undergoing disproportionation (Equation 5.11B) is 0.71.<sup>19,20</sup> System 9 contains 61.3 mol % styrene and thus the mechanism of termination is assumed to be combination. A 0.0103 g sample of the terpolymer in the counting cocktail had 1188.5 counts per minute and thus a  $\bar{M}_n = 32,660$ .<sup>21</sup> This agrees well with the GPC results ( $\bar{M}_n = 26,800$ ). Disparity in values of  $\bar{M}_n$  could be a result of the difference in the method of purification of the labelled and unlabelled sample, or they could be due to a difference in hydrodynamic volume measured by GPC versus the poly(styrene) standards. A slight milkiness in the counting

cocktail might have caused internal quenching of the fluorescent species (fewer counts) and thus have given a slightly higher  $\bar{M}_n$  than the actual value. In any case, the value obtained by GPC, which is easier to obtain experimentally, is relatively accurate for polymers with greater than 60 mol % styrene. Polymers are characterized by GPC before the removal of blocking groups to give a minimum distortion of the hydrodynamic volume relative to pure poly(styrene).

### Conclusions

Monomers are the clay of an organic polymer chemist. The art lies in their arrangement to give shape and physical character to the model polymer.

Terpolymers with a wide variety of components and compositions have been synthesized. The terpolymer composition equation has been modified to eliminate consideration of the interactions of  $[M_2]$  and  $[M_3]$  in polymerization process for the prediction of polymer composition. This method is most accurate at low  $[M_2]$  and  $[M_3]$  feeds, where the reactivity ratios are well characterized particularly in the case of small values ( $r < 0.15$ ), and for pure reactants. Equation 5.12 is also useful for  $[M_1] = [M_2] > [M_3]$  if the reactivity of  $[M_1]$  and  $[M_2]$  is similar.

Polymers of known composition can be characterized for molecular weight before protecting groups are removed. It has been shown that GPC has adequate accuracy for our purposes. The methods for controlling molecular weight have been demonstrated, but these techniques are not further utilized in this dissertation.



Finally, a polymer of predictable composition and molecular weight can be chemically modified to tailor the physical properties of the polymer such as water solubility or structural rigidity. Most of the work centered on polymers containing a  $[SS^-]$  solubilizing group. This approach was abandoned when polymers containing  $[SS^-]$  and an amine functionality gelled due to the formation of hydrophobic polyampholyte complexes.<sup>22</sup> Cationic systems containing benzyltrimethylammonium (VBMA) substituents as well as amines will not gel.

Polymer samples are assigned acronyms to clearly indicate their components. These acronyms are altered to define the chemical modification after polymerization:

1) hydrophobic,  $[S]$ , no modification;

2) water soluble,



3) amine,



4) heme,  $[HDA]$ ,  $[HDME]$ ,  $[HMEMA]$ , no modification;

5) crosslinking agent



Water soluble polymers with specific chemical and physical properties have been synthesized. Do these polymers reversibly carry oxygen and bind  $CO_2$  as a function of pH? Do they have hydrophobic

domains and intramolecular crosslinks? These questions and others will be answered in the next three chapters.

### References

1. Alfrey, T. Jr; Goldfinger, G. J. Chem. Phys., (1944), 12, 332.
2. Valvassori, A; Sartori, G. Adv. Polymer Sci., (1967), 5, 28.
3. Walling, C.; Briggs, E.R. J. Am. Chem. Soc. (1945), 67, 1774.
4. Odian, G. Principles of Polymerization 2nd ed., McGraw Hill, New York, (1981) p. 447.
5. Kelen, T.; Turssanyi, B.; Disselhoff, G. J. Macromol. Sci.-Chem., (1978), A12(1), 35.
6. Brandrup, J.; Immergut, E.H. (ed.) Polymer Handbook 2nd Ed. Wiley-Interscience, New York (1975) pp. II 1, II 45.
7. For a general discussion of the applicability and accuracy of each experimental method see: Billmeyer, F.W. Textbook of Polymer Science 2nd Ed., Wiley-Interscience, New York (1971), p. 62.
8. Cooper, A.R.; Johnson, J.F.; American Laboratory, (1973), 5, 12.
9. The formula to find the specific activity is given below:  

$$\frac{\text{cpm}}{0.05 \text{ ml}} \times \frac{1 \text{ dpm}}{\text{cpm}} \times \frac{10 \text{ ml}}{0.004 \text{ g}} \times \frac{1 \text{ m Ci}}{2.22 \times 10^9 \text{ dpm}} \times \frac{164.21 \text{ g}}{\text{mol}} \times \frac{1}{e} = \frac{\text{m Ci}}{\text{mol}}$$
 where e is the efficiency of counting determined using a toluene standard.
10. Benson, G.A.; Spillane, W.J. Anal. Chem., (1976), 48(14), 2149.
11. Gillis, J. Senior Honors Thesis, University of Massachusetts, Amherst, Massachusetts (1980).
12. Tanikado, T. J. Polym. Sci., (1960), 43, 489.
13. See Table 3.11.
14. Procedure adapted from: Tsuchida, E.; Osada, Y.; Sunanda, K. J. Polym. Sci., (1972), A(1) 10, 3397.

15. Wessling, R.A.; Pickelman, D.M. J. Dispersion Sci. Tech., (1981), 2  
(2-3), 281.
16. Stahl, G.L.; Walter, R.; Smith, C.W. J. Org. Chem., (1978), 43,  
2285.
17. Greene, T.W. Protective Groups in Organic Synthesis, Wiley-  
Interscience, New York, (1981), p. 222.
18. Bonta, G.; Gallo, B.M.; Russo, S.; Uliana, C. Polymer, (1976),  
17, 217.
19. Bamford, C.H.; Dyson, R.W.; Eastmond, G.C. Polymer, (1969), 10,  
885.
20. Bamford, C.H.; Eastmond, G.C.; Whittle, D. Polymer, (1969), 10,  
771.

21. The equation for determining the molecular weight is as follows:

$$\frac{\text{dpm}}{\text{cc}} \times \frac{\text{cc}}{\text{g polymer}} \times \frac{1 \text{ m Ci}}{2.22 \times 10^9 \text{ dpm}} \times \frac{1 \text{ g AIBN}}{5.52 \times 10^{-3} \text{ m Ci}} \times \frac{1 \text{ mol}}{164.21} \times$$

$$\frac{1}{e} \times \frac{1}{2} = \frac{1}{M_n}$$

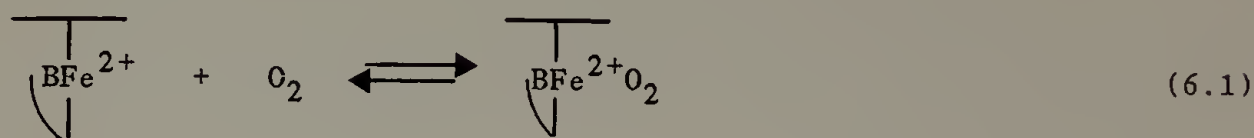
where e is the efficiency of counting determined using a toluene standard.

22. The formation of hydrophobic polyampholyte complexes will be further discussed in Chapter VII.

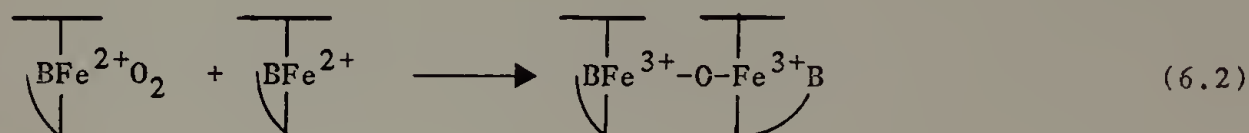
## C H A P T E R VI

### THE OXIDATION KINETICS OF OXYGENATED HEMOGLOBIN MODELS IN AN AQUEOUS ENVIRONEMENT

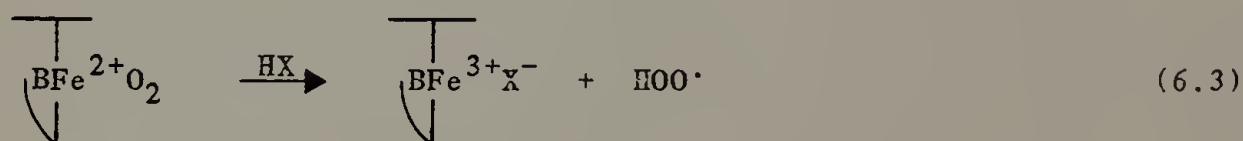
The primary function of a model of hemoglobin is to transport oxygen. This requires a reversible equilibrium between a heme and oxygen dissolved in solution.



Irreversible oxidation to the  $\mu$ -oxo dimer will occur if two heme groups contact each other (see Equation 1.7).<sup>1,2</sup>



Also autooxidation is facilitated by a proton donor solvent (see Equation 1.6).<sup>3,4</sup>



It has been proposed that covalent attachment of a heme group to a polymer chain sterically prohibits heme-heme contact by diluting and dispersing the heme on the polymer chain and thus retarding the oxidation to the  $\mu$ -oxo dimer.<sup>5</sup> Heme groups solvated by hydrophobic domains in the polymer have a slower rate of proton facilitated

autooxidation.<sup>6</sup> Polymer bound hemes in aqueous media reversibly oxygenate with a greater stability than non-polymerized hemes.<sup>7</sup> Most of the work has been performed at lowered temperatures (-10 to -50°C) to slow the rate of oxidation.

### Experimental Procedure

#### Materials

The synthesis of heme polymers used to test reversible oxygenation is given in Chapters IV and V. DMF was purified as described in Chapter II. All solutions were stored in crown cap tubes with neoprene gaskets. A sidearm on the tube with a high vacuum stopcock leading to a ball joint was used to allow the atmosphere to be manipulated efficiently without puncture of the neoprene septum. The source of chemicals used as reducing agents or free radical scavengers is as follows: sodium hydrosulfite (DT) (Fisher), L-ascorbic acid (AS) (Mallinckrodt), aminoiminomethanesulfinic acid (AIMSA) (Eastman, purchased through Fisher), and hydroquinone (HQ) (J.T. Baker). Solutions of reducing agents used to titrate from the oxidized to the reduced form of heme are described below.

Sodium Hydrosulfite (DT) (aprotic media). In a crown cap tube with neoprene gasket, 0.0595 g of sodium hydrosulfite ( $3.3 \times 10^{-4}$  mol) and 0.20 g of 18-crown-6 ( $7.6 \times 10^{-4}$  mol) were degassed. In a separate crown cap tube, 5 ml of anhydrous methanol was degassed. The methanol was added to the DT in a glove bag, under a nitrogen stream and the solution was stirred for 0.5 hr until the DT dissolved in the solution.

The shelf-life of this reducing agent was about 3 days. In some freshly made solutions a bright yellow color appeared very suddenly and disappeared again within an hour. This might have been due to some dissolved anion or decomposition product of the DT.

Sodium Hydrosulfite (DT) (aqueous). A 0.1 M phosphate buffer was prepared from two stock solutions. Stock solution A contained 27.8 g of monobasic sodium phosphate in 1000 ml of distilled water (0.2 M) and B contained 53.65 g of dibasic sodium phosphate ( $\text{Na}_2\text{HPO}_4 \cdot 7\text{H}_2\text{O}$ ) in 1000 ml of water (0.2 M). A buffer of  $\text{pH} = 7.4$  and 0.1 M concentration was obtained by the combination of 19.0 ml of A and 81.0 ml of B and dilution to a total volume of 200 ml. In a crown cap tube, 5 ml of the phosphate buffer was degassed and then was mixed with solid oxygen-free DT (0.1 g,  $5.74 \times 10^{-4}$  mol) in a glove bag. The reducing agent was stored under nitrogen in a glove bag and remained useful for 2 - 4 days.

Aqueous DT was used in conjunction with a free radical scavenger, hydroquinone. Hydroquinone solutions were prepared by combining 0.1 g ( $9.1 \times 10^{-4}$  mol) of the solid with 10 ml of the phosphate buffer and the mixture was thoroughly degassed. Aqueous hydroquinone solutions were stored in the dark under a nitrogen atmosphere and remained colorless for several weeks.

Ascorbate (AS) (aqueous). A solution of 0.1020 g of L-ascorbic acid ( $5.8 \times 10^{-4}$  mol) in 5 ml of  $\text{H}_2\text{O}$  was titrated with a 1 M KOH solution to a  $\text{pH} = 7 - 8.5$ . The total volume was adjusted to 10 ml and the solution was degassed and stored at  $7^\circ\text{C}$ . Solutions of AS were stable for approximately 7 days.



Aminoiminomethanesulfinic acid (AIMSA) (aqueous). A solution of 0.1 g of AIMSA ( $9.2 \times 10^{-4}$  mol) in 5 ml of  $H_2O$  was titrated with 1 M KOH to pH = 7.4. The total volume was adjusted to 10 ml and the solution was degassed and stored at 7°C.

#### Solutions For Oxygenation Studies

The concentration of heme or heme-polymer in solution was adjusted to give the absorbance for the Soret of the oxidized species equal to three. The extinction coefficients determined for the monomers were assumed correct for the heme-containing polymers. Aqueous heme polymer solutions were concentrated using ultrafiltration (Amicon - Model 52) through either a UMIO (old) or YMIO (new) membrane with a molecular weight cut off of 10,000.

Heme monomers. The solutions for oxygenation of HDA, HDME, EMEMA in pure DMF were prepared by dissolving approximately  $3.3 \times 10^{-8}$  moles of heme per ml of DMF. The solution was degassed in a crown cap tube by three to five cycles of freezing, evacuation and then thawing. Heme solutions were stored in a glove bag under a blanket of nitrogen for no more than 5 days.

S/HDA; S/HDME. Solution of 0.0680 g of S/HDME (0.18 mol % HDME) in 25 ml of DMF and 0.0682 g of S/HDA (0.14 mol % HDA) in 25 ml of DMF were degassed in crown cap tubes and stored as described for the monomer solutions.

S/SS<sup>-</sup>/HDA. This terpolymer was synthesized from 0.0981 mol of styrene, 0.0021 mol of MSS,  $1.014 \times 10^{-4}$  mol of HDA, and 0.0011 mol of AIBN in 15 ml of DMF. The heme was polymerized in the reduced state

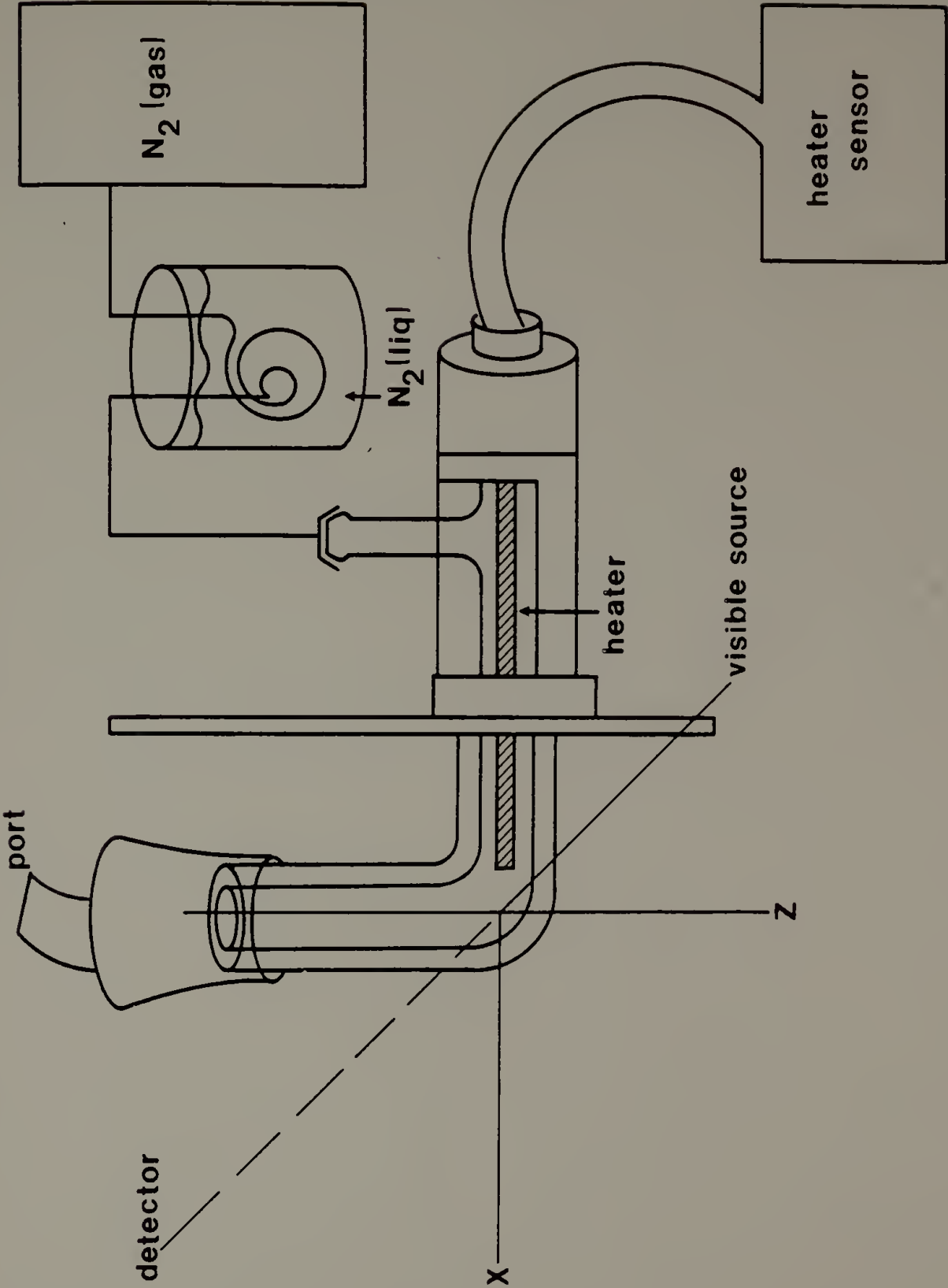
with a carbon monoxide sixth ligand, as described in Chapters IV and V. The polymer contained 0.4 mol % HDA. It was rendered water soluble via techniques described in Chapter V and concentrated using ultrafiltration. Solutions of S/SS<sup>-</sup>/HDA in pure water or water/ethylene glycol (1/1) were degassed by flushing with nitrogen for 30 min in a crown cap tube. (Freezing of solutions of S/SS<sup>-</sup>/HDA in H<sub>2</sub>O caused the polymer to precipitate from solution and it would not redissolve without the addition of organic solvents.) These solutions were stored under nitrogen in a glove bag for no more than five days.

S/SS<sup>-</sup>/APMA/HMEMA. The synthesis of this tetrapolymer was described in Chapter V. It was rendered water soluble by base hydrolysis of the methylsulfonate group and concentrated by ultrafiltration. The concentrated solution was diluted with the desired quantity of DMF or ethylene glycol to give about 0.25 weight % polymer dissolved in solution. The tetrapolymer in organic/aqueous solution mixtures of 9/1, 8/2, 65/35, (DMF/H<sub>2</sub>O) or 1/1 (ethylene glycol/H<sub>2</sub>O) were degassed by cycles of freezing, evacuation and thawing. These solutions were stored under nitrogen in a glove bag for no more than five days.

#### Equipment

A schematic of the low temperature dewar designed to regulate the temperature of a sample for the Beckman Acta MVI spectrophotometer is shown in Figure 6.1. The temperature was adjusted using a Varian Temperature Controller and probe calibrated by a copper-constantan thermocouple connected to a digital thermometer with an internal ice point. The equilibrium temperature was attained in a 3 ml sample after

Figure 6.1. A schematic of the low temperature dewar designed to regulate sample temperature for the Beckman Acta MVI spectrophotometer.

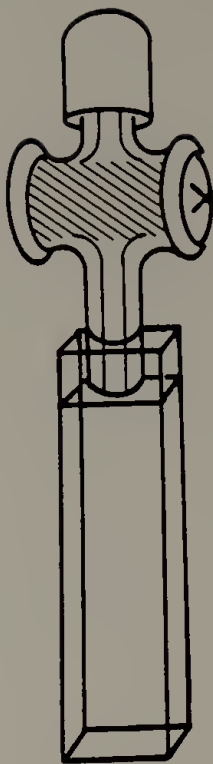


30 minutes. The temperature gradient from the top to the bottom of a sample was less than  $2^{\circ}\text{C}$ . The glass dewar was not completely optically transparent and thus the absorbance of the spectrum obtained was not absolutely quantitative. The spectra for a single sample with various ligands or oxidation states can be compared on a quantitative basis. The face plate for the spectrophotometer sample chamber was custom made to accommodate the low temperature equipment. The visible sample cell was purchased from Hellma and the seal, consisting of a ground glass joint leading to a stopcock, was modified. The modification included a reduction of the total length, the substitution of a 'screw-head' for the stopcock handle and the widening of the free end to fit a rubber septum with a 6.6 mm stopper diameter (Figure 6.2). The seal and the cell were securely held together by a rubber band to prevent accidental separation of the two pieces.

### Procedure

The procedure for sample handling, reduction and monitoring of the oxygenation/oxidation kinetics was identical for all samples. The samples were transferred from the crown cap tube to the sample cell in a glove bag under a heavy flow of nitrogen via a syringe. The sample was sealed quickly. Reducing agents and the hydroquinone (HQ) solution were stored in the glove bag. A 50  $\mu\text{l}$  syringe (Hamilton) was filled with the reducing agent or HQ solution and these were removed from the glove bag with the sample. A spectrum of the sample was taken and then the sample was titrated by 0.5 - 1.0  $\mu\text{l}$  aliquots of the reducing agent to give approximately 90% reduction. (The ratio of the absorbance of the 100%

Figure 6.2. The visible sample cell used in kinetic studies of the oxidation of oxygenated heme models.





reduced to the 100% oxidized at a given wavelength was a constant.) If a free radical scavenger was to be used, 4  $\mu$ l of the hydroquinone solution ( $9.1 \times 10^{-8}$  mol/ $\mu$ l) was added before the titration with reducing agent. The reduced sample was cooled for 30 - 45 minutes and 20 ml of oxygen was bubbled through the sample. The height of the  $\beta$  peak (530 - 537 nm) of the oxygenated species was followed as a function of time (Figure 6.3). After 4 - 6 hours the sample was warmed to 25°C to give a constant absorbance value ( $\sim$  30 min) and then cooled to the oxygenation temperature to give a constant absorbance ( $\sim$  60 min) which was the  $A_{\infty}$  value.

### Calculations

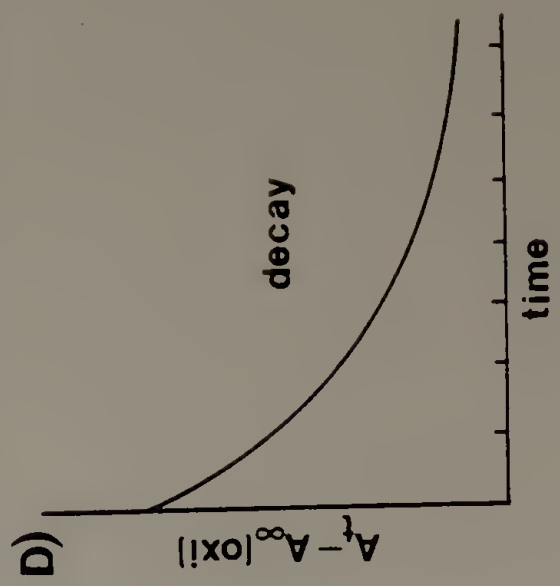
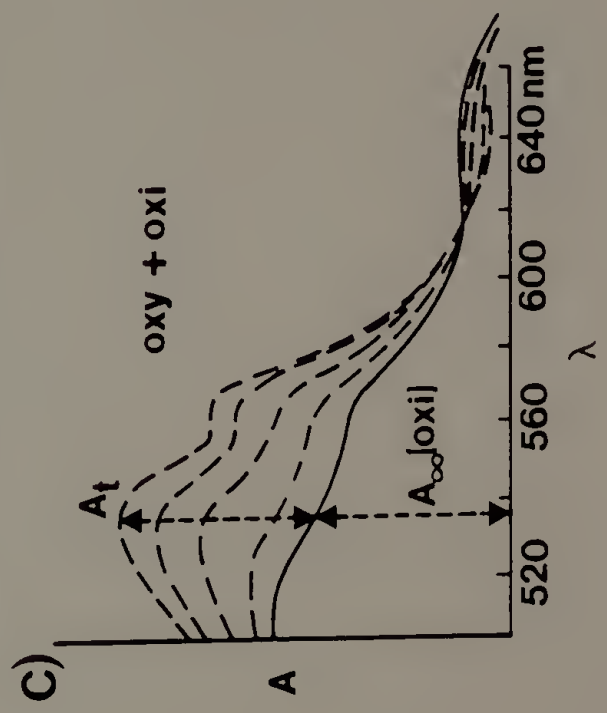
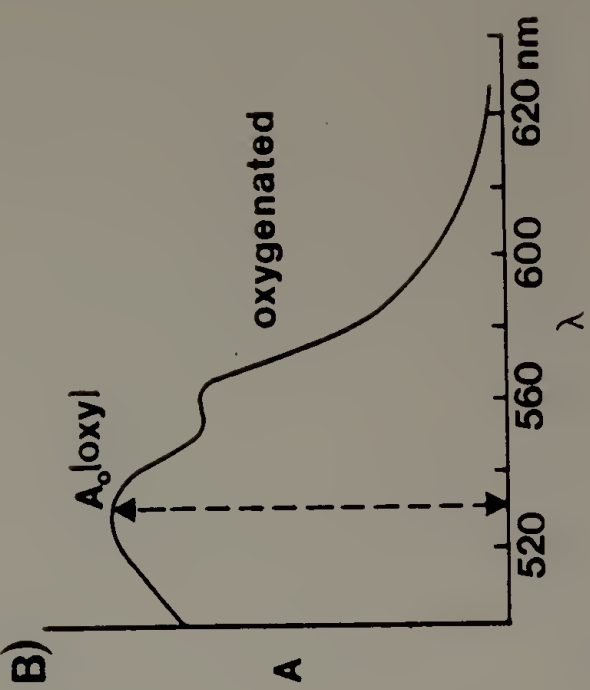
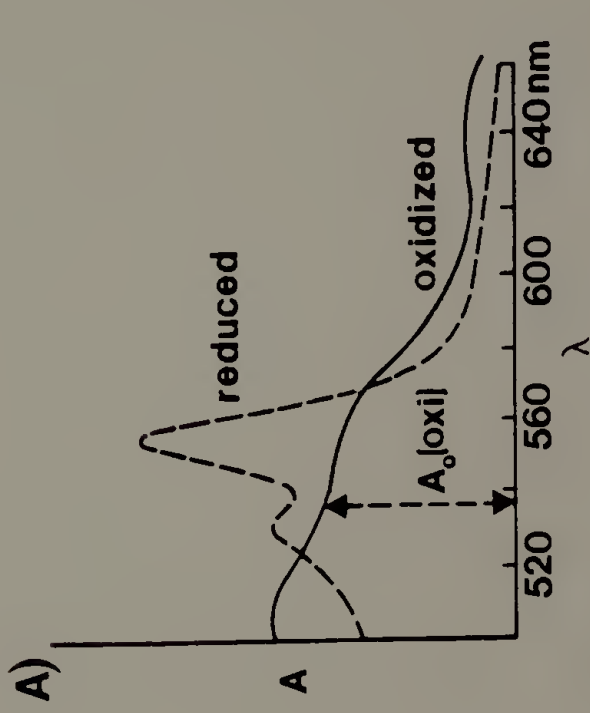
The absorbance  $A_t$  of the mixture of oxygenated and oxidized heme was obtained from the decay curve (as shown in Figure 6.3) at regular time intervals. The value of  $A_{\infty}$  was subtracted from  $A_t$  to give the total absorbance of the oxygenated species. The kinetic order of  $A_t - A_{\infty}$  versus  $t$  was obtained by trial and error plotting of the data: for first-order kinetics one must plot  $\ln(A_t - A_{\infty})$  versus time and for second-order kinetics one must plot  $1/(A_t - A_{\infty})$  versus time. A linear plot with a correlation coefficient of 0.99 was used as conclusive evidence for a description of kinetic behavior.

## Results and Discussion

### Solution Preparation

The kinetics of the oxidation of an oxygenated heme are strongly influenced by the sample age and purity, the type of reducing agent

Figure 6.3. Representative visible spectra observed during kinetic studies: (A) The sample is titrated with reducing from agent the oxidized (——) to the reduced (-----) state. (B) Oxygen is injected and an oxygenated spectrum is observed. (C) The decay of the spectrum from the oxygenated to the oxidized state is observed as a function of time. (D) The decay of the maximum of the  $\beta$  peak is recorded as a function of time.

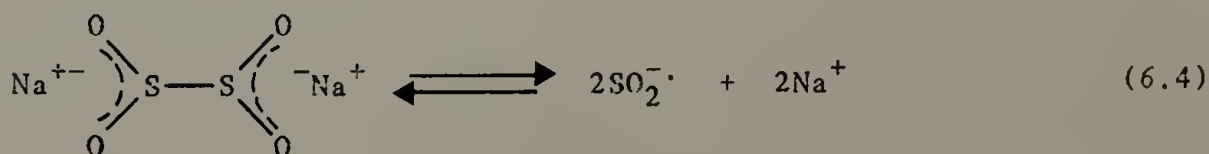


used, the choice of solvent and temperature as well as a host of less obvious factors. For these reasons, solutions of heme and heme-containing polymers were degassed thoroughly to reduce contamination by dissolved oxygen. The solutions were stored under nitrogen for a maximum of five days to ensure high purity i.e. eliminate the possibility of an oxygen leak. A mixture of DMF and water is one of the most commonly used solvent systems in the study of heme model systems. DMF is degraded slowly in the presence of light, water or oxygen, thus the purity of a DMF/H<sub>2</sub>O mixture (9/1) is reduced significantly after storage for a few days.

#### Reducing Agents

The choice and quantity of reducing agent used to reduce a heme containing system to the ferrous state is crucial in a kinetic study. An ideal reducing agent should be highly pure and rapidly reduce the ferric porphyrin without side reactions. Excess reducing agent can give false oxygenated spectra and can increase the stability of the oxygenated species.<sup>8,9</sup>

Sodium hydrosulfite, Na<sub>2</sub>S<sub>2</sub>O<sub>4</sub>, (commonly called sodium dithionite, DT) has been used extensively to reduce a variety of substances in aqueous solution including heme derivatives. The S-S bond is very weak resulting in the dissociation into a pair of SO<sub>2</sub><sup>-</sup> radical anions which are thought to be the reducing species.<sup>10</sup>



The dithionite ion rapidly reduces dioxygen to water thus the reducing agent solutions were prepared in a nitrogen atmosphere to avoid loss of the reductant.

Mincey and Traylor<sup>11</sup> developed a novel system whereby sodium dithionite was used in an aprotic media, thus allowing the study of the oxygenation of model hemes that are sensitive to proton facilitated autooxidation. A crown ether capable of complexing the sodium ion, 18-crown-6, was employed to solubilize the dithionite in nonaqueous media. Two moles of crown ether were required to solubilize one mole of sodium dithionite. Concentrations of up to 0.3 M were achieved in methanol. Mincey and Traylor claimed that the rate of reduction of dioxygen by the crown ether complex of dithionite is very slow in aprotic solvents. Thus, in the presence of oxygen, the complex selectively reduces hemin to yield an oxygenated ferrous heme i.e. an excess of the complex would give a false oxy spectrum.

Despite Mincey and Traylor's undocumented claim that the reaction was quick and quantitative, we observed the reaction of the DT/18-crown-6 complex to be quite slow. After addition of a microliter quantity of the reducing agent to the ferric heme in DMF the absorbance of the reduced species increased with the equilibration time of 15 - 30 minutes. Older solutions of the reducing complex (24 - 48 hr old) required even longer times to reach the fully reduced state. The reduction procedure requires titration of the reducing agent to 80 - 90% completion. There is no way to standardize the purity of the reducing agent and thus the rate of reduction. Therefore one can easily add an

excess of the DT/18-crown-6 complex causing false oxy species or enhanced stability of the oxy species to be observed.

In nonaqueous systems, four-coordinate hemins such as HDME are ligated by some component of the dithionite reducing system. Visible spectra for a S/HDME copolymer in DMF at 25°C are shown in Figure 6.4. The initial oxidized spectrum is characteristic of HDME with a chloride counterion. With the addition of DT/18-crown-6 complex, the spectrum changes to a strange shape characteristic of some type of heme-DT interaction ( $\lambda_{\text{max}} = 565 \text{ nm}$ ). Addition of oxygen to completely reduced S/HDME ( $\lambda_{\text{max}} = 554 \text{ nm}$ ) also yields this spectrum. The original oxidized spectrum with a chloride counterion is again obtained from the heme-DT complex with the addition of a few microliters of 1% HCl. Addition of excess pyridine to the heme-DT complex yields a hemochrome characteristic of the six-coordinate bis-pyridine adduct ( $\lambda_{\text{max}} = 548, 512 \text{ nm}$ ). This suggests that the dithionite anion or a degradation product of the dithionite is a counterion for the four-coordinate ferric porphyrin.

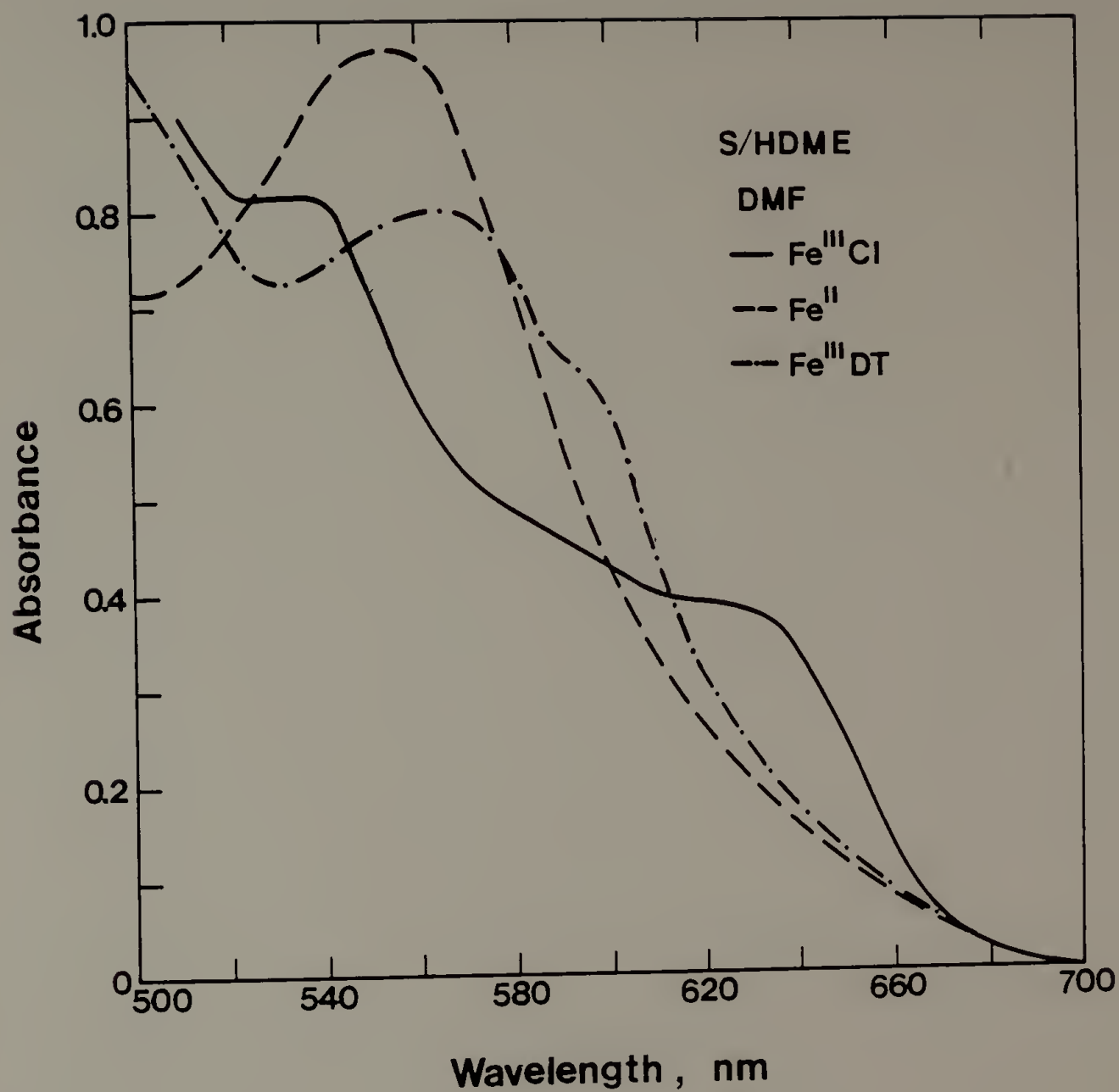
A second technique to reduce hemin in water immiscible solvents by shaking with an aqueous solution of dithionite was devised by Brault and Rougee<sup>12</sup> and Momenteau.<sup>13</sup> This method fails when the solvent is water miscible or if excess oxygen is present. This technique was adapted by Tsuchida<sup>14</sup> to allow the use of water miscible aprotic solvents. A hemin-polymer solution in methylene chloride was extracted with sodium dithionite under a carbon monoxide atmosphere, the layers were separated and the organic layer evaporated to dryness under a CO stream. The solid ferrous heme-polymer was then dissolved in an oxygen-free aprotic

Figure 6.4. The visible spectra of S/HDME copolymer in DMF:

(——) oxidized state with a chloride counterion,

(-----) reduced state,  $\lambda_{\text{max}} = 552 \text{ nm}$ ; (-'-) oxidized  
state with a dithionite counterion.





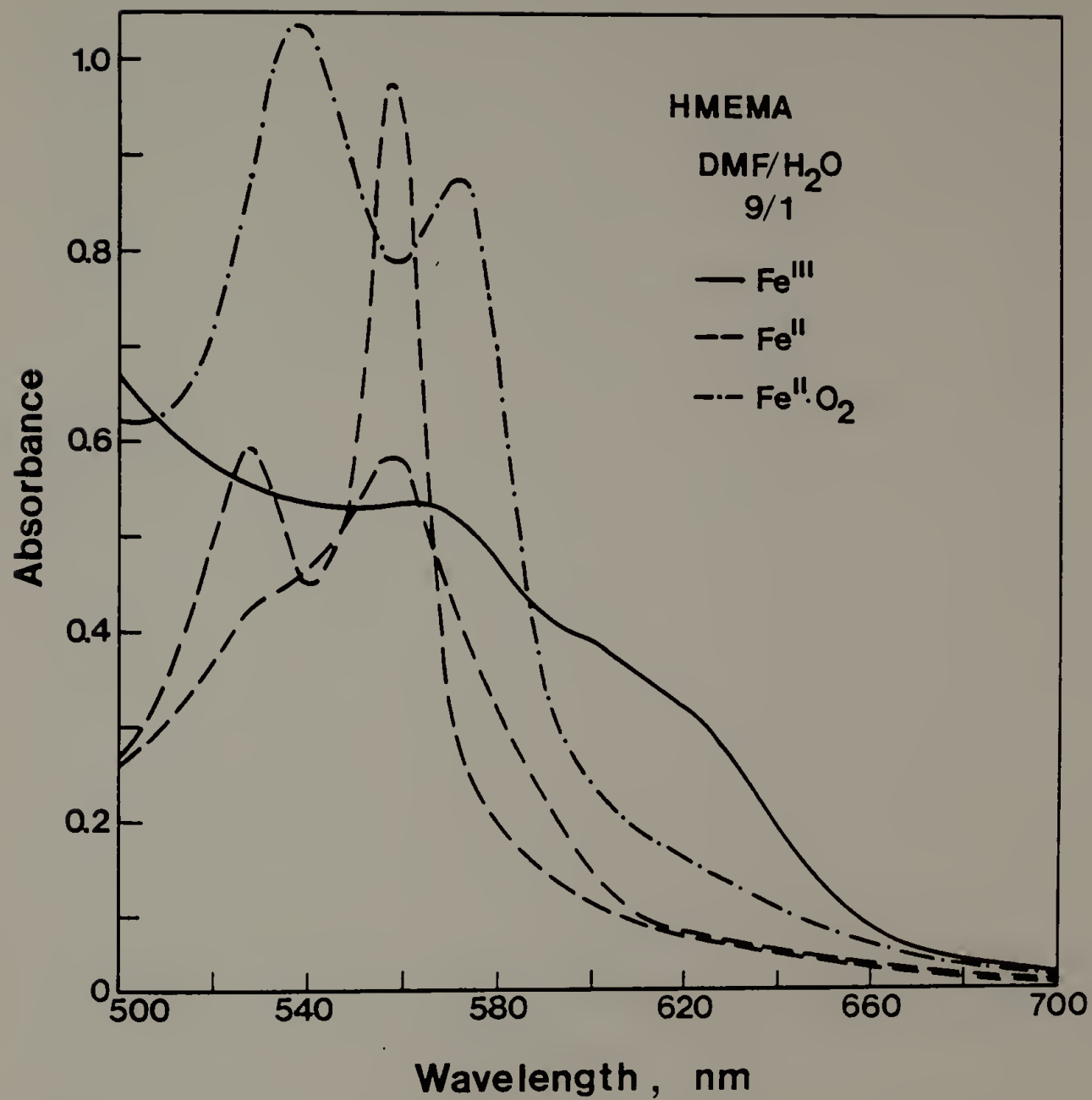
solvent (e.g. DMF). These techniques are extremely time consuming and hemes which are oxidatively unstable are easily oxidized by oxygen contaminants. HDME (FeIII) monomer was approximately 80% reduced using this technique in our laboratory. The total concentration of heme dissolved in an average sample is  $3.5 \times 10^{-5}$  moles/l, thus a very small amount of oxygen contamination would totally oxidize the sample.

The simplicity of hemin reduction by DT in water has encouraged many researchers to use solvent systems which contain 10 vol. % water or more. Tsuchida and coworkers<sup>14,15</sup> have used aqueous sodium dithionite as a reducing agent and denied contribution of the DT or its residue to the reversible oxygenation of heme models on the following basis: i) a small excess of sodium dithionite (5 times the quantity of hemin in solution) was used for the reduction and no trace remained before oxygen exposure, ii) the porphyrin ring was degraded and no oxygenation was observed for a large excess of dithionite, iii) organic reductants such as L-ascorbic acid formed an oxy adduct with the same spectrum and the same lifetime as with the dithionite reducing agent.

We attempted to repeat Tsuchida's experiment<sup>15</sup> in which HMEMA, the five-coordinate model compound, reversibly oxygenated following first-order kinetics with a  $t(1/2) = 98$  min in DMF/H<sub>2</sub>O (9/1) at -30°C. Figure 6.5 shows the visible spectra of the  $\alpha$  and  $\beta$  bands of HMEMA in the oxidized, reduced ( $\lambda_{\max} = 557, 527$  nm) and oxygenated ( $\lambda_{\max} = 572, 537$  nm) states. As the temperature of the sample was decreased the peak heights increased as shown in Figure 6.5 for the reduced species. At -30°C the reduced species is clearly six-coordinate with the sixth

Figure 6.5. The visible spectra of HMEMA in DMF/H<sub>2</sub>O (9:1):

(——) oxidized state, (-----) the reduced state at room temperature (small) and -30°C (tall) where  $\lambda_{\text{max}}$  = 527,557 nm, (-·-) the oxygenated state at -30°C where  $\lambda_{\text{max}}$  = 537,572 nm.

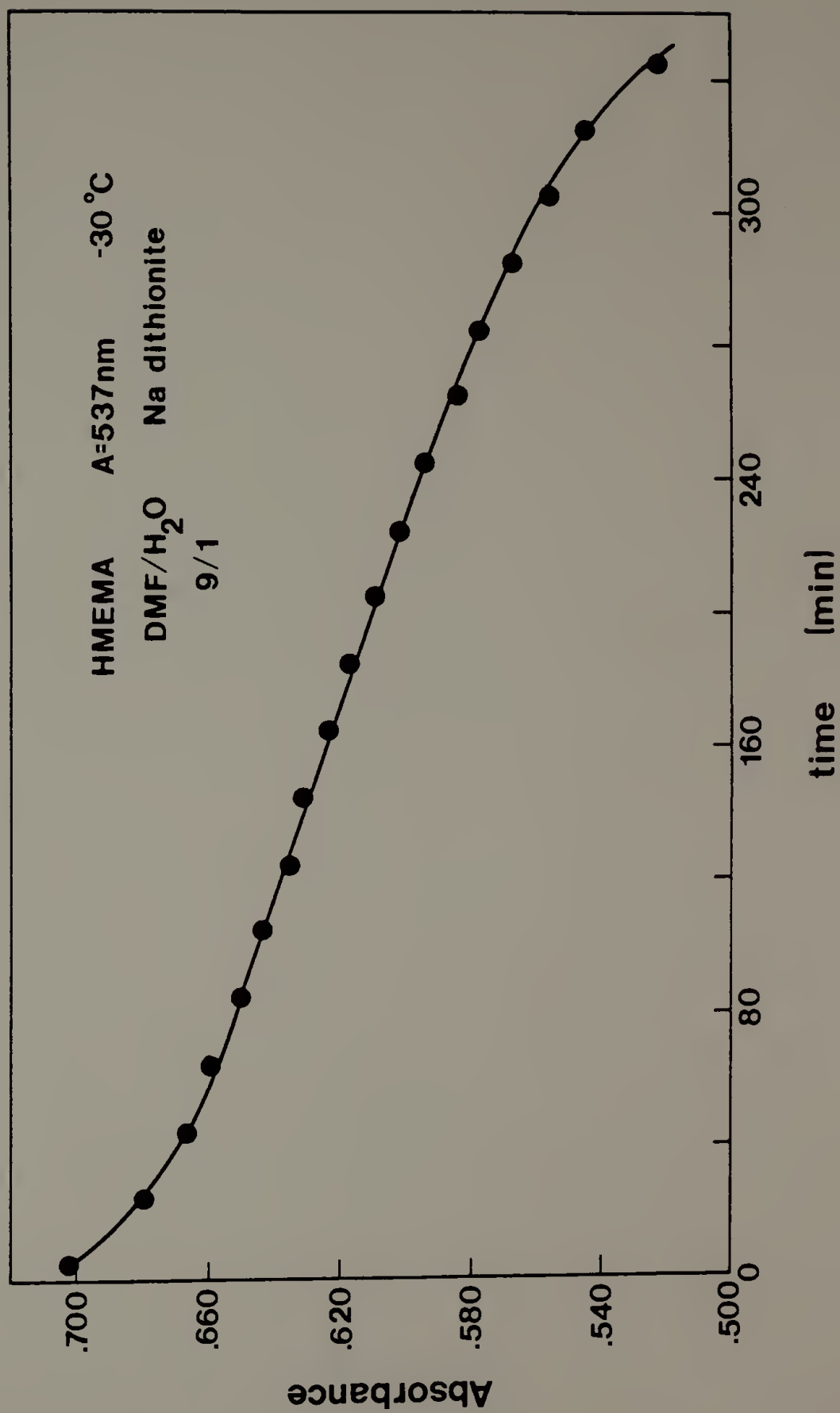


ligand presumably a solvent molecule. A representative decay curve from the oxygenated to the oxidized species monitored at  $\lambda = 537$  nm ( $\beta$ -peak) under the above experimental conditions is shown in Figure 6.6. As previously stated, the reduction of the heme sample was approximately 85% complete. A 3 ml sample contained about  $9 \times 10^{-8}$  moles of heme and thus theoretically 1  $\mu$ l of perfectly pure sodium dithionite in water ( $9.1 \times 10^{-8}$  moles) would exactly reduce the heme solution. Trace contaminants of oxygen in the solvent consumed some of the added DT thus 1-4  $\mu$ l of DT was required for the partial reduction. In instances where even a slight excess of DT was added the solution was discarded.

The decay observed in the first 3 hr was first-order with a half life of 60 - 180 minutes, depending on the purity and age of the sample and the reducing agent solution. After 3 hr the curve in Figure 6.6 has an inflection point and the rate of decay accelerates. Also, the absorbance of the oxidized species at  $A_{\infty}$  was significantly less than that of the starting solution,  $A_0$  (oxi) at all wavelengths. Half-life values in the range of Tsuchida's were obtained by using  $A_{\infty}(\text{oxi}) = A_0(\text{oxi})$ . The value of  $A_{\infty}(\text{oxi})$  determined at the end of the experiment yielded a half-life six times that for  $A_0(\text{oxi}) = A_{\infty}(\text{oxi})$ .

To understand the variables involved in the oxygenation of HMEMA, the absorbance spectrum of a heme solution at room temperature was monitored over a two hour period. Variables of light, oxygen and added aqueous sodium dithionite were studied. Only samples containing aqueous dithionite in an oxygen atmosphere degraded, regardless of the presence of light. This suggests that some degradation product of sodium

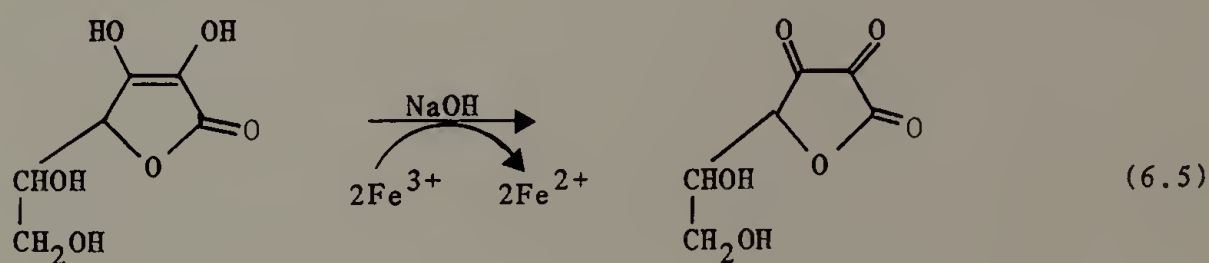
Figure 6.6. The decay in absorbance observed for the reaction of HMEMA from the oxygenated to the oxidized state using a dithionite reducing agent in DMF/H<sub>2</sub>O (9/1) at -30°C, (A at 537 nm).





dithionite causes the porphyrin to be degraded and thus a loss of absorbance is observed with time. This is commensurate with Tsuchida's claims that in the presence of a large excess of added dithionite the heme degrades. The degradation might be due to the  $\text{SO}_2^-$  radical anion or a degradation product of dithionite. These experiments raised an important question: what effect does added sodium dithionite have on the kinetics and rate of the oxidation of ferrous porphyrins? Are Tsuchida's results concerning the half-life and order of decay meaningful (assuming  $A_\infty(\text{oxi}) = A_0(\text{oxi})$  at short times)?

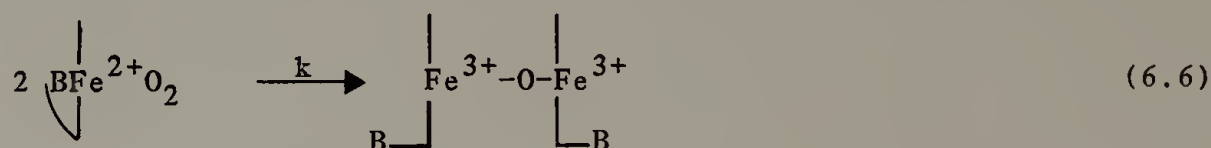
The next obvious step was to study organic reducing agents such as L-ascorbic acid to see if they indeed reproduced the results using DT as a reductant. The preparation of L-ascorbate (AS) was described by Minnaert.<sup>16</sup> The oxidation of L-ascorbate to dehydroascorbate is catalyzed at neutral to basic pH and generates two electrons.<sup>17</sup>



The oxygenation of HMEMA in DMF/ $\text{H}_2\text{O}$  (9/1) was studied at  $-10^\circ\text{C}$  using ascorbate as the reductant. The reduction was fairly quick at room temperature. After each addition, 5 minutes was allowed for equilibration. (At low temperatures the reduction was prohibitively

slow.) No more than 1  $\mu$ l AS ( $5.8 \times 10^{-8}$  mol), approximately a 0.3 fold excess, was used in the reduction reaction. A plot of the decay in absorbance at 537 nm as a function of time for three samples is given in Figure 6.7. The initial concentration of oxygenated hemes represented by  $A_0(\text{oxy}) - A_\infty(\text{oxi})$  differs because heme concentration and the exact fraction of the reduced hemes vary from sample to sample. The curves are shifted along the x-axis to demonstrate that the rate of decay is only dependent on the concentration of oxygenated heme in solution ( $A_t(\text{oxy} + \text{oxi}) - A_\infty(\text{oxi})$ ).

A second-order treatment<sup>18</sup> of the oxidation of HMEMA (FeII) assuming



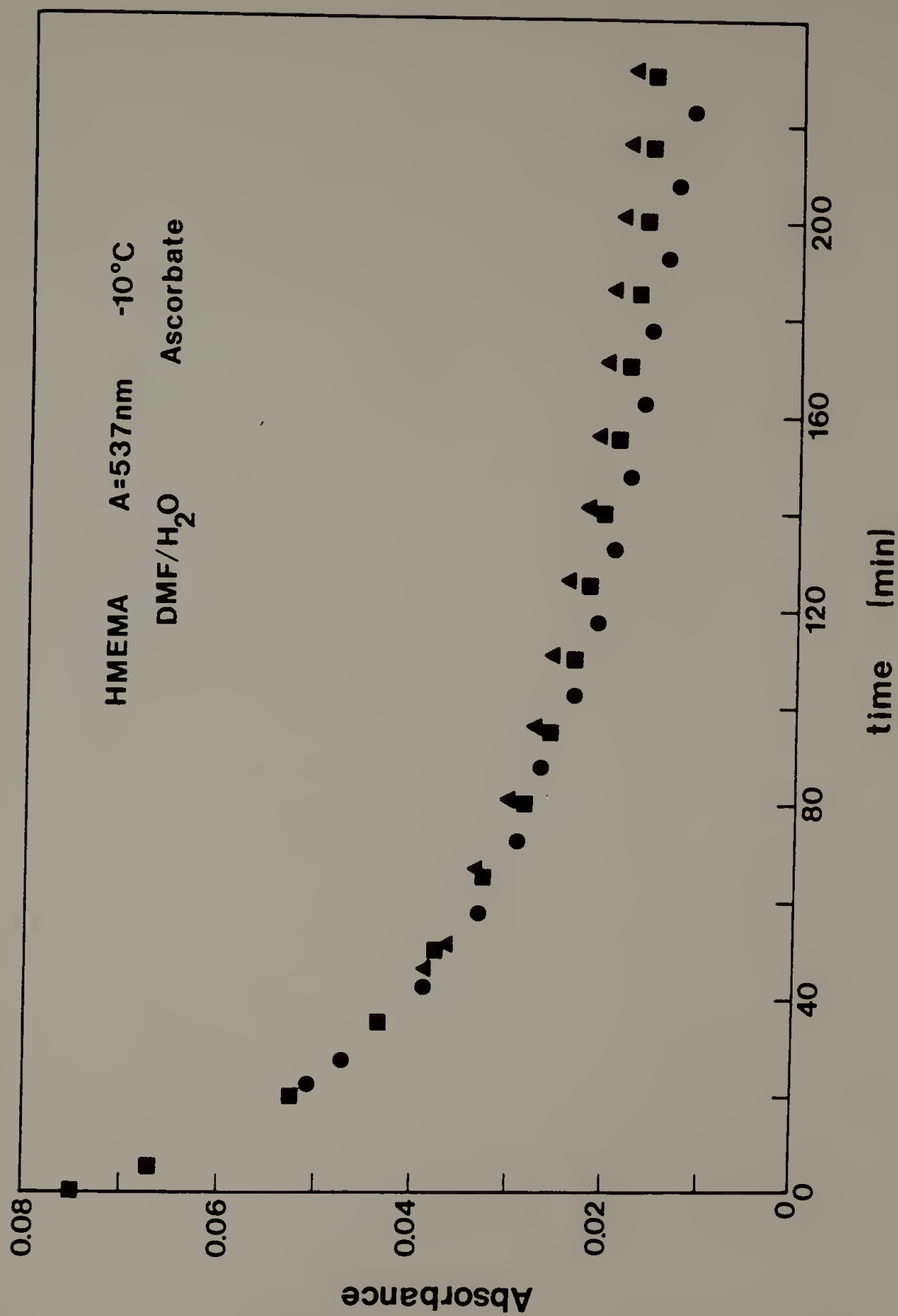
gives the following rate expression:

$$\frac{-d[\text{Fe}^{2+}\text{O}_2]}{dt} = k[\text{Fe}^{2+}\text{O}_2]^2 \quad (6.7).$$

Integration of the rate equation yields

$$\frac{1}{[\text{FeO}_2]_t} - \frac{1}{[\text{FeO}_2]_0} = kt \quad (6.5).$$

Figure 6.7. The decay in absorbance observed for the reaction of HMEMA from the oxygenated to the oxidized state using an ascorbate reducing agent in DMF/H<sub>2</sub>O (9/1) at -10°C, (A at 537 nm). Different symbols indicated different experiments which have been shifted along the x axis to align the curves. This demonstrates that the rate of decay depends on the concentration of the oxygenated species.



If

$$c[\text{FeO}_2]_t = (A_t - A_\infty) \quad (6.9)$$

where  $c$  is a constant which combines the molar extinction coefficient and the pathlength, then a plot of  $1/(A_t - A_\infty)$  versus time yields a line of slope  $= k$  and intercept  $= 1/(A_o(\text{oxy}) - A_\infty)$ . A plot of the data from Figure 6.7 by a second-order method yields straight lines with an average rate constant ( $k$ ), for the three runs, of  $0.23 \pm 0.03 \text{ M}^{-1} \text{ min}^{-1}$  (Figure 6.8). The half-life,  $\tau$ , of a second-order reaction is dependent on the initial concentration defined in this case by  $A_o(\text{oxy})$ ,

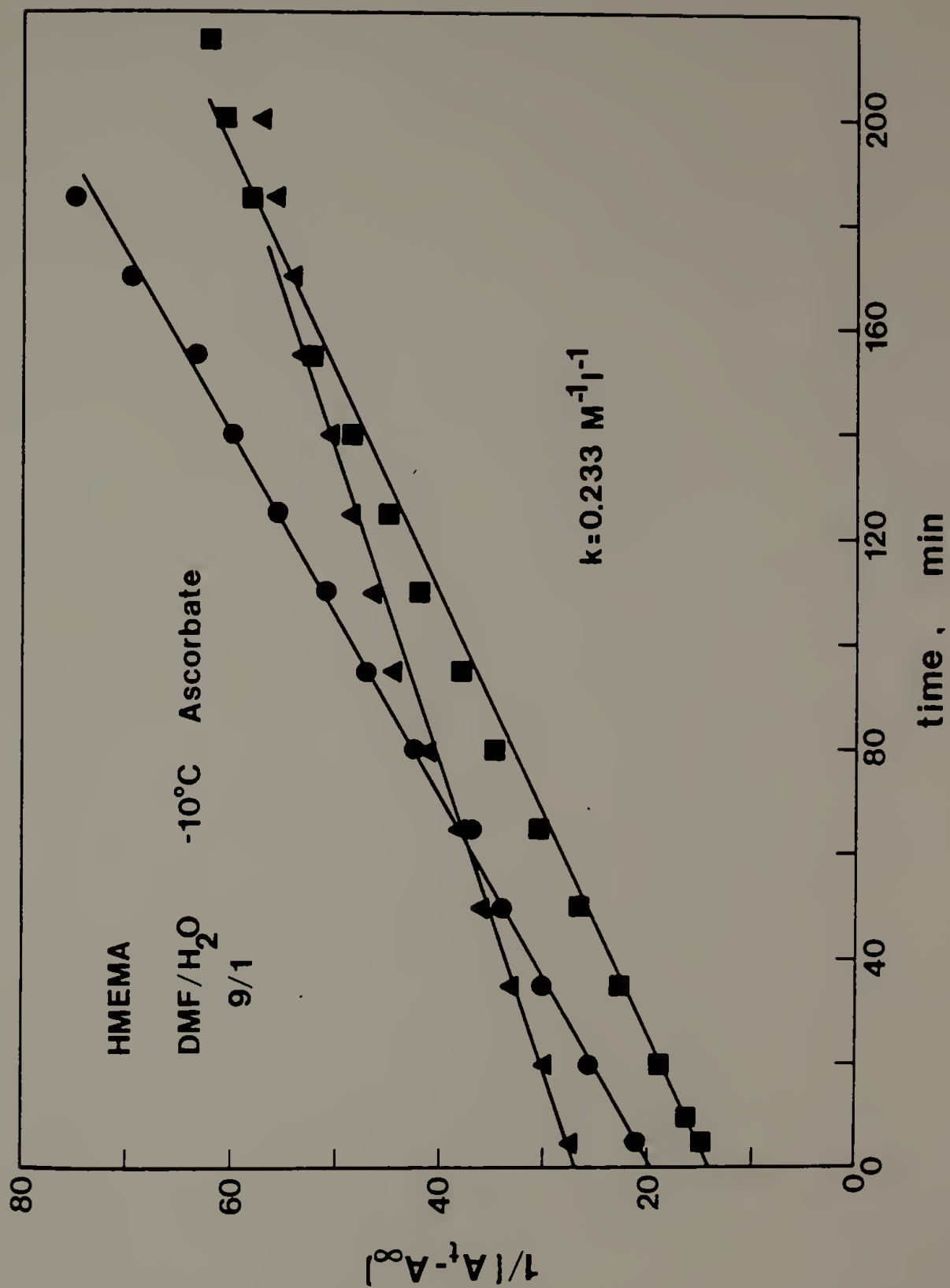
$$\tau = \frac{1}{[A_o(\text{oxy})]k} \quad (6.10)$$

Some loss in absorbance (i.e.  $A_o(\text{oxi}) > A_\infty$ ) was noted for the ascorbate reducing system although it was much less than for aqueous sodium dithionite. The reduction of hemin by AS with traces of oxygen generates hydrogen peroxide<sup>18</sup> which may act to decompose the porphyrin ring.

A second organic reducing agent, aminoiminomethanesulfinic acid (AIMSA) was tested briefly. A large excess of AIMSA (45 - 130 fold excess) was required to give partial reduction of hemin. Also the reaction appeared to be quite slow, making AIMSA an unsuitable reducing agent.

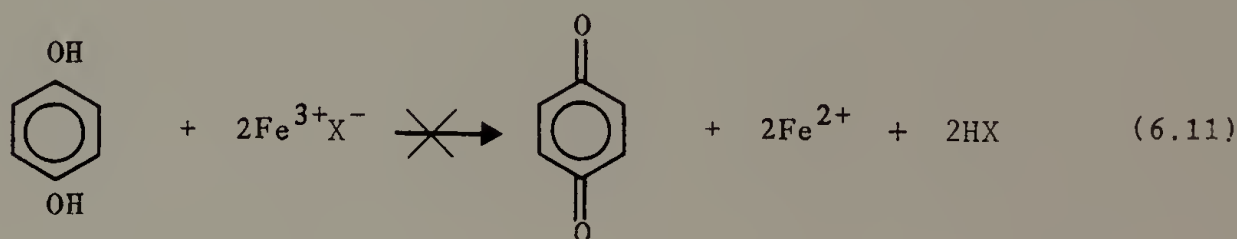
In all the reducing agent systems studied, the heme was degraded by

Figure 6.8. A second-order plot of the kinetic data for the oxy/oxi equilibrium of HMEMA using an ascorbate reducing agent in DMF/H<sub>2</sub>O (9/1) at -10°C (A at 537 nm). The data shown here extends linearly for more than 6 hr. Different symbols indicate different experiments and the average slope is  $0.2329 \pm 0.05$  M<sup>-1</sup> min<sup>-1</sup>.

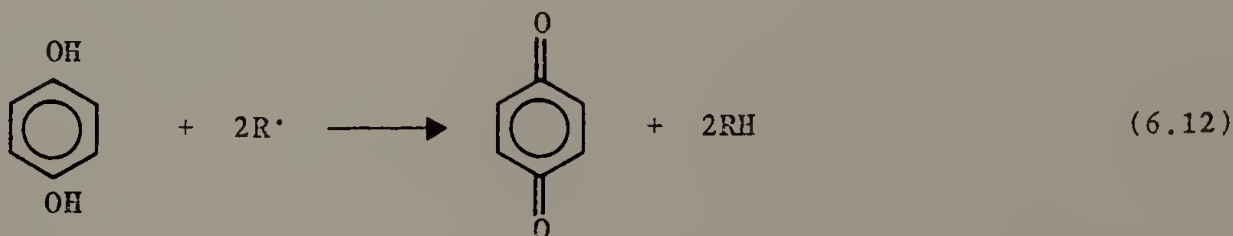




the presence of some type of radical. The degradation of iron porphyrins by hydrogen peroxide formed from the autooxidation of a reducing agent, such as L-ascorbic acid, have been widely studied because of their relationship to the natural process of heme degradation.<sup>19-22</sup> Introduction of a free-radical scavenger, such as hydroquinone, which does not interfere with the redox reaction being studied but could prevent oxidation of the porphyrin and its degradation to bile pigments allows the true oxidation kinetics to be observed. The redox chemistry of iron porphyrins with quinones and hydroquinones was studied by Castro and coworkers.<sup>23</sup> They demonstrated that hydroquinone does not reduce high-spin iron(III) porphyrins.



Our experiments with HMEMA verified this conclusion. Thus hydroquinone acts as a radical scavenger,



without interfering in the redox reaction. The oxidation product, benzoquinone, can't oxidize six-coordinate, low-spin iron(II) porphyrins

thus there is no chance of a reaction occurring between any of the solutes i.e. iron III and iron II porphyrins, benzoquinone and hydroquinone. Addition of hydroquinone (HQ) in kinetic studies gave repeatable results, for the oxygenation equilibria without the complication of degradation of the porphyrin macrocycle and was independent of effects due to sample or reducing agent age.

### Kinetic Studies

Attempts to oxygenate hemin dimethylester (HDME) or hemin bis-3-(1-imidazolyl)propylamide (HDA) at  $-30^{\circ}\text{C}$  in DMF were unsuccessful. The samples were completely oxidized within the 30 seconds required for the oxygen injection and initial spectrum to be taken. Traylor and coworkers<sup>9</sup> studied the oxygenation of these monomers using flash photolysis techniques, in an  $\text{O}_2/\text{CO}$  atmosphere at  $22^{\circ}$  in an aqueous system and found they were completely and irreversibly oxidized. Tsuchida and coworkers<sup>14</sup> showed that HDA (FeII) was irreversibly oxidized at  $-30^{\circ}\text{C}$  in a 9/1 (DMF/ $\text{H}_2\text{O}$ ) solvent upon introduction of oxygen. A copolymer of S/HDA failed to reversibly oxygenate at  $-30^{\circ}\text{C}$  in DMF. Figure 6.9 shows the  $\alpha$  and  $\beta$  bands of the visible spectra of the S/HDA copolymer in the oxidized and reduced state and with a carbon monoxide ligand. To study the effect of the hydrophobic domains on the oxygenation/oxidation of HDA a terpolymer of S/ $\text{SS}^-$ /HDA was synthesized. This terpolymer did not reversibly oxygenate at  $-30^{\circ}\text{C}$  in an ethylene glycol/water (1/1) solvent system. The visible spectra of the  $\alpha$  and  $\beta$  bands for this terpolymer broaden as the volume % water is increased in the sample (Figure 6.10). This could indicate that the imidazole groups are being solvated by the

Figure 6.9. The visible spectra of S/HDA in DMF: (——) oxidized state (-----) reduced state, ( $\lambda_{\text{max}} = 522,552$  nm) and (-·-) with a CO ligand in the reduced state ( $\lambda_{\text{max}} = 534,562$  nm).

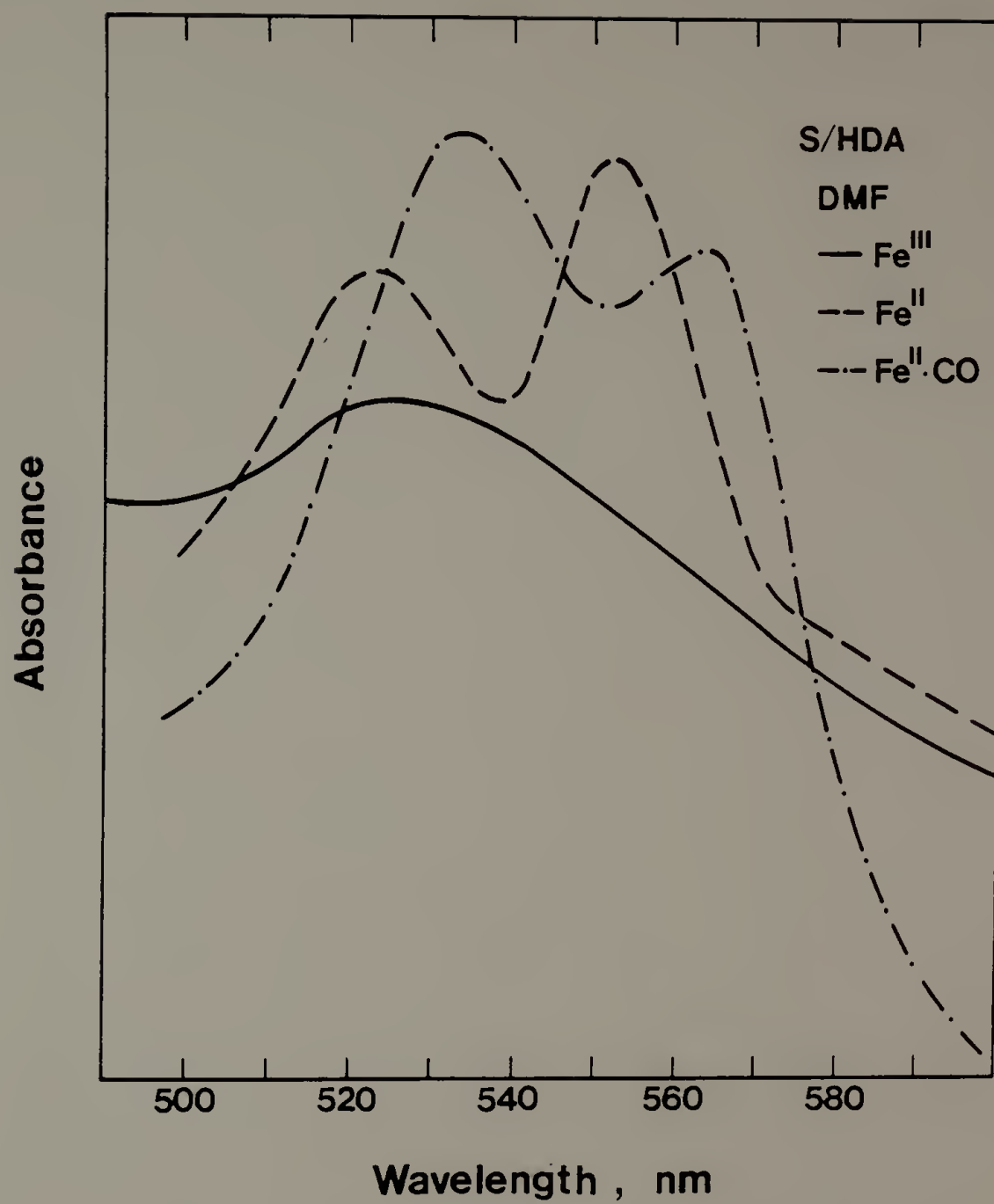
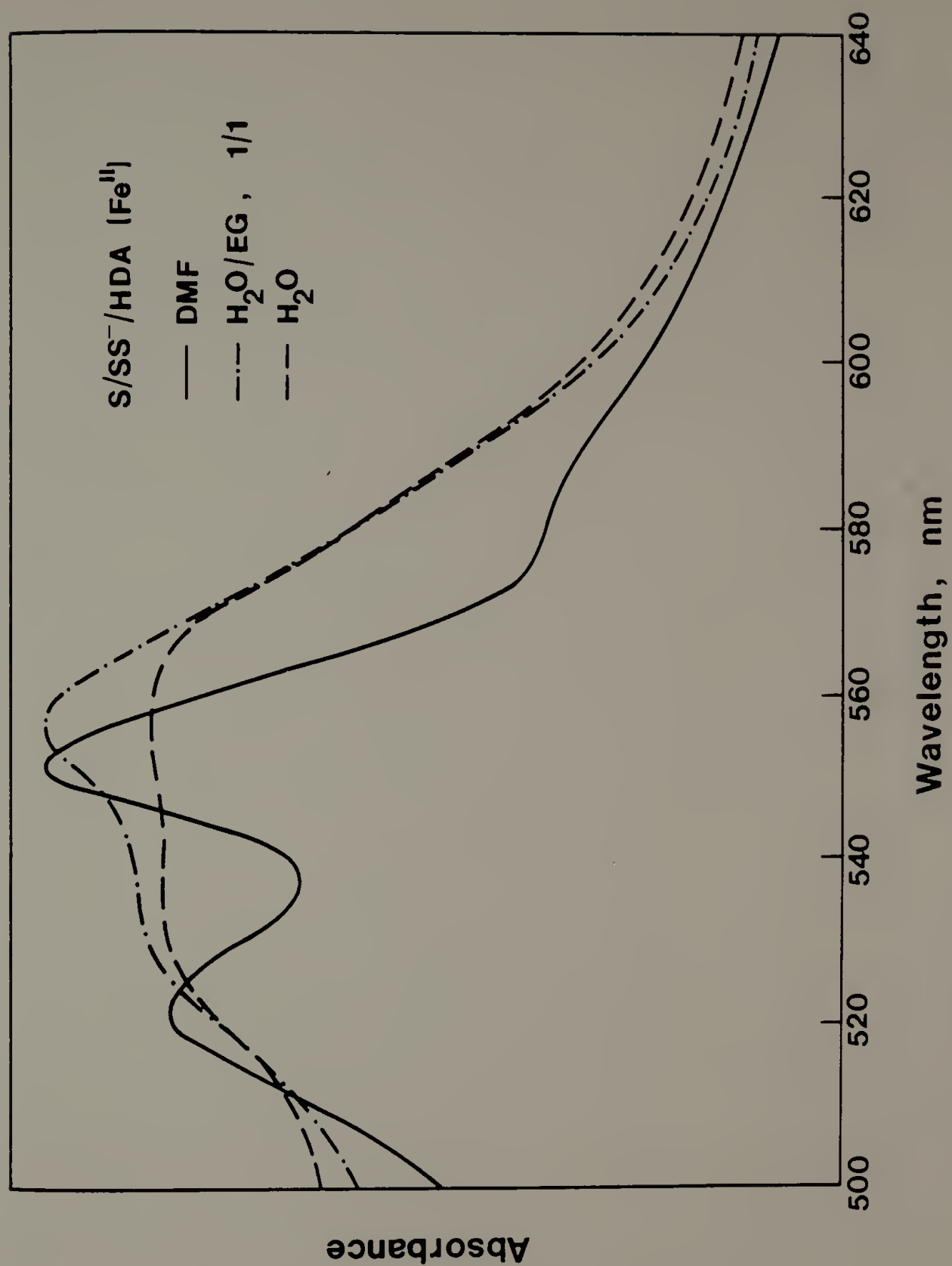


Figure 6.10. The effect of solvent on the visible spectra of S/SS<sup>-</sup>/HDA (Fe II): (—) DMF, (-·-) water/ethylene glycol (1/1) and (-----) water. The  $\alpha$  and  $\beta$  bands broaden as the concentration of water is increased suggesting an interaction of this heme group and water.



water and there is a significant fraction of four-coordinate heme in solution. Certainly the environment of the porphyrin ring of HDA is affected by the increase in the concentration of water. The imidazole groups increase the polarity of hemin, making it relatively water soluble.

The kinetics of the oxygenation of hemin mono-3-(1-imidazolyl)propylamide monomethylester HMEMA was investigated at  $-10^{\circ}\text{C}$  in DMF/ $\text{H}_2\text{O}$  (9/1) using 4  $\mu\text{l}$  HQ and 4  $\mu\text{l}$  DT or less in the reduction. Four decay curves ( $(A_t - A_{\infty})$  versus time) were superimposable when shifted as a function of time. A second-order plot of the data spanning nearly seven hours of decay was linear and had a slope of  $0.15 \pm 0.02 \text{ M}^{-1} \text{ min}^{-1}$  (Figure 6.11). Tsuchida<sup>14</sup> claimed that HMEMA was slow to oxygenate in DMF/ $\text{H}_2\text{O}$  at  $-30^{\circ}\text{C}$  and required 15 minutes of exposure to oxygen to fully oxygenate. This was never observed in the course of our experiments! The spectrum of HMEMA (FeII) at  $-10^{\circ}\text{C}$  is clearly that of the six-coordinate species with the sixth ligand being a solvent molecule (Figure 6.5). However, this solvent ligand does not effectively compete with oxygen at the sixth coordination site. HMEMA did not reversibly oxygenate (i.e. it was immediately oxidized) in ethylene glycol/water (1/1) at  $-30^{\circ}\text{C}$ .

A tetrapolymer of S/SS<sup>-</sup>/APMA/HMEMA was synthesized to examine the effect of the covalent incorporation of a heme unit in the backbone of a polymer chain. Visible spectra of this tetrapolymer in the oxidized, reduced and oxygenated state are shown in Figure 6.12. The wavelength of the maximum of the  $\alpha$  and  $\beta$  peaks in polymerized HMEMA is shifted 3 -



Figure 6.11. A second-order plot of the kinetic data for the oxy/oxi equilibrium of HMEMA using a dithionite reducing agent with hydroquinone as a free radical scavenger at  $-10^{\circ}\text{C}$  in DMF/ $\text{H}_2\text{O}$  (9/1). The curve is a representative experiment and the slope is  $0.15 \pm 0.02 \text{ M}^{-1} \text{ min}^{-1}$ .

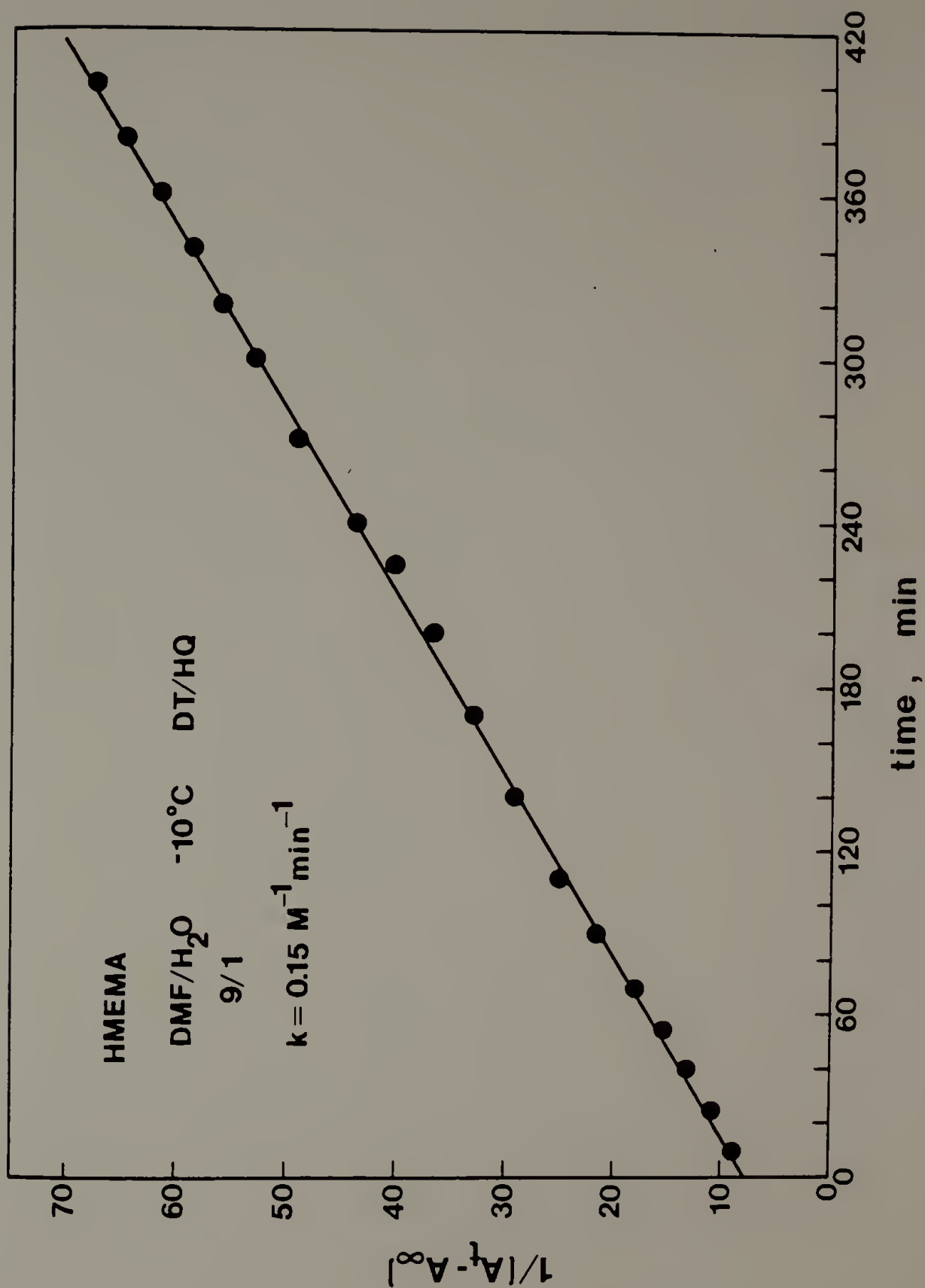
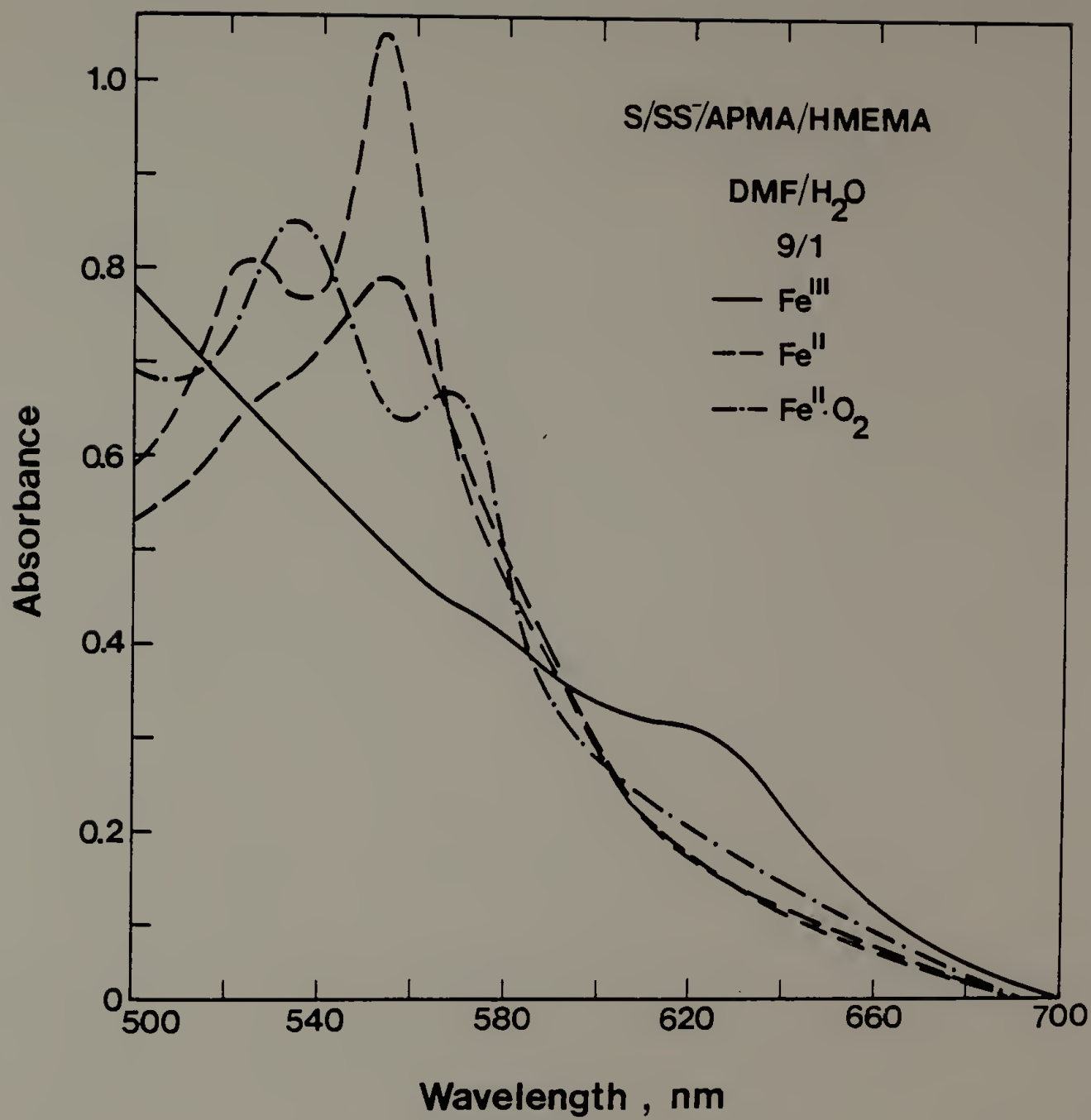


Figure 6.12. The visible spectra of  $S/SS^-/APMA/HMEMA$  in  $DMF/H_2O$  (9/1): (—) oxidized at room temperature, (-----) reduced at room temperature (small) and  $-30^\circ C$  (tall) ( $\lambda_{max} = 533,525$  nm) and (-·-) oxygenated at  $-30^\circ C$  ( $\lambda_{max} = 535,568$  nm).



5 nm lower than that of HMEMA monomer (Figure 6.5) (reduced: 557 → 553 nm, 527 → 525 nm, oxygenated: 572 → 568 nm, 537 → 533 nm). This is due to the polymerization of one of the vinyl groups, and thus a small loss of conjugation.

The oxygenation/oxidation equilibria of S/SS<sup>-</sup>/APMA/HMEMA (before photolysis of the azide) was studied at -10°C in DMF/H<sub>2</sub>O, (9/1) and (8/2). The rate of oxidation appeared to be independent of the solvent composition. A second-order kinetic plot of the data is linear after approximately 60 minutes in both cases (Figure 6.13). The rate constant for several replicate experiments gave  $k = 0.10 \pm 0.02 \text{ M}^{-1} \text{ min}^{-1}$  for (9/1) and  $k = 0.08 \pm 0.02 \text{ M}^{-1} \text{ min}^{-1}$  for (8/2). These rates are virtually identical within experimental error. To evaluate the non-linear data at times less than 60 minutes, the second-order plot was extrapolated back to  $t = 0$ . From this line the theoretical value of  $(1/A_t - A_\infty)_G$  was obtained. After taking the reciprocal,  $(A_t - A_\infty)_G$  was subtracted from the experimental value of  $A_t - A_\infty$ . The values of  $A_{\text{exp}} - A_G$  versus time obey first-order kinetic behavior, i.e. a plot of  $\ln(A_{\text{exp}} - A_G)$  versus time is linear (Figure 6.14).

First order kinetics imply that the reaction



is unimolecular and the rate expression,

$$\frac{d[\text{Fe}^{2+}\text{O}_2]}{dt} = k[\text{Fe}^{2+}\text{O}_2] \quad (6.14)$$

Figure 6.13. A second-order plot for the oxy/oxi equilibrium of S/SS<sup>-</sup>/APMA/HMEMA in DMF/H<sub>2</sub>O, (●, 9/1 and ■ 8/2). A representative experiment is shown in each case. and the average rate constant is  $k = 0.10 \pm 0.02 \text{ M}^{-1} \text{ min}^{-1}$  for (9/1) and  $k = 0.08 \pm 0.02 \text{ M}^{-1} \text{ min}^{-1}$  for (8/2). These rates are identical within experimental error.

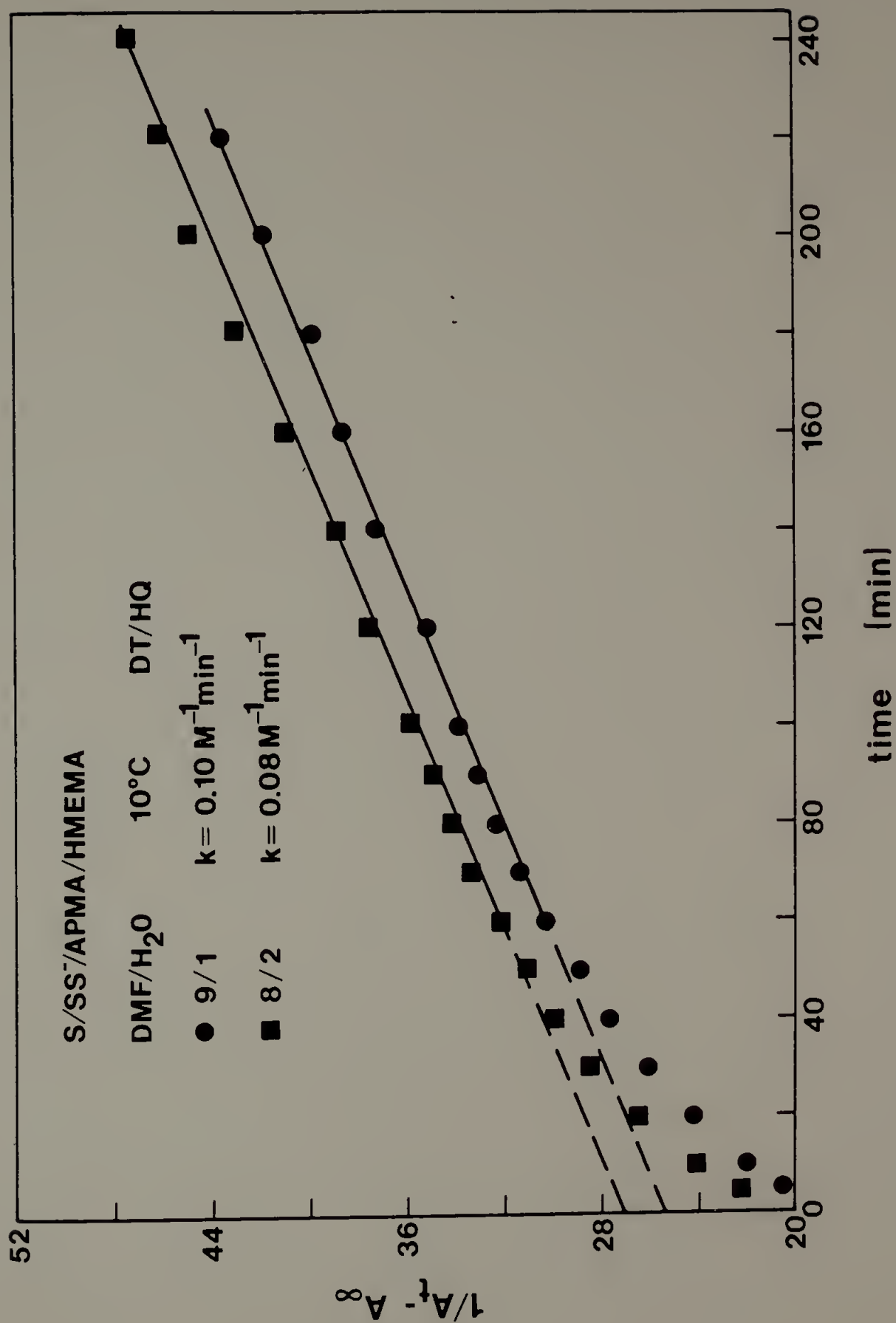
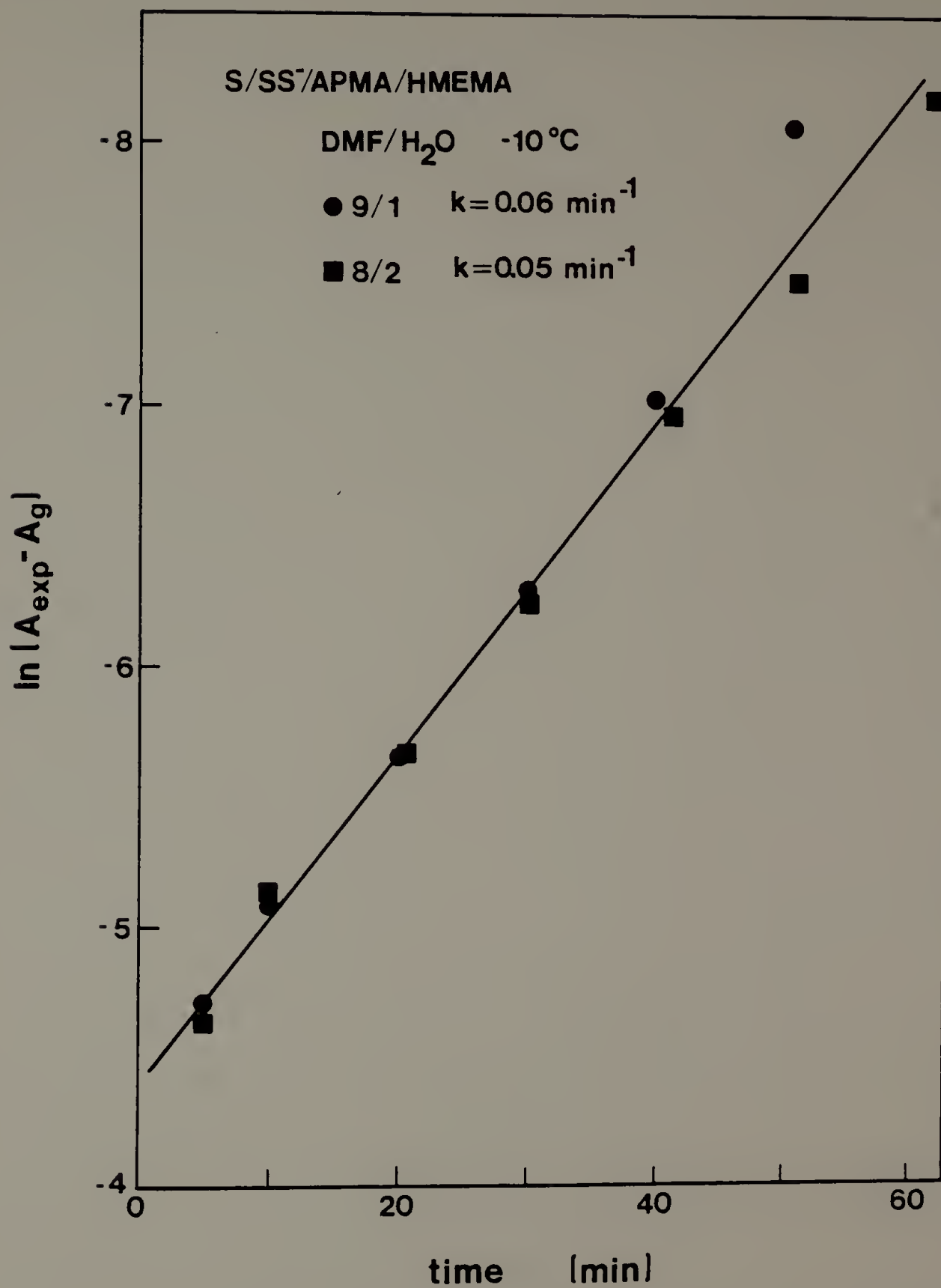




Figure 6.14. A first-order plot for the oxy/oxi equilibrium of S/SS<sup>-</sup>/APMA/HMEMA over the first hour of the kinetic study. The contribution of the second-order process has been subtracted from the experimental data to yield this line. The line is from a single representative experiment. The half-life of the first-order decay in DMF/H<sub>2</sub>O is as follows: ( ● ) 9/1, 11.4 min and ( ■ ) 8/2,  $\tau = 12.7$  min.



can be integrated to yield

$$\ln(A_t - A_o) = -kt + \ln(A_o(\text{oxy}) - A_\infty) \quad (6.15)$$

assuming

$$[\text{Fe}^{2+}\text{O}_2]\text{C} = A_t - A_\infty \quad (6.16).$$

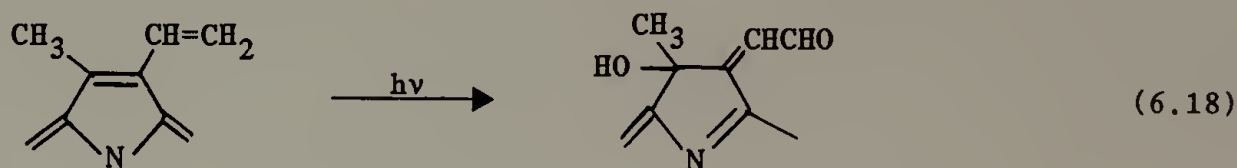
The half-life is independent of the initial concentration of oxygenated heme,

$$\tau = \frac{\ln 2}{k} \quad (6.17).$$

From Equation 6.17 the half-life of the first-order portion of the decay curve in (9/1) DMF/H<sub>2</sub>O is 11.4 min ( $k = 0.061 \text{ min}^{-1}$ ) and  $\tau = 12.7 \text{ min}$  ( $k = 0.054 \text{ min}^{-1}$ ) in (8/2) DMF/H<sub>2</sub>O. These results suggest that increasing concentration of water from 10 to 20 vol. % has no effect on the rate or mechanism of decay from the oxygenated to the oxidized species. Samples of S/SS<sup>-</sup>/APMA/HMEMA in DMF/H<sub>2</sub>O (6.5/3.5) at -10°C and ethylene glycol/water (1/1) at -30°C were oxidized completely and rapidly by the addition of oxygen to the reduced state. Perhaps there is a critical concentration of water at which proton facilitated autooxidation is the primary mechanism of decay.

A tetrapolymer of S/SS<sup>-</sup>/APMA/HMEMA was irradiated at 254 nm in water to photocrosslink the azide. The polymer solution was diluted with DMF

to a (9/1) mixture of DMF/H<sub>2</sub>O. This polymer did not reversibly oxygenate at -10°C! Visible spectra of the tetrapolymer, shown in Figure 6.15, are shifted 3 - 5 nm from the unirradiated sample. Protoporphyrins are relatively unstable to light and in the presence of molecular oxygen degrade to photoporphyrin.<sup>24,25</sup>



The loss of conjugation causes a shift to lower wavelengths and the product is significantly more polar. It is likely that the intense ultraviolet radiation used to photolyze the azide group causes oxidation of the unreacted vinyl group on HMEMA making the heme group hydrophilic and increasing the likelihood of proton facilitated autooxidation.

### Conclusions

Solution purity is an essential requirement for good kinetic studies of the oxidation reactions of model heme systems. As we have demonstrated, the selection of a reducing agent influences the rate and kinetic order observed. Impurities, such as peroxide radicals, can accelerate the rate of heme oxidation in a Fenton-like reaction.

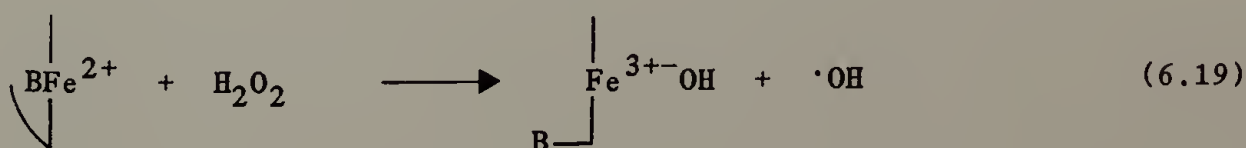
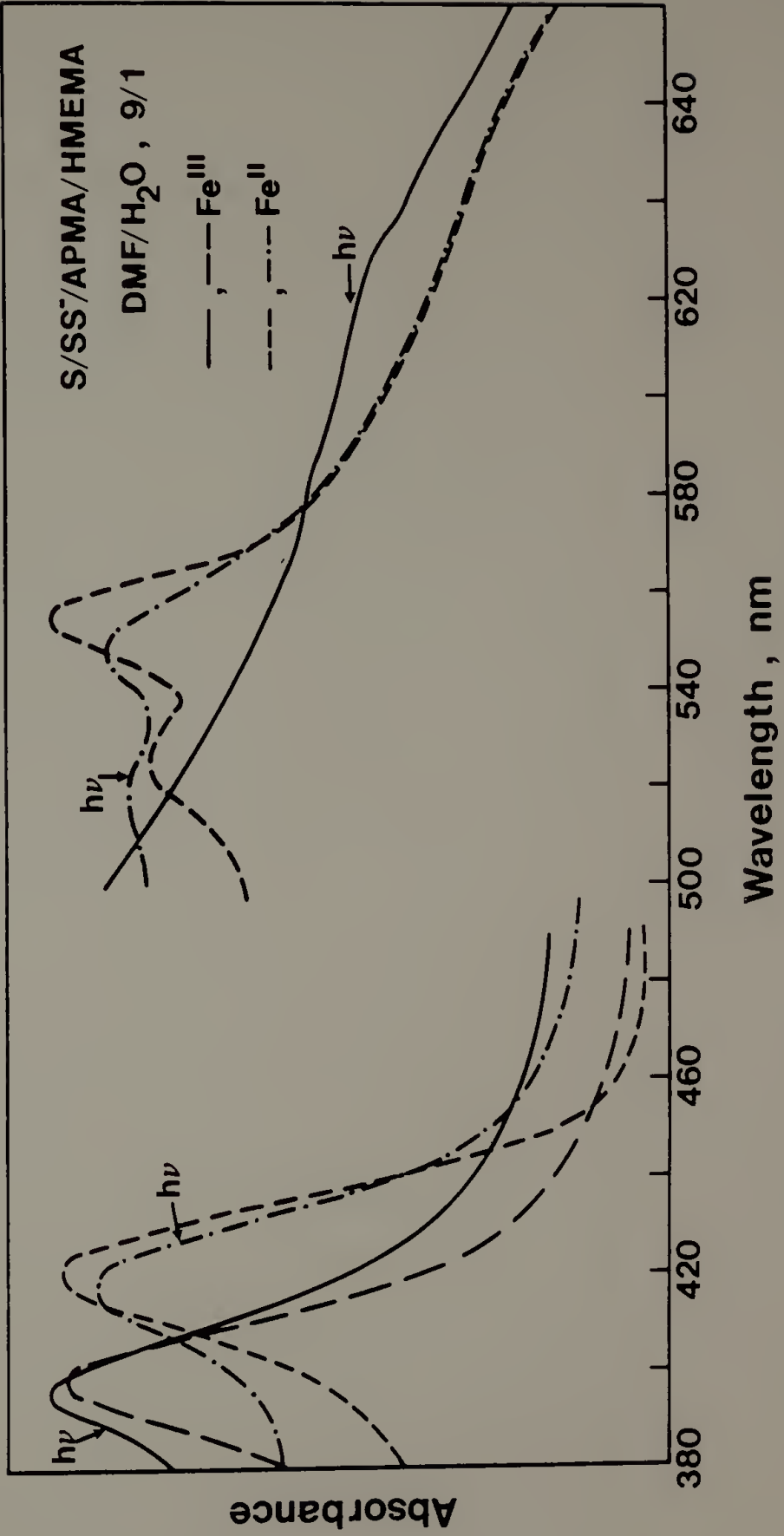


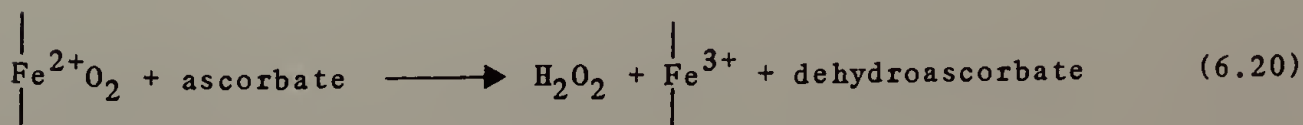
Figure 6.15. Visible spectra of S/SS<sup>-</sup>/APMA/HMEMA before and after irradiation with ultraviolet light. The  $\alpha$  and  $\beta$  bands of the oxidized species (—) are unchanged after irradiation however the Soret shifts from  $\lambda_{\text{max}} = 400$  nm, (---) to  $\lambda_{\text{max}} = 396$  nm, (—). The absorbances of the reduced spectrum (----) at  $\lambda_{\text{max}} = 422$ , 525 and 555 nm shift to  $\lambda_{\text{max}} = 418$ , 520 and 555 nm (-'-) after irradiation.



Many reducing agents such as sodium dithionite or ascorbate generate peroxides in the presence of oxygen and thus catalyze the oxidation reaction.

In current work by Tsuchida<sup>14,15</sup> where heme-polymers showed oxidative stability, aqueous dithionite was used for the reductions and first-order kinetics were reported. They have not speculated on the mechanism of the oxidation reaction. Our results show that Tsuchida's systems have not been studied carefully enough. Using aqueous dithionite we have repeated Tsuchida's results for HMEMA ( $t(1/2) = 98$  min) at  $-30^{\circ}\text{C}$  in DMF/ $\text{H}_2\text{O}$  (9/1) and shown them to be influenced by the age and volume required of the reducing agent and solution purity. The exact composition of a dithionite solution is not well documented but it is likely that the degradation fragments in the presence of dissolved oxygen (contaminants or intentionally introduced) are some type of radicals which enhance the oxidation of heme. This is supported by Tsuchida's observation that in the presence of excess dithionite the porphyrin ring is degraded and no oxygenation is observed. One must question at what point the added DT can be considered an excess, obviously the 5/1 excess DT/heme used by Tsuchida and coworkers is not satisfactory.

The use of ascorbate as a reductant gives second-order kinetics for HMEMA (DMF/ $\text{H}_2\text{O}$  (9/1),  $-10^{\circ}\text{C}$ ) with  $k = 0.23 \text{ M}^{-1} \text{ min}^{-1}$ . In the presence of oxygen, ascorbate reacts to form hydrogen peroxide.





The hydrogen peroxide then can react to oxidize ferrous heme in a reaction dependent on the concentrations of ferrous heme and hydrogen peroxide. Thus ascorbate accelerates the rate of oxidation of model hemes.

In the presence of a free radical scavenger, hydroquinone, the oxidation of HMEMA at  $-10^{\circ}\text{C}$  (DMF/ $\text{H}_2\text{O}$  (9/1)) is second-order with  $k = 0.15 \text{ M}^{-1} \text{ min}^{-1}$ . Slow oxygenation of this model reported by Tsuchida<sup>14</sup> was not observed. The mechanism of the oxidation is likely a dimerization process. The rate of oxidation of chelated heme models was found to be second-order in heme and inversely proportional to the oxygen concentration by Chang et al.<sup>26</sup> With a large excess of dissolved oxygen, the oxidation of HMEMA is simply second-order in dissolved heme. This means that even in a solvent of 10 vol. % water, dimerization is the primary mechanism of heme oxidation!

Oxidatively unstable heme models, such as HDME and HDA, were not stabilized by incorporation in a polymer chain. For heme dimethylester, a four-coordinate structure makes it vulnerable to both dimerization and autooxidation. Heme diamide has a six-coordinate structure with equal affinity for imidazole or dioxygen. The instability of HDA (FeII) to oxygen might be due to the propensity of this model to form dimers in solution, especially at lowered temperatures,<sup>27</sup> which would increase the possibility of oxidation by dimerization to the  $\mu$ -oxo dimer. The two imidazole groups on HDA increase the polarity, thus increasing the solvation by water as evidenced by the broadening of the peaks in the electronic spectra. This enhances proton facilitated autooxidation.

Polymer-bound HMEMA oxidized by two different mechanisms. The first 60 minutes of decay (DMF/H<sub>2</sub>O, -10°C) showed both first- and second-order processes were occurring. Approximately 20% of the hemes were oxidized by a first-order process. The half-life of the first-order process was about 12 minutes, thus after 60 min the concentration of the heme which decayed by a first-order process was approximately 3% of the original value. We conclude that the first-order process is due to the local environment of the polymer chain around the heme, because it is not observed for non-polymerized hemes. The rate and percent of HMEMA oxidized by the first-order process is independent of the fraction of water in the sample.

The mechanism of degradation is probably proton facilitated autooxidation (Equation 6.3). In a large excess of water the rate expression for oxidation would solely depend on the heme concentration. If  $[H^+]$  is a constant, then

$$\frac{d[Fe^{2+}O_2]}{dt} = k'[Fe^{2+}O_2] \quad (6.21)$$

where  $k'$  represents the rate constant of the pseudo first-order process. Explanations for the observed first-order decay can be hypothesized by examining the local environment of a heme group. The concentration of water near a heme would be increased by a sodium sulfonate neighbor. It is unlikely that the conformation of a random polymer in a DMF/H<sub>2</sub>O mixture would create hydrophobic domains giving hemes which are accessible and non-accessible to proton facilitate autooxidation.

Tsuchida and coworkers<sup>6</sup> studied the viscosity of a water soluble polymer-heme complex and showed that addition of DMF to the polymer solution destroyed the polymer-heme hydrophobic interaction. The imidazole group of HMEMA has a  $pK_a$  of approximately 3.6.<sup>28</sup> Therefore, it is unlikely that a heme-sulfonate interaction due to ionic attraction which would increase the local concentration of water and enhance oxidation could occur in DMF/H<sub>2</sub>O that is slightly basic (pH = 7.4). There is a possibility that a fraction of the hemes are stacked together on the chain causing dimerization that is observed to be a first-order process. It seems most likely that some of the hemes have a neighboring sulfonate group which increases the nearby concentration of water, causing proton facilitated oxidation.

The rate constant for the second-order process in DMF/H<sub>2</sub>O ((9/1) and (8/2)) at -10°C is  $\sim 0.085 \text{ M}^{-1} \text{ min}^{-1}$ . This means that the polymer bound HMEMA is slightly more stable (1.5 times) than monomeric heme. The mechanism of oxidation is likely to be dimerization because the kinetics are second-order in heme concentration. This suggests that incorporation of a heme in a polymer with a random conformation is not sufficient to prevent the contact of two heme groups and subsequent dimerization. The polymer chain reduces the probability of heme-heme contact but doesn't eliminate it.

In solvent systems containing a larger volume percent of water, such as DMF/H<sub>2</sub>O (6.5/3.5) and ethylene glycol/water (1/1) there is no stability towards oxidation. The mechanism is presumably proton facilitated autooxidation. Irradiation of the tetrapolymer for

photocrosslinking causes the unpolymerized vinyl group to be oxidized making the heme more hydrophillic. After irradiation, polymer bound HMEMA no longer reacts reversibly with oxygen. It is likely that this is also due to proton facilitated autooxidation.

Table 6.1 summarizes the systems studied, the rate constants and the half-lives. In general, we can conclude that the heme and all substituents on the porphyrin ring must be hydrophobic to prevent proton facilitated autooxidation. Also, a random polymer is a useful heme carrier but does not provide sufficient steric hindrance to prohibit heme-heme contact. Two novel hydrophobic analogs of HMEMA, a ten-carbon and six-carbon ester were synthesized at the conclusion of this work which can be tested to verify the hypothesis that increasing heme hydrophobicity would enhance the stability of the oxygenated state.

Table 6.1

Summary of the Kinetics of the Oxygenation/Oxidation Reactions of Heme Model Systems.

System	Solvent	T (°C)	Kinetics	Rate	$\tau$	
HMEMA	DMF/H <sub>2</sub> O	(9/1)	-10	Second-Order	0.15 M <sup>-1</sup> min <sup>-1</sup>	-
S/SS <sup>-</sup> /APMA/HMEMA	DMF/H <sub>2</sub> O	(9/1)	-10	First-Order and Second-Order	0.06 min <sup>-1</sup> 0.10 M <sup>-1</sup> min <sup>-1</sup>	11.4 min
		(8/2)	-10	First-Order and Second-Order	0.05 min <sup>-1</sup> 0.083 M <sup>-1</sup> min <sup>-1</sup>	12.7 min
		(65/35)	-10	no oxy		
	H <sub>2</sub> O/EG	(1/1)	-30	no oxy		
S/SS <sup>-</sup> /APMA/HMEMA (after hv)	H <sub>2</sub> O	1°	no oxy			
	H <sub>2</sub> O	1°	no oxy			
	DMF/H <sub>2</sub> O	(9/1)	-10	no oxy		
HDME	DMF	-30	no oxy			
S/HDA	DMF	-30	no oxy			
S/SS <sup>-</sup> /HDA	H <sub>2</sub> O	1°	no oxy			
	H <sub>2</sub> O/EG	(1/1)	-30	no oxy		

### References

1. Hammond, C.J.; Wu, C.S. Adv. Chem. Ser., (1968), 77, 186.
2. Cohen, I.A.; Caughey, W.S. Biochemistry, (1968), 7, 636.
3. Brunori, M.; Falcioni, G.; Fioretti, E.; Giordina, B.; Ratillo, E. Eur. J. Biochem., (1975), 53, 99.
4. Wallace, W.J.; Caughey, W.S. Biochemical and Clinical Aspects of Oxygen, Academic Press, New York, (1979), p. 69.
5. Nishide, H.; Sehine, M.; Tsuchida, E. Polymer Journal, (1982), 14(8), 629.
6. Tsuchida, E.; Nishide, H.; Ohno, H. J. Inorg. Biochem., (1982), 17, 283.
7. A literature survey is given in Chapter I.
8. Nishide, H.; Mihayashi, K.; Tsuchida, E. Biopolymers, (1979), 18, 739.
9. Traylor, T.G.; Chang, C.K.; Geibel, J.; Berzinis, A.; Mincey, T.; Cannon, J. J. Am. Chem. Soc., (1979), 101(22), 6716.
10. Kice, J.L. Sulfur in Organic and Inorganic Chemistry, Vol. I, Sinning, A. (ed.), Marcel Dekker, New York, (1971), p. 153.
11. Mincey, T.; Traylor, T.G. Bioinorg. Chem., (1978), 9, 409.
12. Brault, T.; Rougee, M. Biochemistry, (1974), 13, 4591.
13. Momenteau, M. Biochim. Biophys. Acta, (1973), 304, 814.
14. Tsuchida, E.; Nishide, H.; Sato, Y.; Kaneda, M. Bull. Chem. Soc. Jpn., (1982), 55, 1890.
15. Tsuchida, E.; Nishide, H.; Sato, Y. J. Chem. Soc. Chem. Commun., (1982), 556.



16. Minnaert, K. Biochim. Biophys. Acta, (1961), 54, 26.
17. Benatti, U.; Morelli, A.; Guida, L.; DeFlora, A. Biochem. Biophys. Res. Commun., (1983), 111(3), 980.
18. An excellent summary of the kinetic approach can be found in:  
Levenspiel, O. Chemical Reaction Engineering 2nd Ed. J. Wiley and Sons, New York, (1972), pp. 47-92.
19. Falk, J.E. Porphyrins and Metalloporphyrins, Elsevier Pub. Co., New York, (1964), p. 20.
20. Gray, C.H. The Bile Pigments, Methuen, London, (1953).
21. Lemberg, R.; Legge, J.W. Haematin Compounds and Bile Pigments, Interscience, New York, 1949.
22. O'Carra, P. in Porphyrins and Metalloporphyrins, Smith, K.M. (ed.), Elsevier Pub. Co., New York, (1975), p. 123; Fuhrhop, J.-H., Ibid., p. 625.
23. Castro, C.E. J. Am. Chem. Soc., (1977), 99(24), 8032.
24. Inhoffen, H.H.; Brockman, H.; Bliesner, K.M. Liebigs Ann. Chem., (1969), 730, 173.
25. Hoff, F.R.; Whitten, D.G. Reference 22, p. 667.
26. Chang, C.K.; Powell, D.; Traylor, T.G. Croat. Chem. Acta, (1977), 49, 295.
27. Momenteau, M.; Rougee, M.; Loock, B. Eur. J. Biochem., (1976), 71, 63.
28. Geibel, J.; Cannon, J.; Campbell, D.; Traylor, T.G. J. Am. Chem. Soc., (1978), 100(11), 3575.



## C H A P T E R VII

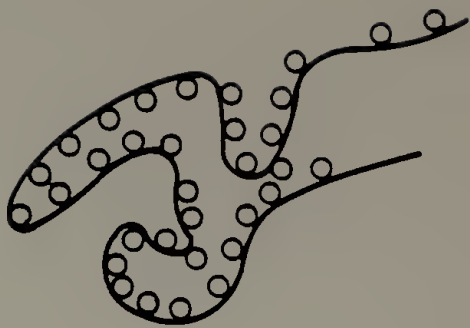
### CHARACTERIZATION OF HYDROPHOBIC DOMAINS IN WATER SOLUBLE POLYMERS AND THE GELATION OF HYDROPHOBIC POLYAMPHOLYTES

Hydrophobic intramolecular interactions are important in determining the unique conformation of hemoglobin and other proteins. In our model of hemoglobin, ionic moieties (15 - 20 mol %) give water solubility and thus these polymers must be characterized as hydrophobic polyelectrolytes. At low concentrations of ionic groups some polyelectrolytes exist in a hypercoiled conformation,<sup>1</sup> which is due to intramolecular micelle formation caused by hydrophobic interactions.<sup>2</sup> Sodium phenylsulfate, N-ethylpyridinium bromide and N-trimethylbenzyl ammonium are all relatively hydrophobic ionic groups in our polymers and thus are also important in determining polymer solution properties.<sup>3</sup> Contracted hydrophobic polyelectrolytes, 'polysoaps', can solubilize water insoluble substances in their hydrophobic domains<sup>4,5</sup> making them promising carriers for heme groups which are oxidatively unstable in a water environment.

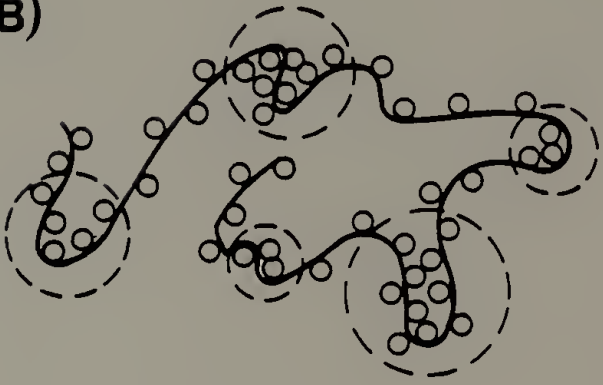
The structure of polysoaps has been studied in both aqueous and organic media. If the cohesive power of the lipophilic group is very strong, most of these groups will aggregate to make a compact structure in water. The macromolecule can be small enough to form a single micelle (Figure 7.1A) or large enough to contain several micelles (Figure 7.1B).<sup>6,7</sup> Intermolecular interactions with other polysoaps are favored (Figure 7.1C) where hydrophobic portions of the polymer chain

Figure 7.1. The structure of polysoaps in solution: (A) The polymer forms a single micelle; (B) Several micelles are found in a single polymer molecule; (C) A few polysoap molecules aggregate to give a single micelle.

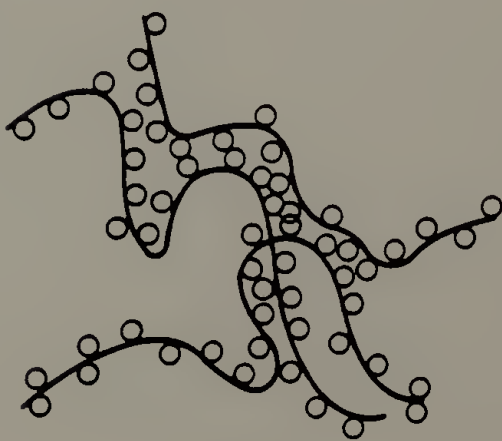
A)



B)



C)



are forced into contact with the aqueous media. Some of the ionic groups are incorporated in the interior of the molecule and extend the chain by disrupting van der Waals attractions. The hydrophobic association is decreased by the addition of nonpolar organic solvents, such as tetrahydrofuran. However, in a polar organic solvent, such as DMF, hydrophobic interactions are still important in determining solution properties.<sup>8</sup> The effect of alkyl group length, temperature, ionic strength and added protein denaturants<sup>9</sup> on hydrophobic polyelectrolytes has been characterized.<sup>10</sup>

An unforeseen consequence of incorporating both anionic and cationic functional groups in the model polymer was the synthesis of novel hydrophobic polyampholyte complexes. Intermacromolecular complexes have been previously considered of four types:<sup>11</sup> polyelectrolyte complexes,<sup>12</sup> hydrogen-bonding complexes, stereocomplexes and charge transfer complexes. Applications for intermacromolecular complexes include flocculation and waste treatment, novel membrane applications, mechanochemistry, matrix polymerization, metal-free ionomers,<sup>13</sup> and new biocompatible materials.<sup>14</sup> Biological systems (e.g. DNA, RNA and proteins) form specific interpolymer complexes which are interesting as templates for polymerization and models of self-assembly to give a specific three dimensional structure.

The majority of intermacromolecular complexes are formed by mixing solutions of two polymers to obtain a precipitate or coacervate which is only soluble in a complex solvent system, e.g. water/acetone/KBr.<sup>15-18</sup> An exception to this approach is the work of Salamone et al.<sup>13,19</sup> who

polymerized styrene with divinyllic cation-anion monomer pairs such as 3-methacrylamido-propyldimethylammonium 2-acrylamido-2-methylpropane-sulfonate by solution copolymerization. These polyampholytes were characterized as ionomers. The major problems of this method are the limited solubility of all components in a solvent system, heterogeneity of the reaction during polymerization and a large variance in monomer reactivity (i.e.  $r_1 \neq r_2$ ).

### Experimental Procedure

#### Materials

The source of chemicals used in these experiments is as follows: 4-(2-hydroxyethyl)-1-piperazineethane sulfonic acid (HEPES), sodium laurelsulfate, Oil Red EGN, tetramethylammonium hydroxide, tetraethylammonium hydroxide and tetrabutylammonium hydroxide were purchased from Aldrich, sodium 2,2-dimethyl-2-silapentane-5-sulfonate (DSS) was purchased from Thompson-Packard and Aldrich, potassium thiocyanate was purchased from Fischer, cesium iodide was purchased from Alfa Inorganics, Tween 20 and sodium deoxycholic acid were purchased from Sigma and Tergitol NP40 was purchased from Union Carbide.

The synthesis of most of the terpolymers used in this work is given in Chapter V, the others are described below.

S/SS<sup>-</sup>/AEMA.<sup>20</sup> In a round bottom flask, 17.9 ml of styrene (0.19 mol), 5.71 g of MSS (0.029 mol), 1.21 g of AEMA ( $9.4 \times 10^{-3}$  mol), 0.185 g of AIBN ( $1.1 \times 10^{-3}$  mol) and 100 ml of DMF were combined and flushed with nitrogen. The mixture was polymerized at 60°C for 6 hr and then

precipitated into isopropanol. Elemental analysis: C, 77.41; H, 7.09; N, 1.69. Composition: S, 60.1; MSS, 24.3; AEMA, 15.6. The polymer was rendered water soluble by base hydrolysis in DMF followed by dialysis into water.

S/MSS/BNAHD. In a crown cap tube with a sidearm, 9.12 g of styrene (0.088 mol), 0.485 g of MSS ( $2.44 \times 10^{-3}$  mol), 2.23 g of BNAHD ( $7.84 \times 10^{-3}$ ), 0.078 g of AIBN ( $4.72 \times 10^{-4}$  mol) and 7 ml of DMF were combined, degassed, and polymerized for 90 min at 60°C. The polymer was precipitated into methanol and air dried. Elemental analysis: C, 83.99; H, 7.59; N, 1.11. Composition: S, 75.5; MSS, 13.2; BNAHD, 11.3.

The methylsulfonate group was hydrolyzed with dilute base in DMF, the solution was neutralized and then made acidic with HCl in ethyl acetate. The polymer could not be solubilized in water by dialysis.

#### Surfactant Solutions

Standard solutions of surfactants at twenty times the critical micelle concentration were made in 25 ml of deionized distilled water as follows: 0.0459 g of Tween 20, 0.1175 g of sodium deoxycholic acid, 0.1188 g of sodium laurelsulfate and 0.0291 g of Tergitol NP40. Standard surfactant solutions (30  $\mu$ l) were added to five identical concentrated solutions of (2.8 weight %) S/SS<sup>-</sup>/AEMA in water, 0.3 ml, to give twice the critical micelle concentration. The pH of each sample was adjusted to 7.5 - 8.2. Samples containing surfactant gelled more quickly than the control sample, although the sample containing sodium deoxycholic acid gelled somewhat more slowly than the others. The time



required for gelation was evaluated as the time at which the solution did not flow when the sample tube was inverted: sodium laurelsulfate, 4 hr; Tween 20 and Tergitol NP40, 8 hr; sodium deoxycholic acid 24 hr and control, 36 hr. These times are estimates and only useful for sample comparison at an identical concentration and pH.

#### Qualitative Comparison of Counterion Effect

A sample of S/SS<sup>-</sup>/NAHD in water was divided into 4 fractions and the fractions were dialyzed against 0.1 weight % of the following: NaCl, tetramethylammonium hydroxide (TMA), tetraethylammonium hydroxide (TEA) and tetrabutylammonium hydroxide (TBA). The sample of TBA gelled within 5 minutes in the dialysis tube. All of the other solutions were quite viscous. After 24 hr the samples were removed from the tubes and the pH was adjusted to 7.5. The viscosity was evaluated by measuring the time required for 1 ml of the solution to pass through the capillary of a 2 ml pipet. The viscosity of the solutions (the viscosity is proportional to the flow time) was in the order of  $\text{TMA}^+ \leq \text{Na}^+ < \text{TEA}^+$  (8.71 sec, 11.24 - 8.69 sec, 9.27 sec) with the  $\text{TBA}^+$  too gel-like to measure. It was observed that the flow time of the polymer solution with the  $\text{Na}^+$  counterion decreased with repetitive runs from 11.24 sec to 8.69 sec for a 1 ml volume. The error of the measurement for four runs was  $\pm 0.2$  sec.

#### Dye Solubilization

Composition Effect. A 3.2 weight % solution of S/4VPQ/NAHD (60.9/23.9/15.5) and a 1.5 weight % solution of S/4VPQ/NAHD (35.4/47.3/17.3) were diluted to give 1.0, 0.5, 0.1 and 0.05 percent



solutions. A small amount of finely ground Oil Red EGN was added and the samples were sealed in vials. Solutions were shaken for 14 days at room temperature. Each solution was filtered through an E fritted-glass filter (4 - 8  $\mu\text{m}$ ) with a bed of celite 545 (to protect the filter). One milliliter of the filtrate was diluted with 1 ml of methanol and the absorbance of the dye at 510 nm was measured to determine the dye concentration. The sample was further diluted (by 1/10 or 1/20) and the ultraviolet absorbance at 256 nm was measured to determine the polymer concentration. The extinction coefficient,  $\epsilon$ , of the stock solutions at 256 arising from the styrene and pyridinium groups pendant on the terpolymers was observed to be  $\epsilon = 10,700 \text{ (g/ml)}^{-1} \text{ cm}^{-1}$  for 60/24/16 and  $\epsilon = 27,900 \text{ (g/ml)}^{-1} \text{ cm}^{-1}$  for 36/47/17. The extinction coefficient of Oil Red EGN was  $\epsilon = 21,200 \text{ M}^{-1} \text{ cm}^{-1}$ .

Crosslinking Effect. A 2.86 weight % solution of S/SS<sup>-</sup>/APMA, (84.5/13.5/2.0) was diluted to 1.0% and half was irradiated at 254 nm for 12 hr. The two samples, S/SS<sup>-</sup>/APMA and S/SS<sup>-</sup>APMA-hv, were further diluted to give 0.5, 0.1 and 0.05 weight % solutions. A small amount of dye was added and they were shaken for 14 days. Insoluble dye uptake was evaluated as described above. Samples of 1.0% and 0.5% precipitated due to the agitation. The irradiated solution precipitate was colorless indicating that no dye was solubilized before precipitation. The extinction coefficient of S/SS<sup>-</sup>/APMA was found to be  $2300 \text{ (g/ml)}^{-1} \text{ cm}^{-1}$ . (For styrene  $\epsilon \approx 2000 \text{ (g/ml)}^{-1} \text{ cm}^{-1}$ ).

Ionic Strength Effect. A stock solution of S/4VPQ/NAHD (36/47/17) was diluted to give a 0.52 weight % solution for 5 samples. A stock

solution of NaCl, (0.5655 g/10 ml, 0.968 M) was added to each sample to give the following molarities of NaCl: 0.0133 M (50  $\mu$ l), 0.02767 M (100  $\mu$ l), 0.0553 M (200  $\mu$ l), 0.0829 (300  $\mu$ l) and 0.1328 M (500  $\mu$ l). The sample volume was adjusted with distilled water to give 500  $\mu$ l of total volume added. A small amount of dye was added and the samples were shaken for two weeks. Slight variations in solution concentration between samples were corrected by normalization of the dye absorbances to one concentration (0.28 weight %).

pH Effect. A solution of S/SS<sup>-</sup>/AEMA (60.1/24.3/15.6) was diluted to give a 0.68% solution. This solution was divided into five samples and the pH was adjusted with 0.968 M NaOH (0.968 M NaCl was added to each sample to adjust all solutions to the same ionic strength) to give pH = 3.8, 7.4, 8.8, 9.3 and 11.0. After 18 hr the solution pH had equilibrated to pH = 6.24, 6.9, 8.1 and 10.7 respectively. Oil Red EGN was added and the solutions were shaken for 14 days. Only the sample at pH = 10.7 had solubilized dye. For the other samples, virtually all the dissolved polymer (99%) precipitated from solution and thus was removed by filtration regardless of pH (demonstrated by the ultraviolet spectrum). The precipitates were pink indicating that either some dye was solubilized before the polymer precipitated or the dye was absorbed on the polymer surface after precipitation.

### Light Scattering

Light scattering in solution, both static and dynamic, was studied using an argon-ion laser at 514.5 nm and a Langely Ford 64 - channel correlator. Instrumentation is thoroughly described by Ford.<sup>21</sup>

A 2.86% solution of S/SS<sup>-</sup>/APMA (84.5/13.5/2.0) was divided into two 5 ml samples and one sample was irradiated for 20 hr. It gelled within two hours of cooling. The dynamic scattering of the unirradiated sample at a 90° angle and 23°C was measured using both a 10 μsec and 50 μ sec sample time. Although the baseline showed some error, the radius of the unirradiated sample was estimated to be 2500 Å! A static measurement of the intensity versus angle for both the irradiated and unirradiated solution at 20°, 30°, 40°, 50°, 70° and 90° was performed. The above solutions were unfiltered.

A series of solutions of S/SS<sup>-</sup>/APMA ranging from 0.004 weight % to a 2.0 weight % were prepared to study the dynamic scattering as a function of concentration. A wide variety of filters (cellulose ester, poly(vinylchloride) and poly(tetrafluorotethylene)) of varying pore sizes (0.22 μm, 0.5 μm and 0.6 μm) were tested but all were rapidly clogged, particularly when the solution concentration was 0.5% or larger. The radius of samples with an estimated concentration ranging from 0.004 to 0.10 weight % was found to be 160 Å.

### Electron Microscopy

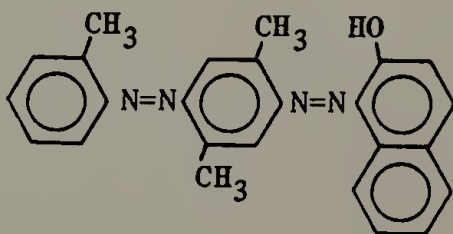
Preliminary electron microscopy work was done by L.C. Dickinson and Y. Cohen. Samples of S/SS<sup>-</sup>/APMA-hv gel were sonicated into dilute solution and then a drop of solution was freeze-dried on a carbon-coated copper grid. A sample of S/SS<sup>-</sup>/AEMA (60.1/24.3/15.6) in DMF was dialyzed against a 0.75% CsI solution with the pH=11. The pH was adjusted to 7.05 and gelation was observed within 10 minutes. Carbon-coated copper grids were dipped in the solution, before gelation, and

then were air-dried. Gelled samples of S/SS<sup>-</sup>/AEMA were prepared using a Balzar freeze-etch apparatus. A sample of gel was frozen in liquid freon to 77°K and then fractured at -100°C with a horizontally rotating steel knife. The sample was prepared under high vacuum and was allowed to stand for a given time to etch the sample (0 - 2 min). The sample was shadowed with platinum at a 45° angle and then carbon at a 90° angle. The sample was warmed and the replica cleaned in an acid solution. All samples were studied by transmission electron microscopy.

### Results and Discussion

#### Hydrophobic Domains

The ability of a water soluble polymer to solubilize a water insoluble dye is evidence that the polymer behaves like a contracted polysoap. The procedure for the dye solubilization experiments was adapted from work by Ito et al.<sup>5</sup> The structure of the oil soluble dye, Oil Red EGN, is shown below.



(7.1)

Oil Red EGN has  $A_{\text{max}} = 514 \text{ nm}$  with an extinction coefficient of  $21,000 \text{ M}^{-1} \text{ cm}^{-1}$ .

The effect of polymer composition on the capacity of a terpolymer to solubilize dye was investigated for two random polymers of S/4VPQ/NAHD

with a composition of either 60/24/16 or 36/47/17. Four different concentrations of each polymer solution were shaken with an excess of Oil Red EGN and the amount of dye solubilized after two weeks was observed (Table 7.1). A small amount of dissolved polymer was lost from each solution during the filtration process (precipitated on the sintered glass filter) and so polymer concentration was measured using the ultraviolet absorbance maximum. The ethyl pyridinium moiety is a relatively hydrophobic ionic group. The pH of the solution was 6.0 - 7.0 therefore the amine group on NAHD was protonated.<sup>22</sup> Thus, NAHD and 4VPQ would contribute to both the ionic and hydrophobic character of the polymer.

The polymer containing a larger percentage of styrene, 60/24/16, solubilized more dye than 36/47/17 at all concentrations (Figure 7.2). The larger the number of hydrophobic groups on a polymer the greater the extent of hydrophobic domain formation and the greater the capacity to solvate a water insoluble substance in those domains. This result is predictable but also demonstrates the quantitative use of dye solubilization to probe the existence and extent of hydrophobic domains in water soluble polymers.

The concentration of solubilized dye was normalized to give the moles of dye solubilized in a 1.0 weight % polymer solution i.e the solubilizing power. One would expect that the capacity to solvate a dye would be linear with respect to solution concentration. However, a plot of the solubilizing power ( $[\text{dye}]100 \text{ ml/g}$ ) versus the solution concentration demonstrates that solubilizing power increases sharply



Table 7.1

Data for Oil Red EGN Uptake in Terpolymers of S/4VPQ/NAHD

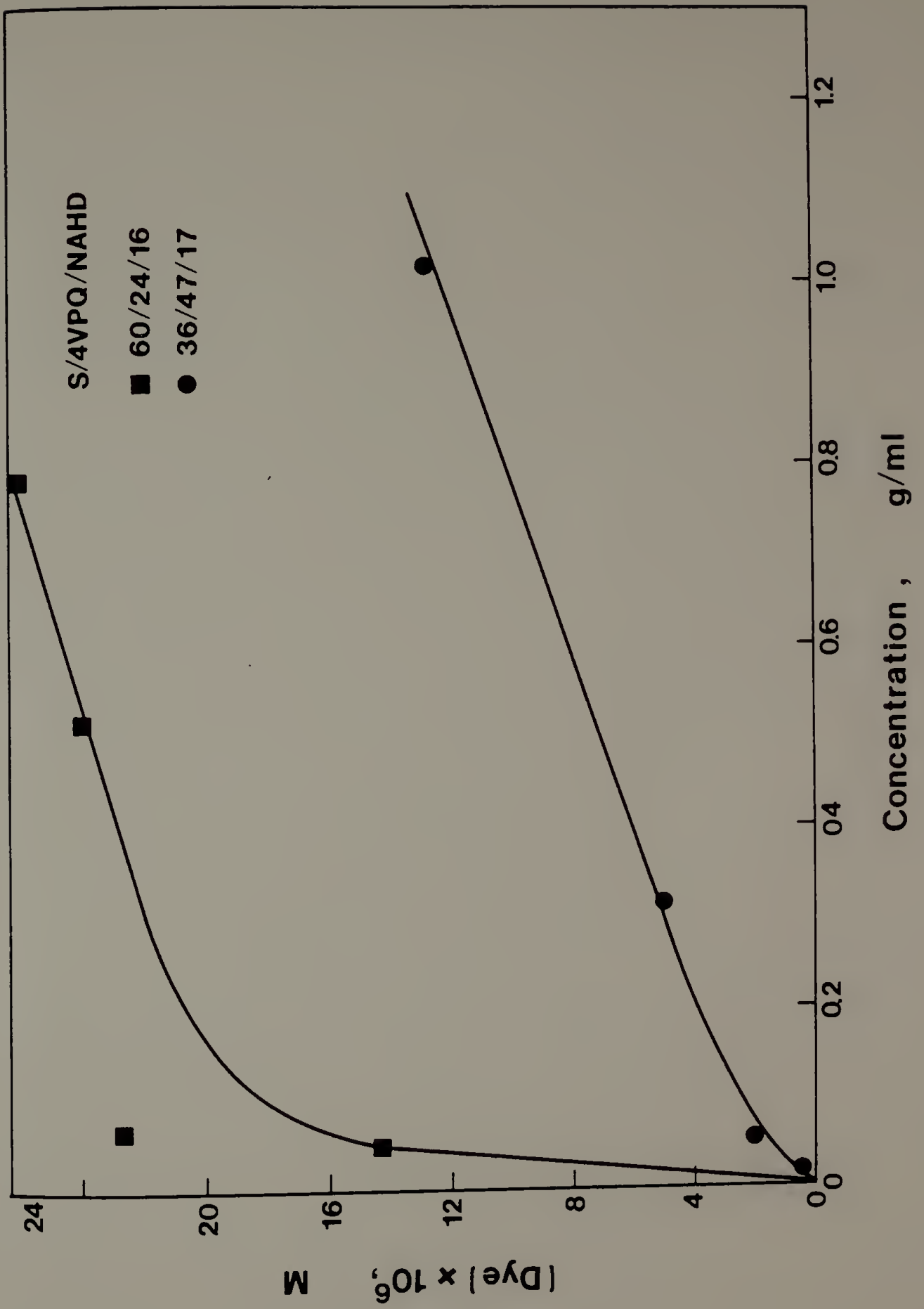
weight % (g/ml $\times 10^2$ ) <sup>a</sup>	A	$\lambda_{\max}$ (nm)	[Dye] (M) $\times 10^5$	S <sup>b</sup> (M) $\times 10^5$
36/47/17				
0.020	0.010	510	0.47	2.35
0.056	0.042	510	1.98	3.56
0.316	0.108	510	5.09	1.61
1.019	0.272	510	12.8	1.25
60/24/16				
0.049	0.304	513	14.3	29.5
0.067	0.482	513	22.7	33.7
0.318	0.506	515	23.9	7.5
0.690	0.552	515	26.5	3.77

<sup>a</sup>Weight % polymer was determined from the absorbance at 256 nm;  
 $\epsilon(36/47/17) = 17,900 \text{ (g/ml)}^{-1} \text{ cm}^{-1}$  and  $\epsilon(60/24/16) = 10,700 \text{ (g/ml)}^{-1} \text{ cm}^{-1}$ .

<sup>b</sup>Solubilizing power (S) is defined as the moles of dye solubilized in a  
 1.0 weight % solution of polymer.

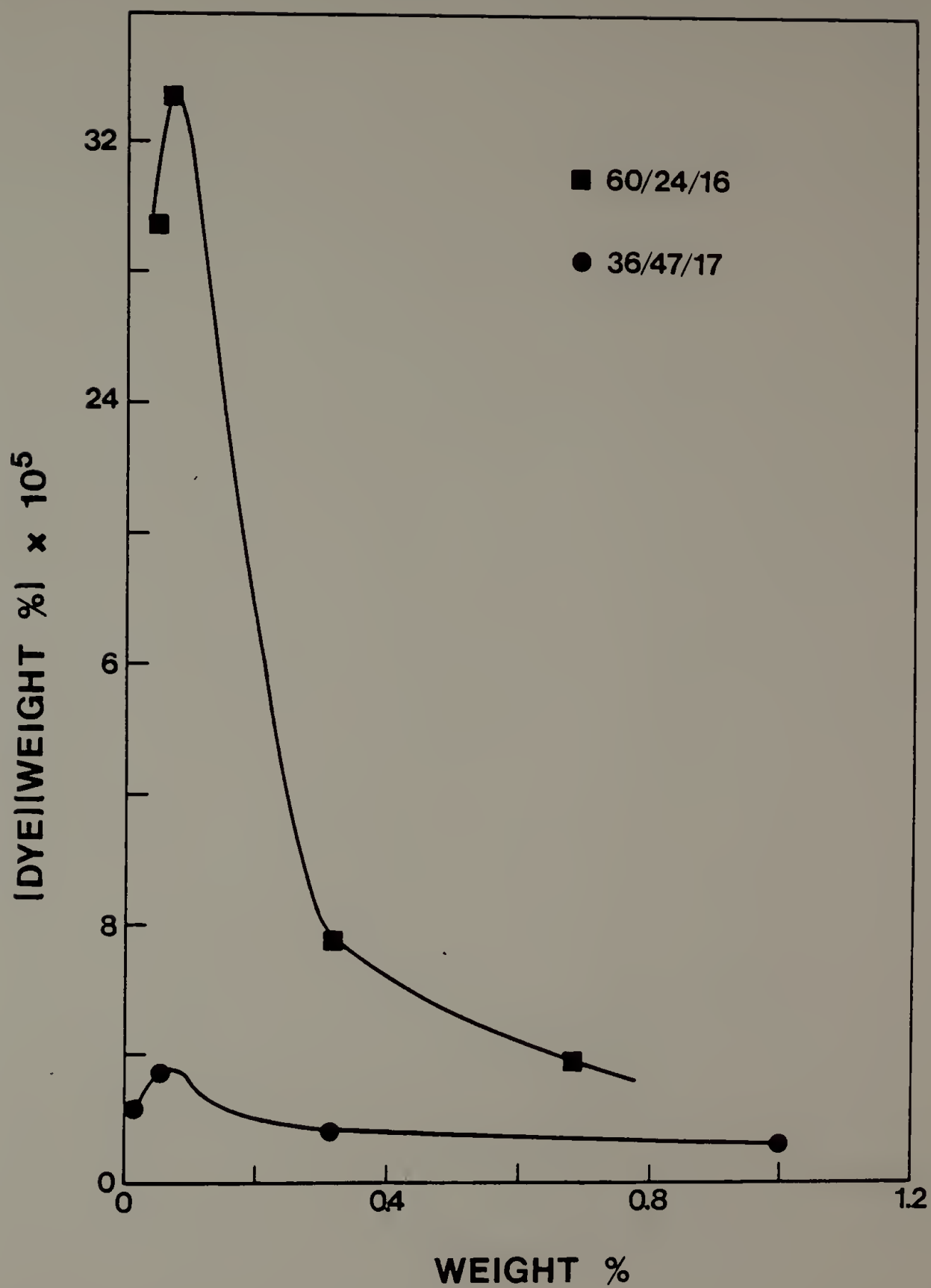
Figure 7.2. Dye solubilization as a function of polymer composition and concentration for S/4VPQ/NAHD: (■) 60/24/16 and (●) 36/47/17.





with dilution (Figure 7.3). With a composition of 36/47/17 there is a 2.8 times enhancement of solubilization at 0.056 weight % as compared to 1.018 %. This difference was more dramatic for 60/24/16 where the solubilizing power at 0.049% was 7.8 times larger than at 0.69%. This increase in solubilizing power with increasing dilution for polysoaps was also observed by Ito and coworkers<sup>5</sup> and they proposed this effect was due to interactions of the polar portion of the dye with the aqueous environment. A red-shift in the absorption maximum of the dyes solubilized in polysoaps was reported as evidence of the polar interaction of the polymer and dye molecule. The absorbance maximum of Oil Red EGN in a sodium laurelsulfate solution was  $\lambda_m = 514$  nm. In 60/24/16, where the effect of dilution on solubilizing power was most pronounced, the absorbance maximum was between 513 - 515 nm. Although ionic forces might be important in determining the extent of solubilization a second plausible explanation exists. Polymer aggregation might also reduce the number of sites available for dye solubilization. As the concentration of a solution containing a hydrophobic polyelectrolyte is increased the likelihood of intermolecular interactions increases. The ionic forces cause the polymers to repel one another yet the van der Waals forces stabilize the polymer in solution by decreasing the interfacial area between the hydrophobe and water (i.e. by decreasing the free energy of association).<sup>6</sup> Above a critical concentration the polymers solvate each other by aggregation thus reducing their capacity to carry a water insoluble dye. For S/4VPQ/NAHD this critical concentration is between 0.1 - 0.2

Figure 7.3. Solubilizing power versus sample concentration for two terpolymers of S/4VPQ/NAHD: ( ■ ) 60/24/16 and ( ● ) 36/47/17.

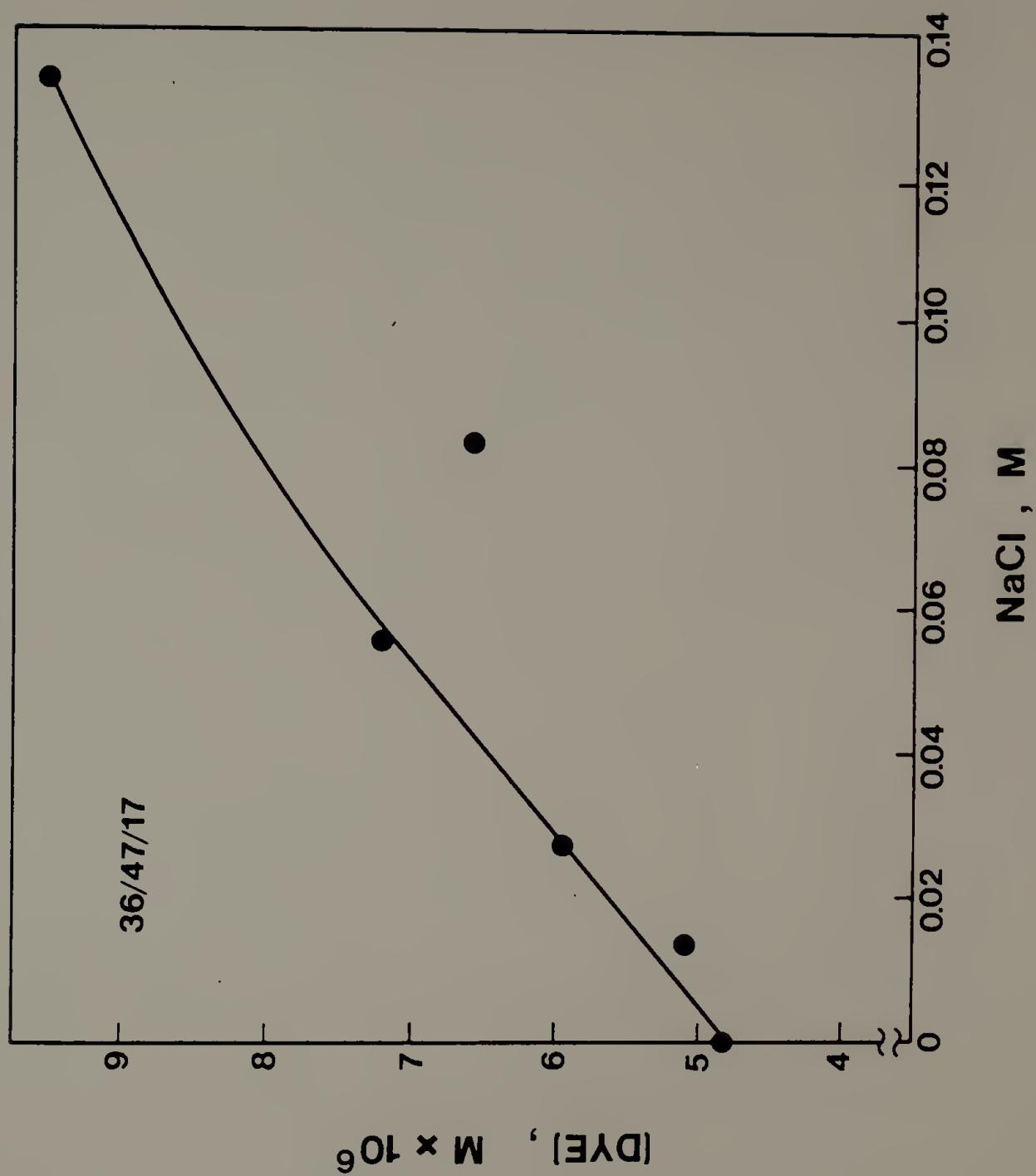


weight %. This is the same concentration range observed to be nonlinear for the anionic polysoaps of Ito et al.<sup>5</sup> One would expect more aggregation in 60/25/16 than in 36/47/17 because of the higher hydrophobic content and this explains the more dramatic decrease in solubilizing power with increasing concentration.

The effect of ionic strength on the presence of hydrophobic domains was investigated for S/4VPQ/NAHD, 36/47/17. Dye solubilization as a function of ionic strength is shown in Figure 7.4. A tenfold increase in ionic strength gave a twofold increase in dye solubilization in a 0.28 weight % polymer solution. For ionic polysoaps, added electrolytes suppress the electrical repulsion between ionic groups and thus decrease the free energy of hydrophobic association and increase the contraction of a polysoap.<sup>6</sup> In a relatively contracted state, where there are more hydrophobic associations, a polymer molecule can solvate more of an 'oil' soluble substance.<sup>23</sup> According to the above hypothesis, one would predict that increasing the ionic strength to the point of intermolecular aggregation would decrease the capacity of a polymer to solvate dye. This could explain the leveling-off evident in the plot of dye uptake as a function of ionic strength. Additional dye uptake experiments at high ionic strength are needed to conclusively demonstrate this principle.

Attempts to examine the radius of S/SS<sup>-</sup>/APMA polymer dissolved in aqueous solutions by dynamic light scattering were hampered by their inability to be filtered, particularly in solutions with concentrations greater than 0.1 weight %. Pore sizes up to 0.6  $\mu\text{m}$  were tested using a

Figure 7.4. Dye solubilization as a function of ionic strength for S/4VPQ/NAHD (36/47/17). A tenfold increase in ionic strength gave a twofold increase in dye solubilization.





range of filters (cellulose-ester, poly(vinylchloride) and poly(tetrafluoroethylene)) and all clogged.<sup>24</sup> In a dilute filtered solution (approximately 0.1%) the Stokes radius was found to be 160 Å (assuming a spherical particle shape). In an unfiltered, concentrated solution (2.86%) the Stokes radius was estimated to be 2500 Å. GPC analysis of unhydrolyzed S/MSS/APMA from the same polymerization reaction gave  $\bar{M}_n = 19,700$  and  $\bar{M}_w = 44,600$ . These estimates are accurate enough to conclude that concentrated polymer solutions are aggregated, however, the critical concentration for aggregation was not determined.

#### Hydrophobic Polyampholyte Complexes

Gelation of our water soluble model polymers was first observed for a terpolymer, S/SS<sup>-</sup>/APMA (85/13/2), after irradiation by ultraviolet light. The polymer solution (2.86 weight %) gelled after standing undisturbed for one week (not during irradiation). The gel was soluble in several organic solvents including DMF, acetone and methanol! Also, the gel could be sonicated in a large volume of water to form a clear solution. Obviously the gelation was not caused by covalent crosslinks to form an insoluble network structure.

Dye solubilization experiments for S/SS<sup>-</sup>/APMA before and after irradiation (as a function of concentration) were only qualitative because the turbidity of some samples interfered with absorption measurements. Solutions with initial concentrations of 0.5 and 1.0 weight % S/SS<sup>-</sup>/APMA precipitated from solution with shaking to give final concentrations of 0.14 and 0.01 weight % of dissolved polymer remaining respectively. This is another indication of polymer

aggregation at concentrations of 0.5% or more. It appeared that the unirradiated solutions solubilized more dye than the irradiated ones: a 0.125 weight % (unirradiated) solution solubilized 1.5 times more dye than a 0.165 weight % (hv) solution relative to a 1.0% standard. This might simply be an effect of dilution, however, precipitates from the 1.0 and 0.5% (hv) samples had noticeably less pink color than the precipitates from the unirradiated samples.

Static light scattering as a function of angle for S/SS<sup>-</sup>/APMA (a 2.86% sample before and after hv) showed less scattering for the gel than for the unirradiated sample at all angles studied (Figure 7.5). This is a qualitative indication that the conformation of the polymer in solution has probably contracted during the gelation process. The solution concentration and its inability to be filtered limit the usefulness of light scattering techniques.

The next system observed to gel was S/SS<sup>-</sup>/NAHD (61/32/7) in a 3.6 weight % solution containing 1% 4-(2-hydroxyethyl)-1-piperazine ethanesulfonic acid (HEPES) at a pH of 7.74. The gel was the consequence of preparing a sample for <sup>13</sup>C-NMR to study carbamate formation and the pK<sub>a</sub> of the amine group as a function of pH. Attempts to find the pK<sub>a</sub> of the free amine on S/SS<sup>-</sup>/NAHD by titration were abandoned because the time required for pH equilibration after addition of an acid or base were prohibitively long. This is shown in Figure 7.6 for 20 ml of a 1.8 weight % solution of S/SS<sup>-</sup>/NAHD upon addition of 100  $\mu$ l 0.0987 M NaOH. Equilibrium was attained after approximately 6 hr. Gelation of S/SS<sup>-</sup>NAHD was time dependent and required approximately 18

Figure 7.5. Static light scattering as a function of angle for S/SS<sup>-</sup>/APMA (a 2.86 weight % solution): (●) before irradiation with ultraviolet light and (■) after irradiation. The irradiated sample scattered less light than the unirradiated at all angles.

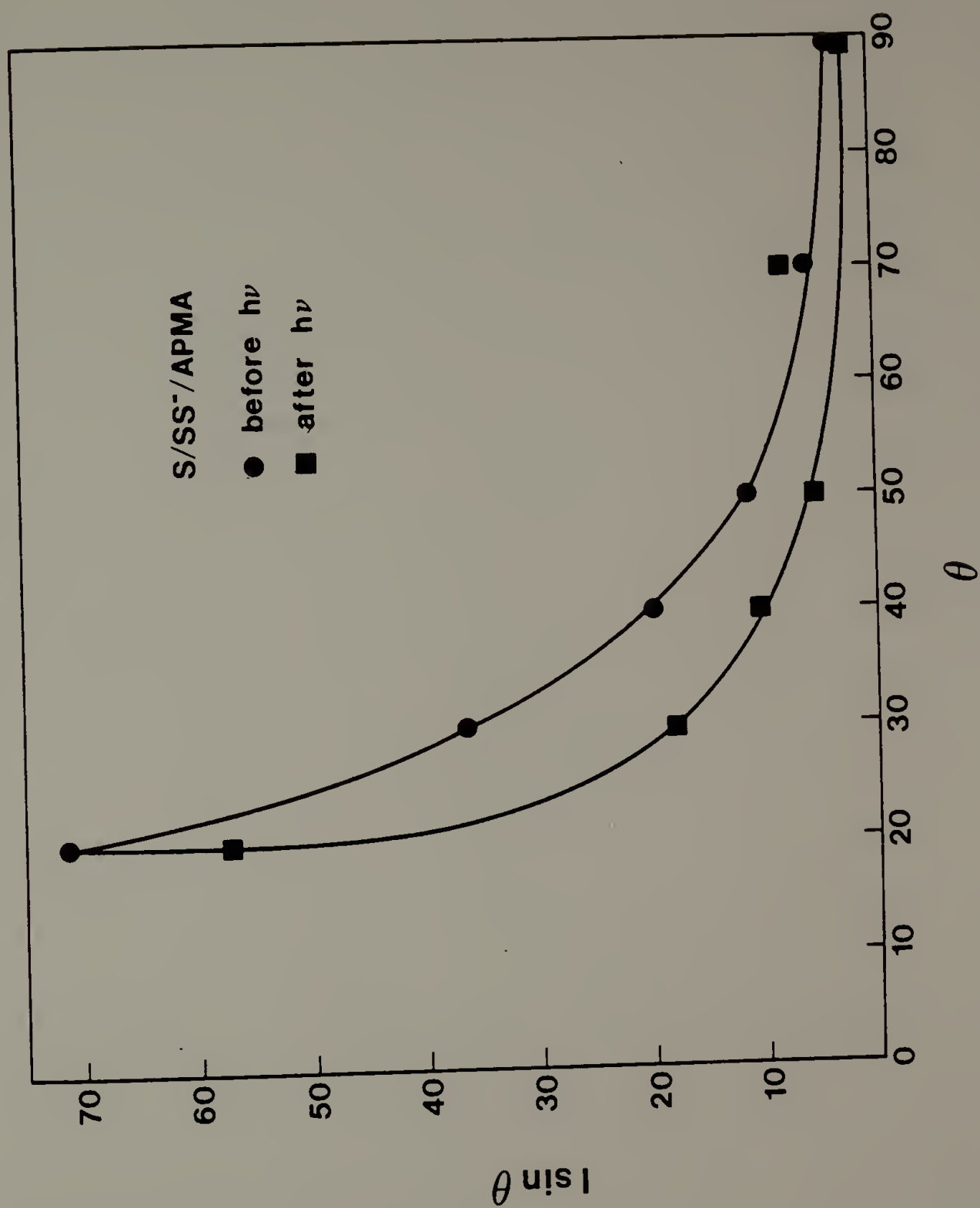
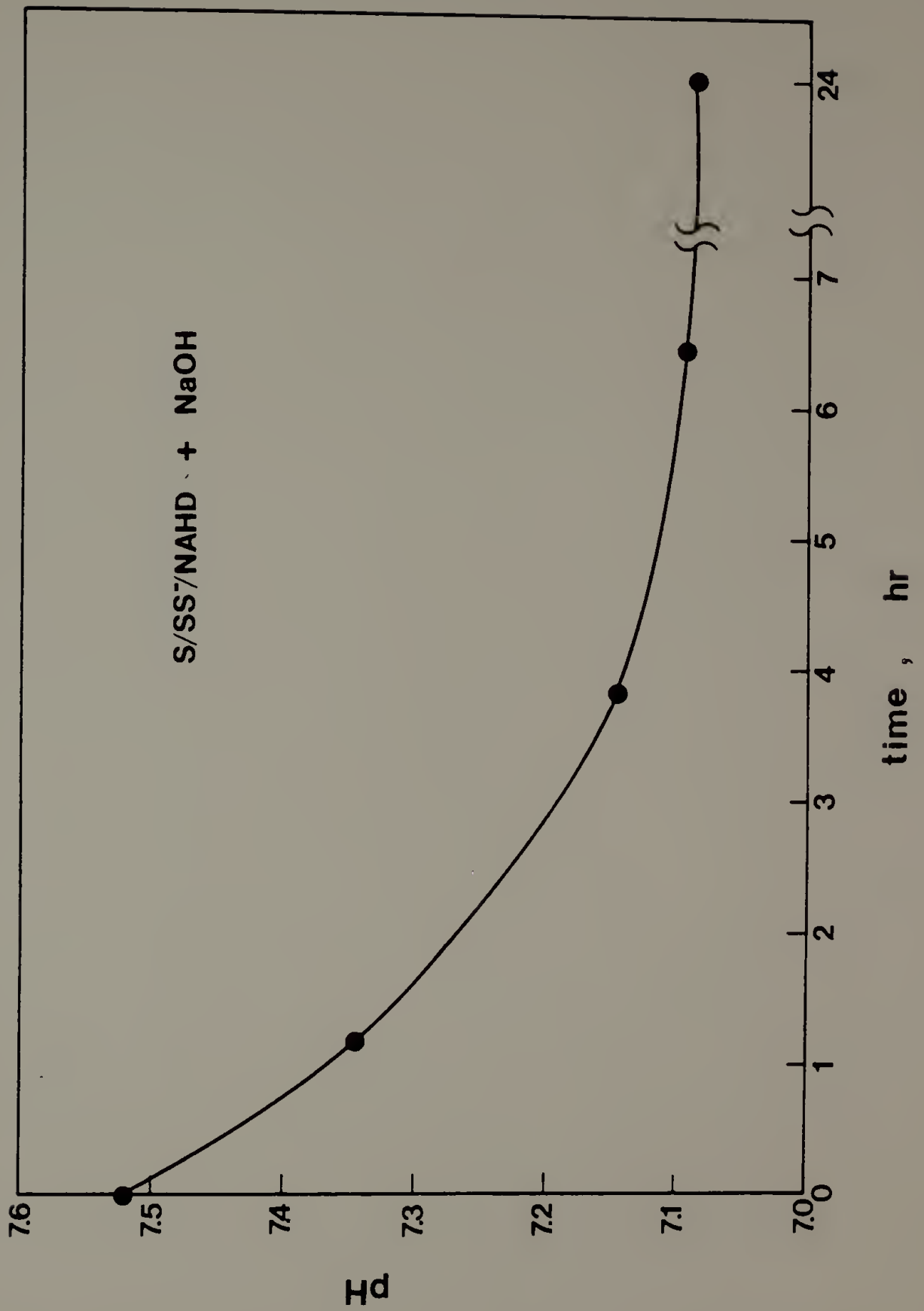


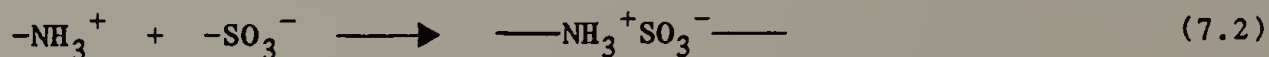
Figure 7.6. The pH equilibration as a function of time for a solution of S/SS<sup>-</sup>/NAHD (20 ml, 1.8 weight %) with the addition of 100  $\mu$ l of 0.0987 M NaOH.



hr. The gel was soluble in polar organic solvents such as DMF. A second terpolymer containing less sodium styrene sulfonate (76/13/11) was not water soluble despite the fact that other polymers containing 13%  $\text{SS}^-$  are water soluble.

In preliminary work in our laboratory, Gillis<sup>20</sup> had synthesized a terpolymer of S/MSS/AEMA. A sample of this terpolymer was subjected to base hydrolysis. Addition of a few drops of dilute hydrochloric acid to the concentrated polymer solution caused localized gelation within a few seconds and gelation of the entire solution within 12 hr. Again, the gel was soluble in polar organic solvents.

Experimental observation of gelation in S/ $\text{SS}^-$ /APMA, S/ $\text{SS}^-$ /NAHD and S/ $\text{SS}^-$ /AEMA was related to the sample concentration and pH and exhibited a time dependence indicative of a metastable state. The most likely explanation is that these polymers form polyelectrolyte complexes. The protonated amine interacts with the sulfonate anion to create an ionic crosslink:



Common solvents for polyelectrolyte complexes such as 20% KSCN, 20% NaBr, 1 g of NaBr/3 ml of  $\text{H}_2\text{O}$ /1 ml of acetone, 1 N HCl and 1 N NaOH did not solubilize the gels. Simple polar organics such as DMF or acetone were all that was necessary to dissolve the gels. Therefore hydrophobic interactions hold a significant role in the gel's molecular structure. These hydrophobic polyampholytes were imagined as aggregated polymer

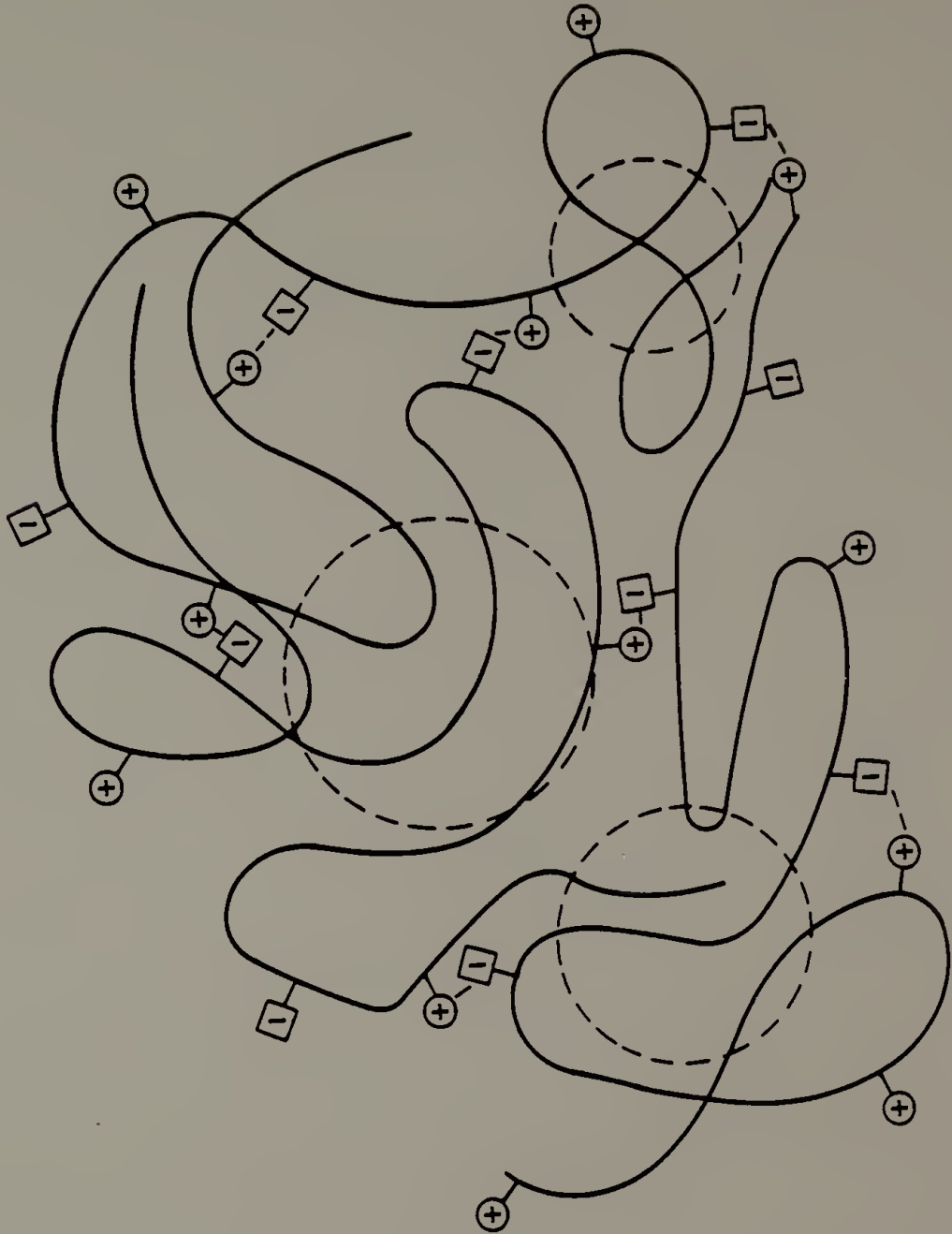


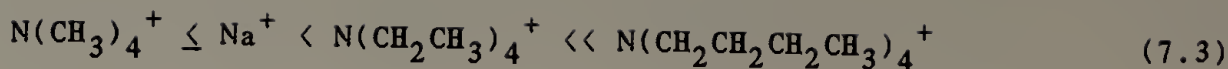
molecules tied together by ionic crosslinks (Figure 7.7). The slow equilibration of pH after addition of acid or base is a measure of the time required for the conformation of the polymer to change to allow the amine to be protonated or deprotonated. Both anionic and cationic groups are somewhat hydrophobic and this may enhance their interaction.

The effect of pH on complex formation was examined by shaking solutions of S/SS<sup>-</sup>/NAHD with Oil Red EGN at five different pH's ranging from 6.2 to 10.8. After two weeks, samples with a pH less than 8.7 precipitated completely from solution (less than 1% of the original polymer remained). This is an indication that the  $pK_a$  of NAHD is not sufficiently lowered by the hydrophobic environment of the polymer chain. Probably, fluctuations in chain conformation cause the amine to move into the aqueous environment and allow the amine to be protonated at  $pH \leq 8.7$ . In the polymer solution at  $pH = 10.7$  the amine groups were unprotonated and the polymer solubilized dye as an ordinary polysoaps.

To evaluate the effect of counterions on the rate and extent of gelation, four solutions of S/SS<sup>-</sup>/NAHD were dialyzed against 0.1% solutions of NaCl, tetramethyl ammonium hydroxide (TMA<sup>+</sup>), tetraethylammonium hydroxide (TEA<sup>+</sup>) and tetrabutylammonium hydroxide (TBA<sup>+</sup>). To some extent the ionic strength of these added ions contracts the polymers closer to their theta dimensions. The TBA<sup>+</sup> counterion caused the polymer to have a gel-like property. In general the viscosity of the solutions increased with increasing hydrophobicity of the counterion:

Figure 7.7. A schematic of the structure proposed for a hydrophobic polyampholyte gel: ( $\oplus$ ) cations, ( $\ominus$ ) anions and the hydrophobic domains are enclosed by dashed lines (---).





Hydrophobic interactions between tetraalkylammonium cations and styrene sulfonate have been observed to cause negative volume changes.<sup>25</sup> The positive volume changes observed here can be attributed to a release of electrostricted water molecules at the charged site. The viscosity of the terpolymer solution with a sodium counterion decreased after being forced through a narrow capillary. This is evidence that a shearing force disrupts the polymer structure in solution.

A variety of surfactants were investigated as a means to prevent gelation.<sup>27</sup> Two non-ionic surfactants were studied: Tween 20, a polyethylene sorbitan monolaurate, with a critical micelle concentration (CMC) of 60 mg/l and Tergitol NP40 a polyethylene glycol. Sodium laurelsulfate, a strong detergent with a CMC = 8.2 mM and sodium deoxycholic acid, a cholesterol-like surfactant with a CMC = 4 - 6 mM were also studied. In all cases, added surfactant at twice their CMC actually enhanced the rate of gelation. Sodium laurelsulfate enhanced the rate of gelation most dramatically, followed by the two non-ionics and then sodium deoxycholic acid. The ionic head group of sodium laurelsulfate can form an ionic crosslink with a protonated amine and at the same time the hydrophobic tail enhances the hydrophobic interaction. This might also explain the slightly increased rate of gelation for sodium deoxycholic acid, however the hydrophobic interaction would not be as strong because the fused-ring structure is more rigid, limiting its conformation and thus its interaction. For the non-ionic

surfactants the mechanism by which gelation is enhanced is less obvious. Perhaps they simply increase hydrophobic aggregation.<sup>28,29</sup>

Added solutes consisting of short chain molecules containing an anionic group, such as HEPES, DSS, or sodium acetate, accelerated the gelation of the hydrophobic polyampholytes. These slightly hydrophobic molecules might behave like sodium laurilsulfate and increase gelation via ionic and hydrophobic interactions. In cationic polymer solutions (e.g. S/4VPQ/NAHD) anionic solids caused the polymer to precipitate and adsorb to the solid like a gum. Salts such as NaCl or CsI greatly enhanced the rate of gelation. The added electrolytes suppress ionic attraction between the anionic and cationic moieties, however, they also decrease the free energy of hydrophobic association and thus increase the contribution of hydrophobic interaction to the gelation process.

Characterization of hydrophobic polyelectrolyte complexes is complicated by the fact that, before gelation, the polymer is in a mesostate and the properties such as viscosity, turbidity etc. are time dependent.<sup>30</sup> Ordinary characterization techniques are not useful after gelation. Electron microscopy is a technique which yields domain size and gel macrostructure but is fraught with artifacts, particularly in water soluble gels.<sup>31</sup> Preliminary work by Y. Cohen using freeze fracture techniques looks promising but has not yet detailed the gel structure. The different potential applications of these hydrophobic polyampholytes require specific characterization methods such as membrane permeability or biocompatibility.

### Conclusions

Hydrophobic domain formation is favored at high hydrophobe content, high ionic strength and low solution concentration. Dye solubilization is a quantitative method which can be used to compare model polymers and the effectiveness of their structure in providing a hydrophobic domain for the heme group. In a 0.26 weight % polymer solution of S/SS<sup>-</sup>/APMA-hv (84.5/13.5/2)  $1.49 \times 10^{-5}$  moles of dye were solubilized per liter. A tetrapolymer of S/SS<sup>-</sup>/APMA-hv/HMEMA (84/13/2.7/0.16) has  $3.38 \times 10^{-5}$  moles heme in one liter of 0.25 weight % solution. This means that in pure water only about half of the heme groups are solubilized by the hydrophobic domains. Some inaccuracies are a result of the assumption that Oil Red EGN and the hemin derivatives are equally solubilized in a polysoap. Future work should utilize solubilization of a specific hemin derivative to avoid errors of this nature.

Polymer composition can be tailored to maximize hydrophobic domain concentrations at a given ionic strength. Polymers which are salt sensitive (i.e. insoluble in buffer solutions) are undesirable as models of hemoglobin. Buffers are a convenient method of maintaining a constant pH. Polymers containing a large quantity of styrene are extremely sensitive to added salts. Polymers containing moderate quantities of hydrophobic units exhibit improved dye solubilization with increasing ionic strength. The optimum model polymer should be totally unaggregated at a given ionic strength and concentration. Evidence of aggregation was seen in the increased capacity of polymers to solubilize dye with dilution. This effect was more dramatic for a more hydrophobic



polymer where aggregation would be likely to be observed. Light scattering data suggests that at some solution concentration larger than 0.1 weight % hydrophobic polyelectrolytes are quite aggregated.

Novel hydrophobic polyampholytes have been synthesized. They are the first class of random polymers to incorporate anionic, cationic and hydrophobic groups in each polymer chain. The synthetic method, whereby blocked monomers are polymerized, allows these three types of monomers to be polymerized to give any type of composition. Before unblocking, the polymer is soluble in a wide variety of solvents. After gelation the system is still soluble in polar organic solvents. The gelation process is dependent on concentration, pH, counter ion, added solutes and salt. It is also likely that polymer composition and temperature affect the rate of gelation and the structure of the gel. These properties make the polymer interesting for many applications. The pH dependence could be altered by quaternization of the amine group after polymerization to yield a permanent cation. At low concentrations of anions and cations these polymers act as ionomers.<sup>13</sup> The procedure to synthesize novel hydrophobic polyampholytes is general and has a potential application for many systems of widely varying properties.



### References

1. Dubin, P.L.; Strauss, U.P. J. Phys. Chem., (1970), 74, 2842.
2. Strauss, U.P. "Micellization, Solubilization and Microemulsions", Mittal, K.L. (ed.), Plenum Press, New York (1977), Vol. II, p. 895.
3. Turro, N.; Okubo, T. J. Am. Chem. Soc., (1982), 104(11), 2985.
4. Strauss, U.P.; Williams, B.L. J. Phys. Chem., (1961), 65, 1390.
5. Ito, K.; Yamashita, Y. J. Colloid Sci., (1964), 19, 28.
6. Nakagawa, T.; Inoue, H. Kolloid-Z. u. Z. Polymere, (1964), 195(2), 7.
7. Strauss, U.P.; Barbieri, B.W. Macromolecules, (1982), 15, 1347.
8. Ito, K.; Yamashita, Y. J. Colloid Sci., (1964), 19, 152.
9. Dubin, P.L.; Strauss, U.P. J. Physical Chem., (1973), 77(11), 1427.
10. Dubin, P.L.; Strauss, U.P. Polyelectrolytes and Their Applications, Rembaum, A.; Selegny, E. (eds.), D. Reidel Pub. Co., Dordrecht Holland, (1975) p. 3.
11. Tsuchida, E.; Abe, K. Adv. Polym. Sci., (1982), 45, pp. 1-123.
12. Philipp, B.; Dawydoff, W.; Linow, K.-J. Z. Chem., (1982), 1, 1.
13. Salamone, J.C.; Mahmud, N.A.; Mahmud, M.U.; Nagabhushanam, T.; Watterson, A.C. Polymer, (1982), 23, 843.
14. Kataoka, K.; Tsuruta, T. Makromol. Chem., (1980), 181, 1363.
15. Shinoda, K.; Hayashi, T.; Yoshida, T.; Sakai, K.; Nakajima, A. Polym. J., (1976), 8(2), 202.
16. Abe, K.; Koide, M.; Tsuchida, E. Macromolecules, (1977), 10(6), 1259.

17. Ohno, H.; Nii, A.; Tsuchida, E. Makromol. Chem., (1980), 181, 1227.
18. Kurokawa, Y.; Shirakawa, N.; Terada, M.; Yui, N. J. Appl. Polym. Sci., (1980), 25, 1645.
19. Salamone, J.C.; Tsai, C.C.; Olson, A.P.; Watterson, A.C. J. Polym. Sci.: Polym. Chem. Ed., (1980), 18, 2983.
20. S/SS<sup>-</sup>/AEMA was synthesized by J. Gillis, purity of the reactants is unknown.
21. Ford, N.C. "Dynamic Light Scattering: Applications of Photon Correlation Spectroscopy", Pecca, R. (ed.), Plenum Pub. Co., New York, in publication.
22. The  $pK_a$  of the free amine of NAHD in a hydrophobic polyelectrolyte is discussed in Chapter VIII.
23. Tokiwa, F. J. Phys. Chem., (1968), 72, 1214.
24. R.A. Wessling (Dow Chemical Co.) studied cationic polysoaps containing a quaternized ammonium group and found that they could not be filtered (Private Communication 1983). The coiled structure probably collapses (i.e. precipitates) when forced through a small hole such as the pore in a membrane.
25. Tondre, C.; Kale, M.; Zana, R. Eur. Polym. J., (1978), 14, 139.
26. Tondre, C.; Zana, R. J. Phys. Chem., (1972), 76, 3451.
27. For a review of surfactant chemistry: Helenius, A.; Simons, K. Biochim. Biophys. Acta, (1975), 415, 29.
28. Tokiwa, F.; Tsujii, Bull. Chem. Soc. Jpn., (1973), 46, 2684.
29. Cabane, B. J. Phys. Chem., (1977), 81(17), 1639.

30. See Reference 11 p. 16.

31. Tokyama, K.; Miller, W.G. Nature, (1981), 289, 813.

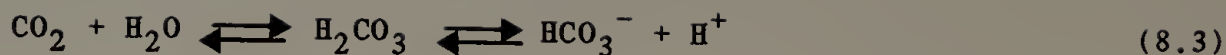
## C H A P T E R   V I I I

### CARBAMATE FORMATION IN AMINE CONTAINING POLYMERS TO MIMIC CO<sub>2</sub> TRANSPORT BY HEMOGLOBIN

The reaction of carbon dioxide with amino groups of the N-terminal valines of hemoglobin to form carbamates is of great physiological importance.<sup>1,2</sup> Approximately 60% of the dissolved CO<sub>2</sub> in the tissue is transported to the lungs by this mechanism. Bound CO<sub>2</sub> is a heterotropic effector, influencing oxygen binding in hemoglobin.<sup>3</sup>

Techniques to study carbamate formation in proteins include gasometric methods,<sup>4</sup> chemical chromatographic techniques,<sup>5,6</sup> X-ray crystallography,<sup>7</sup> the study of abnormal hemoglobins,<sup>8</sup> <sup>13</sup>C Fourier transform nuclear magnetic resonance (FT-NMR)<sup>9,10</sup> and other less direct methods. <sup>13</sup>C FT-NMR has the advantage of being a quantitative nondestructive technique of visualizing carbamate formation over a wide range of conditions. Experimental use of isotopically enriched carbon dioxide (<sup>13</sup>CO<sub>2</sub>) up to 90% gives an 80-fold increase in sensitivity. The carbamate resonance is characteristically a few parts per million downfield of the bicarbonate resonance. The pH dependence of carbamate formation follows a bell shaped curve given by the following equilibria:





where  $K_a$  is the dissociation constant of the amine group and  $K_c$  is the formation constant of the carbamate group. At low pH, the concentration of unprotonated amine is limited and at high pH the concentration of dissolved  $\text{CO}_2$  is limited. Reaction 8.1 is virtually instantaneous (less than 1  $\mu\text{sec}$ ) because it is an ionic reaction. Reaction 8.2 is also fast (less than 0.1 sec) and represents two reactions: the combination of the amine and  $\text{CO}_2$  to form a carbamic acid followed by the dissociation of that acid.<sup>4</sup> At physiological pH the concentration of  $\text{CO}_3^{2-}$  in solution is quite small thus reaction 8.3 represents the most important equilibria for  $\text{CO}_2$  dissolved in solution. Reaction 8.3 is rather slow comparatively, with ten minutes necessary to reach equilibrium at 20°C.

The mole fraction of carbamate (Z) in an amine containing sample is dependent on the pH and the concentration of dissolved  $\text{CO}_2$ .

$$Z = \frac{K_c K_a [\text{CO}_2]}{K_c K_a [\text{CO}_2] + K_a [\text{H}^+] + [\text{H}^+]^2} \quad (8.5)$$

Variations in ionic strength due to increasing  $p\text{CO}_2$  at a constant pH can cause saturation of anion binding sites as well as cause conformational changes which affect carbamate formation. For this reason Gurd and coworkers<sup>11</sup> have developed experimental methods maintaining constant total carbonates. This simplified the determination of Z. For

hemoglobin, Z was determined experimentally from the integration of the undecoupled NMR spectrum by the following relation:

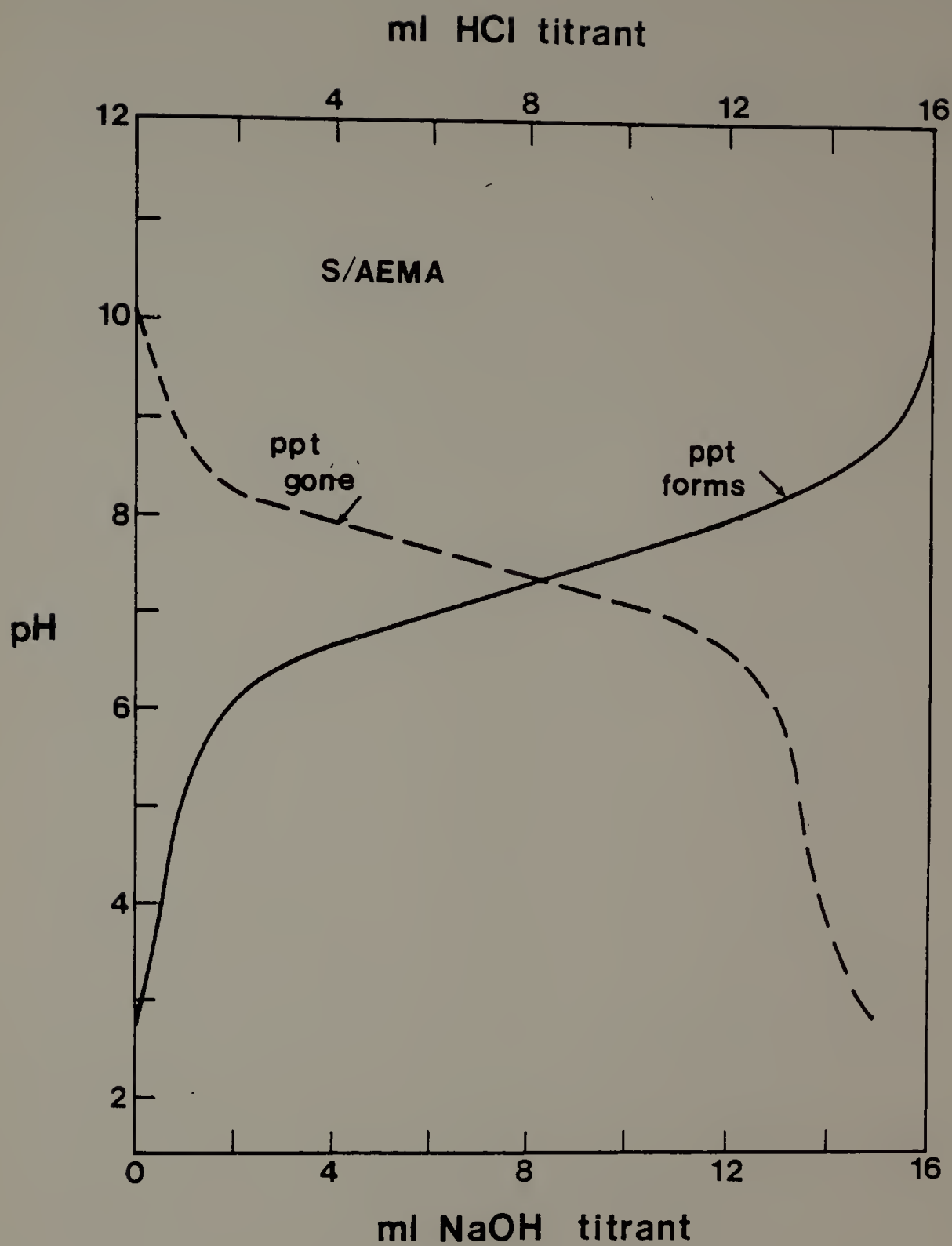
$$Z = \frac{I_{cam}}{I_{co}} \times \frac{(0.011)}{\bar{X}^{13}CO_2} \times 328 \quad (8.6)$$

where  $I_{cam}$  and  $I_{co}$  are the intensities of the carbamate resonance and the sum of the naturally abundant  $^{13}C$ -carbonyl carbon atoms of the 328 peptides in an  $\alpha\beta$  dimer respectively. The measured mole fraction of  $^{13}C$  enriched carbonates,  $\bar{X}^{13}CO_2$ , was determined by mass spectroscopy and 0.011 is the natural abundance of  $^{13}C$ . Quantitative results from the  $^{13}C$ -NMR technique depend on the quality of the NMR spectrum as well as the accurate knowledge of the pH,  $^{13}C$  enrichment and total carbonates.

Two different alkyl amines were selected to carry carbon dioxide at physiological pH, 2-aminoethyl methacrylate (AEMA), and N-methylacrylylhexamethylenediamine (NAHD). Gillis<sup>12</sup> studied the titration of a copolymer of styrene and AEMA (68.7 mol % AEMA) and demonstrated that the  $pK_a$  of the amine was approximately 7.5 (Figure 8.1). As the amine group was titrated from the protonated to the unprotonated state the polymer precipitated from solution (pH = 8.5). In this copolymer AEMA functioned as both a water solubilizing group and a carbon dioxide carrying group. The expected  $pK_a$  of AEMA is between 8.5 - 9.5, thus the local environment of the polymer chain appeared to lower the  $pK_a$  of AEMA. No attempt was made to evaluate the effect of added electrolytes (NaOH or HCl) or polymer composition on the  $pK_a$  of AEMA. It was proposed that NAHD would be more hydrophobic than AEMA and

Figure 8.1. A titration curve of S/AEMA (0.4 g, 31.3/68.7) in water with 0.0885 M NaOH and 0.983 M HCl.





therefore would be unprotonated at physiological pH in a hydrophobic polyelectrolyte.

### Experimental Procedure

#### Materials

Monomer synthesis is described in Chapter II and polymer synthesis and modification in Chapter V. HEPES (4-(2-hydroxyethyl)-1-piperazineethanesulfonic acid) and D<sub>2</sub>O (99.9% isotopic purity) were obtained from Aldrich Chemical Co. DSS (sodium 2,2-dimethyl-2-silapentane-5-sulfonate) was from Thompson-Packard, Inc. <sup>13</sup>Sodium acetate with the carbonyl group enriched to give 90% isotopic purity was purchased from Merck, Sharp and Dohme Canada, Ltd. <sup>13</sup>CO<sub>2</sub> was obtained from Monsanto Chemical Corp. at 90% enrichment and sodium carbonate and sodium bicarbonate were obtained from Stohler Isotope Chemicals at 90% and 99% isotopic enrichment respectively. Water was distilled and deionized before use. <sup>13</sup>C-NMR sample tubes (Taperlock) were purchased from Wilmad Glass Co. and had a ground glass joint at the top of the tube which allowed samples to be sealed, degassed and stored with the desired atmosphere. The sample tube was sufficiently light and symmetrical to be spun at velocities between 20 - 35 Hz without difficulty.

#### Standards

DSS was used as a reference for chemical shift. In a few instances DSS was an internal reference with 0.03 g used for a 1.5 ml sample. For the most part DSS interacted with polymers to salt them out of solution

or increase the rate of gelation and thus a saturated aqueous ( $D_2O$ ) solution of DSS, 50  $\mu$ l in a capillary, was used as an external reference. The chemical shift of HEPES as function of pH was characterized over the range of 6.45 - 8.30 for use as an internal pH standard. HEPES has an apparent  $pK_{a1} = 3$  and  $pK_{a2} = 7.53$  at  $20^\circ C$ .<sup>13</sup> Decoupled spectra of these standards in  $D_2O$  with a  $90^\circ$  rf pulse and no pulse delay were taken to determine their chemical shift. It was assumed that the pH measured with a Radiometer PHM64 Research pH meter was equal to pD. A  $^{13}C=O$  standard,  $^{13}$ sodium acetate (50  $\mu$ l, 0.319 M), was sealed in a capillary and used as an external standard to quantitate the amount of carbamate formed in solution, analogous to the envelope of protein carbonyls of hemoglobin used to quantitate carbamate formation by the N-terminal valines by Gurd and coworkers.<sup>10</sup>

#### Sample Preparation

Samples for  $^{13}C$  spectra included S/4VPQ/NAHD (36/47/17, 1.58 weight % and 61/24/15, 2.28 weight %) and AEMA monomer in  $H_2O$ . The solutions were diluted with 10 vol %  $D_2O$  to provide a lock for the NMR. The pH of the solution was adjusted two different ways. In the first method  $CO_2$  (not enriched with  $^{13}C$ ) was flushed through a sample and the pH was adjusted by the addition of a solution of 0.142 M NaOH in  $D_2O$ . In this method, neither the amount of isotopic enrichment nor the ionic strength was a constant from sample to sample. In the second method a volume of NaOH was added to the sample and sample handling in the air was kept to a minimum to avoid contamination by atmospheric  $CO_2$ . The sample and standard were placed in the NMR tube and degassed by evacuation.

Solutions of S/4VPQ/NAHD were quite frothy and thus the samples were repeatedly evacuated for short periods and then allowed to stand to allow the foam to subside. After degassing, 760 mm of 90%  $^{13}\text{CO}_2$  were placed over the sample and the sample was allowed to equilibrate for 12 - 18 hr. Samples were degassed again, blanketed with 760 mm  $^{13}\text{CO}_2$  and allowed to stand at least 1 hr before the NMR spectrum was taken. After the spectrum was taken and the sample tube was opened, the pH of the sample was measured immediately.

### $^{13}\text{C}$ Fourier Transform NMR Measurements

Spectra were taken on a Varian CFT20 20 MHz  $^{13}\text{C}$  FT-NMR instrument. Data was acquired using gated decoupling with a pulse width of  $30^\circ$  and a pulse delay of 5 s. The advantage of using these acquisition parameters will be fully discussed later in this chapter. Integral areas were recorded digitally. The peak areas for a sample with a delay time of 5 and 10 s were found to be equal, thus 5 s was a sufficient relaxation time for quantitative data to be obtained. A good spectrum was obtained after 12,000 transients giving a resolution of peak position of  $\pm 0.06$  ppm. Temperature was maintained at  $30^\circ\text{C}$  with a Varian temperature controller.

## Results and Discussion

### Gated Decoupling and the $^{13}\text{C}$ FT-NMR Method

The technique of gated decoupling, first described by Freeman, Hill and Kaptein,<sup>14</sup> only became useful with the advent of Fourier transform instrumentation. In this method protons are irradiated just before the

radiofrequency pulse. The decoupler is then switched off after accumulation of the free-induction decay (FID) and continuing through the period of the pulse delay (Figure 8.2).<sup>15</sup> The spectra obtained using this technique have the simplicity of decoupled spectra but the nuclear Overhauser effect (NOE) is eliminated. This occurs because the saturation of proton resonances has a nearly instantaneous effect on scalar spin-spin coupling but the NOE builds up with the time constant of the spin-lattice relaxation time,  $T_1$ .<sup>16</sup> Thus during the accumulation time the NOE does not have time to build up and peak area is quantitative.

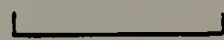
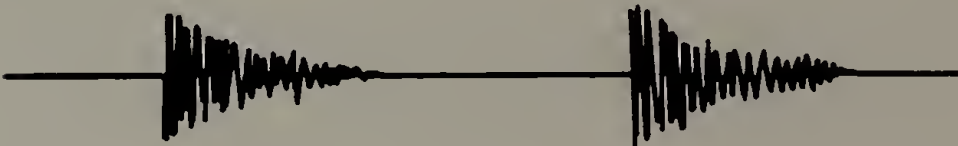
The length of the radiofrequency pulse determines the angle of tipping of the magnetization from the large DC magnetic field. For the pulse angle of  $90^\circ$  used by Gurd et al. the delay time of five times  $T_1$  was required to allow 98% of the nuclei to relax to the equilibrium value (i.e. aligned with the applied magnetic field). It isn't necessary to use a  $90^\circ$  pulse because there will be some component of the magnetization vector in the x-y plane regardless of the angle, although this will decrease with decreasing angle. It is more efficient to pulse more often and obtain more scans of weaker signals.<sup>17</sup> At a  $30^\circ$  pulse the repetition rate of  $1 \times T_1$  is usually sufficient to obtain quantitative data. A pulse delay of 5 s was found adequate to obtain quantitative spectrum. Care was exercised in sample placement in the probe to ensure the small sample volumes (less than 1.5 ml) were entirely contained within the receiver coil.

Figure 8.2. The timing necessary to obtain gated decoupling.

**RF Pulse**

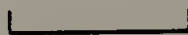


**Data**



**FID accumulation time**

**Decoupler**



**pulse decay**



### HEPES as an Internal pH Standard

The chemical shift of the  $^{13}\text{C}$  resonances in HEPES was characterized as a function of pH (Figure 8.3). The spectra at the pH extremes of 6.46 and 8.3 is given in Figure 8.4. HEPES has been used by Gurd and coworkers<sup>10</sup> as an internal pH standard because a chemical shift for a two-carbon resonance arising from the piperazine ring titrates with an acid limit at 49.17 and 51.32 ppm (using an external carbon disulfide reference). In our experiments the pH sensitive two carbon piperazine ring resonance titrated between 51.90 and 53.6 ppm relative to internal DSS. A second pH sensitive carbon joining the ethylsulfonate with the piperazine ring with a chemical shift between 58.1 and 60.3 ppm was observed. HEPES was observed to accelerate gelation in hydrophobic polyampholytes and caused precipitation of cationic polymers, such as S/4VPQ/NAHD and thus was only used for the  $^{13}\text{C}$  NMR spectra of monomers.

### $^{13}\text{C}$ Carbamates in Model Systems

The  $^{13}\text{C}$  NMR spectrum of AEMA in  $\text{D}_2\text{O}$  with a  $^{13}\text{CO}_2$  atmosphere at a pH of 6.9 is given in Figure 2.1 (HEPES and DSS internal standards). The carbamate resonance is observed slightly downfield from the carbonate-bicarbonate resonance at 166.41 ppm. The carbamate resonance of valine at pH = 8.56 was reported at 164.0 ppm.<sup>11</sup> As was mentioned in Chapter II, AEMA rearranges in basic solution via a five-membered ring intermediate to form the more stable amide tautomer in nearly equal proportion with AEMA monomer. AEMA is not a good choice to model the  $\text{CO}_2$  uptake of valine in hemoglobin because of the rearrangement in neutral solution and thus further investigation to quantitate carbamate

Figure 8.3. The  $^{13}\text{C}$  chemical shifts of HEPES as a function of pH between pH = 6.5 to 8.3. Carbons D and E are particularly sensitive to protonation of the piperazine nitrogen.

Assignment:

- a) 60.55 - 61.20 ppm
- b) 49.85 - 50.00
- c) 53.85 - 54.40
- d) 51.90 - 53.60
- e) 58.1 - 60.30
- f) 54.35 - 54.65

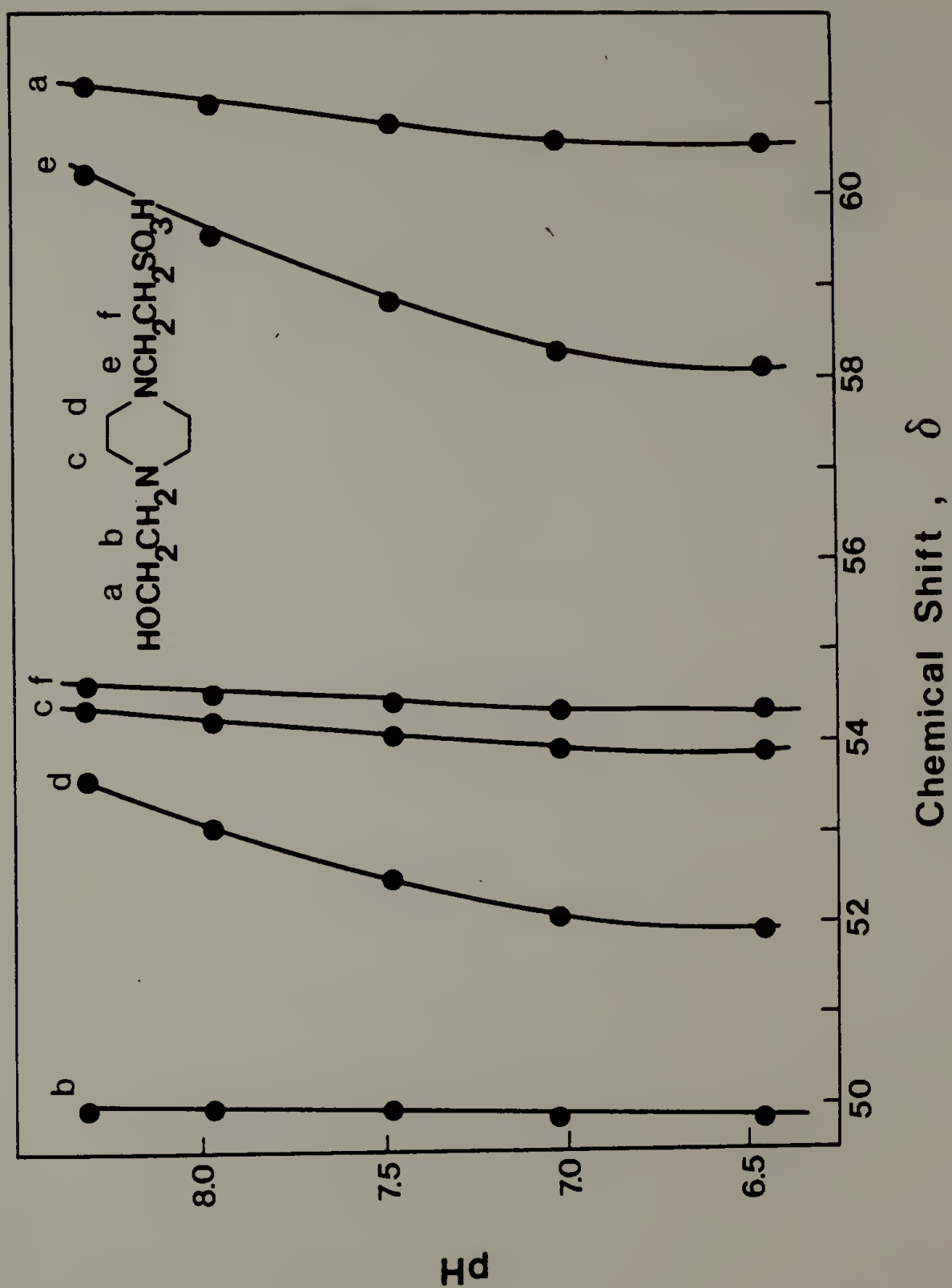
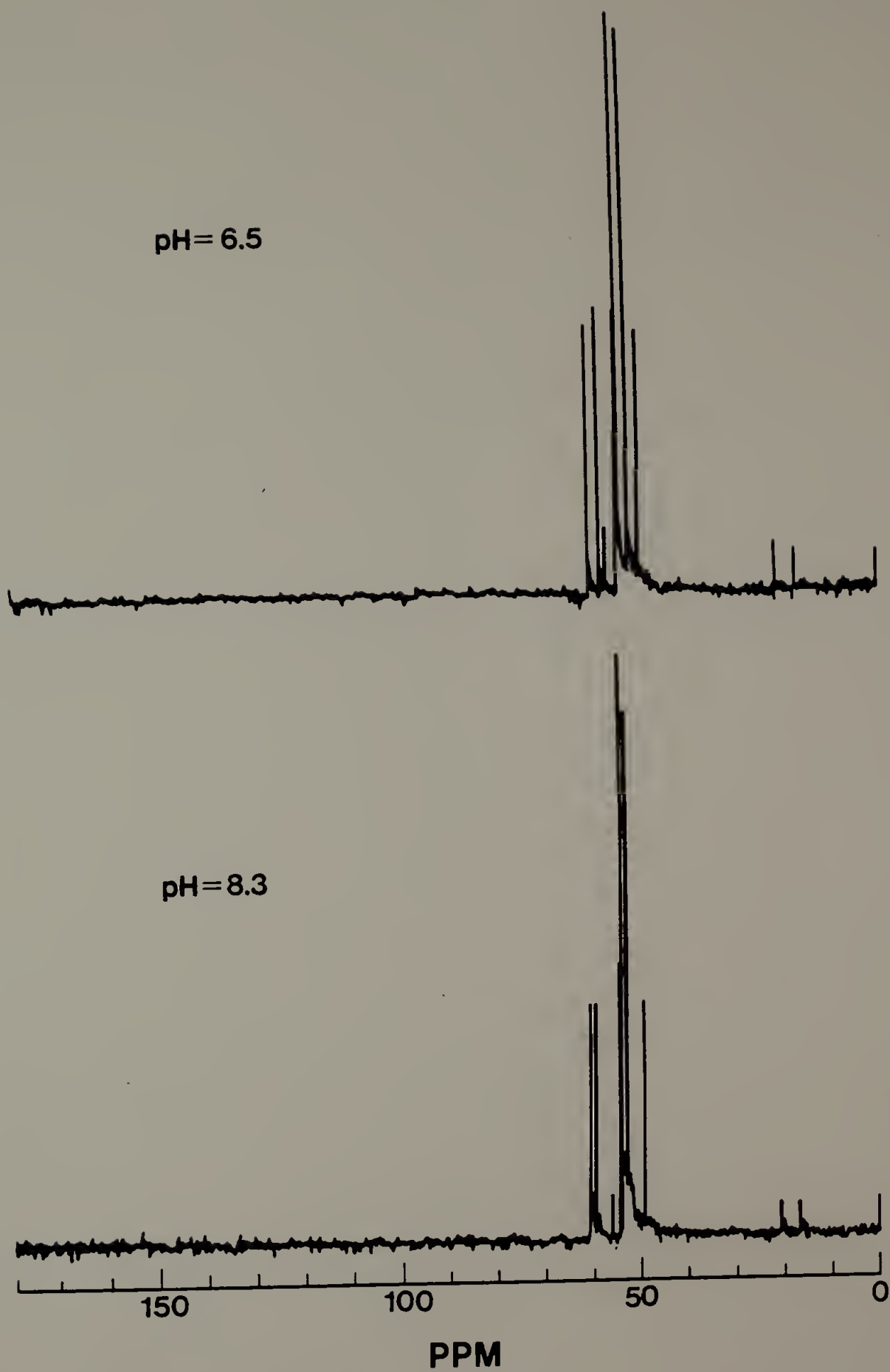


Figure 8.4. Representative  $^{13}\text{C}$ -NMR spectra of HEPES at pH = 6.457 and pH = 8.30. The small peaks at  $\delta = 0.0$ , 17.58, 21.64 and 56.93 ppm are the DSS standard.



formation in AEMA-containing polymers was abandoned.

The  $^{13}\text{C}$  NMR spectra of terpolymers of S/4VPQ/NAHD (61/24/15 and 36/47/17) were taken at a variety of pH values (6.0 – 9.5) and ionic strengths (up to 2.8 M NaOH). Using an external DSS standard the chemical shift of  $\text{CO}_2$  was 127.3 ppm and the resonance for the carbonate-bicarbonate exchange varied as a function of pH between 162.7 ppm and 164.35 ppm (Figure 8.5). Gurd reported these resonances at 124.5 ppm and 160 – 164.4 ppm respectively. The  $^{13}\text{C}$ -carbonyl of the sodium acetate external standard was observed at 184.06 ppm. The literature value for the chemical shift of this carbon, relative to dioxane in  $\text{H}_2\text{O}$  is 181.9 ppm.<sup>18</sup> One can estimate that the sodium acetate standard contains  $1.46 \times 10^{-5}$  moles of  $^{13}\text{C}=\text{O}$ . A 1.5 weight % polymer solution containing 14.5 mol % NAHD would have  $2.28 \times 10^{-5}$  moles of NAHD in a 1.5 ml sample. In a solution enriched 90% by  $^{13}\text{CO}_2$ , the theoretical amount of carbamate which could be observed is  $2.05 \times 10^{-5}$  moles and thus the maximum peak area observed would be 1.4 times larger than that of the external  $^{13}\text{C}=\text{O}$  standard.

None of the aqueous solutions of polymerized NAHD exhibited carbamate formation in the range of physiological pH. In Figure 8.6 the  $^{13}\text{C}$  spectrum between 100 – 200 ppm for a 2.6 weight % solution of 61/24/15 at pH = 7.30 containing  $3 \times 10^{-4}$  moles of NaOH at 760 mm  $^{13}\text{CO}_2$  is given. The sample was not flushed with enriched  $\text{CO}_2$  therefore the isotopic enrichment of  $^{13}\text{CO}_2$  is nearly 90%. The only resonances visible are those of the dissolved  $^{13}\text{CO}_2$ , bicarbonate-carbonate exchange and external sodium acetate. At a pH = 8.7 the concentration of dissolved

Figure 8.5. The chemical shift of the  $^{13}\text{C}$  bicarbonate-carbonate resonance as a function of pH.



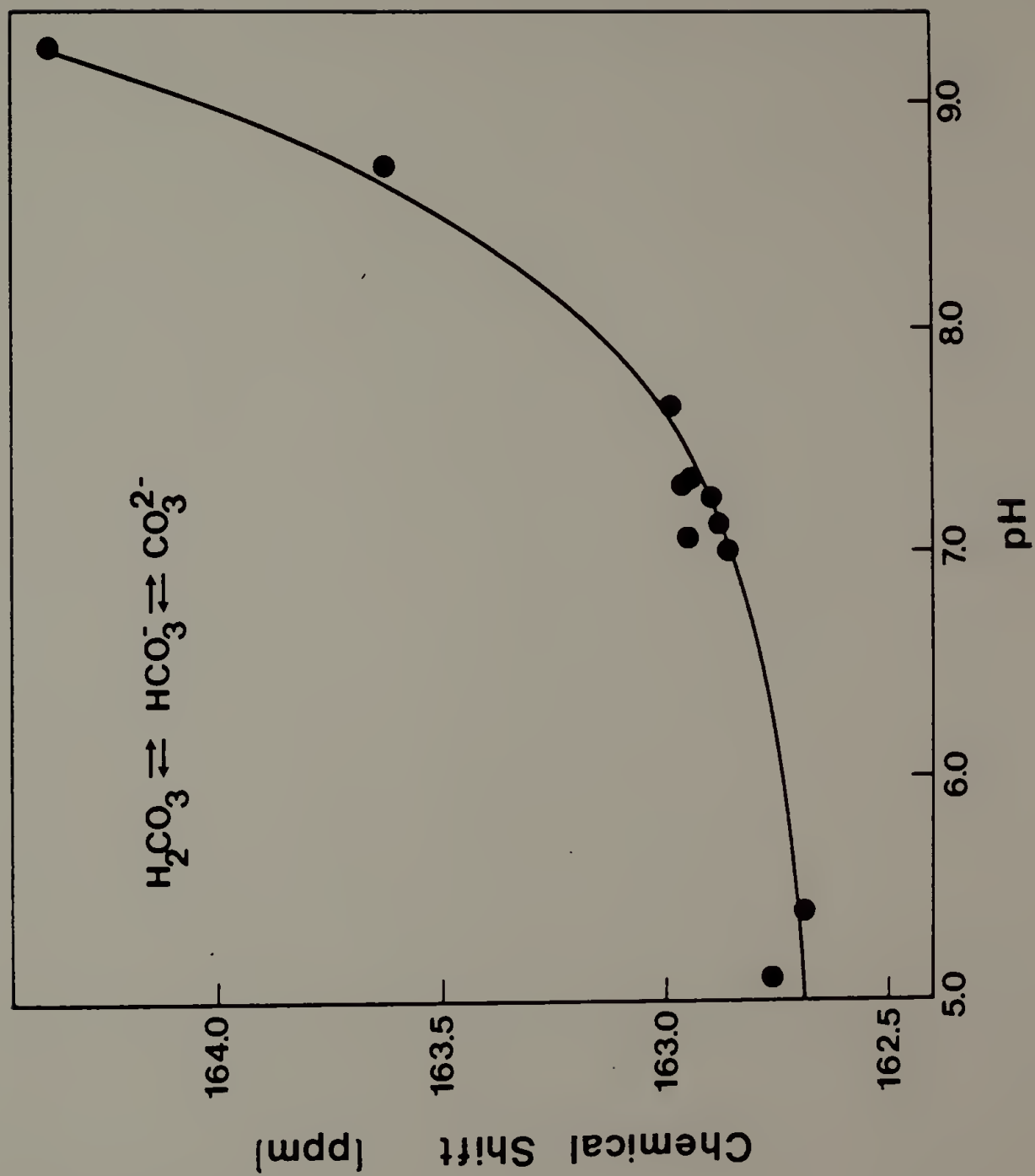
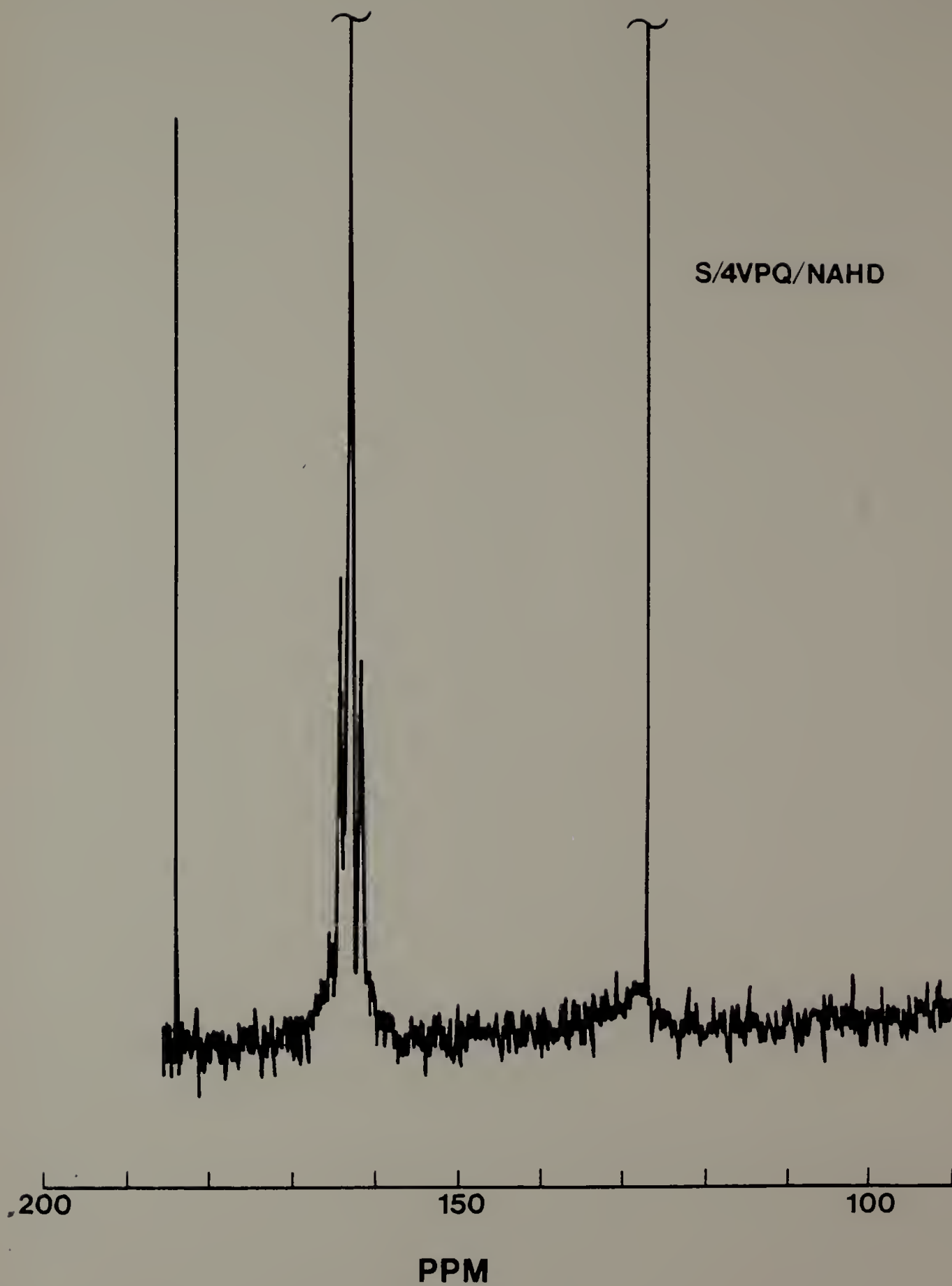


Figure 8.6. The  $^{13}\text{C}$ -NMR of S/4VPQ/NAHD (61/24/15) at pH = 7.3 at 760 mm  $^{13}\text{CO}_2$ . The only resonances visible are those of the dissolved  $^{13}\text{CO}_2$  at 127.3 ppm, the bicarbonate-carbonate exchange at 162.95 ppm and the external standard  $\text{CH}_3^{13}\text{CO}_2\text{Na}$  at 184.06 ppm.



CO<sub>2</sub> is negligible as was observed by the <sup>13</sup>C NMR spectrum. At higher pH (greater than 9.5) the yellow color of the free amine is evidence that the amine is unprotonated however the concentration of dissolved CO<sub>2</sub> is quite low.

### Conclusions

Polymers containing AEMA and NAHD do not effectively model the capacity of hemoglobin to react with dissolved CO<sub>2</sub> to form carbamates. The pK<sub>a</sub> of AEMA is in the proper range to carry CO<sub>2</sub> as a carbamate but the rearrangement of this monomer hinders its usefulness. One of the premises upon which NAHD was selected to carry CO<sub>2</sub> was that the hydrophobic nature of the amine would cause it to 'prefer' to be solvated in the hydrophobic domain of the polyelectrolyte thus lowering the pK<sub>a</sub> of the amine group. It seems that the hydrophobic domains in these random flexible vinyl terpolymers are not sufficiently static to lower the pK<sub>a</sub> of NAHD. Fluctuations in the polymer conformation allow the amines to be protonated at physiological pH and have the pK<sub>a</sub> one would expect of them in a purely aqueous system.

To quantitate carbamate formation in hydrophobic polyelectrolytes one must have a constant ionic strength to avoid the effect of added electrolytes on the polymer conformation. A buffered system is highly desirable to avoid large fluctuations in pH under a CO<sub>2</sub> atmosphere. Also, high pressures of <sup>13</sup>CO<sub>2</sub> tend to swamp out the sodium acetate <sup>13</sup>C standard (as well as the signal for the carbamate) and thus lower the sensitivity of this method. Careful, refined experimental techniques

are required to use  $^{13}\text{C}$  FT-NMR to quantitatively define the reaction of  $\text{CO}_2$  with model amine-containing polymers to form carbamates.

### References

1. Kilmartin, J.V.; Rossi-Bernardi, L. Biochem. J., (1971), 124, 31.
2. Gurd, F.R.N.; Matthew, J.B.; Wittebort, R.J.; Morrow, J.S.  
Biophysics and Physiology of CO<sub>2</sub>, Bauer, C.; Gros, G.; Bartels, H.  
(eds.), Springer-Verlag, New York, (1980), p. 89.
3. Roughton, F.J.W. Handbook of Physiology, Section 3: Respiration,  
Fenn, W.O.; Rahn, W. (eds.), American Physiological Society,  
Washington, Vol. 1, p. 767.
4. Roughton, F.J.W.; Rossi-Bernardi, L. Proc. Roy. Soc. B., (1966),  
164, 381.
5. Perrella, M.; Rossi-Bernardi, L.; Roughton, F.J.W. Oxygen Affinity  
of Hemoglobin and Red Cell Acid-Base Status, Alfred Benzon  
Symposium IV, Rørth, M.; Astrup, P. (eds.), Academic Press, New  
York, (1972), pp. 178-204.
6. Perrella, M.; Rossi-Bernardi, L. in Methods in Enzymology, Vol. 76  
Hemoglobins, Antonini, E.; Rossi-Bernardi, K.; Chiancone, E.  
(eds.), Academic Press, New York, 1981, pp. 487-496.
7. Arnone, A. Nature, (1974), 247, 143.
8. Bauer, C.; Baumann, R.; Engels, U.; Pacyna, B. J. Biol. Chem.,  
(1975), 250, 2173.
9. Matthew, J.B.; Morrow, J.S.; Wittebort, R.J.; Gurd, F.R.N. J.  
Biol. Chem., (1977), 252, 2234.
10. Morrow, J.S.; Matthew, J.B.; Gurd, F.R.N. in Ref. 6, pp. 496-511.
11. Morrow, J.S.; Keim, P.; Gurd, F.R.N. J. Biol. Chem., (1974),  
249(23), 7484.

12. Gillis, J. Senior Honors Thesis, University of Massachusetts, 1980.
13. Good, N.E.; Winget, G.D.; Winter, W.; Connolly, T.N.; Izawa, S.; Singh, R.M.M. Biochem., (1966), 5, 467.
14. Freeman, R.; Hill, H.D.; Kaptein, R. J. Magn. Resonance, (1972), 7, 327.
15. For a good review of FT-NMR and gated decoupling see: Cooper, J.T. Spectroscopic Techniques for Organic Chemists, Wiley-Interscience, New York (1980) pp. 136-200.
16. Opella, S.J.; Nelson, D.J.; Jardetzky, O. J. Chem. Phys., (1976), 64(16), 2533.
17. Christiansen, K.A.; Grant, D.M.; Shulman, E.M.; Walling, C. J. Phys. Chem., (1974), 78, 1971.
18. Sadtler Standard Spectra:  $^{13}\text{C}$ -NMR, #976C, 1976.



## CHAPTER IX

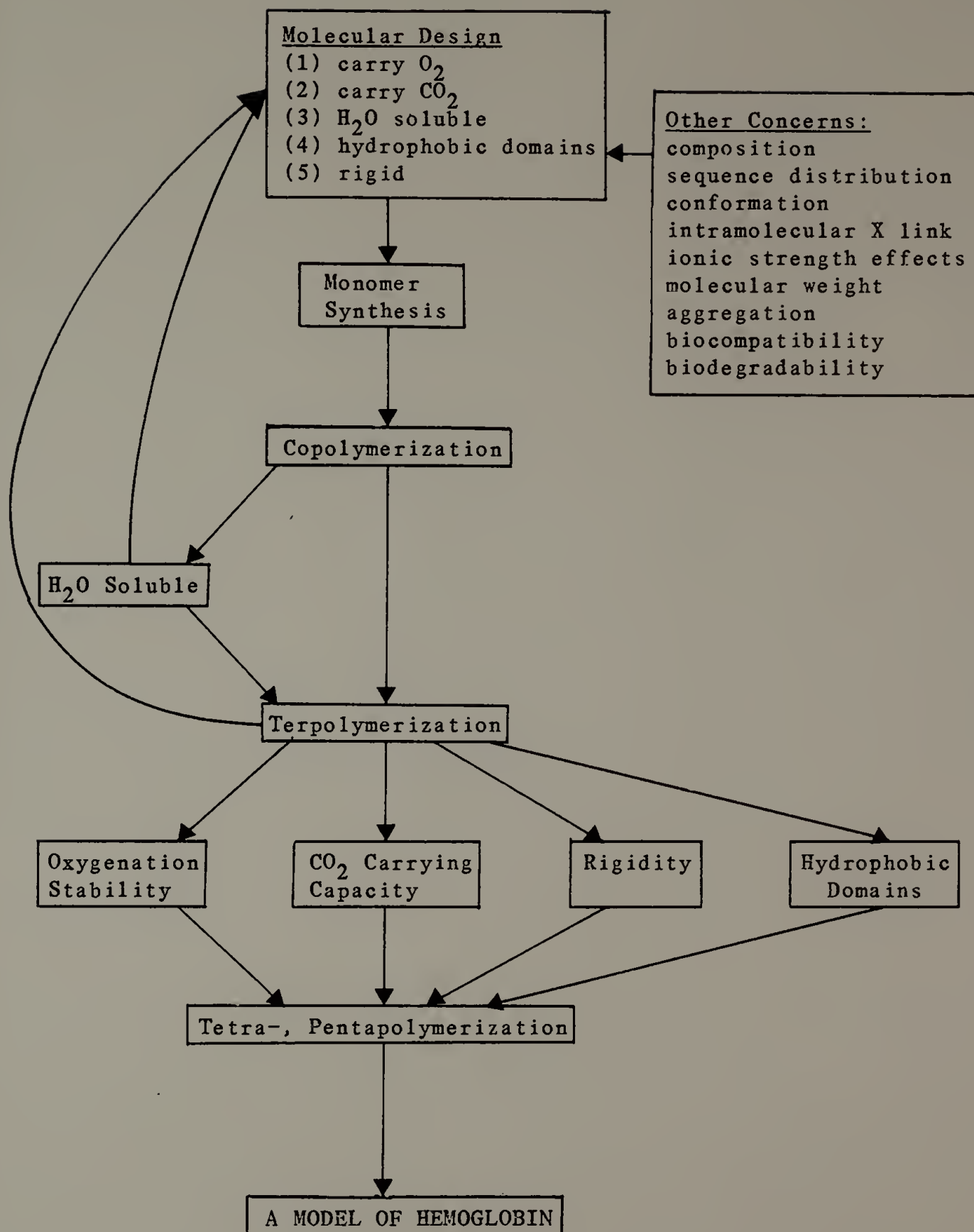
### SUGGESTIONS FOR FUTURE WORK

The potential application of polymers which mimic the functions of hemoglobin or other biological molecules (e.g. enzymes, antibodies) ensures that scientific investigation in the area of biomimetic chemistry will intensify in the future. The combination of imaginative organic synthesis with meticulous characterization of physical properties is necessary for the success of work of this nature.

A flow chart showing the progression of work towards the synthesis of a model of hemoglobin is given in Figure 9.1. One must carefully consider the ramifications of each single idea throughout the scheme. Each functional monomer must exhibit nearly random behavior in copolymerization. Interaction of functional units, as was observed for the novel hydrophobic polyampholytes, must be avoided to prevent aggregation of the polymer or gelation in solution.

One of the fundamental principles upon which this dissertation was based was that incorporation of a heme unit in the polymer chain would prevent heme-heme contact and dimerization to the  $\mu$ -oxo dimer. Also, the polymer would provide a hydrophobic environment for the heme to prevent autooxidation. By studying the kinetics of the oxidation reaction it appears that polymer bound hemes in DMF/H<sub>2</sub>O (9/1) at -10°C oxidize via dimerization at one-half the rate of non-bound hemes. The polymer provides some steric hindrance but not enough to give the heme good stability. Future heme models must be more sterically hindered. A

Figure 9.1. Flow chart for the synthesis of a polymer which can mimic the functions of hemoglobin.



picket-fence heme where methacrylamido groups replace the pivalamido groups would be polymerizable and make heme reactivity more nearly equal that of the other monomers in the system. One could imagine that four vinyl groups held in close proximity, as in ferrous meso-tetra( $\alpha,\alpha,\alpha,\alpha$ -o-methacrylamidophenyl)porphyrin, might have some preference for homopropagation over heteropropagation thus increasing the steric hindrance even more. The synthesis of the  $\alpha,\alpha,\alpha,\alpha$  derivative will be time consuming and this model heme does not have a covalently bound axial base. Therefore, an imidazole type monomer must be incorporated at between 5 - 10 mol % in the model polymer.<sup>2</sup> Other researchers have terpolymerized 1-vinylimidazole or 1-vinyl-2-methylimidazole with styrene and a heme model compound for this purpose. These imidazole monomers are not resonance stabilized and thus are significantly less reactive than heme or styrene. A more resonance stabilized monomer could be synthesized by simply reacting methacrylyl chloride with 3-(1-imidazolyl)propylamine to yield N-methacrylyl-3-(1-imidazolylpropyl)-amide. Incorporation of both the picket-fence and imidazole derivative in the polymer chain will maximize steric interactions which will help decrease the rate of dimerization. Steric hindrance of on the  $\alpha$  side of the porphyrin ring would prevent imidazole binding and give a 5-coordinate heme. The picket-fence heme would be significantly more hydrophobic than HMEMA which would increase solubilization in hydrophobic domains and slow the rate of autooxidation. In future work, the role of the polymer chain is reduced to that of a carrier for the functional units.

Intramolecular crosslinking of the polymer to give rigidity is not a particularly profitable avenue of research. A random polymer with solution properties of a hydrophobic polyelectrolyte is still a relatively flexible molecule. A significant amount of intrachain crosslinking would be required to prevent fluctuations in conformation. The azide functional unit is a non-selective crosslinking agent. Thus as the concentration of this photoreactive moiety is increased the likelihood of interchain reaction also increases. The characterization of the efficiency of the crosslinking reaction and the extent of intramolecular crosslinking (versus intermolecular crosslinking) is quite challenging. One must observe a contraction of the polymer in dilute solution via light scattering or intrinsic viscosity. Ultra-violet irradiation of heme-containing polymers for the intramolecular crosslinking reaction resulted in heme degradation and oxidative instability.

Hydrophobic domains are important for the protection of hemes from autooxidation. Solubilization experiments using water insoluble substances provides a means of visualizing hydrophobic domains in hydrophobic polyelectrolytes. Future solubilization experiments should utilize heme model compounds as the insoluble dye to make extrapolation of results to heme polymers more feasible. Systems studied should include a range of copolymer compositions (hydrophobe/hydrophile) and ionic strengths. The results should be used to tailor the composition of the copolymer at a desired ionic strength. It is imperative that the model polymer be able to tolerate added electrolytes without gelation or

precipitation. Buffer compatibility for control of pH and ionic strength in model polymer systems would facilitate experiments such as oxygenation studies or carbamate formation as a function of pH. An examination of different hydrophobic and hydrophilic monomers would be quite useful. The hydrophobicity of polymers containing VBCQ can be varied by incorporating long chain alkyl groups into the quaternary ammonium moiety.<sup>3</sup> Investigation of nonionic water solubilizing groups, such as N-vinylpyrrolidone, might provide new polymers which can mimic the functions of hemoglobin.

Model polymers in which amine monomers were incorporated to carry CO<sub>2</sub> in the form of carbamates at physiological pH were not useful because the pK<sub>a</sub> of the amine group was not sufficiently lowered by solubilization in the hydrophobic domains of the polymer. In future work model amines should be selected which have a pK<sub>a</sub>  $\approx$  7.4 in aqueous solution. Strong electron withdrawing groups or conjugation with an aromatic ring lowers the pK<sub>a</sub> of an amine. One must be cautious, however, since decreasing the basicity will also decrease the reactivity of the amine with dissolved CO<sub>2</sub>. Tyrosineamide has a pK<sub>a</sub> = 7.33,<sup>4</sup> thus derivatives of this readily available material are promising monomer candidates. If the free amine of tyrosineamide was blocked using a amine protecting agent like BOC-ON, the N-t-butylcarboxytyrosineamide could be reacted with methacrylyl chloride to yield an ester with suitable properties.

Our perspective on the role of the polymer in the model of hemoglobin has changed from that where the polymer chain provides both



hydrophobic domains and steric hindrance to a more passive role as a water soluble carrier of the functional units. Free radical polymerization via a vinyl group has several advantages: the reactivity of that vinyl group can be varied by varying the monomer selection, a wide variety of novel monomers can be imagined and the experimental techniques are quite simple. Other interesting systems could be used. Emulsion polymerization techniques would yield a novel model of hemoglobin. The core-shell morphology of these colloidal systems would be quite amenable to the protection of a heme group in a hydrophobic environment. Block copolymer model systems have the potential advantage of water solubility with clearly defined hydrophobic domains. Polymerizable vesicles offer a means of encapsulating hemes or heme polymers to enhance oxidative stability.<sup>5</sup> Biocompatibility of these model systems, for use as artificial blood, is a complication which is an important consideration in future investigations.

The synthesis of a polymer which can mimic the functions of hemoglobin is a complex and challenging problem. It is essential to approach biomimetic chemistry with flexibility: to be open to new ideas and to eliminate rigidly preconceived notions. The structure of hemoglobin has evolved over hundreds of millions of years. The scientist who attempts to model the structure and function of this elegant protein does so with admiration for its complexity and a sense of humility for the knowledge of humankind.



### References

1. Dolphin, D.; McKenna, C.; Murakami, Y.; Tabushi, I. (eds.)  
Biomimetic Chemistry: Adv. Chem. Sci., 191, American Chemical Society, Washington, D.C. 1980.
2. This estimate is based on work by: Nishide, H.; Shinohara, K.; Tsuchida, E. J. Polym. Sci. Polym. Chem. Ed., (1981), 19, 1109.
3. Wessling, R.A.; Pickelman, D.M. J. Dispersion Sci. Tech., (1981), 2, 281.
4. Weast, R.C. (ed.) Handbook of Chemistry and Physics, 56th Edition, CRC Press, Cleveland, (1975), p. D-149.
5. Gros, L.; Ringsdorf, H.; Schupp, H. Angew. Chem. Int. Ed. Engl., (1981), 20, 305.

APPENDIX A. SPECTRA OF ORGANIC COMPOUNDS

Figure A.1. Proton NMR of methyl p-(2-bromoethyl)benzenesulfonate (CDCl<sub>3</sub>/TMS).

Assignment:

- a) 3.60 ppm
- b) 3.15 ppm
- c) 7.52 ppm
- d) 7.90 ppm
- e) 3.71 ppm

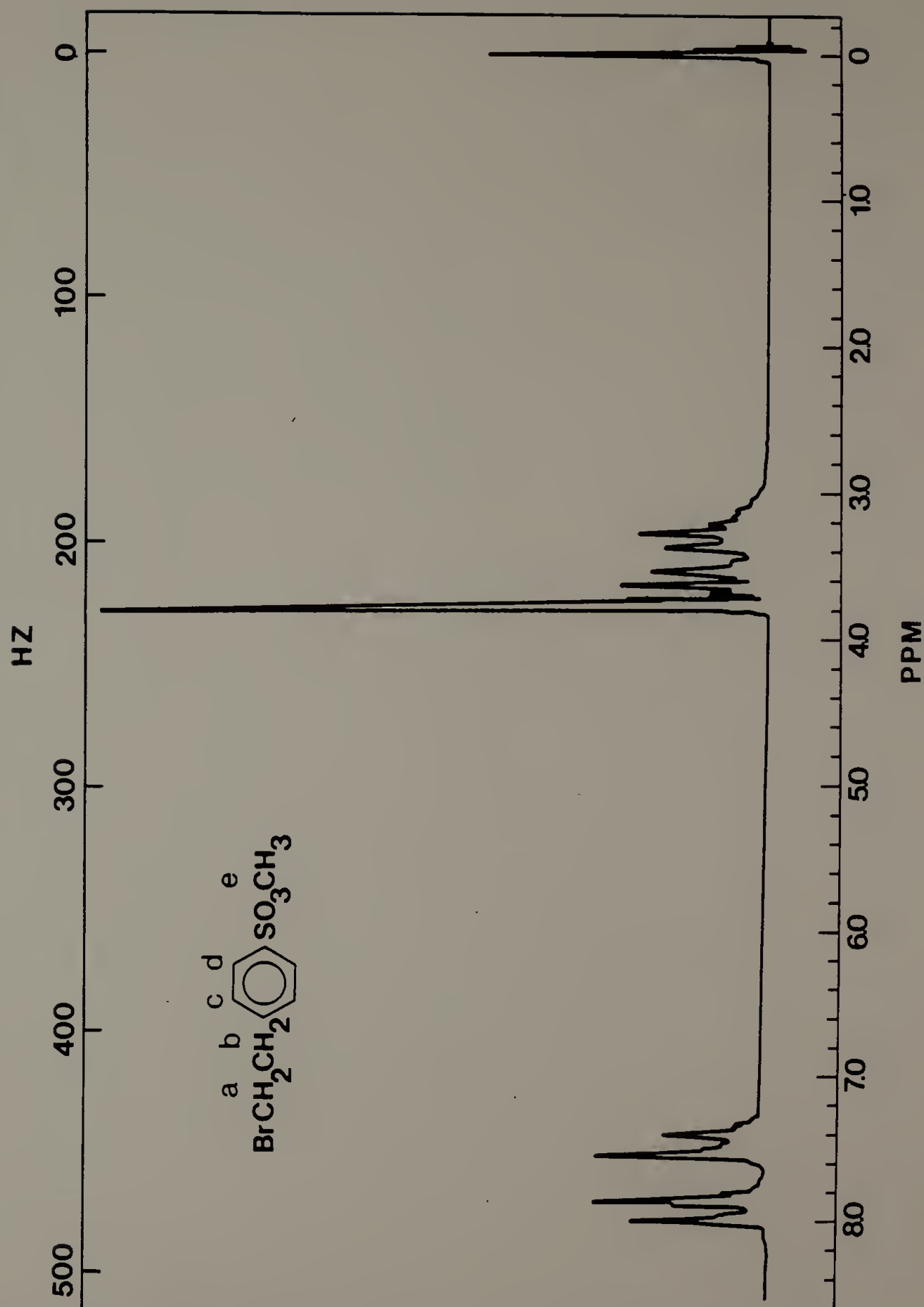


Figure A.2. Proton NMR of methyl p-vinylbenzenesulfonate  
(CDCl<sub>3</sub>/TMS).

Assignment:

- a) 5.37, 5.81 ppm
- b) 6.70 ppm
- c) 7.50 ppm
- d) 7.85 ppm
- e) 3.71 ppm

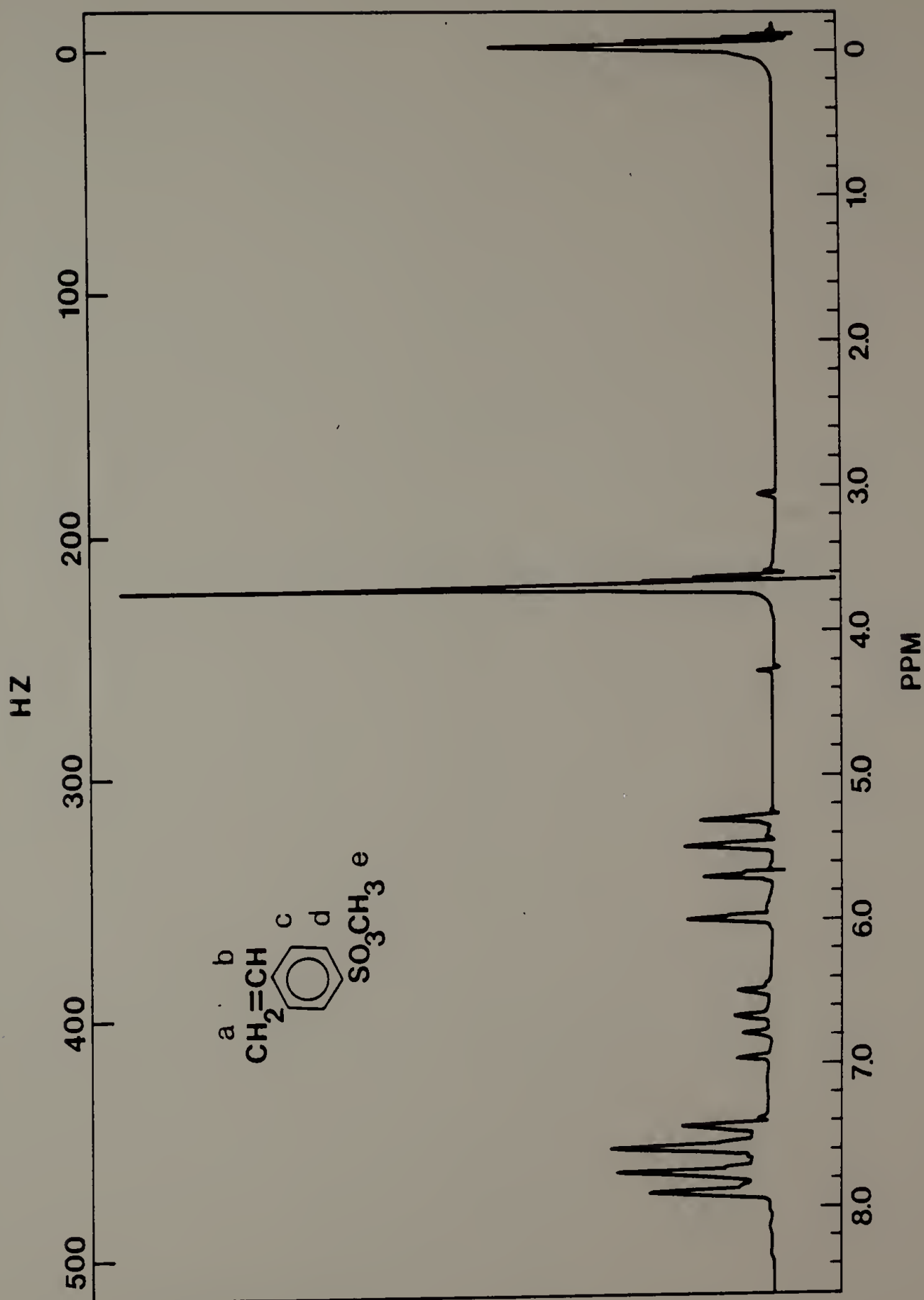


Figure A.3. Infrared spectrum of methyl p-vinyl-  
benzenesulfonate (neat).



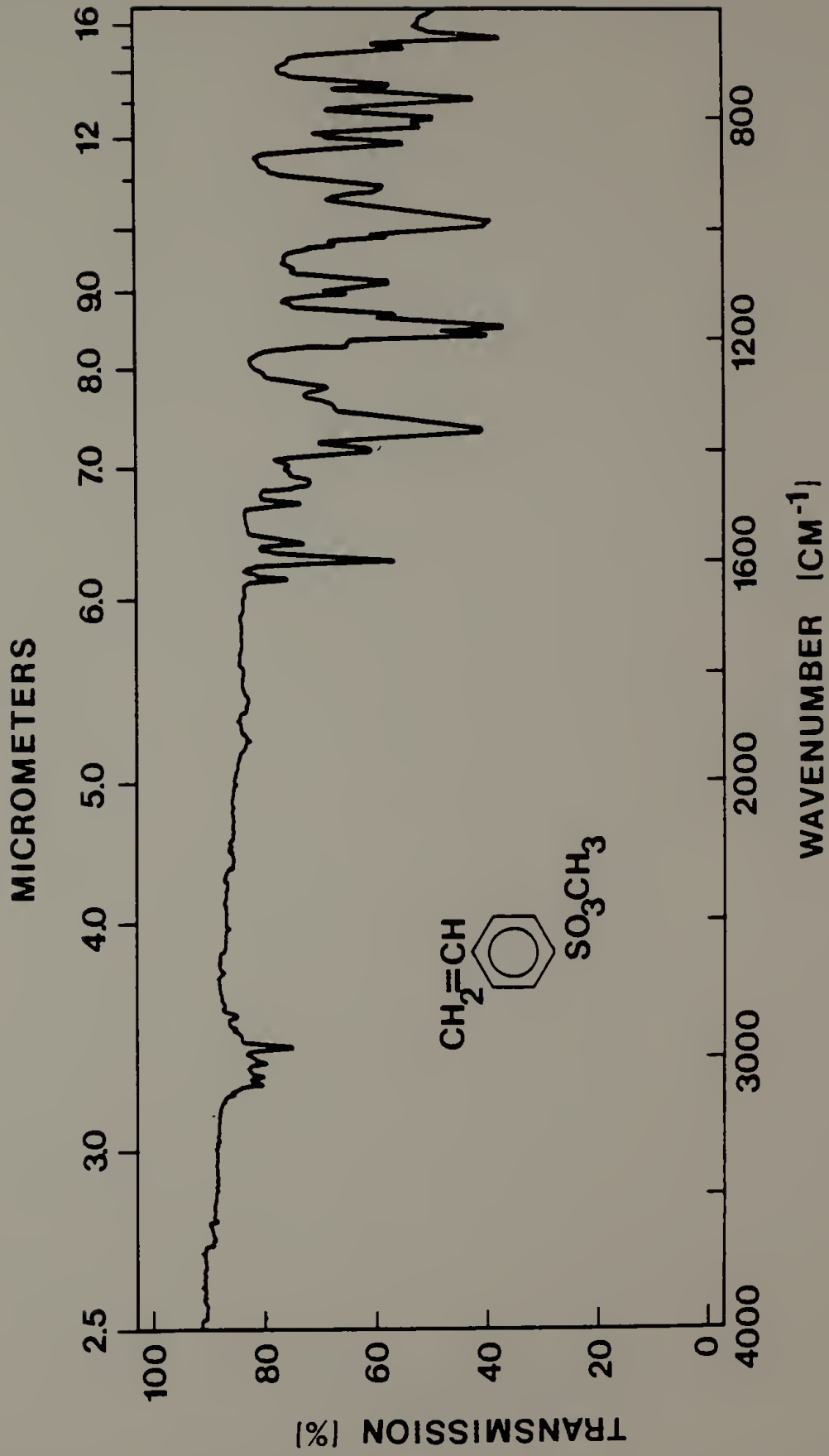


Figure A.4. Carbon-13 NMR of methyl p-vinylbenzenesulfonate  
(CDCl<sub>3</sub>/TMS).

Assignment:

- a) 118.19 ppm
- b) 135.15 ppm
- c) 133.86 ppm
- d) 126.91 ppm
- e) 128.39 ppm
- f) 143.07 ppm
- g) 56.42 ppm

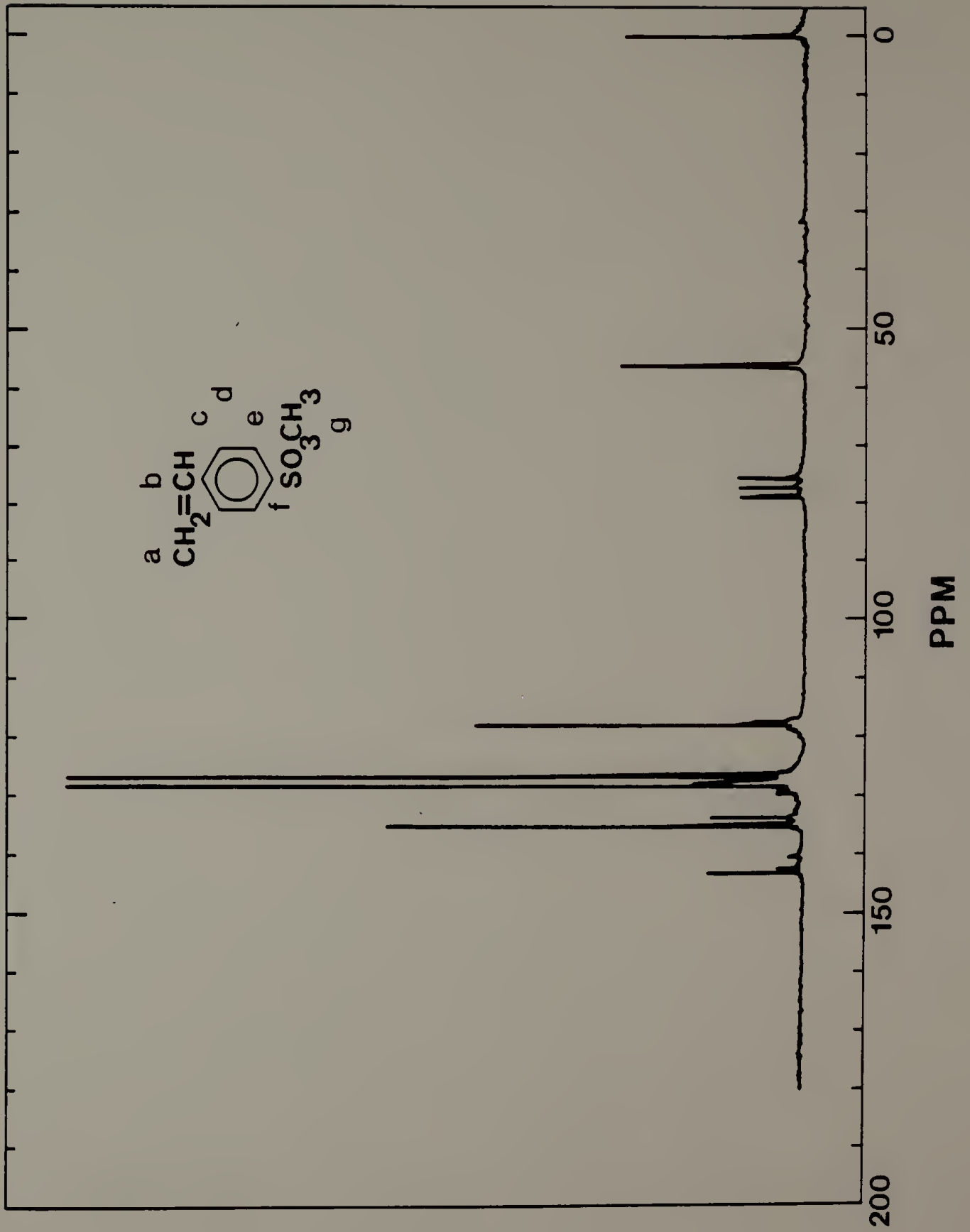


Figure A.5. Infrared spectrum of ferric protoporphyrin IX dimethylester (KBr).

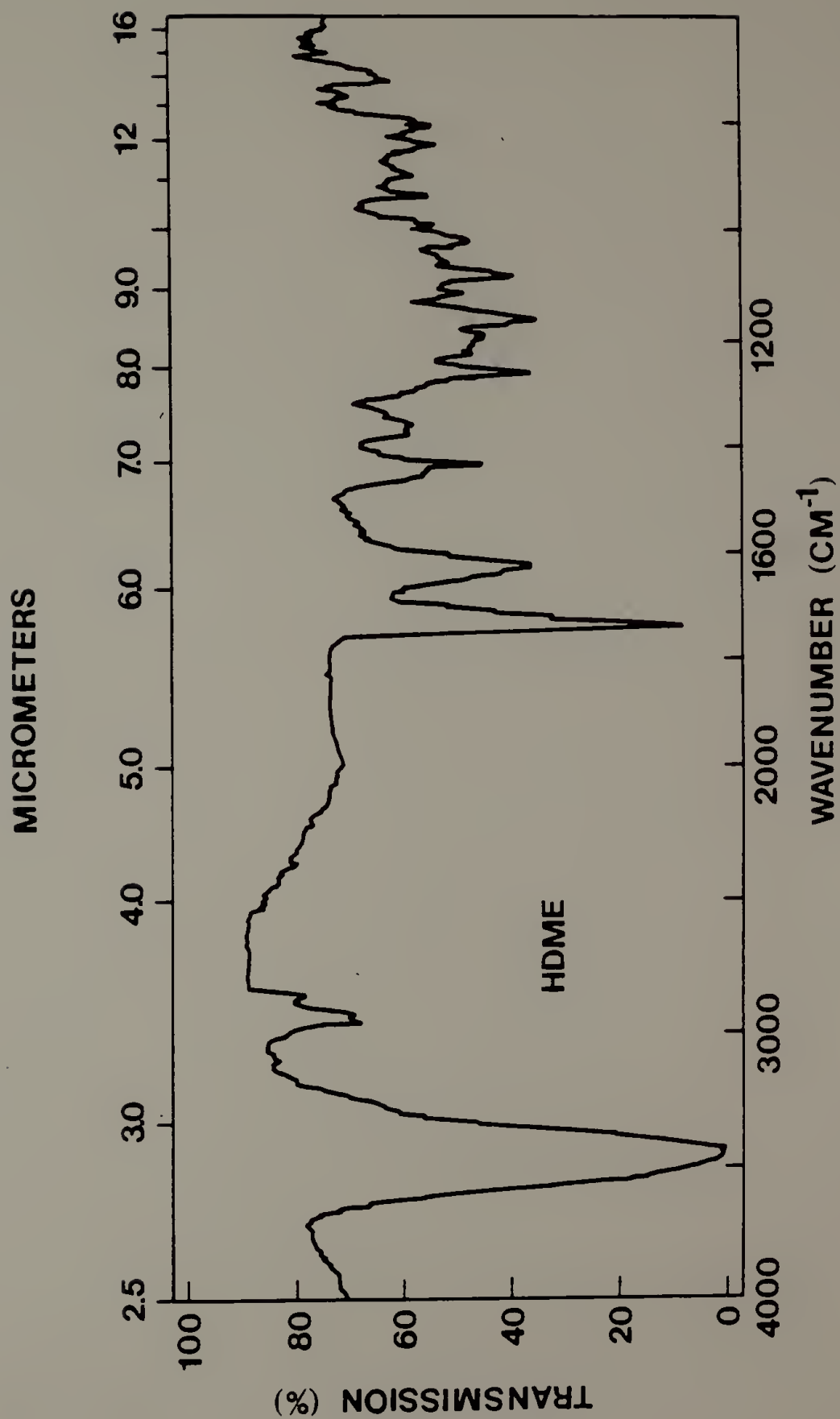


Figure A.6. Proton NMR of 3-(1-imidazolyl)propylamine  
(CDCl<sub>3</sub>/TMS).

Assignment:

- a) 2.60 ppm
- b) 1.85 ppm
- c) 4.00 ppm
- d) 7.03 ppm
- e) 6.95 ppm
- f) 7.49 ppm

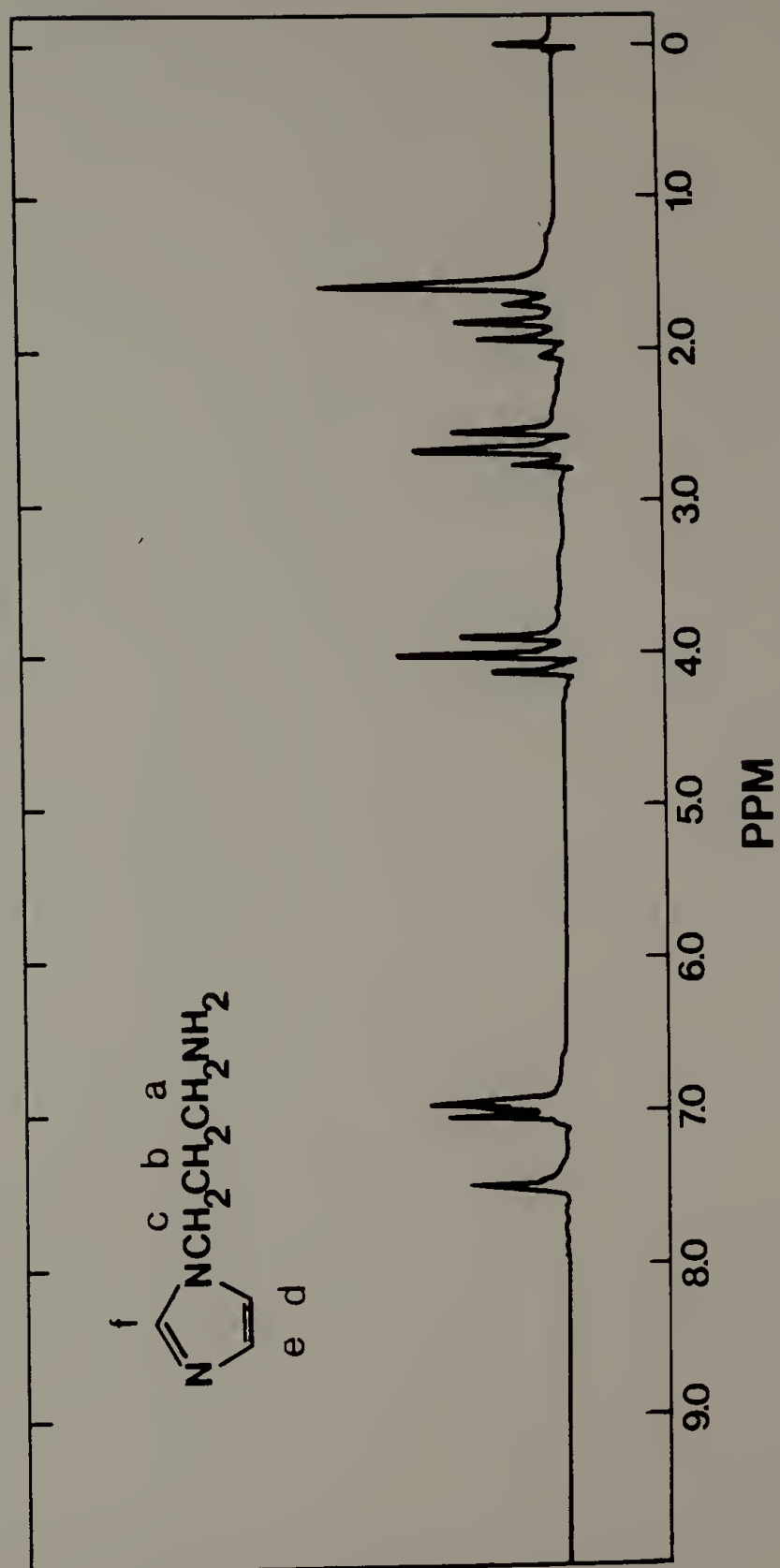




Figure A.7. Infrared spectrum of 3-(1-imidazolyl)propylamine  
(neat).

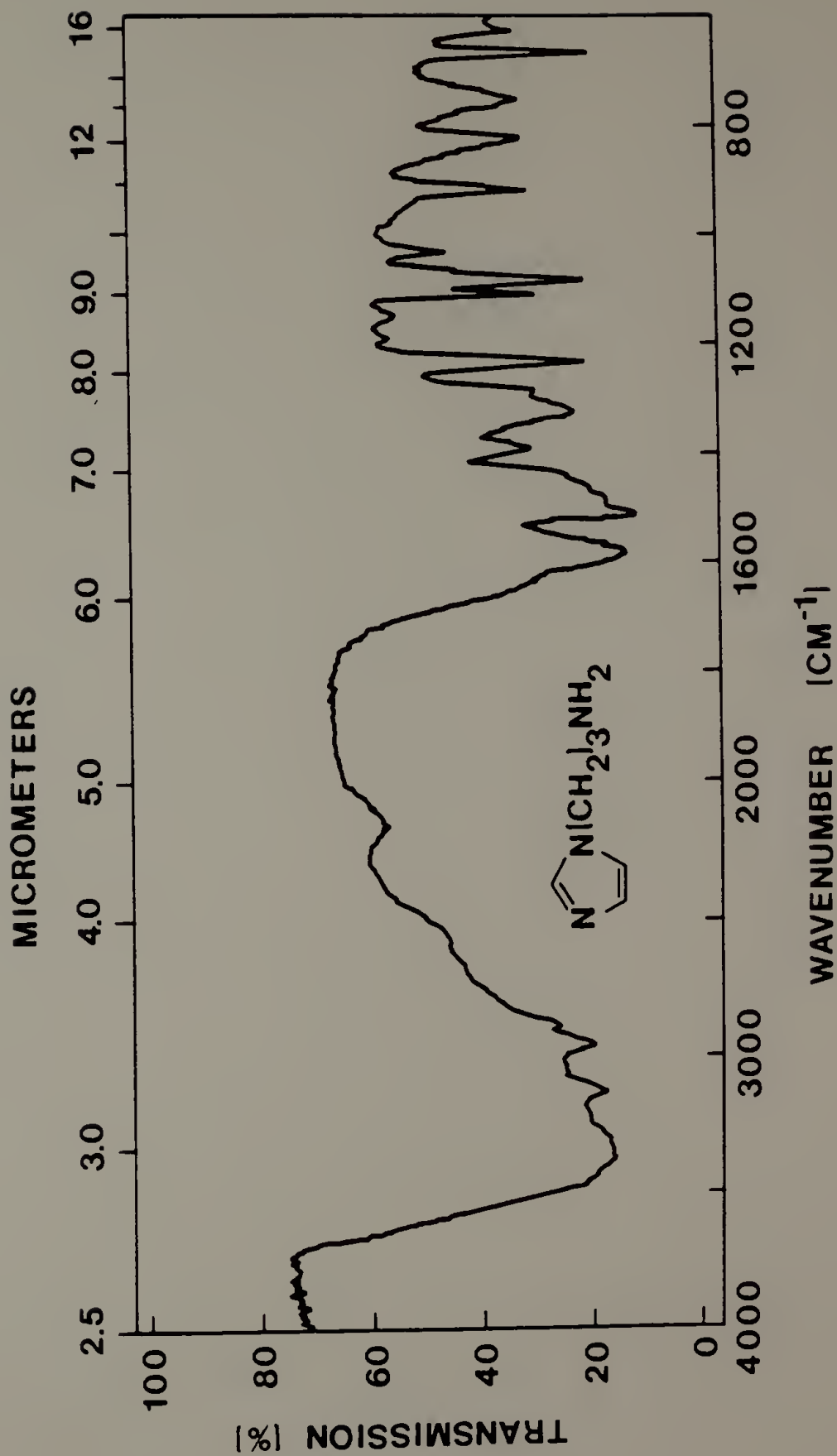


Figure A.8. Infrared spectrum of ferric protoporphyrin IX di-3-(1-imidazolyl)propylamide (KBr).

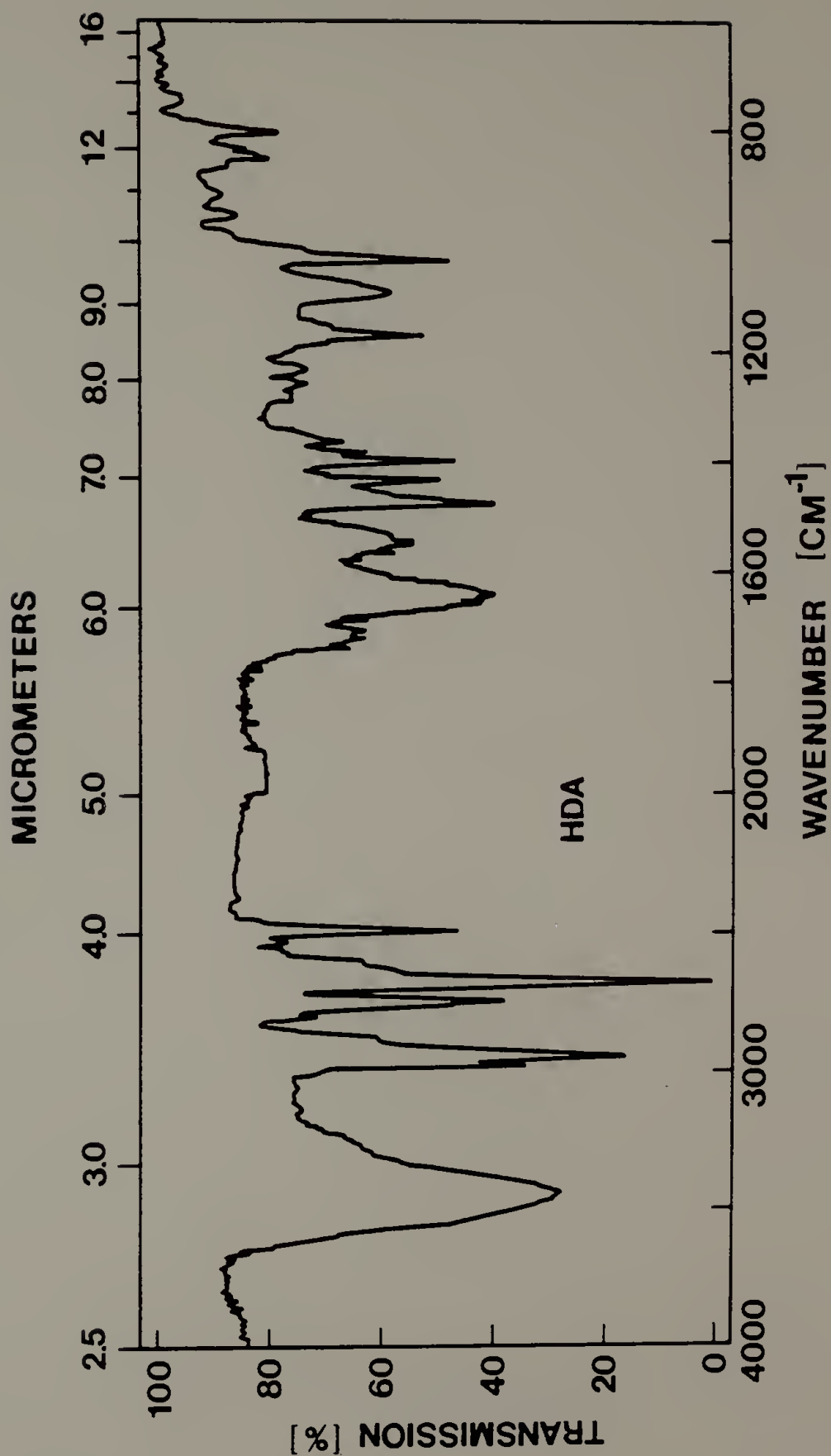


Figure A.9. Infrared spectrum of ferric protoporphyrin IX mono-3-(1-imidazolyl)propylamide monomethylester (KBr).

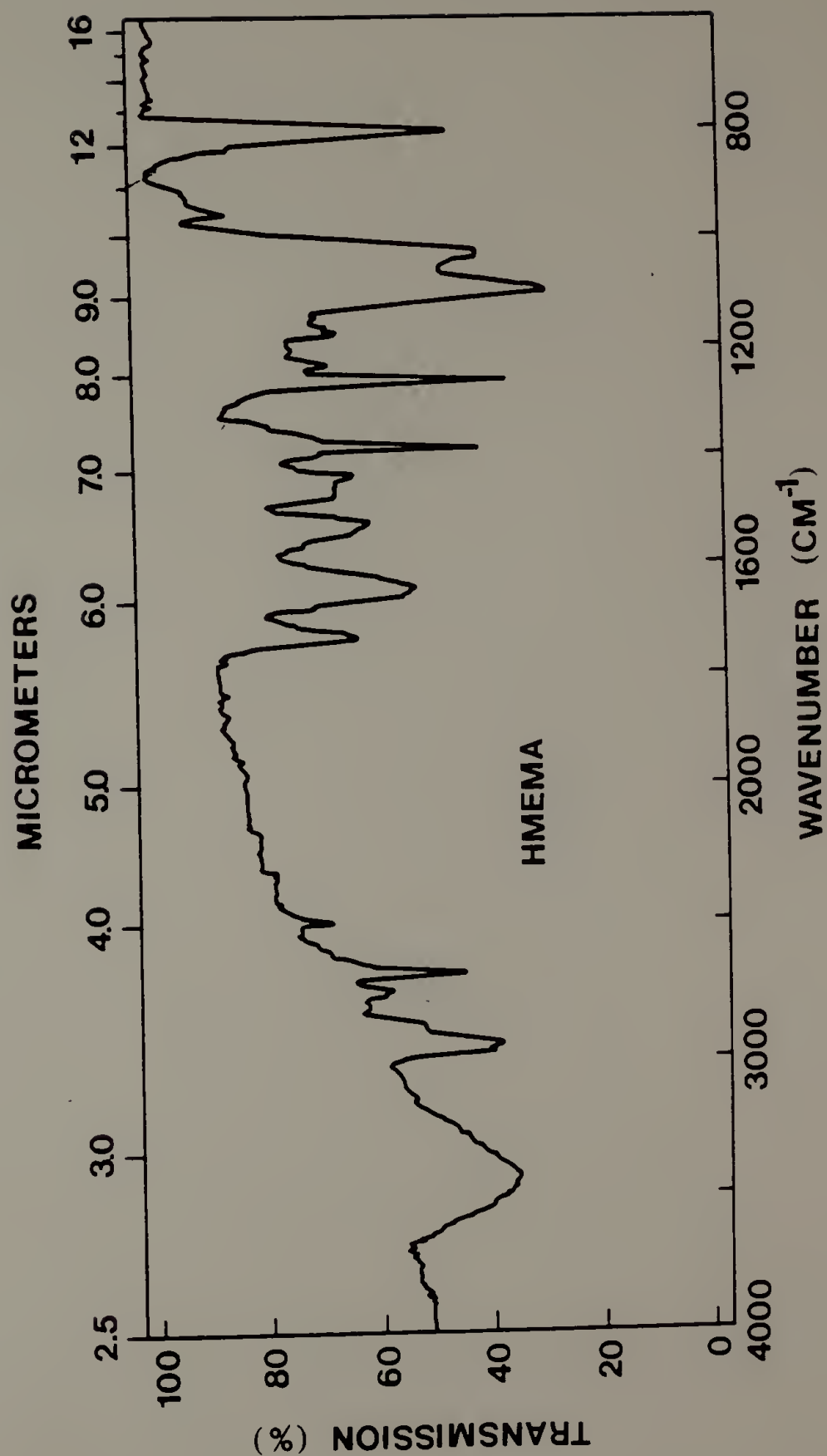


Figure A.10. Infrared spectrum of N-tert-butyloxycarbonyl-2-aminoethyl methacrylate (KBr).



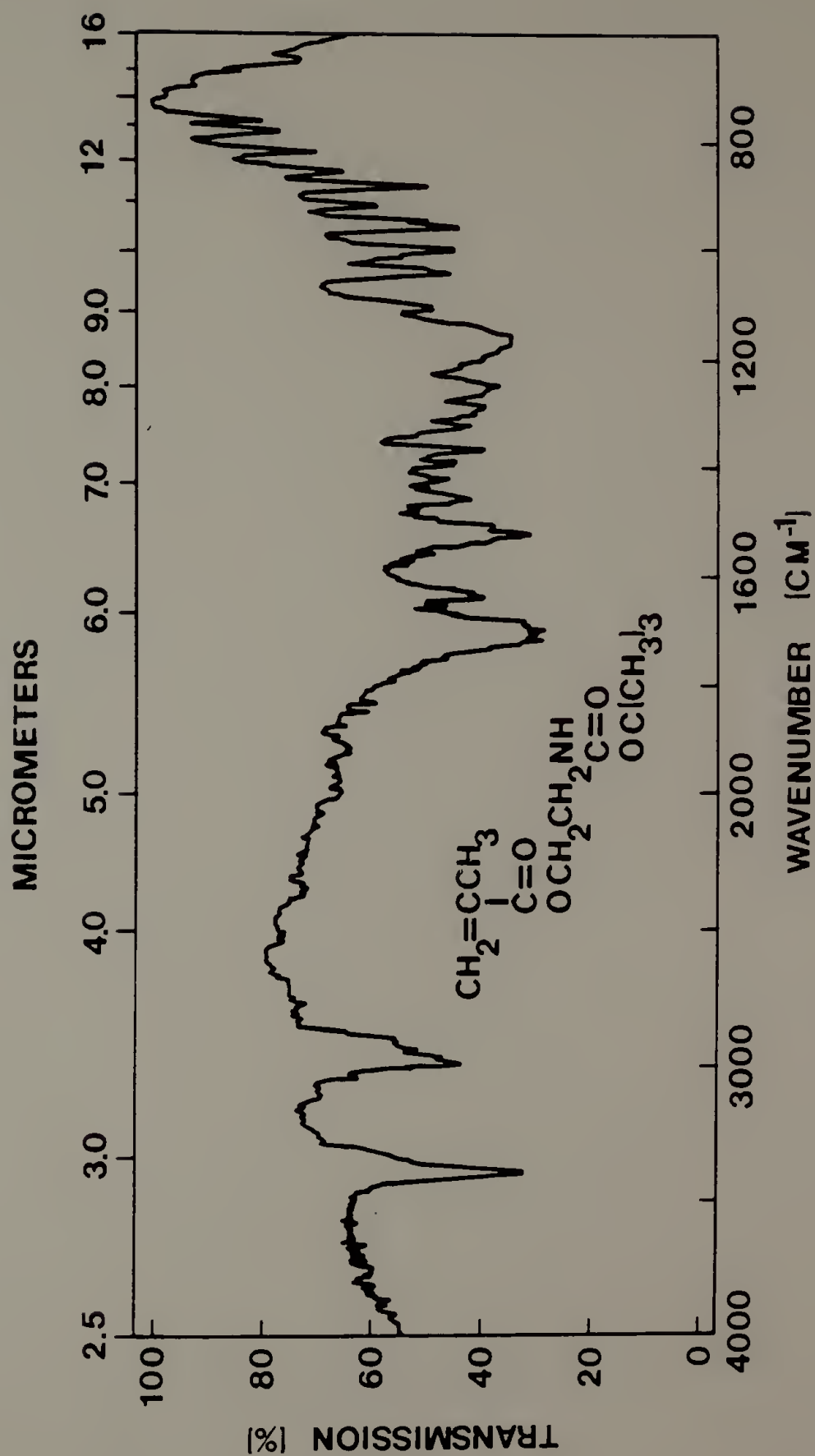


Figure A.11. Proton NMR of N-tert-butyloxycarbonyl-2-aminoethyl methacrylate ( $\text{CDCl}_3/\text{TMS}$ ).

Assignment:

- a) 5.60, 6.05 ppm
- b) 1.98 ppm
- c) 4.25 ppm
- d) 3.48 ppm
- e) 4.83 ppm
- f) 1.51 ppm

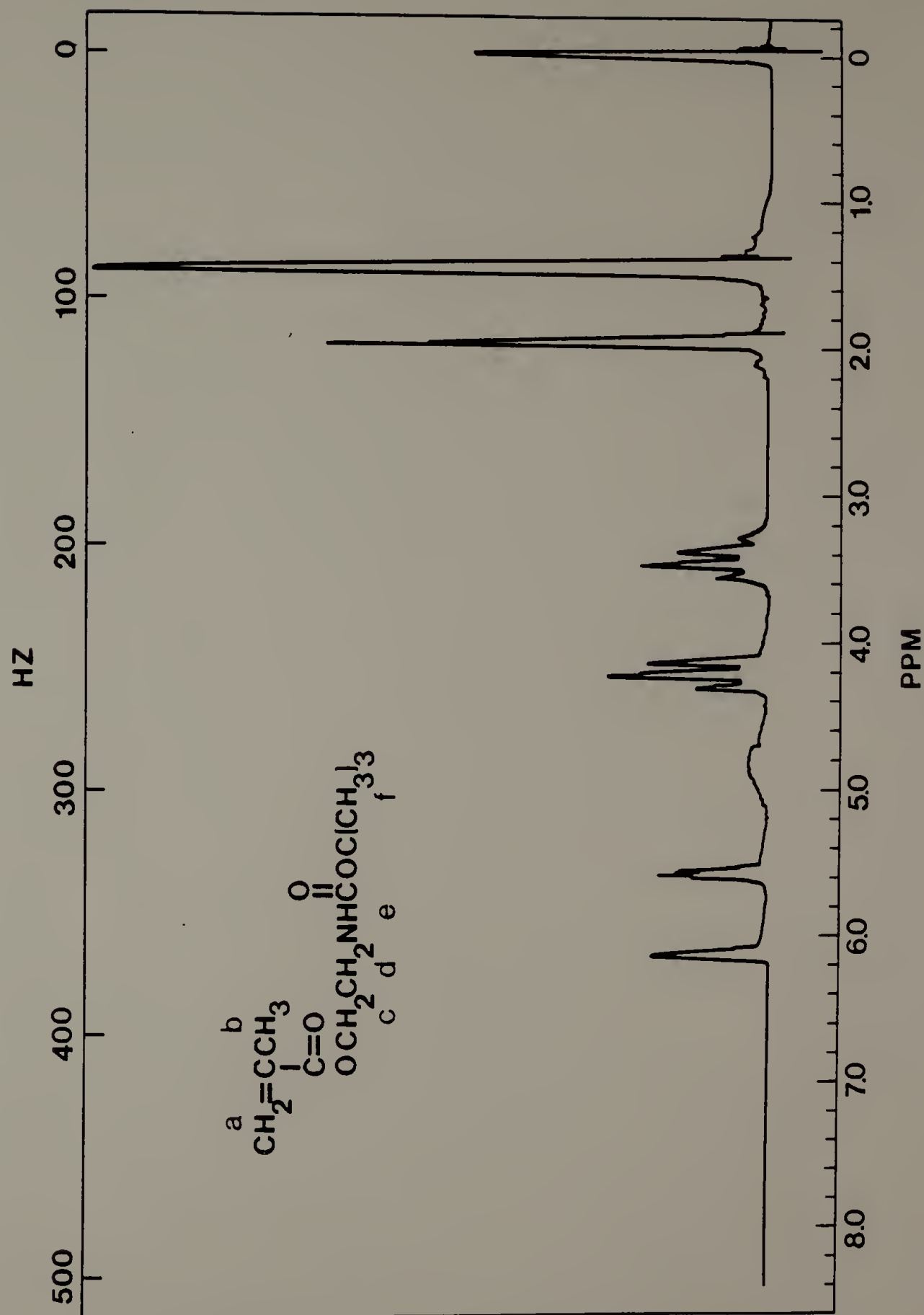


Figure A.12. Carbon-13 NMR of N-tert-butyloxycarbonyl-2-aminoethyl methacrylate ( $\text{CDCl}_3/\text{TMS}$ ).

Assignment:

- a) 125.82 ppm
- b) 136.09 ppm
- c) 18.26 ppm
- d) 167.26 ppm
- e) 63.92 ppm
- f) 39.72 ppm
- g) 155.90 ppm
- h) 79.37 ppm
- i) 28.37 ppm

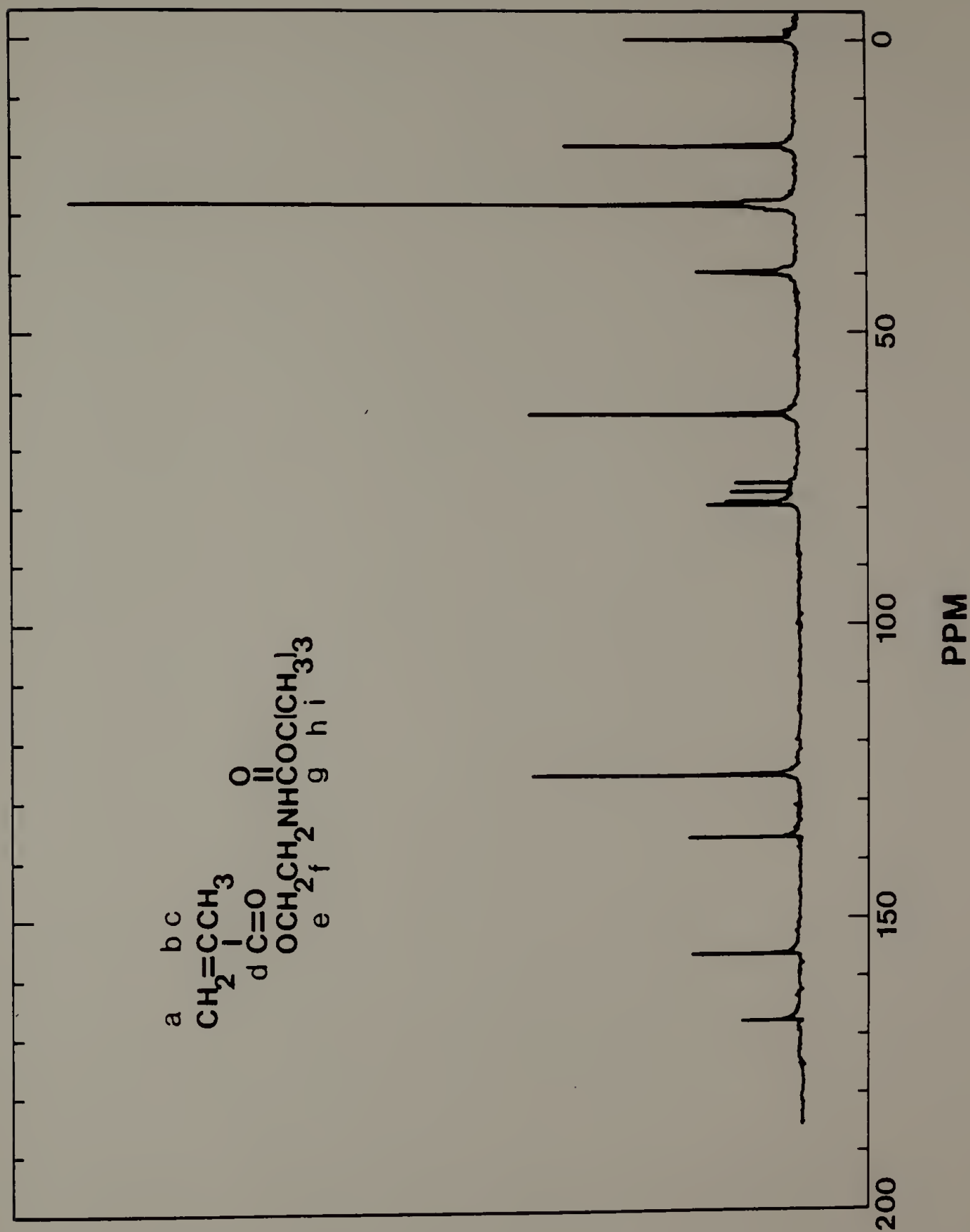


Figure A.13. Infrared spectrum of N-tert-butyloxycarbonyl-N'-(2-methacrylyl)-1,6-diaminohexane (KBr).

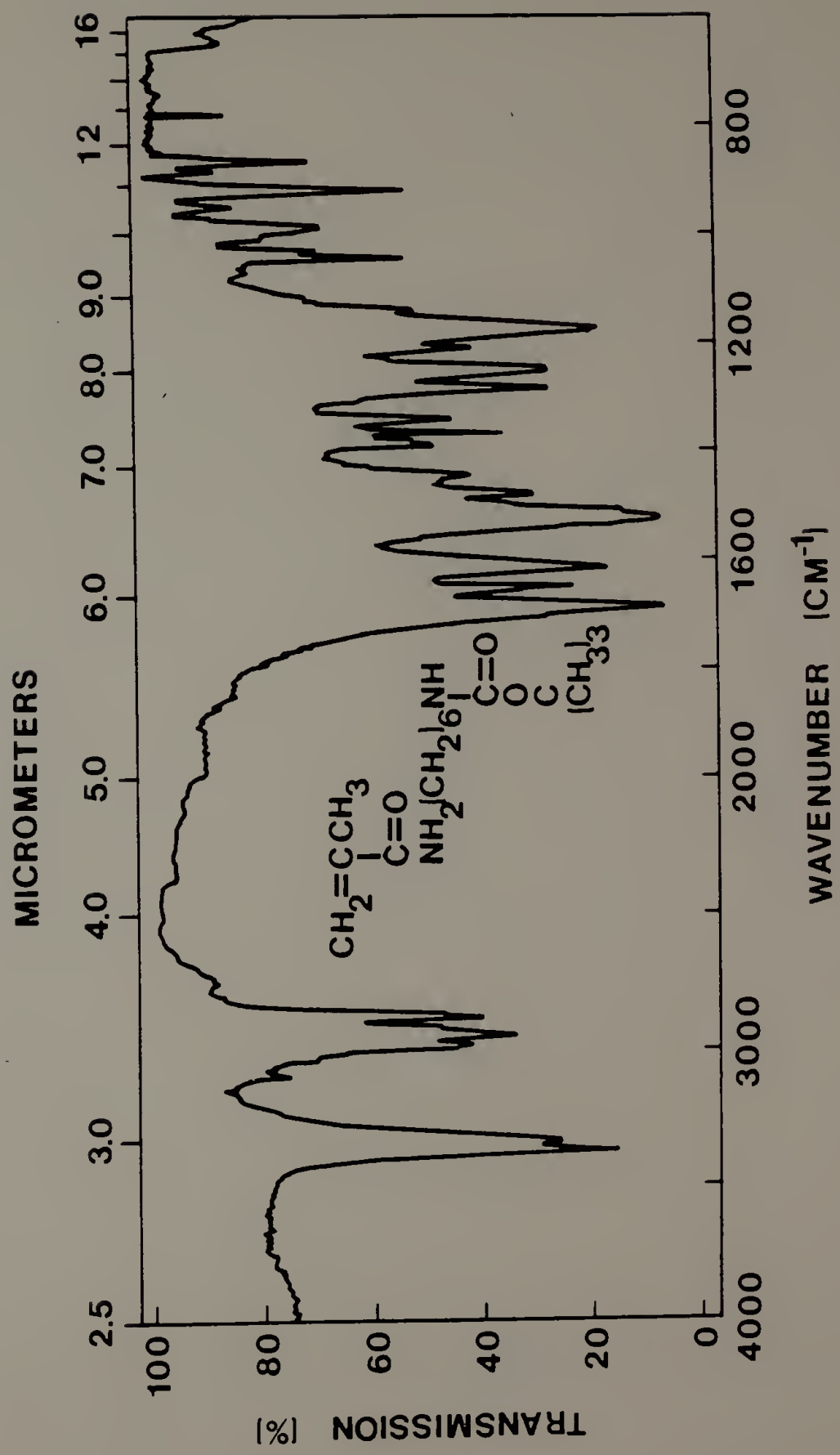


Figure A.14. Proton NMR of N-tert-butyloxycarbonyl-N'-(2-methacrylyl)-1,6-diaminohexane (CDCl<sub>3</sub>/TMS).

Assignment:

- a) 5.33, 5.72 ppm
- b) 1.98 ppm
- c) 6.12 ppm
- d) 3.18 ppm
- e) 4.66 ppm
- f) 1.51 ppm



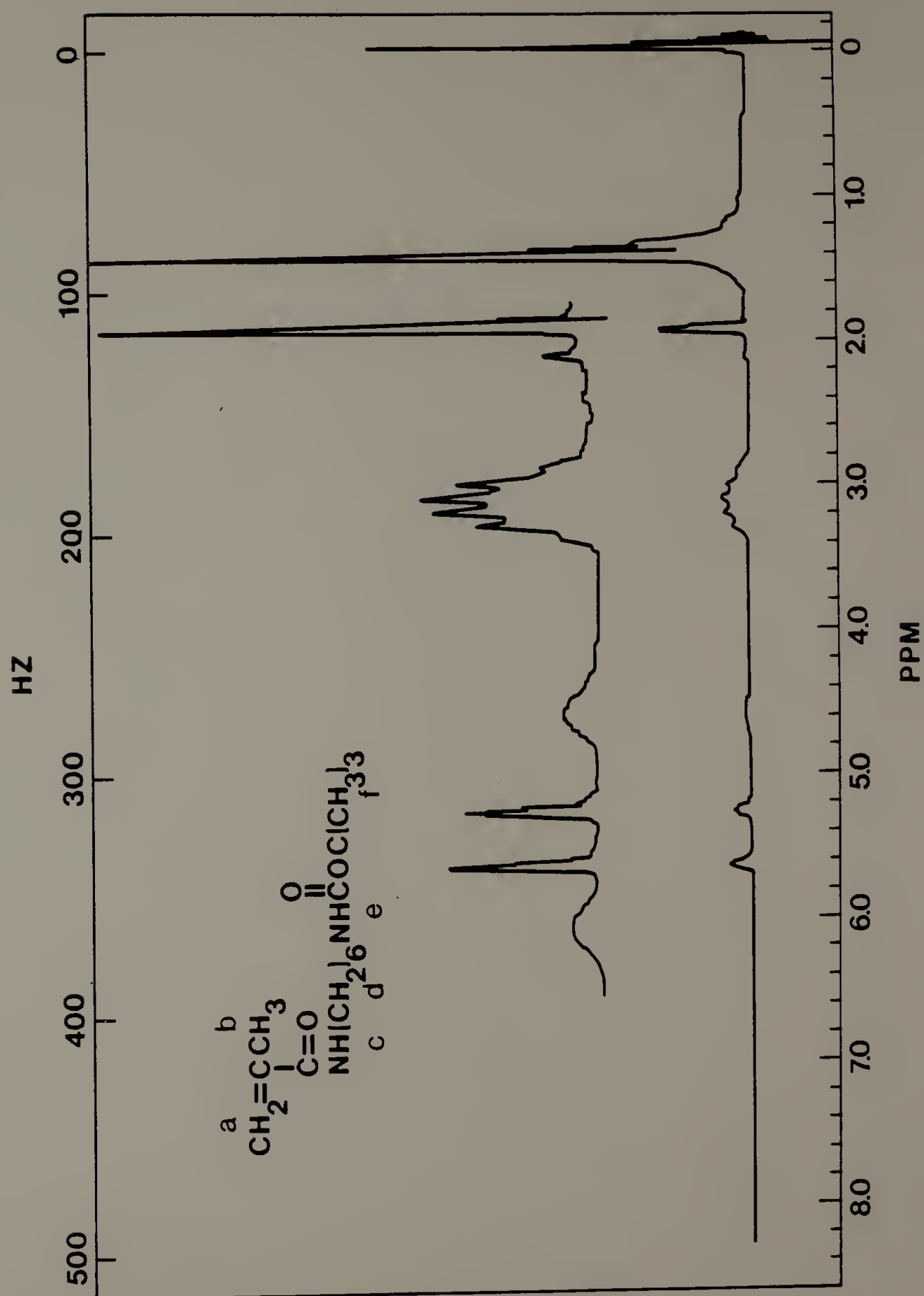


Figure A.15. Carbon-13 NMR of N-tert-butyloxycarbonyl-N'-(2-methacrylyl)-1,6-diaminohexane (CDCl<sub>3</sub>/TMS).

Assignment:

- a) 119.16 ppm
- b) 140.37 ppm
- c) 18.79 ppm
- d) 168.59 ppm
- e) 40.41 ppm
- f) 29.54 ppm
- g) 26.41 ppm
- h) 26.26 ppm
- i) 29.04 ppm
- j) 39.45 ppm
- k) 156.19 ppm
- l) 79.08 ppm
- m) 28.51 ppm

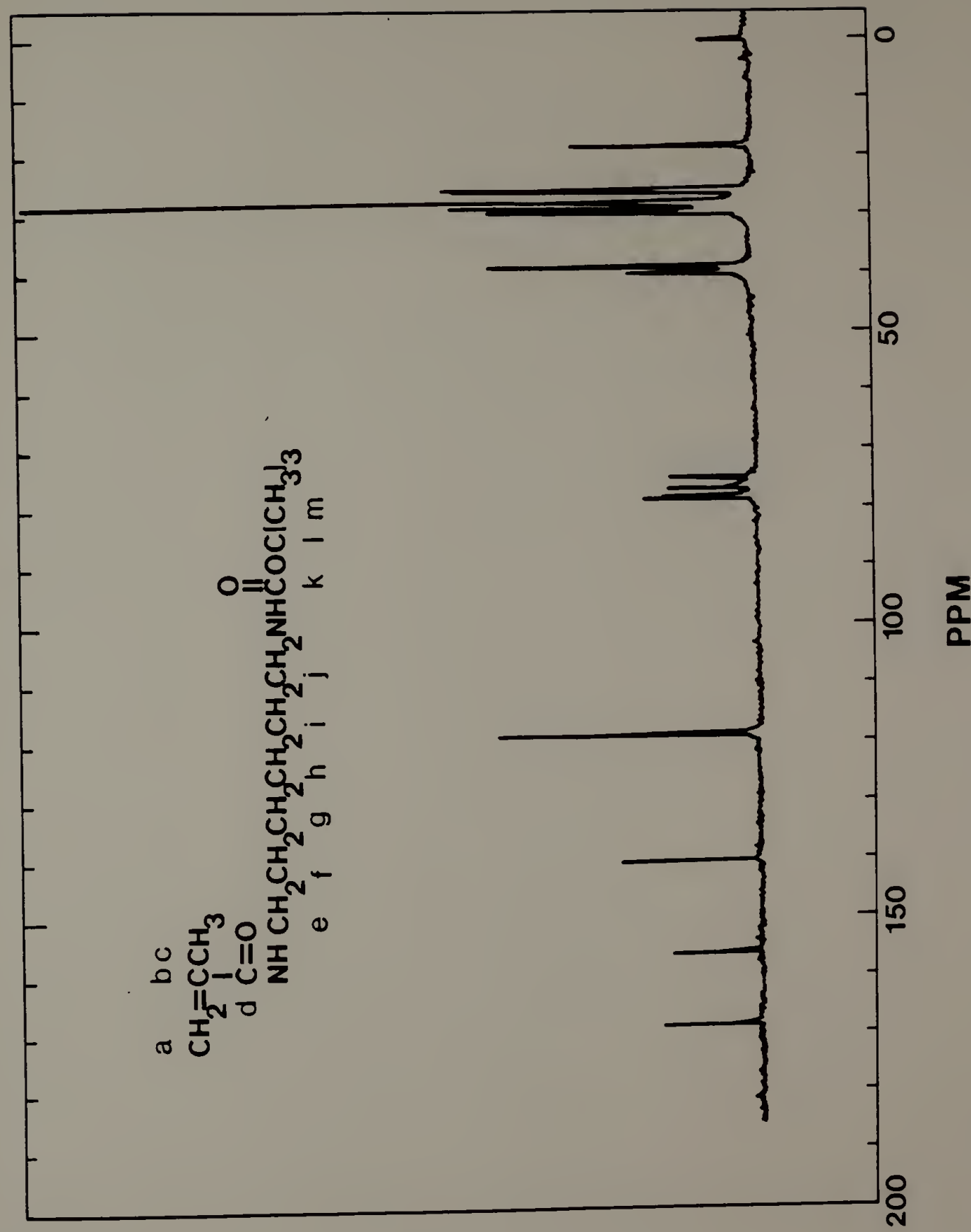


Figure A.16. Infrared spectrum of p-azidophenol (neat).

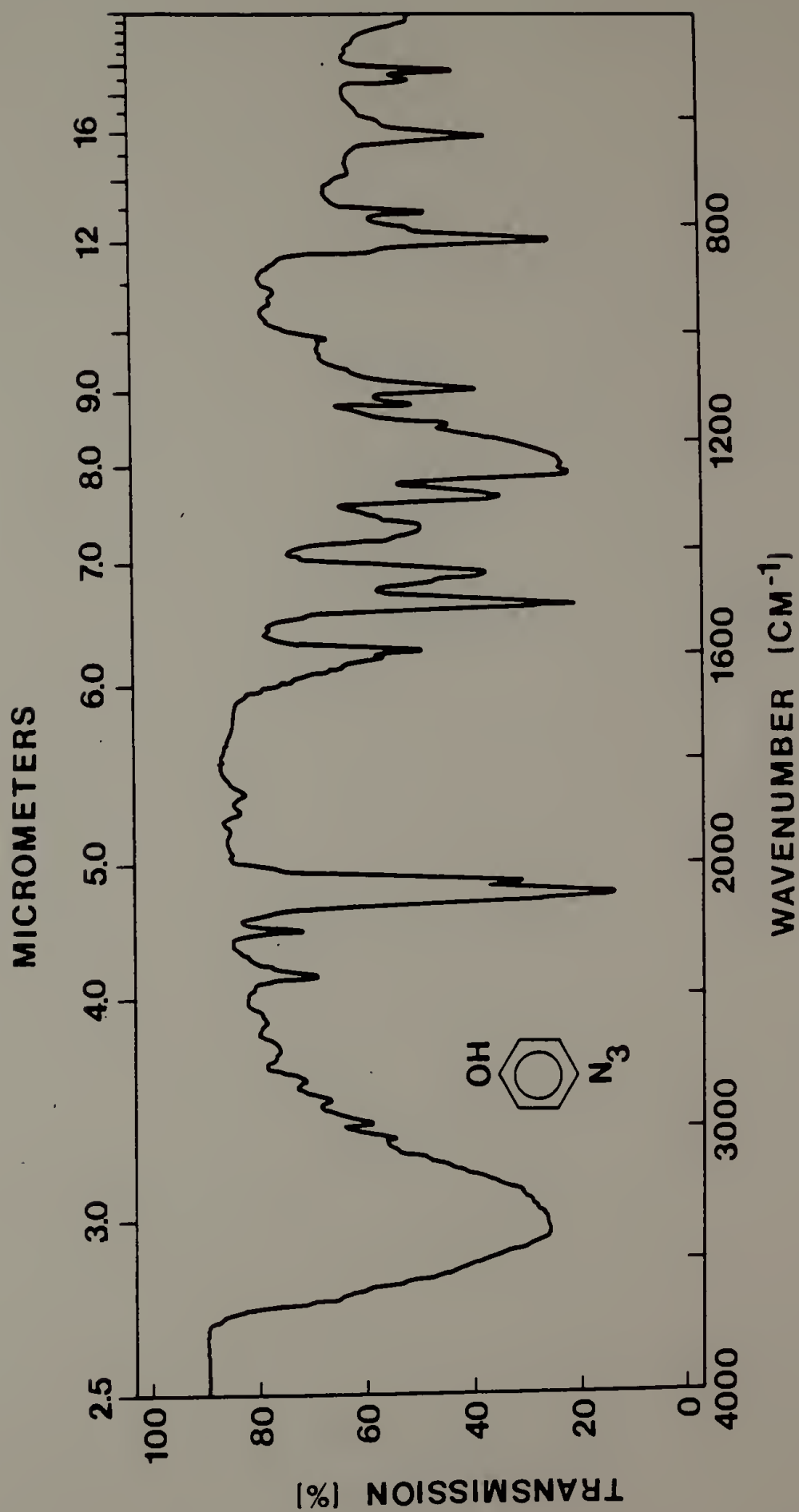


Figure A.17. Infrared spectrum of p-azidophenyl methacrylate  
(KBr).

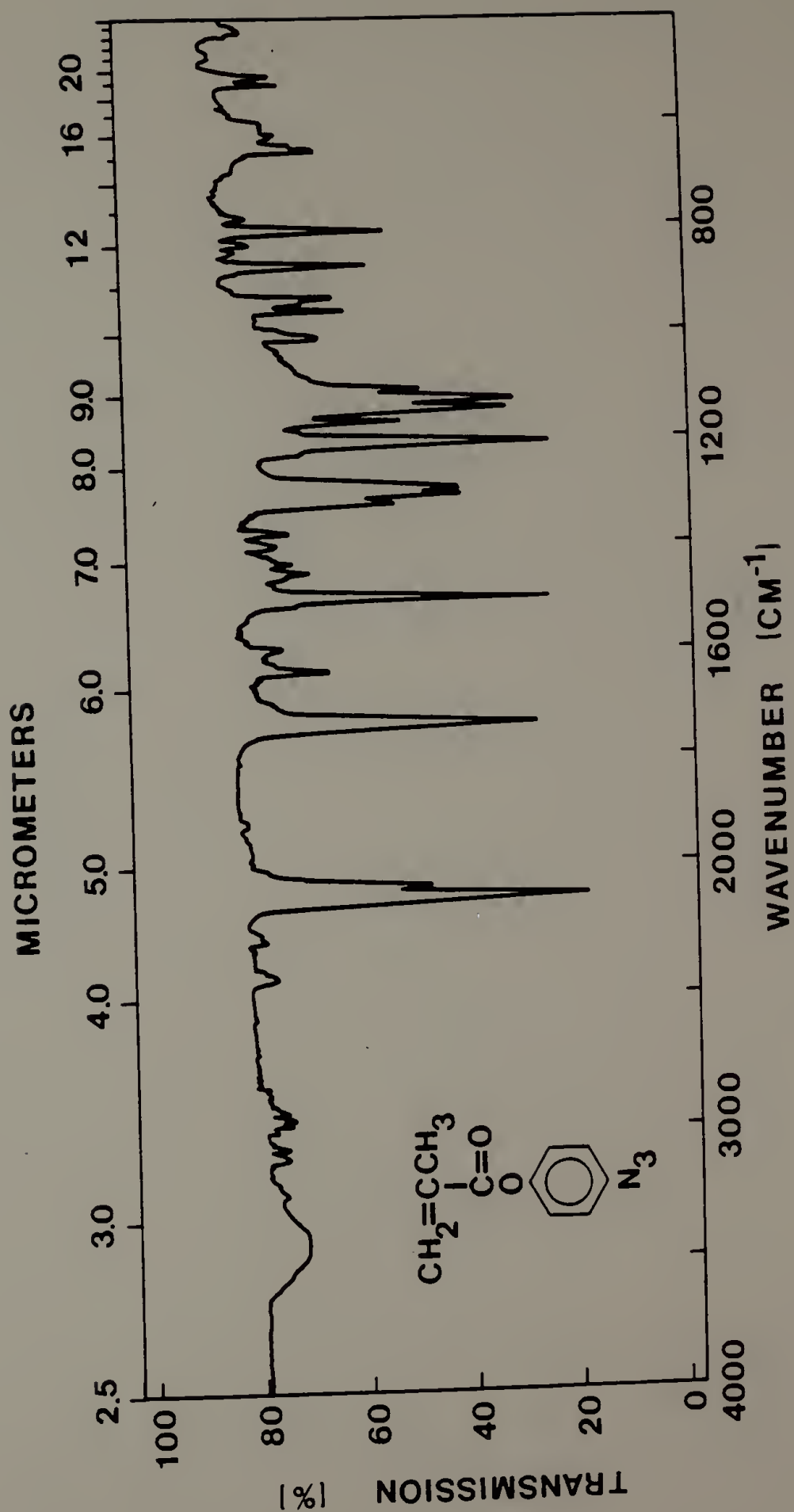


Figure A.18. Proton NMR of p-azidophenyl methacrylate ( $\text{CDCl}_3/\text{TMS}$ ).

Assignment:

- a) 5.75, 6.35 ppm
- b) 2.10 ppm
- c) 7.10 ppm



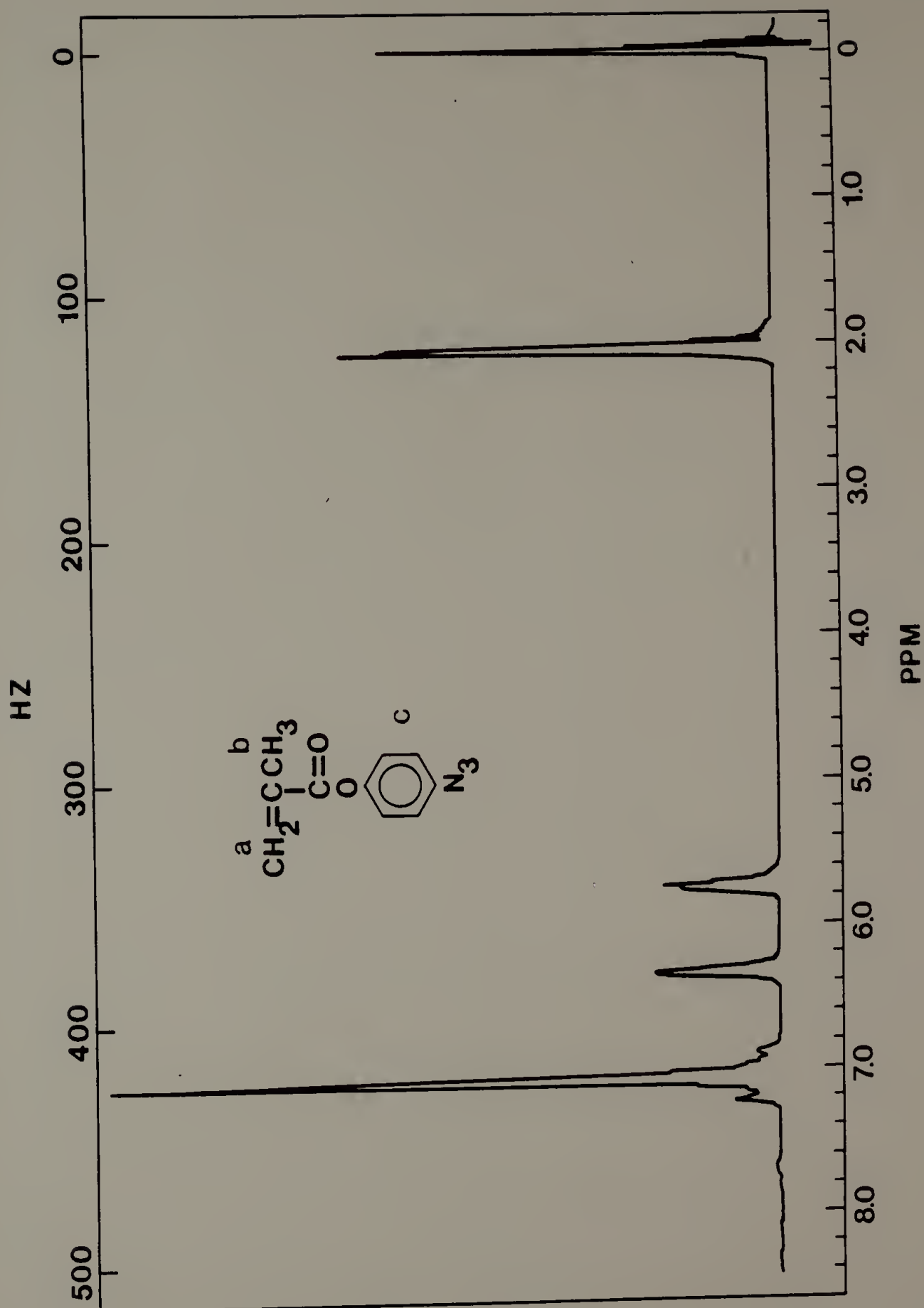


Figure A.19. Carbon-13 NMR of p-azidophenyl methacrylate  
(CDCl<sub>3</sub>/TMS).

Assignment:

- a) 127.32 ppm
- b) 135.81 ppm
- c) 18.36 ppm
- d) 165.67 ppm
- e) 147.90 ppm
- f) 123.05 ppm
- g) 119.80 ppm
- h) 137.50 ppm

